Effect of Foetal and Adult Stem Cells in Acute and Chronic Kidney Diseases

Thesis

EFFECT OF FOETAL AND ADULT STEM CELLS IN ACUTE AND CHRONIC KIDNEY DISEASES

Thesis submitted by

Cinzia Rota

for the degree of

Doctor of Philosophy

Discipline of Life Sciences

Open University Research School, London, UK

"Mario Negri" Institute for Pharmacological Research, Bergamo, Italy

Director of Studies

Dr. Ariela Benigni

Second Supervisor

Dr. Patricia Murray

SEPTEMBER 2012

DATE OF SUBMISSION : 27 SEPTEMBER 2012

DATE OF AWARD : 4 MARCH 2013

EFFECT OF FOETAL AND ADULT STEM CELLS IN ACUTE AND CHRONIC KIDNEY DISEASES

Cinzia Rota
"Mario Negri" Institute for Pharmacological Research
Open University Research School, London
Doctor of Philosophy
September 2012

ABSTRACT

Acute kidney injury (AKI) and chronic kidney disease (CKD) are serious illnesses associated to high mortality and unsatisfactory therapeutic treatments. In search for new therapies, it has become evident that stem cells could be a possible option for patients with AKI and CKD.
The evidence of the renoprotective effect of bone marrow-mesenchymal stem cells (BM-MSCs) in experimental model of AKI, prompted us to study the effect of stem cells isolated from sources that are more accessible as cord blood (CB) and amniotic fluid. Infusion of hCB-MSCs in immunodeficient mice with AKI ameliorated renal function and tubular structure, prolonging survival. Moreover, transplanted hCB-MSCs localized in peritubular areas, limiting oxidative stress and apoptosis. By virtue of stem cell capacity to produce growth factors, hCB-MSCs were able to induce the pro-survival factor Akt in tubular cells and subsequently their proliferation.
Using the well-established model of AKI in immunodeficient mice, we studied the pro-regenerative effect of amniotic fluid stem (hAFS) cells. Infusion of hAFS cells in cisplatin-mice improved renal function and limited tubular damage, although not to control level, and prolonged animal survival. These cells engrafted injured kidney predominantly in peritubular region and through a paracrine mechanism are able to exert an anti-apoptotic effect, to activate Akt and stimulate proliferation of tubular cells. We enhanced the therapeutic potential of hAFS cells by cell pre-treatment with GDNF, which markedly ameliorated renal function and tubular injury by increasing stem cell homing to the tubulointerstitial compartment.
In AKI models, the renoprotective effect of BM-MSCs is well established, however the role of these stem cells in model of CKD is controversial and not demonstrated so far. Therefore, we tested the effect of BM-MSCs in a model of adriamycin-induced nephropathy. Repeated infusions of BM-MSCs limited podocyte loss, and normalized distribution of parietal epithelial cells along the Bowman's capsule, reducing glomerulosclerosis. Moreover, through the local release of growth factors as VEGF, BM-MSCs were able to provide a local pro-survival environment that limited glomerular inflammation and microvascular rarefaction.

CONTENTS

Principles of the main techniques and instruments

LIST OF ABBREVIATIONS

ADR	adriamycin
AF	amniotic fluid
AIF	apoptosis-inducing factor
AKI	acute kidney injury
APAF1	apoptotic protease activating factor 1
ARF	acute renal failure
ATN	acute tubular necrosis
bFGF	basic fibroblast growth factor
BM	bone marrow
BM-MSCs	bone marrow-derived mesenchymal stem cells
BrdU	bromodeoxyuridine
BSA	bovine serum albumin
BUN	blood urea nitrogen
CB	cord blood
CDK	cyclin dependent kinase
CKD	chronic kidney disease
DAB	3,3'-diaminobenzidine
DMEM	Dulbecco's modified eagle's medium
EGF	epidermal growth factor
EGFP	enhanced green fluorescent protein
ESRD	end-stage renal disease
FACS	fluorescence activated cell sorting
FCS	foetal calf serum

FITC	fluorescein isothiocyanate
FSC	forward scatter
FSGS	focal segmental glomerulosclerosis
G-CSF	granulocyte colony stimulating factor
GDNF	glial cell line derived neurotrophic factor
GFR	glomerular filtration rate
hAFS cells	amniotic fluid stem
HB-EGF	heparin-binding EGF-like growth factor
hCB-MSC	human cord blood mesenchymal stem cell
HGF	hepatocyte growth factor
hMSC	human mesenchymal stem cell
HPF	high power field
HSC	haematopoietic stem cell
ICAM-1	intercellular adhesion molecule-1
IGF-1	insulin-like growth factor 1
IL-β	interleukin-β
IL-6	interleukin-6
IL-11	interleukin-11
LCA	*Lens Culinaris Lectin*
LIF	leukaemia inhibitory factor
MAPK	mitogen activated protein kinase
MCP-1	monocyte chemotactic protein-1
m-CSF	macrophage colony-stimulating factor
MHC	major histocompatibility complex
MOMP	mitochondrial outer membrane permeabilization
MSC	mesenchymal stem cell

NCAM	neural cell adhesion molecule
NCDs	non-communicable disease
PAS	periodic acid-Schiff's reagent
PBS	phosphate buffer saline
PCNA	proliferating cell nuclear antigen
PE	phycoerythrin
PTEC	proximal tubular epithelial cell line
RANTES	regulated and normal T cell expressed and secreted
ROS	reactive oxygen species
RRT	renal replacement therapy
SCF	stem cell factor
SDF-1	stromal cell-derived factor
SP	side population
SSC	side scatter
TGF-β	transforming growth factor β
TNF-α	tumor necrosis factor α
VCAM-1	vascular cell adhesion molecule
VEGF	vascular endothelial growth factor

ACUTE KIDNEY INJURY

CHAPTER 1

INTRODUCTION

1.1 Acute kidney injury

Acute kidney injury (AKI), formerly known as "acute renal failure" (ARF) is a common clinical problem with increasing incidence, serious consequences, unsatisfactory therapeutic options, and an enormous financial burden to society (Devarajan *et al.*, 2006). AKI is a complex disorder that comprises multiple causative factors and occurs with varied clinical manifestations that range from minimal but sustained elevation in serum creatinine to anuric renal failure. AKI is classically characterized by the rapid deterioration of renal function, with at least a 50% decrease in glomerular filtration rate (GFR) that leads to accumulation of nitrogenous wastes such as blood urea nitrogen (BUN) and creatinine (Devarajan *et al.*, 2006).

The incidence of AKI in hospitalized patients has generally been reported to be in the 2%-7% range, with an incidence of 5% to greater than 10% in the intensive care unit (ICU) patients (Lamiere N *et al.*, 2006; Waikar S *et al.*, 2008). Despite advances in preventive strategies and support measure, over the last 20 years, the incidence of AKI has remained stable, probably due to the therapeutic use of new more aggressive nephrotoxic drugs, more invasive procedures and increasing age of the patient population. Moreover, AKI has remained associated with high morbidity and mortality, particularly in ICU, where mortality rates may exceed 50%. In addition to mortality rates, there are chronic consequences even in patients survive their acute illness, with a high

risk to develop or exacerbate chronic kidney disease (Coca *et al.* 2009; Hsu *et al.* 2009).

Traditionally, the causes of acute kidney injury are classified as *pre-renal* due to inadequate perfusion, *intrinsic, renal* or *parenchymatous* due to injury to renal parenchyma, and *post renal* or *obstructive* due to obstruction of outflow (Figure 1.1). The *pre-renal* AKI occurs when there is a volume depletion caused by renal or extra renal losses, fluid sequestration, or inadequate perfusion pressure (Lattanzio *et al.* 2009). Patients with *pre-renal* AKI can exhibit, at least at the beginning of the disease, intact glomerular and tubular structure. Among hospitalized patients, *pre-renal* AKI can be consequence of liver dysfunction, nephritic syndrome, intestinal obstruction, decreased cardiac output (cardiogenic shock, myocarditis, myocardial infarction, etc.); in surgical patients, *pre-renal* azotemia is a common cause of peri- and post-operative renal dysfunction. Moreover, among the *pre-renal* causes of AKI, there are peripheral vasodilatation (hypotension, sepsis, hypoxemia, etc), renal vasoconstriction (prostaglandin synthesis inhibition, sepsis, hepatorenal syndrome, hypercalcemia) or efferent arteriole vasodilatation. If the underlying cause is corrected, the AKI is rapidly reversible.

In *intrinsic* AKI, the decrease in GFR is secondary to intrinsic renal damage mainly affecting tubules (acute tubular necrosis, ATN), interstitium (acute tubulointerstitial nephritis), glomeruli and/or vessels (acute glomerulonephritis, vascular occlusion). Injury to the

tubules most often is caused by ischemia or nephrotoxins, and ATN has composed by three phases: initiation, maintenance, and recovery. The classic course of "self-limited" ATN is the steady rise in serum creatinine levels (injury stage), followed by stabilization, and an eventual decline in those measures during 7 to 21 days. Acute interstitial nephritis is an interstitial disturbance that often results from an allergic reaction to drug. Symptoms include fever, rash, and serum and urine eosinophil counts may be elevated. Autoimmune disease, infection and infiltrative disease also can lead to interstitial nephritis (Lattanzio *et al.* 2009). Glomerulonephritis, an uncommon cause of AKI, has systemic manifestations as fever, rush and arthritis. Urine finding include red blood cell casts, haematuria, and proteinuria. Finally, vascular disease can occur on the micro- and macrovascular levels. Microvascular disease is commonly secondary to small-vessel thrombosis or occlusion. Macrovascular causes should include renal stenosis or thrombosis, aortic disease or acute dissection (Lattanzio *et al.* 2009).

Post-renal causes of AKI result in obstruction of the outflow tracts of the kidney. It can be due to congenital anomalies, prostatic hypertrophy, retroperitoneal fibrosis and, less frequently, to bilateral renal calculi or to malignant conditions. Drugs and infections might also cause post-renal AKI. Approximately 10% of AKI cases are the result of post-renal causes that are readily reversible (Lattanzio *et al.* 2009).

AKI is usually treated by targeting the underlying causes. In

certain situations, such as when a patient has glomerular disease, microvascular disease or obstructive disease, rapid diagnosis and treatment are necessary to prevent permanent renal damage. However, once AKI develops, supportive therapy is critical to maintain fluid and electrolyte balances, minimize nitrogenous waste production and sustain nutrition. Before the development of renal replacement therapy, many people with AKI died from severe electrolyte imbalance (hyperkalemia, acidosis) or from the uraemic toxins themselves. The treatment of AKI with renal replacement therapy has the objective to maintain fluid and electrolyte, acid-base, and solute homeostasis, to prevent further insults to the kidney and to promote healing and recovery. However, modern dialysis techniques, such as continuous renal replacement therapy, have had no significant impact on overall mortality. Over the last thirty years, despite advances in supportive care, very little clinical progress has been made for decreasing renal dysfunction and mortality. The quest for a pharmacological therapy that could improve survival after an AKI episode has been largely unsuccessful. Numerous pharmacologic agents have been tested with successful results in preventing or ameliorating experimental AKI (Star *et al.*, 1998). However, none of these substances have been translated successfully to clinical practice. Negative clinical trial experience with dopamine, furosemide, mannitol, calcium channel blockers, atrial natriuretic peptide and several other hormonal or pharmacological substances has been reported (Grino *et al.*, 1994; Haug *et al.*, 1993).

Several studies have also evaluated the role of growth factors as epidermal growth factor (EGF), insulin growth factor-1 (IGF-1) and hepatocyte growth factor (HGF), possibly because their mitogenic and pro-survival activity (Nigam *et al.*, 2000; Toubeau *et al.*, 1994), but also because many types of renal cells express the receptor for this growth factors. In an animal model of ATN, EGF treatment enhanced renal tubule cell regeneration and accelerated the recovery of renal function. (Coimbra *et al.*, 1990; Humes *et al.*, 1989; Norman *et al.*, 1990). The same was obtained with IGF-1. In ischaemic and toxic ATN, the pre-treatment with IGF-1 or treatment within 24 hours of damage accelerated renal recovery (Ding *et al.*, 1993; Miller *et al.*, 1992). Administration of HGF in a mouse model of AKI induced by cisplatin, at the time of renal injury, accelerated renal recovery by reducing serum urea nitrogen and the severity of pathological changes (Kawaida *et al.*, 1994; Miller *et al.*, 1994).

Although in animal models good results have been obtained, clinical trials in humans with AKI have failed to show substantial benefit of these growth factors as cure of a disease that contributes significantly to morbidity and mortality in severely ill patients. (Franklin *et al.*, 1997; Hirschberg *et al.*, 1999).

The failure of the pharmacological therapies tested, increasingly makes necessary to identify new treatments. At this purpose, a large body of literature reported an emerging role for stem cells, discussed later in this chapter, in the regenerative mechanisms of the kidney.

1.1.1 Pathophysiology of acute kidney injury

The following part of the chapter will focus primarily on acute tubular necrosis (ATN), the most common cause of acute kidney injury. In the ischaemic and nephrotoxin ATN the straight portion of the proximal tubules is mainly damaged, however the proximal convoluted tubules are involved as well. ATN is characterized by a rapid loss of cytoskeletal integrity and cell polarity with shedding of the proximal tubule brush border, mislocalization of adhesion molecules and other membrane proteins such as sodium/potassium ATPase, along with apoptosis and necrosis (Bonventre *et al.*, 2003). Effacement of the tubular brush border, loss of proximal tubule cell microvilli, simplification of the basolateral surface of tubular epithelial cells, flattening of tubular epithelium and dilatation of tubular lumina also occurs (Figure 1.2).

Pigmented, granular or hyaline casts are present in the lumina of distal nephron segments in ATN. The major component of casts is the unique Tamm-Horsfall glycoprotein that is normally produced by the ascending thick limb of Henle and is present in the urine. Its polymerization within the renal tubules occurs under conditions of dehydration, and increasing sodium, calcium and hydrogen ion concentrations result in cast formation.

With severe injury, in many regions of the tubule the basement membrane remains the only barrier between the filtrate and the peritubular interstitium. Backleak of the filtrate can then occur,

especially when the pressure in tubule is increased owing to intratubular obstruction (Zuk *et al.*, 2001). Biochemical pathways that lead to cell necrosis are activated by severe cell injury and include: cell energy (ATP) store depletion, increased concentration of reactive oxygen species, intracellular acidosis, increased activity of phospholipases, release of proteases from the tubular cell brush border, loss of lipid transmembrane protein polarity in the tubular-cell apical and basolateral surface membranes leading to relocation of sodium/potassium ATPase to the apical cell membrane.

A more detailed description of the pathophysiological changes in nephrotoxic ATN is described for cisplatin induced renal damage as follows in this chapter.

1.1.2 Cisplatin nephrotoxicity

Acute kidney injury can be induced in experimental models by ischemia/ reperfusion, or by toxic insults like folic acid, cisplatin and glycerol. In this study, cisplatin-induced injury was chosen, because this animal model faithfully mimics the events leading AKI in human patients. So, this section of the introduction focuses on features of cisplatin nephrotoxicity and goes deeper inside the mechanisms underlying cisplatin toxicity.

Tubular cells of the kidney are particularly vulnerable to toxicant-mediated injury due to their exposure to circulating chemicals and

transport processes that result in high intracellular concentrations. Drugs and chemicals may act at different sites in the kidney, and their nephrotoxicity is influenced by several factors like:

- direct toxic effect of drugs on cells of the nephron;
- pharmacologic activity of some substances and their effects on renal function;
- high metabolic activity of particular segments of the nephron;
- multiple transport systems, which can result in intracellular accumulation of drugs and chemicals;
- high intratubular concentration with possible precipitation and crystallization of some drugs.

Cisplatin (cis-diamminedichloroplatinum II), whose biological activity was discovered in the early sixties (Rosenberg *et al.*, 1965; Rosenberg *et al.*, 1967), is one of the most remarkable successes in "the war of cancer". Cisplatin and related platinum-based therapeutics are currently used in the treatment of neoplasia with a wide spectrum of efficacy against several solid tumours like testicular, head, neck, ovarian, cervical, nonsmall cell lung carcinoma and many other type of cancer (Pabla *et al.*, 2008; Madias *et al.*, 1978). One of the major limiting factors in the use of cisplatin is the side effect in normal tissue, associated to ototoxicity, gastrointestinal toxicity, myelosuppression, allergic reactions and nephrotoxicity (Hartmann *et al.*, 2003; Pabla *et al.*, 2008). The prevalence of cisplatin nephrotoxicity is high, occurring in about one-third of patient undergoing cisplatin treatment. For years,

different approaches have been tried to minimize the side effects, one strategy used with some success is to hydrate the patients during cisplatin treatment (Pabla *et al.*, 2008). Despite these efforts, the side effect of cisplatin, in particularly nephrotoxicity, remain a major factor that limits the use and efficacy of cisplatin in cancer therapy.

Following intravenous administration, cisplatin undergoes extensive protein binding (more than 90%). The unbound fraction, low in molecular weight and neutral in charge, is freely filtered at the glomerulus, not reabsorbed and appears unchanged in the urine. The mechanism of intracellular transport of cisplatin is not clear and may vary from on cell type to another, however, in the renal system, the organic cation transporters (OCTs) have been implicated in cisplatin uptake (Pabla *et al.*, 2008; Ludwig *et al.*, 2004). In particular, OCT2 is critical for cisplatin uptake in the kidney (Ciarimboli *et al.*, 2005). Cisplatin is activated when the drug is inside the cell where the chloride ligands in the cis-position are replaced by water molecules forming a hydrated drug that can react with nucleophylic sites. The product is a highly reactive electrophylic molecule (Townsend *et al.*, 2002).

The cytotoxicity of cisplatin is probably due to a combination of insults, including peroxidation of the cell membrane, mitochondrial dysfunction, inhibition of protein synthesis and DNA injury.

DNA injury and subsequent cellular events. Cisplatin binds to DNA, leading to the formation of inter- and intrastrand cross-links. Cross-linking results in defective DNA templates and arrest of DNA synthesis

and replication (Wang *et al.*, 2005; Heiger-Bernays *et al.*, 1990; Jamieson *et al.*, 1999). DNA damage may lead to p53 activation (Figure 1.3) by phosphorylation, and the protein accumulates in the nucleus to regulate the expression of numerous genes associated with cell cycle arrest, DNA repair and apoptosis as cyclin dependent kinase (CDK) inhibitor $p21^{Waf1/Cip1}$, growth arrest and DNA damage inducible *gadd45a* gene, and the pro-apoptotic *bax* gene (Morgan *et al.*, 1997; Bullock *et al.*, 2001; Delmastro *et al.*, 1997; Hershberger *et al.*, 2002).

Apoptosis and necrosis. Tubular cell death, in the form of both necrosis and apoptosis, is a common histopathological feature of cisplatin toxicity. Depending on the dose of cisplatin, renal tubular cells undergo either necrosis or apoptosis (Lieberthal *et al.*, 1996). Necrotic cell death was observed when a high concentration of cisplatin (millimolar) was used, while lower concentration of cisplatin (micromolar) led to apoptosis (Lieberthal *et al.*, 1996).

Several pathways of apoptosis have been implicated in cisplatin nephrotoxicity, including the intrinsic pathway focused on mitochondria, the endoplasmic reticulum (ER)-stress pathway and the extrinsic pathway mediated by death receptors.

Intrinsic or mitochondrial pathway has emerged as the major apoptotic pathway in cisplatin nephrotoxicity (Figure 1.4). Cellular stress activates Bax and Bak, the pro-apoptotic Bcl-2 family proteins, which form porous defect on the outer membrane of mitochondria (MOMP, mitochondrial outer-membrane permeabilization) (Jiang *et al.*, 2006).

MOMP leads to the release of apoptogenic factors, like cytocrome c, AIF (apoptosis-inducing factor), Smac/DIABLO, endonuclease G and others, from the organelles (Pabla *et al.*, 2008; Green *et al.*, 1998). Cytocrome c after being released into the cytosol, binds to apoptotic protease activating factor 1 (APAF1) causing oligomerization and apoptosome formation. The apoptosome, finally, recruits and activates pro-caspase 9, which after proteolytic processing activates downstream caspase-3 and-7 (Figure 1.4). These caspases are responsible for apoptotic hallmarks, such as chromatin condensation, plasma membrane asymmetry and cellular blebbing (Pabla *et al.*, 2008; Green *et al.*, 1998).

Smac, after being released into cytosol, can bind and antagonize the caspase inhibitor proteins IAPs to further augment caspase activation. In contrast, AIF, once released from mitochondria, accumulates in the nucleous to induce apoptosis in a caspase-independent manner (Pabla *et al.*, 2008; Green *et al.*, 1998).

A direct involvement of the receptor-mediated apoptotic pathway, the extrinsic pathway, has also been demonstrated in renal tubular cells (Figure 1.4). In the extrinsic pathway, binding of the death receptors as Fas, TNFR-1 and 2 (tumor-necrosis factor-α receptor), by ligands at the plasma membrane leads to the recruitment and activation of caspase-8, which further activate downstream caspases to induce apoptosis (Figure 1.4). (Strasser *et al.*, 2000).

It is important consider that although the classical apoptotic pathways

activated by cisplatin involve caspase, not all the apoptosis is mediated by caspase. The mechanism of caspase-independent apoptosis is currently unclear, probably might involve AIF.

Mitochondrial dysfunction and oxidative stress. Oxidative stress has been recognized as an important factor that contributes to cisplatin nephrotoxicity (Baliga *et al.*, 1999). Increase of various reactive oxygen species (ROS) occurs during cisplatin treatment *in vitro* (Brady *et al.*, 1990) and *in vivo* (Gordon *et al.*, 1986; Davis *et al.*, 2001; Satoh *et al.*, 2003). Once incorporated by the cells, cisplatin is converted into a highly reactive form, which induce depletion and inactivation of glutathione, a well-recognized cellular antioxidant, leading to the accumulation of endogenous ROS and oxidative stress within the cells (Pabla *et al.*, 2008). Cisplatin may also induce mitochondrial dysfunction and increase ROS production via the disrupted respiratory chain (Pabla *et al.*, 2008). Moreover, there is evidence that ROS increase p53 (Nakamura *et al.*, 2001) with subsequent activation of the cell death program.

In various experimental models, have been demonstrated the renoprotective effect of antioxidants as dimethylthiourea (DMTU), melatonin, selenium, vitamin E, N-acetylcysteine and many others (Ramesh *et al.*, 2005; Jiang *et al.*, 2007; Dickey *et al.*, 2005; Tsuruya *et al.*, 2003; Sener *et al.*, 2000; Naziroglu *et al.*, 2004). However, whether these antioxidant chemicals are renoprotective in human patients during cisplatin-based chemotherapy is uncertain.

Inflammation. In the case of cisplatin nephrotoxicity, several cytokines and chemokines as tumor necrosis factor-α (TNF-α), transforming growth factor β (TGF-β), RANTES, MIP-2, and monocyte chemotactic protein-1 (MCP-1) are significantly up-regulated in the kidney (Ramesh *et al.*, 2002). In the inflammatory response trigger by cisplatin, TNF-α appears to be a key upstream regulator. Ramesh et al. showed that pharmacological inhibition of TNF-α afforded protection from cisplatin nephrotoxicity (Ramesh *et al.*, 2002). Moreover, a significant up-regulation of the expression of ICAM-1, that serves as a ligand for the β_2 integrins, LFA-1 and Mac-1 on leukocytes, was found in kidneys from cisplatin-treated rats and mice (Kelly *et al.*, 1999; Ramesh *et al.*, 2002).

All this evidence suggests a pro-inflammatory role of cisplatin in its nephrotoxicity.

1.2 Repair and recovery in kidney disease

In a physiological setting, the kidney has been regarded as an organ with minimal cell turnover and limited capacity for repair. However, after injury, an increased cell proliferation is the driving event that directs towards tissue recovery. After ischemia/reperfusion injury, regeneration of tubules is evident on the third day, after ten days

50% of the tubules have been regenerated (Ysebaert *et al.*, 2000) and complete restoration of tubular structure is reached after 4 weeks (Humes *et al.*, 1994; Witzgall R *et al.*, 1994). This functional property of the kidney to regenerate supports the hypothesis that resident cells can be involved in restoring structure and function. What remains to be determined is whether reparative programme depend on (Figure 1.5):

- cells originating from de-differentiation of tubular cells
- stem or progenitor cells that reside in a specific niche in the kidney
- extrarenal stem cells that, recruited to the kidney following damage, exert a paracrine effect/or differentiate into renal cells.

1.2.1 De-differentiation of terminally differentiated cells

Seemingly, terminally differentiated resident tubular cells may have a role in kidney repair during cell turnover or after damage. In fact, using healthy juvenile rats in which the kidney is fully developed but the nephrons still grow in length, Vogetseder *et al.* have demonstrated that mitotic cells (BrdU-retaining cells) displayed characteristic features of the epithelium (Vogetseder *et al.*, 2005). Moreover, the same group has observed that the generation of new cells in the S3 segment of the proximal tubule was due to the division of differentiated, normally slow-cycling cells, suggesting that differentiated tubular cells are self-renewing (Vogetseder *et al.*, 2007).

The cells that survive to damage might proliferate and generate

identical cells or dedifferentiate and subsequently re-enter the cell cycle. The positive correlation between differentiated tubule markers and mitosis markers in healthy kidneys supports the idea that resident tubular epithelial cells could fuel regeneration. The de-differentiation hypothesis is also attractive due to the precedence set by nephron development, i.e. that the tubules arise from mesenchyme that is induced to become epithelium.

After the insult occurs, renal tubular cells rapidly lose their brush border and dedifferentiate into a more mesenchymal phenotype. This process seems to be followed by migration of the dedifferentiated cells into regions where cell necrosis, apoptosis or detachment have resulted in denudation of the tubular basement membrane (Figure 1.5). There, they proliferate and eventually redifferentiate into an epithelial phenotype, completing the repair process (Cantley *et al.*, 2005). It is thought that the release, at the tubular sites of injury, of growth factors such as insulin-like growth factor 1 (IGF-1) and hepatocyte growth factor (HGF), coordinates this response of dedifferentiation, migration, proliferation and eventually redifferentiation (Schena FP, 1998).

Tubular cell dedifferentiation, which recapitulates in the patterns of gene and protein expression kidney development, was shown by the finding that tubular cells acquire an immature mesenchymal phenotype with re-expression of Vimentin, Pax-2 and neural cell adhesion molecule (NCAM) in post-ischemic recovery (Witzgall *et al.*, 1994; Imgrund *et al.*, 1999; Abbate M *et al.*, 1999). A vimentin positive

phenotype, normally not expressed in the mature nephron, is acquired by the proximal tubular cells during the recovery phase after ischaemia/reperfusion injury (Witzgall *et al.*, 1994). NCAM, a dedifferentiation marker for renal cells, is expressed in post-ischaemic proximal tubular cells of the severely injured S3 segment (Abbate M *et al.*, 1999). Moreover, it is implicated in the control of cell shape and migration and is rapidly down regulated during the conversion to a more mature phenotype. The loss of the highly specialized phenotype is reflected also by decreased expression of the apical brush border markers, gp330 and DPP-IV. While de-differentiating, these cells also express the transcription factors Pax-2, a factor involved in kidney development (Dressler, 1996), Egr-1 and c-fos (Ouellette *et al.*, 1990). Cell adhesion molecules, such as integrins, also change their distribution: after ischaemia/reperfusion injury, β1-integrins are relocated to the lateral borders of the cell, like in immature epithelial cells where they are implicated in the control of cell migration (Zuk *et al.*, 2001).

A great support for proximal tubular cell survival derives from distal tubular epithelial cells, which in response to ischemia/reperfusion injury, release reparative and prosurvival factors and protect the sensitive proximal tubules from injury (Gobe *et al.*, 2007).

1.2.2 Renal stem/progenitor cells in the adult kidney

Stem cells of adult organs have traditionally been viewed as multipotent precursor cells capable of maintaining, generating and replacing mature cell types within their own specific tissue, as a consequence of physiological cell turnover or tissue injury (Blau *et al.*, 2001). A stem cell is define as a cell that, upon division, can self-renew and give rise to a transit-amplifying progenitor, that acquires a more differentiated state, but exhibits a high capacity for growth. Adult stem cells support homoeostasis in tissue with high rates of turnover as blood, skin and intestine, but also in organs formerly believed to have no regenerative potential as the lung and brain (McCampbell *et al.*, 2012).

Renal stem/progenitor cells in the adult kidney have been identified looking for cells expressing stem-cell markers or cells in the kidney with functional properties of stem cells, as that stem cells cycle infrequently. The search for renal stem/progenitor cells in adult kidney has not identified a multipotent cell able to self-renew and make more than 20 specialized renal cell type, but has revealed the presence of different population of stem/progenitor cells in distinct localizations within the nephron. These sites include the glomeruli, the tubuli, the renal papilla and the interstitium (Benigni *et al.*, 2010).

Multipotent progenitor cells expressing the stem cell markers CD24 and CD133 were immunoisolated from Bowman's capsules in adult human glomeruli (Sagrinati *et al.*, 2006). These parietal epithelial

cells (PECs) exhibited clonogenic self-renewal and were able to generate podocytes and tubular cells in vitro. Moreover, in a mouse model of AKI, tubular regeneration occurred in animals that received an injection of $CD24^+CD133^+$ PECs (Sagrinati *et al.*, 2006). Further molecular characterization of $CD24^+CD133^+$ human PECs revealed that this group is heterogeneous, and includes cells that express markers typical of differentiated podocytes, like nestin and podocalyxin (PDX) (Ronconi *et al.*, 2009). Human PECs are spatially organized in a continuum along the Bowman's capsule, with $CD24^+CD133^+PDX^-$ cells present closest to the urinary pole, $CD24^+CD133^+PDX^+$ cells (named transitional cells) localised between urinary and vascular pole, and differentiated podocytes negative for CD24 and CD133 and positive for PDX present near vascular pole (Ronconi *et al.*, 2009). Only PDX^- population of cells exhibited multipotency *in vitro* and were able to ameliorate renal function, reducing proteinuria, once injected into mice with adriamycin-induced renal injury (Ronconi *et al.*, 2009). Genetic labelling has been used to mark the PECs and irreversibly track their progeny in newborn and adolescent mice, demonstrating that PECs migrate into the glomerular tuft and become podocytes. These finding provide evidence that these cells are responsible for podocyte renewal (Appel *et al.*, 2009).

Similarly, multipotent progenitor cells expressing CD24 and CD133 were found in the tubular compartment of human kidneys. This population was first identified by searching for $CD133^+$ cells in tubular

fractions on the basis of the correlation between this antigen and the PECs (Sallustio *et al.*, 2010). Moreover Sallustio *et al.*, found that a subset of the $CD133^+$ tubular cells co-expressed CD24 and, by clonogenic analysis, the $CD24^+CD133^+$ cells could differentiate into multiple cell types *in vivo*. This tubular population also had a similar gene signature to $CD24^+CD133^+$ glomerular cells by microarray (Sallustio *et al.*, 2010). Tubular cells expressing both CD24 and CD133 were found in proximal and distal segments, although the frequency was not quantified. More recently, another research group discovered and characterized a human multipotent population of cells positive for CD24 and CD133 (Lindgren D *et al.*, 2011). In this case, the isolation strategy was based on the high ALDH (aldehyde dehydrogenase) activity associated with stemness. Kidney cells with $ALDH^{high}$ activity were isolated from the renal cortex and had an increased capacity to form sphere-like clusters of epithelial cells in culture, and were capable of anchorage-independent growth features seen in several types of multipotent stem cells. By whole-genome expression profiling, the $ALDH^{high}$ cells showed high levels of CD24, CD133, vimentin and cytokeratins 7 and 19 (Lindgren D *et al.*, 2011). Cells expressing CD133 were also isolated from the tubular fraction of the healthy human renal cortex (Bussolati *et al.*, 2005). These cells, that expressed PAX-2, demonstrated self-renewal capacity and were able to differentiate towards renal epithelium and endothelium *in vitro*. When injected into mice with glycerol-induced acute kidney injury, these cells homed the injured kidney and integrated in tubules

(Bussolati *et al.*, 2005).

Since a detailed repertoire of unique cell surface marker proteins expressed on renal stem/progenitor cells is unknown, an alternative strategy for identification has been based on the property that stem cells cycle infrequently to maintain the pool of cells for tissue turnover and repair. Slow-cycling cells can be identified by their retention of the proliferative marker bromodeoxyuridine (BrdU). On the basis of this concept, Maeshima *et al.* demonstrated the existence of label-retaining cells in proximal, distal and collecting tubules of normal rat kidneys (Maeshima *et al.*, 2003). Further studies showed the presence of these cells in the interstitium that were capable of re-expressing the mesenchymal cell markers Vimentin and e-cadherin after ureteral obstruction (Yamashita et al., 2005).

Based on the same method that uses BrdU incorporation, Oliver *et al.* found that the interstitium of the renal papilla is a niche for kidney stem cells (Oliver *et al.*, 2004). During recovery from ischaemia, BrdU-positive cells disappeared from papilla, suggesting that they can be involved in kidney repair. *In vitro*, renal papillary cells co-expressed epithelial (ZO-1) and mesenchymal (α-smooth muscle actin) markers. Under specific culture conditions, they gave rise to a heterogeneous cell population, with some cells expressing nestin, a marker of neuronal stem cells, and with other cells expressing class III β-tubulin, a marker of fully differentiated neurons, suggesting that isolated papillary cells were pluripotent. When injected into the renal cortex, papillary cells

incorporated into parenchyma (Oliver *et al.*, 2004).

Iwatani and co-worker have isolated from the kidney a stem cell-rich population termed side population (SP), using a method first set up by Goodell *et al.* (Goodell *et al.*, 1996) that uses the high capacity of stem cells to extrude a Hoechst dye, and that therefore identifies these cells as Hoechst^{low} cells (Iwatani *et al.*, 2004). In the kidney, side population cells have been found residing in the renal interstitial space and once systemically infused in experimental model, their therapeutic benefit has been modest. The beneficial effect of SP cells observed in animal models of kidney diseases as adriamycin nephropathy (Challen *et al.*, 2006), cisplatin-induced AKI (Hishikawa *et al.*, 2005) and chronic kidney disease (Imai *et al.*, 2007), is likely due to paracrine effect of SP cells.

For future application in the regenerative medicine field, it would be relevant to identify the factors regulating cell growth and differentiation of stem or progenitor cells. Isolation, *in vitro* expansion and transplantation of these cells could represent a new therapeutic approach.

1.2.3 Role of extra-renal stem cells in kidney repair

In the addition to the repair capabilities of the tubular cell itself, and the possibility that endogenous renal stem cells participate in kidney repair, in the last few years it has become very clear that bone marrow-derived stem cells, contribute to turnover and regeneration after injury to several regions of the kidney (De Broe, 2005). Bone

marrow-derived stem cells have remarkable plasticity to the extent that they can give rise to all type of blood cells but they can also differentiate into multiple lineages other than their tissue of origin (Wagers *et al.*, 2004).

Evidence of the contribution of bone marrow-derived stem cells in the renal cell turnover and regeneration was obtained by Poulsom *et al.*, examining kidney biopsies from male patients who have received kidney transplant from female donors (Poulsom *et al.*, 2001). In men receiving a kidney transplant from female donors, Y chromosome containing tubular epithelial cells was observed in kidneys suffering damage as a consequence of acute tubular necrosis (Poulsom *et al.*, 2001). Similarly, in male patients with resolving ATN who had received a kidney transplant from a female donor, Gupta *et al.* have demonstrated that extrarenal stem cells of bone marrow origin, can participate in the regenerative response following ATN, differentiating in renal tubular epithelial cells (Gupta *et al.*, 2002).

The idea that bone marrow contains cells that home to the tubular epithelium has been further explored in mice. Poulsom *et al.* found that female mice recipients of male bone marrow grafts showed co-localization of Y chromosomes and the tubular epithelial marker *Lens culinaris lectins*, in up to 8 % of tubular epithelial cells, indicating that bone marrow cells can traffic into the kidney and participate in the normal tubular epithelial cell turnover (Poulsom *et al.*, 2001). More recently, the same group observed, in a mouse model of AKI-induced

by folic acid, that bone marrow- derived stem cells contributed to regeneration. In female mice lethally irradiated and transplanted with male bone marrow cells, the authors determined that the number of Y-chromosome-positive tubular cells increases following folic acid-induced tubular injury in the recipient mouse, and that some of these cells undergo division within the tubule. They note, however, that most (90%) renal tubular regeneration came from female indigenous cells, as the cells involved in tubule repair seem to be Y-chromosome-negative (Fang *et al.,* 2005). The finding that proliferation of endogenous tubular cells rather than influx of bone marrow-derived cells provides the bulk of cells involved in tubule repair is supported by the work of Lin and Duffield (Lin *et al.,* 2005; Duffield *et al.,* 2005). Moreover, Lin *et al.,* have documented that transplantation of exogenous bone marrow-derived cells in mice with ischemia/reperfusion injury didn't improve renal function (Lin *et al.,* 2005).

It is not clear whether these cells, eventually coming from the bone marrow, are already present in the kidney prior to injury, functioning as resident stem cells, or whether they are recruited to the kidney at the time of injury (Poulsom *et al.,* 2002). Conflicting results reported by different groups, have generated uncertainty as to whether cells from the bone marrow actually become tubular cells *in vivo*. On the basis of most current data, it seems that even if adult bone marrow-derived cells retain the capacity to differentiate into or fuse with renal tubular cells, it is an uncommon event and does not have a

predominant role in the acute tubule regenerative process.

1.3 Stem cell therapy for kidney repair

As described above, the kidney shows an intrinsic capacity to repair as physiological cell turnover or after injury. However, if the damage has reached a certain point, renal repair is rather limited and the ability to recuperate from the injury may be compromised. For this reason, several groups have begun to explore the capacity of bone marrow-derived stem cells to promote tubule repair after injury, as cell therapy.

The bone marrow contains at least two populations of stem cells, haematopoietic stem cells (HSCs) from which all the cellular blood elements are derived, and mesenchymal stem cells (MSCs), which provide stromal support for haematopoiesis. Presently, MSCs are the preferred stem cell population for cellular therapy in experimental model of AKI (table 1), since HSCs failed to induce kidney repair in animal model of acute kidney damage and ischemia/reperfusion injury (Morigi *et al.*, 2004; Kale *et al.*, 2003).

MSCs are undifferentiated adult stem cells of mesodermal origin that constitute only 0.001-0.01% of the total BM cell population. MSCs are progenitors of skeletal tissue components such as bone, cartilage, haematopoiesis-supporting stroma and adipocytes (Bianco *et al.*, 2001; Pereira *et al.*, 1995; Pittenger *et al.*, 1999; Prockop *et al.*, 1997). Experimental findings have shown the potential of MSCs to

differentiate along multiple cell lineages including neuronal, myogenic and hepatocyte-like cells (Jiang *et al.*, 2002; Kopen *et al.*, 1999; Schwartz *et al.*, 2002; Toma *et al.*, 2002). Moreover, MSCs can be easily isolated and expanded. Our group has demonstrated that intravenous injection of murine BM-MSCs protected renal function and structure in mice with AKI induced by cisplatin, whereas HSCs had no protective effect (Morigi *et al.*, 2004). Murine BM-MSCs minimized tubular damage and accelerated proliferation of tubular cells. Moreover, our group reported the presence of Y-chromosome-positive cells in the injured tubules of MSC-transplanted mice, although the percentage of MSCs-derived tubule cells was not stated (Morigi *et al.*, 2004). The finding that MSCs can protect renal tubules from acute injury and might be directly incorporated into the regenerating tubule has been supported by a study from Herrera *et al.* in a glycerol-induced murine rhabdomyolysis model of acute renal failure (Herrera *et al.*, 2004). However, follow up studies revealed that only 2-2.5% of the injected BM-MSCs showed engraftment, opposed to a previously reported 22% (Herrera *et al.*, 2007).

The renoprotective capacity of MSCs has been confirmed by two studies that have shown an important difference from the earlier findings (Duffield *et al.*, 2005; Togel *et al.*, 2005). In an experimental model of ischemia/reperfusion injury, neither Togel and colleagues nor Duffield *et al.* were able to detect direct engraftment of MSCs within renal tubules. The study by Togel *et al.* showed that intracarotid

administration of MSCs either immediately or 24 h after renal ischemia resulted in significantly improved renal function. These MSCs were, however, only transiently present in the renal vasculature, and were not detected within the renal parenchyma for up to 3 days after infusion (Togel *et al.*, 2005). Examination of gene expression in the MSC-treated kidneys revealed a decrease in pro-inflammatory cytokines and an increase in several growth factors, including basic fibroblast growth factor and transforming growth factor-α. So, these authors concluded that MSCs protected the kidney via paracrine and/or endocrine effects rather than through direct engraftment in the renal tubules. Similarly, in the study of Duffield and colleagues, upon i.v. injection of MSCs, post ischemic functional renal impairment was reduced, but there was no evidence of differentiation of these cells into tubular cells of the kidney (Duffield *et al.*, 2005). These authors found that proliferation of endogenous tubular cells, rather than engraftment of transplanted MSCs, accounted for the kidney repair.

Taken together, there is good evidence that administration of MSCs both protects against AKI in toxic and ischemic rodent models and accelerates recovery phase (Humphrey *et al.*, 2008). Similar to rodent MSCs, our group has recently demonstrated the renoprotective effect of human MSCs in an immunodeficient mouse model of AKI induced by cisplatin (Morigi *et al.*, 2008). Human BM-MSC infusion decreased proximal tubular epithelial cells injury and ameliorated the deficit in renal function, resulting in reduced recipient mortality

(Morigi *et al.*, 2008).

The mechanisms by which MSCs promote kidney remain unclear but an important aspect of the therapeutic effect of MSCs appears to be their ability to home to injured kidney. Several studies have explained the possible mechanism that regulate MSC homing, suggesting an increasingly involvement of inflammation in the MSC engraftment. Ip and co-workers have observed, using specific neutralizing antibody, that MSCs use β-1 integrin to engraft in ischemic myocardium, suggesting that MSC recognition of the endothelial cell VLA-4 adhesion molecule via β-1 integrin was required for engraftment (Ip *et al.*, 2007). P-selectin and vascular cell adhesion molecule (VCAM-1), have been shown to be involve in the initial steps by which transplanted MSCs interact with the vessel wall in the course of extravasation. Using a parallel plate flow chambers and function-blocking antibodies against P-selectin and VCAM-1, Ruster *et al.* have observed a role of these adhesive molecules in the coordinated rolling and adhesion of MSCs on endothelial cells (Ruster *et al.*, 2006). The central role of inflammation and VLA-4/VCAM-1 in MSCs-endothelial interaction has also come from studies of Segers and co-workers (Segers *et al.*, 2006).

Chemotaxis of MSCs to sites of inflammation is also an area of interest. Several mediators have been identified and stromal cell-derived factor-1 (SDF-1) seems to be an attractive candidate. SDF-1 and its receptor CXCR4 are important mediators of leukocyte homeostasis. The post-ischemic kidney has been shown to recruit different leukocyte

populations, including bone marrow-derived stem cells. Therefore, Togel *et al.* have investigated the SDF-1/CXCR4 system in the damaged kidney, and they observed that SDF-1 is expressed in the kidney and is upregulated after renal injury, mobilizing CXCR4-positive cells to the kidney after ischemic injury (Togel *et al.*, May 2005). The role of SDF-1/CXCR4 system in the MSC engraftment in vivo was further investigated by Hung *et al.* (Hung *et al.*, 2007). Short-term exposure of MSCs to low oxygen increased the expression of the chemokine receptors CX3CR1 and CXCR4, inducing an increased in vitro migration of MSCs in response to the fractalkine and SFD-1. Another candidate for MSCs homing is CD44, which is expressed on MSCs and required for renal localization of injected MSCs. Herrera and coworkers observed that CD44 and hyaluronic acid interactions recruited exogenous MSCs in a glycerol-induced mouse model of AKI (Herrera *et al.*, 2007).

As commented above, there is increasing evidence that MSCs facilitate kidney regeneration predominantly by delivering growth factors and cytokines to the site of kidney injury instead of transdifferentiation into renal cells (Krause *et al.*, 2005). The timing of renal epithelial cell proliferation, which is dramatically increased within 24-48 h, appears to be too rapid to be explained by transdifferentiation of extrarenal cells type into epithelial cells. MSCs are able to secrete a broad array of growth factors and cytokines including granulocyte colony-stimulating factor (G-CSF), stem cell factor (SCF), leukemia

inhibitory factor (LIF), macrophage colony-stimulating factor (m-CSF), IL-6 and IL-11, vascular endothelial growth factor (VEGF), basic fibroblast growth factor (bFGF), monocyte-chemoattractant protein (MCP-1), hepatocyte growth factor (HGF) and insulin growth factor-1 (IGF-1) (Haynesworth *et al.*, 1996; Weimar *et al.*, 1998). Togel and co-workers observed that infusion of MSCs enhanced recovery of renal function in rats with ischemia/reperfusion-induced acute renal failure (Lange *et al.*, 2005). Examining MSC-conditioned medium, they found significant level of VEGF, HGF and IGF-1 and they determined that this conditioned medium was capable of enhancing endothelial cell proliferation and differentiation (Togel *et al.*, 2007). Our group, using an in vitro cisplatin-induced proximal tubule cell culture model, have demonstrated that MSCs exert beneficial effects on tubular cell damaged by cisplatin, by producing the mitogenic and pro-survival factor IGF-1 (Imberti *et al.*, 2006). Importantly, we observed that MSCs with IGF-1 knockdown failed to protect mice from cisplatin-induced AKI (Imberti *et al.*, 2006). The Westenfelder laboratory performed a similar study in MSCs with knockdown of VEGF, showing that VEGF knockdown failed to protect the rats from AKI (Togel *et al.*, 2009).

Recently, other than soluble factors, a new mechanism of communication among cells was proven: horizontal transfer of mRNAs contained within shed microvesicles. Bruno et al. found that microvesicles derived from human MSCs induced proliferation and inhibited apoptosis of tubular epithelial cells *in vitro*, while when

injected in SCID mice with glycerol-induced AKI, accelerated the functional recovery of tubular cells (Bruno *et al.*, 2009). The effect of microvesicles was RNA-dependent as microvesicles contained a specific subset of cellular mRNA, such as mRNA associated with proliferation, control of transcription and immunoregulation (Bruno *et al.*, 2009; Tetta *et al.*, 2011).

The therapeutic effect of MSCs can be ascribed not only to their ability to home to injured tissues and secrete trophic mediators, but also to their immunomodulatory roles. MSCs are immunologically privileged and allogenic MSCs do not induce a proliferative T-cell response. The mechanisms for this tolerance include low surface expression of both major histocompatibility complex (MHC) class I and II molecules, and major costimulatory molecules such as CD40, CD80 and CD86 (McTggart *et al.*, 2007). MSCs also exert anti-inflammatory effect on T cells. T cells play an important role in immuno-mediated and ischemic kidney disease, therefore the ability of MSCs to regulate T-cell response is relevant for their therapeutic effect in AKI. Semedo *et al.* observed high level of anti-inflammatory cytokines in kidneys of MSC-treated animals after IRI (Semedo *et al.*, 2007, 421).

Although bone marrow represents the most common tissue source of MSCs, harvesting these stem cells is invasive and their number, frequency, differentiation potential, and life span decline with the age of the donor. Therefore, in the clinical perspective to cure AKI, the search for new sources of MSCs, is of significant value. It has been

reported that stem cells with similar surface expression patterns of MSCs can be isolated from alternative sources as umbilical cord blood, placenta, adipose tissue, amniotic fluid, peripheral blood, and other tissues (Liu *et al.*, 2009).

Since the first successful transplantation of umbilical cord blood in 1988 (Gluckman *et al.*, 1989), cord blood has become an accepted source of haemopoietic stem cells for the treatment of leukaemia, haemoglobinopathy and for the repair of bone marrow following high-dose chemotherapy for solid tumours (Laughlin *et al.*, 2004). However, recent research has revealed that the cord blood is an alternative and extremely rich reservoir contains not only haematopoietic stem cells but also neural and endothelial progenitors and mesenchymal stem cells (Flynn *et al.*, 2007; Sanchez-Ramos 2006; Erices *et al.*, 2000; Lee *et al.*, 2009). Cord blood stem cells have many advantages over embryonic and other adult stem cells. Cord blood represents a potentially unlimited source of stem cells, and its collection is non-invasive and relatively simple to process and store (Seres *et al.*, 2010). Moreover, cord blood raises no ethical issues for basic studies and clinical applications. Based on these advantages, there is considerable interest in the use of cord blood stem cells in regenerative medicine.

On the other hand, in the last 10 years, the amniotic fluid, obtained from amniocentesis, has also been extensively studied as a non-controversial source of a population of stem cells with intermediate characteristics between embryonic and adult stem cells (De Coppi *et al.*,

2007). Moreover, clonal hAFS cell lines had non-tumorigenicity at late passages, when injected into immunodeficient mice. Therefore, hAFS cells may represent a new pluripotential cell source for tissue regeneration without raising any ethical concerns associated with human embryonic stem cell research.

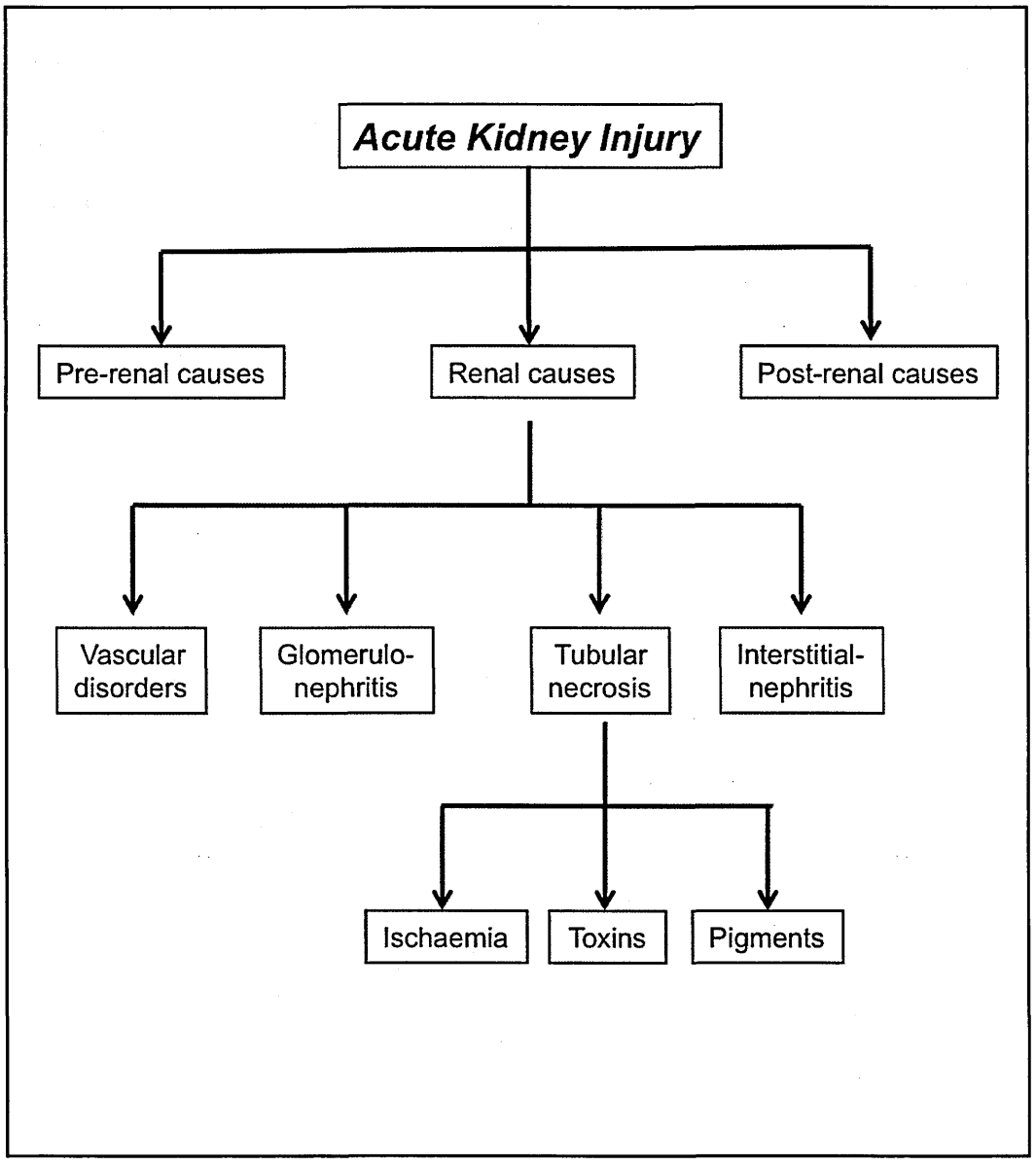

Figure 1.1: Classification scheme of acute kidney injury

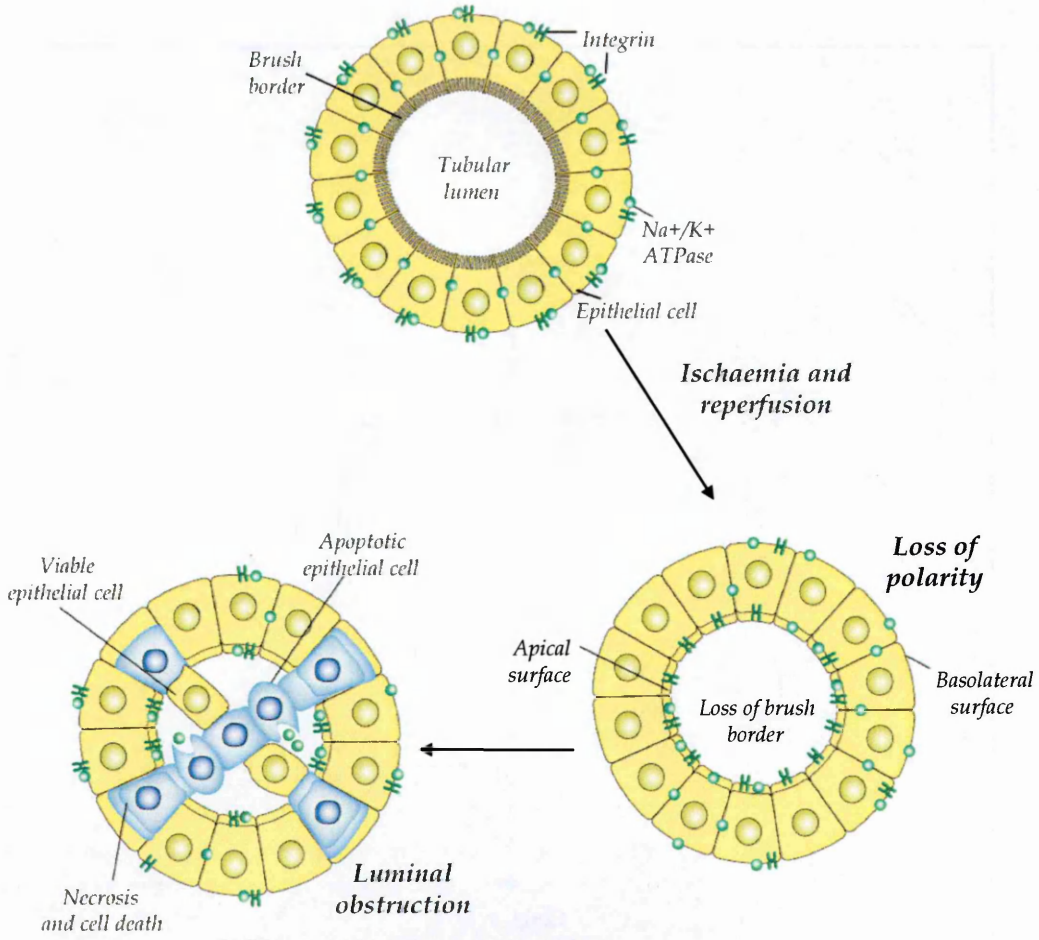

Figure 1.2: Tubular changes in the pathophysiology of ischaemic acute tubular necrosis (Modified from Lameire at al., 2005)

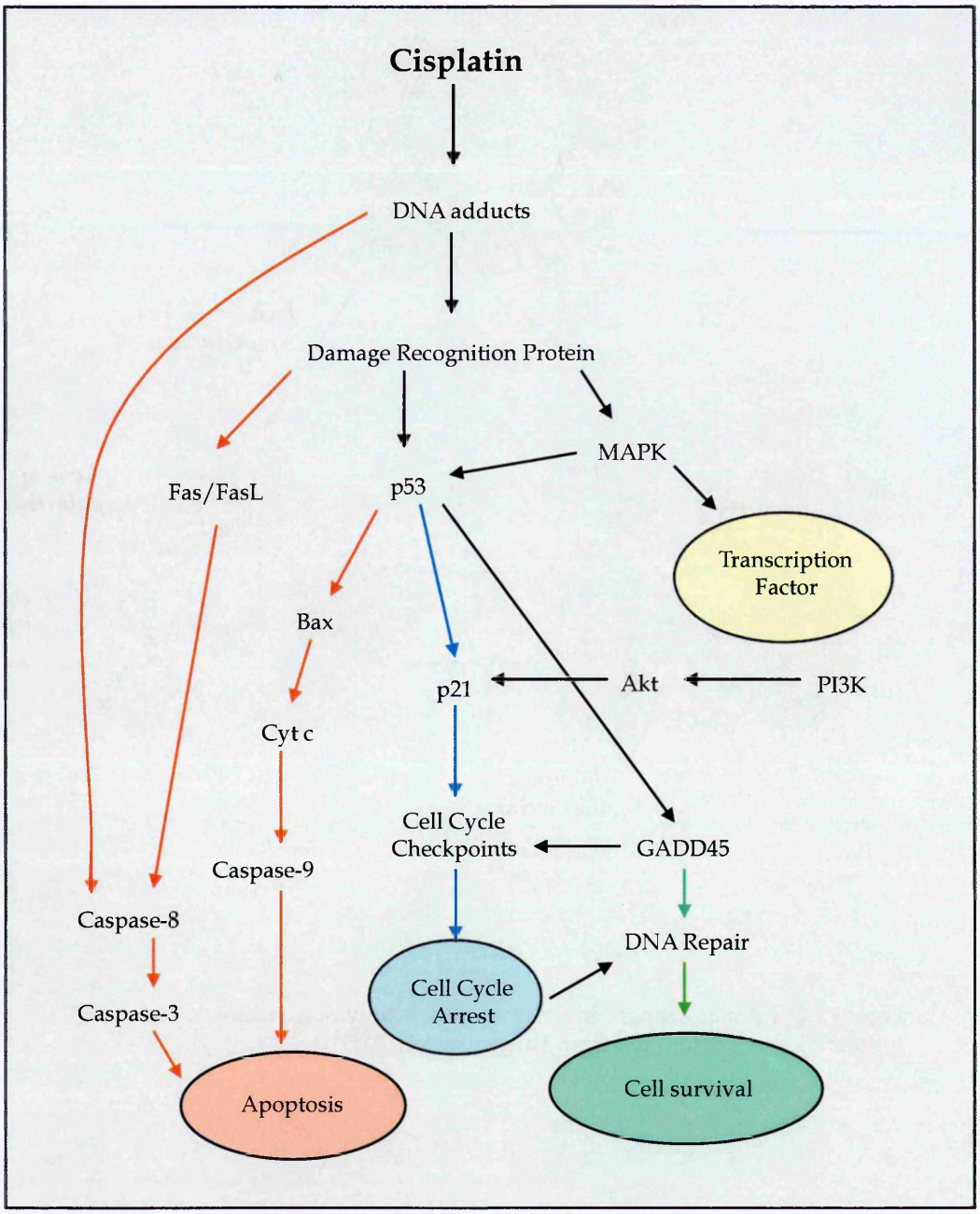

Figure 1.3: Main biological effects of cisplatin

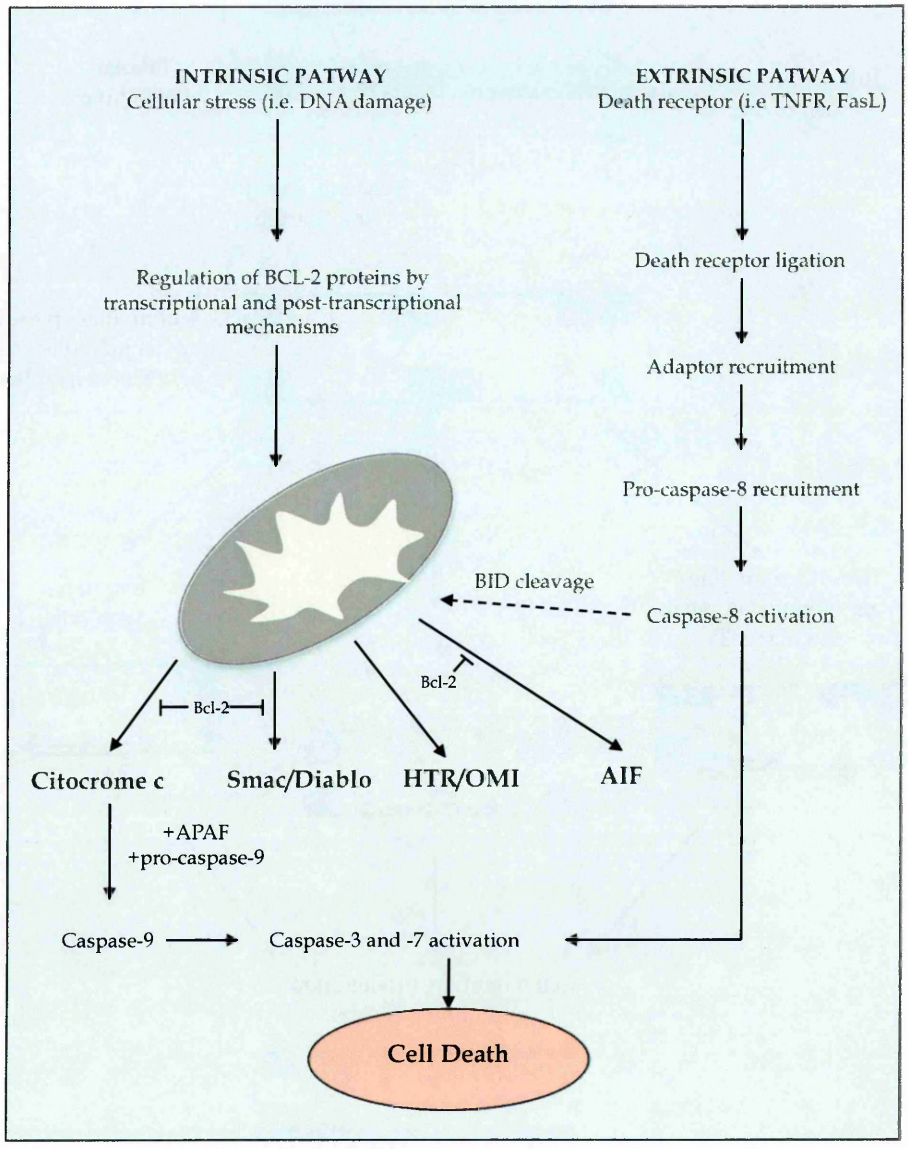

Figure 1.4: Pathways leading to cisplatin- induced apoptosis

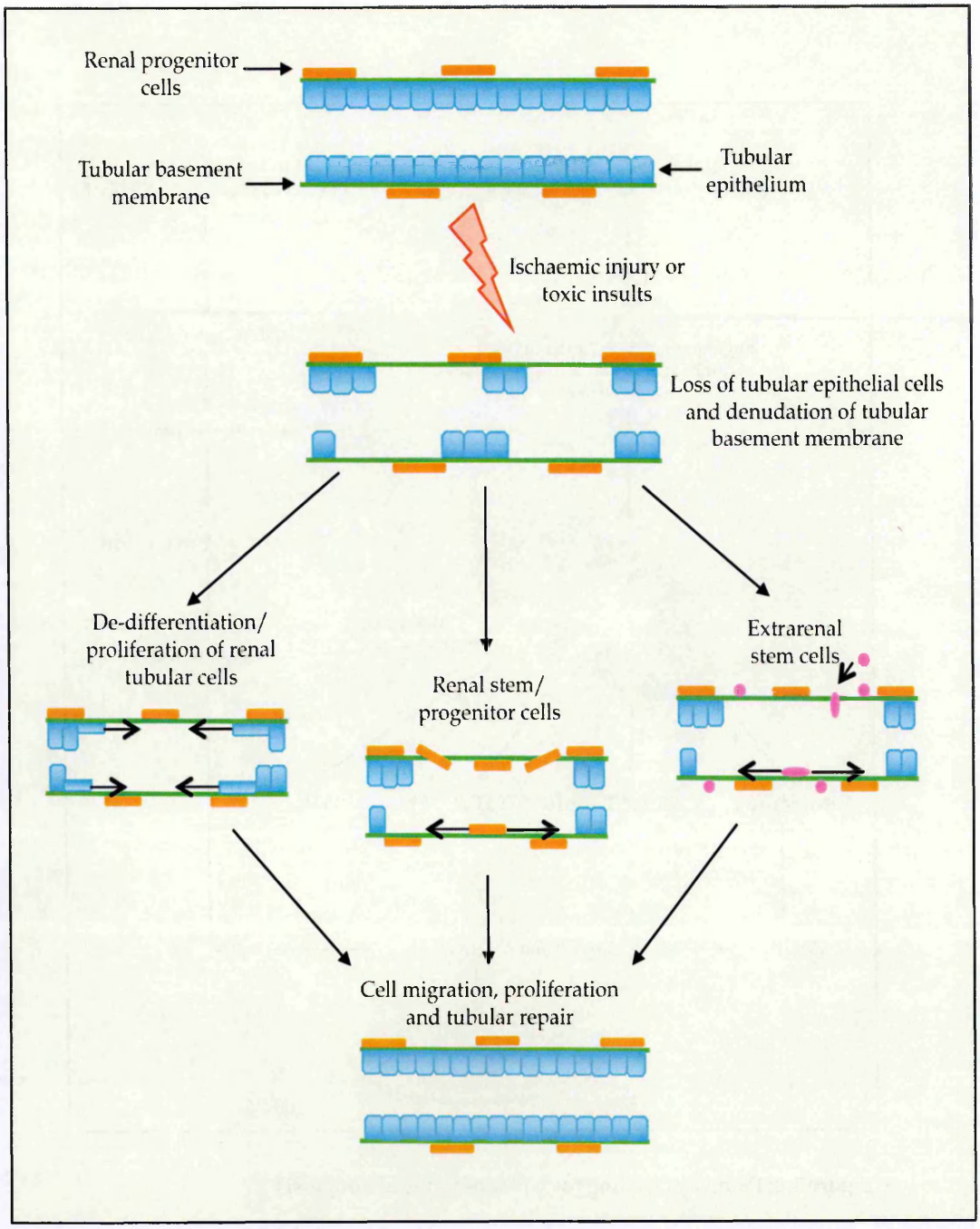

Figure 1.5: Possible mechanisms of renal cell regeneration (Modified from Cantley LG, 2005)

Table 1.1. Summary of studies using mesenchymal stem cells (MSCs) isolated from bone marrow to treat acute kidney injury

Injury model	MSC source	Administration	Features	References
Glycerol-induced kidney injury	1×10^6 GFP+ mouse BM-MSC – female C57BL/6J mice	i.v. injection	↑ proliferation, ↑ morphological recovery, ↑ renal function	Herrera *et al.*, 2004
Cisplatin-induced kidney injury	2×10^5 mouse BM-MSC – male C57BL/6J mice	i.v. injection	↑ renal function, ↑ tubular proliferation, ↑ morphological recovery	Morigi *et al.*, 2004
40 min bilateral IR	1.5×10^6 rat BM-MSC – Sprague–Dawley rats	Infused into thoracic aorta via a carotid artery	↑ renal function, ↓ injury score, ↑ preservation of proximal tubular brush border	Lange *et al.*, 2005
40 min bilateral IR	1×10^6 rat BM-MSC	Intra-aortic delivery via left carotid artery	↑ renal function, ↑ proliferative indexes, ↓ apoptotic indexes, ↓ renal injury, ↓ IL-1β, TNF- α, IFN-γ, iNOS, ↑IL-10, bFGF, TGF-α, Bcl-2	Togel *et al.*, 2005
Cisplatin-induced kidney injury	2×10^5 mouse BM-MSC – male C57BL/6J mice	Tail vein or i.p. injection	↑ renal function, ↑ tubular cell proliferation, ↓ tubular cell apoptosis	Bi *et al.*, 2007
Glycerol-induced kidney injury	1×10^6 mouse CD44+ or CD44-/- BM-MSC – C57BL/6J or Cd44tm1Hbg/J mice	Tail vein	CD44+ BM-MSC: ↑ morphological and functional recovery,CD44-/- BM-MSC: no significant morphological or functional recovery	Herrera *et al.*, 2007
Cisplatin-induced kidney injury	2×10^5 mouse IGF-1 gene silenced BM-MSC – male C57BL/6J mice	i.v. injection	Limited protection of renal function (BUN) and tubular injury	Imberti *et al.*, 2007
60 min bilateral IR	2×10^5 rat BM-MSC – male Wistar rats	i.v. injection	↓ serum creatinine and plasma urea, ↑ PCNA nuclei in MSC treated kidneys, ↑ IL-4, ↓ IL-1β	Semedo *et al.*, 2007
30 min unilateral IR	1×10^5 rat MSC	Intra-arterially infused	↓ apoptosis in kidney regions with MSC still present in microvasculature 24 h post-IR	Togel *et al.*, 2007
Cisplatin-induced kidney injury	5×10^5 human BM-MSC	Tail vein	↑ renal function, ↑ proliferative score, ↓ proximal tubular epithelial cell injury, ↓ apoptotic score, ↓ mortality	Morigi *et al.*, 2010
60 min bilateral IR	2×10^5 rat BM-MSC – male Wistar rats	i.v. injection	↓ serum creatinine, ↑ renal function, low expression of IL-1β, IL-6, TNF-α, high expression IL-4 and IL-10	Semedo *et al.*, 2009
Cisplatin-induced kidney injury	5×10^6 human BM-MSC	i.p. injection	Prolonged survival, ↓ urea nitrogen, ↓ apoptosis, ↑ proliferation	Eliopoulos *et al.*, 2010

1.4 Aim of the study

In literature is widely demonstrated the protective effect of MSCs isolated from bone marrow. However, the considerable amount of findings has highlighted the limits of adult stem cells, i.e. their number, frequency, differentiation potential, and life span that decline with the age of the donor. Therefore, in the clinical perspective to cure AKI, the search for new sources of MSCs, is of significant value. In the last decade, alternative sources of MSCs have been identified, and in particular cord blood (CB) and amniotic fluid (AF) are revealed as a non-controversial and rich reservoirs of fetal stem cells.

Based on this evidence, the aim of this study is to investigate the possible therapeutic effect of human CB-MSCs and human AFS cells in renal repair processes. The administration of stem cells will hopefully improve renal function, preserving renal structure, thus opening new perspectives for future therapies in acute damage. We aim to study the changes in renal function after stem cell injection but also stem cell engraftment into damaged tissue, their possible differentiation into renal epithelial cells and their effects on the tissue regeneration. Moreover, another important goal of this study is to clarify *in vitro* the mechanisms underlying the renoprotective effect of these different populations of stem cells.

CHAPTER 2

MATERIALS

2.1 Mice

NOD-SCID female mice were purchased from Charles River Italia s.p.a., Calco, Italy.

2.2 Cells

Human CB-MSCs. Human cord blood mesenchymal stem cells were kindly supplied from Dr. Lorenza Lazzari, Cell Factory, Fondazione IRCCS Ospedale Maggiore Policlinico Mangiagalli e Regina Elena, Milan, Italy.

Human BM-MSCs. Human bone marrow mesenchymal stem cells were kindly supplied from Dr. Martino Introna, Unit of haematology, Azienda Ospedaliera, Ospedali Riuniti di Bergamo, Bergamo, Italy.

Human dermal fibroblasts were purchased from Istituto Zooprofilassico Sperimentale della Lombardia e dell'Emilia Romagna, Brescia, Italy.

HK2. Human papillomavirus 16 (HPV-16)-transformed proximal tubular cell line was purchased from ATCC (CTR-2190; American Type Culture Collection, Manassas, VA, USA).

Human AFS cells. Human amniotic fluid stem cells were kindly supplied from Dr. Paolo De Coppi, University College London, UK.

2.3 Media, supplements and cell culture reagents

Penicillin-Streptomycin, liquid containing 10,000 units of penicillin and 10,000 µg of streptomycin, GIBCO-Invitrogen, S. Giuliano Milanese (MI), Italy, was used at 1% (1ml/100ml).

L-Glutamine 200 mM, liquid, GIBCO-Invitrogen

"Growth medium" for hCB-MSCs

Alpha MEM GlutaMAX™-I, Gibco-Invitrogen

+ 20% FCS, selected lot purchased from Euroclone, Pero (MI), Italy

+ 2 mM L-Glutamine,

+ 1% penicillin -streptomycin,

"Growth medium" for hBM-MSCs

DMEM, Sigma-Aldrich

+ 5% platelet lysate, supplied by Dr. Martino Introna

+ 2 mM L-Glutamine,

+ 1% penicillin -streptomycin,

"Growth medium" for human dermal fibroblast

MEM, GIBCO-Invitrogen

+ 10% FCS, selected lot, GIBCO-Invitrogen

+ 2 mM L-Glutamine,

+ 1% penicillin -streptomycin,

"Growth medium" for HK2

Dulbecco's Modified Eagle's Medium (DMEM)/Ham's Nutrient Mixture F-12 (DMEM/F-12)

+ 1% penicillin –streptomycin

+ 5% Foetal Calf Serum (FCS), heat-decomplemented

+ 2 mM L-Glutamine

+ 5 pg/ml 3,3',5-Triiodo-L-thyronine

+ 5 ng/ml Hydrocortisone

+ 5 pg/ml Prostaglandin E_1

+ 5 µg/ml Insulin, 2.75 µg/ml Transferrin, 3.3 ng/ml Sodium selenite

+ 10 ng/ml Epidermal growth factor

DMEM/F-12, supplemented with 3150 mg/L glucose, 3574 mg/L HEPES, 55 mg/L sodium pyruvate, without sodium bicarbonate and without L-glutamine, was purchased from Sigma-Aldrich, St Louis Missouri USA-Milan, Italy.

FCS, selected lot purchased from GIBCO-Invitrogen.

3,3',5-Triiodo-L-thyronine sodium salt, powder, purchased from Sigma-Aldrich. To prepare a 400 ng/ml stock solution, the powder was dissolved in 1 ml of NaOH 1 N (Carlo Erba Reagenti, Milano, Italy) and 49 ml of sterile DMEM/F-12. A further dilution of 1/50 was done in DMEM/F-12.

Hydrocortisone-water soluble, powder, purchased from Sigma-Aldrich. A stock solution of 1 mg/ml was prepared in DMEM/F-12.

Prostaglandin E_1, powder, purchased from Sigma-Aldrich. A stock solution of 1 mg/ml was prepared by dissolving the powder in ethanol (Carlo Erba Reagenti) followed by a dilution in PBS 1X to reach the concentration of 10 ng/ml.

Insulin-transferrin-sodium selenite (ITS) 100X, liquid, was purchased from GIBCO-Invitrogen.

Recombinant human epidermal growth factor, powder, purchased from PeproTech Inc., Rocky Hill, New Jersey, USA. A stock solution of 1 μg/ml was prepared in PBS 1X.

"Growth medium" for hAFS cells

Alpha MEM GlutaMAX™-I, Gibco-Invitrogen

+ 15% ES-FBS, GIBCO-Invitrogen

+ 2 mM L-Glutamine, GIBCO-Invitrogen

+ 1% penicillin -streptomycin, GIBCO-Invitrogen

+ 18% Chang B, Irvine Scientific, Santa Ana, CA,

+2% Chang C powder, purchased from Irvine Scientific. A stock solution was prepared reconstituted Chang medium C lyophilized in 50 ml distilled water.

"Test medium" (for *in vitro* experiments)

DMEM, Sigma-Aldrich

+ 2 mM L-Glutamine, GIBCO-Invitrogen

+ 2% FCS, GIBCO-Invitrogen

+ 1% penicillin -streptomycin, GIBCO-Invitrogen

"Inductive media" for hCB-MSCs

Adipogenic Induction and Maintenance Media, Cambrex, Walkersville, MD, USA.

Osteogenic Induction and Maintenance Media, Cambrex, Walkersville, MD, USA.

Chondrogenic inductive medium (0.5 ml, Cambrex) with TGFβ (10ng/ml, Sigma-Aldrich).

"Inductive media" for hAFS cells

DMEM low-glucose medium DMEM, Sigma-Aldrich

+ 10% FBS, GIBCO-Invitrogen

+ 2 mM L-Glutamine, GIBCO-Invitrogen

+ 1% penicillin -streptomycin, GIBCO-Invitrogen

Adipogenic supplements:

1 μM dexamethasone, Sigma-Aldrich

+1 mM 3-isobutyl-1-methylxanthine, Sigma-Aldrich

+ 10 μg/ml insulin, Sigma-Aldrich

+ 60 μM indomethacin, Sigma-Aldrich

Osteogenic supplements:

100 nM dexamethasone, Sigma-Aldrich

+ 10 mM beta-glycerophosphate , Sigma-Aldrich

+ 0.05 mM ascorbic acid-2-phosphate, Wako Chemicals, Richmont, VA, USA.

Trypsin

Trypsin for hCB-MSCs: Trypsin 0.25%/EDTA 50 μM was purchased from GIBCO-Invitrogen

Trypsin for HK2: Trypsin, 0.5% (10X) with EDTA•4Na was purchased from GIBCO-Invitrogen. A solution 1X was aseptically prepared in balanced salt solution without Ca^{++} and Mg^{++}.

Trypsin for human AFS cells: Trypsin 0.05% /EDTA 0.02% solution (w/v) in PBS 1X without Ca^{++} and Mg^{++}. Biochrom, Berlin, Germany.

2.4 Growth factors

Glial cell line-derived neurotrophic factor (GDNF) protein, Abcam Inc, Cambridge, MA, USA.

2.5 Chemicals

Acetone was purchased from Carlo Erba Reagenti, Rodano, Milan, Italy.

Alcian Blue was purchased from Sigma-Aldrich.

Alizarin Red S (sodium alizarin sulfonate) was purchased from Sigma-Aldrich. 2% Solution was prepared by dissolving the powder in distilled water. Solution was stirred and centrifuged at 4000 rpm for 10 minutes. The supernatant was collected and filtered. pH was adjusted at 4.1 with 0.5% ammonium hydroxide.

Cis-diaminedichloroplatinum (cisplatin) was purchased from Sigma-Aldrich or Ebewe Italia Srl, Roma, Italy, as indicated in the Methods.

Dimethyl sulfoxide (DMSO) was purchased from Sigma-Aldrich.

Ethanol (absolute) was purchased from Carlo Erba Reagenti, Rodano, Milan, Italy.

Eukitt was purchased from Bio Optica, Milan, Italy.

Formalin solution, ready to use was purchased from Bio-Optica.

Harris haematoxylin and eosin was purchased from Bio-Optica, Milan, Italy.

Hydrogen peroxide (H_2O_2) solution was purchased from Sigma-Aldrich.

Isofluorane was purchased from Abbot, San Donato Milanese, Milan, Italy.

Mounting medium was purchased from DakoCytomation, Glostrup, Denmark.

Oil Red O was purchased from Sigma-Aldrich. We prepared a 0.5% solution in methanol. Solution was stirred and centrifuged at 4000 rpm for 10 minutes. The supernatant was collected and filtered.

Paraffin, Bioplast Plus, was purchased from Bio Optica.

Paraformaldehyde was purchased from Electron Microscopy Sciences

(Hatfield, PA, USA). In order to prepare a 4% solution, we diluted 8% aqueous solution in PBS 2X under a fume hood.

Periodic acid, Diapath, Martinengo, Bergamo, Italy.

Propylene oxide (1,2-epoxypropane), Electron Microscopy Sciences, EMS, Rome, Italy.

Schiff's reagent, Kaltek srl, Padova, Italy.

Sodium hyposolfite was purchased from Merck. A 5% solution was prepared by dissolving the powder in water.

Toluene was purchased from Sigma-Aldrich.

Trypan Blue (4% solution) was purchased from Sigma-Aldrich. This solution was diluted 1:2 with saline and filtered (0.4 μm filters).

Tissue-Tek Oct Compound was purchased from Sakura Finetek, Torrance, CA, USA.

Von Kossa was purchased from Bio-Optica.

2.6 Buffers and solutions

"Blocking buffer "

Bovine serum albumin (BSA; Sigma-Aldrich) was added to PBS 1X to obtain a final BSA concentration of 1%. The solution was maintained on ice for few minutes to facilitate albumin solubilisation. The solution was then filtered with a 0.2 μm sterile filter.

Citrate buffer 10% concentrated pH 6.0, was diluted 1:10 in PBS 1X and was purchased from DiaPath.

Cacodylate buffer 0.2 M

Sodium cacodylate trihydrate 12.84 g, Sigma-Aldrich

+ 300 ml of water

pH was stabilized at 7.4 with HCl 0.2 N (Merck).

Cacodylate buffer 0.1M pH 7.4

Prepared by diluting (1:1) in water cacodylate buffer 0.2 M, pH 7.4

3,3'-diaminobenzidine (DAB)

One tablet of DAB was put into 25 ml of distilled water. Solution was mixed and 6.5 µl of 30% H_2O_2 was added.

DAB was purchased from Merck.

Duboscq-Brazil solution ready to use, was purchased from DiaPath, Martinengo (BG), Italy.

Epon resin

Solution 1:

5 ml of Durcupam ACM, Fluka (Sigma-Aldrich)

+ 18 ml of Epoxy Embedding Medium, Hardener DDSA, Fluka

Solution 2:

6 ml of Epoxy Embedding Medium, Fluka

+ 300 µl of Epoxy Embedding Medium Accelerator, Fluka

Finally, solution 1 and 2 were mixed.

2.5% glutaraldehyde in 0.1M cacodylate buffer

0.2 M cacodylate buffer, pH 7.4, 19 ml

+ 19 ml of water

+ 2 ml of glutaraldehyde solution at 50%, Fluka (Sigma-Aldrich)

Osmium tetroxide 2%

1 g osmium tetroxide crystalline, Electron Microscopy Sciences

+ 50 ml water.

Freshly prepared working solution was used at concentration 1% in PBS.

"Permeabilizing solution"

TRITON X100 was purchased from Sigma-Aldrich and was diluted to a final concentration of 0.5%, 0.3% or 0.1% in PBS 1X, as indicated in the Methods.

Phosphate buffer saline (PBS) 10X (for cell culture and immunohistochemistry) was purchased from Ambion-Invitrogen. Finally, PBS 1X is prepared diluting 1:10 PBS 10X in water.

Paraformaldehyde-lysine-periodate (PLP) fixative

Solution A: 8% paraformaldehyde, purchased from Electron Microscopy Sciences (Hatfield, PA, USA).

Solution B: 0.05 M Phosphate buffer Stock (pH 7.4)

- Dissolve 0.69 gr of Sodium Phosphate Monobasic Monohydrate in 100 ml of dH_20 (solution I)

-Dissolve 4.45 gr of Sodium Phosphate in 500 ml of dH_20 (solution II)

- Add 95 ml of solution I and 405 ml of solution II.

Solution C:

-Dissolve 9.13 gr of L-Lysine (Sigma-Aldrich) and 1.425 gr of Sodium m-Periodate (Sigma-Aldrich) in 500 ml of Solution B.

Solution D: PLP fixative

- Add 10 ml of solution A and 30 ml of solution C

2.7 Antibodies

For all antibodies, preliminary experiments were performed following manufacturer's suggestions in order to identify the most appropriate concentration.

Antibodies used for hCB-MSC study

- Mouse-anti human antibody **CD45-PC7** (phycoerythrin-Cy7; IM3548) was purchased from Beckman Coulter, and used at the concentration of 1:100.

- Mouse-anti human antibody **CD34-PE** (phycoerythrin; 550619) was purchased from Becton Dickinson, San Josè, CA, USA, and used at the

concentration of 1:100.

- Mouse-anti human antibody **CD146-FITC** (fluorescein isocyanate; 5040-F100T) was purchased from Biocytex, Marseille, France, and used at the concentration of 1:100.

- Mouse-anti human antibody **CD90-PE** (CBL415P) was purchased from Chemicon, Temecula, CA, USA, and used at the concentration of 1:100.

- Mouse-anti human antibody **CD44-FITC** (555478) was purchased from Becton Dickinson, and used at the concentration of 1:100.

- Mouse-anti human antibody **VE-Cadherin-FITC** (ABIN123940) was purchased from Bender MedSystems, Burlingame, CA, U.S.A, and used at the concentration of 1:100.

- Mouse-anti human antibody **alpha SMA-FITC** (F3777) was purchased from Sigma-Aldrich, and used at the concentration of 1:100.

- Mouse-anti human antibody **NG2-PE** (IM3454U) was purchased from Beckman Coulter, and used at the concentration of 1:100.

- Mouse-anti human antibody **CD105-PE** (5100-PE100T) was purchased from Biocytex, and used at the concentration of 1:100.

- Mouse-anti human antibody **CD73-PE** (550257) was purchased from Becton Dickinson, and used at the concentration of 1:100.

- Mouse-anti human antibody **CXCR4-APC** (allophycocyanin; 555976) was purchased from Becton Dickinson, and used at the concentration of 1:100.

- Mouse-anti human antibody **CD56-PE** was purchased from Cymbus, Hampshire, UK, and used at the concentration of 1:100.

- Mouse-anti human antibody **LNGFR-PE** (557196) was purchased from

Becton Dickinson, and used at the concentration of 1:100.

- Mouse-anti human antibody **HLA class I-FITC** (IM1838U) was purchased from Immunotech Beckman Coulter Company, Praha, Czech Republic, and used at the concentration of 1:100.

- Mouse-anti human antibody **HLA class II** (347360) was purchased from Becton Dickinson, and used at the concentration of 1:100.

- Unconjugated mouse-anti human antibody **CK3/12** was purchased from Biodesign, Maine, USA, and used at the concentration of 1:100.

- Unconjugated mouse-anti human antibody **CK19** was purchased from Biodesign, and used at the concentration of 1:100.

- Unconjugated mouse-anti human antibody **BB9** (557813) was purchased from Becton Dickinson, and used at the concentration of 1:100.

- Unconjugated mouse-anti human antibody **SSEA4** (MAB4304) was purchased from Chemicon, and used at the concentration of 1:100.

- Mouse anti-human **HNA** (MAB1281) antibody was purchased from Chemicon and used at the concentration of 1:50.

- Rabbit polyclonal anti-**nitrotyrosine** (06-284) antibody was purchased from Upstate Biotechnology, Billerica, MA, USA, and used at the concentration of 1:2000.

- Monoclonal mouse anti- **PCNA** antibody (clone PC10; P8825) was purchased from Sigma-Aldrich and used at the concentration of 1:250.

- Rabbit anti-**phosphorylated Akt** (Ser 473) (9271) antibody was purchased from Cell Signaling Technology, Danvers, USA, and used at the concentration of 1:100.

- **Biotinylated goat anti-rabbit** IgG antibody (AP132B) was purchased from Chemicon, Temecula, CA, USA, and used at the concentration of 1:50.

- **Biotinylated sheep anti-mouse** IgG antibody (AP302B) was purchased from Chemicon, Temecula, CA, USA, and used at the concentration of 1:50.

- **FITC-conjugated goat-anti-mouse** antibody was purchased from Exalpha, Maynard, MA, USA, and used at the concentration of 1:50.

- **PE-conjugated goat-anti-mouse** antibody was purchased from Exalpha, and used at the concentration of 1:50.

- **Isotype immunoglobulins IgG1 PE-FITC** (FCMAB230P; FCMAB229F) was purchased from Chemicon, and used at the concentration of 1:50.

- **Isotype immunoglobulins IgG1 PC7** (6607099) was purchased from Beckman Coulter, and used at the concentration of 1:50.

- **Isotype immunoglobulins IgG1 APC** (554681) was purchased from Becton Dickinson, and used at the concentration of 1:50.

- **Cy3-conjugated goat anti rabbit** antibody (111-165-003) was purchased from Jakson Immunoresearch, West Baltimore, Pike, USA, and used at the concentration of 1:50.

- **Cy3-conjugated goat anti-mouse** antibody (115-165-146) was purchased from Jackson Immunoresearch, and used at the concentration of 1:50.

Antibodies used for hAFS study

- Mouse monoclonal antibody anti-**CD117** (c-Kit, SC53147, Santa Cruz Biotechnology, Santa Cruz, CA, USA), and used at the concentration of 1:100.

- Mouse anti-human antibody **CD29 FITC** (610468) was purchased from Becton Dickinson, and used at the concentration of 1:100.

- Mouse anti-human antibody **CD44 FITC** (555478) was purchased from Becton Dickinson, and used at the concentration of 1:100.

- Mouse anti-human antibody **CD73 PE** (550257) was purchased from Becton Dickinson, and used at the concentration of 1:100.

- Mouse anti-human antibody **CD90 FITC** (555595) was purchased from Becton Dickinson, and used at the concentration of 1:100.

- Mouse anti-human antibody **CD105 PE** (560839), was purchased from Becton Dickinson, and used at the concentration of 1:100.

- Mouse anti-human antibody **CD80 FITC** (557226) was purchased from Becton Dickinson, and used at the concentration of 1:100.

- Mouse anti-human antibody **CD86 PE** (557344) was purchased from Becton Dickinson, and used at the concentration of 1:100.

- Mouse anti-human antibody **Oct-4 FITC** (SC-5279) was purchased from Santa Cruz, and used at the concentration of 1:100.

- Mouse anti-human antibody **SSEA-4 FITC** (SC-21704) was purchased from Santa Cruz, and used at the concentration of 1:100.

- Mouse anti-human antibody **HLA-ABC FITC** (IM1838U) was purchased from Immunotech, Marseille, France, and used at the concentration of

1:100.

- Mouse anti-human antibody **HLA-DR PE** (IM1639) was purchased from Immunotech, and used at the concentration of 1:100.

- Mouse anti-human **CD105** antibody (M352701) purchased from DakoCytomation, Glostrup, Denmark, and used at the concentration of 1:100.

- Rabbit anti-**phosphorylated Akt** (Ser 473) antibody (9721) was purchased from Cell Signaling Technology, Danvers, USA, and used at the concentration of 1:100.

- Mouse **anti-Ki-67** antibody (NCL-L-ki67-MM1), was purchased from NovoCastra Laboratories Newcastle upon Tyne, UK.

- Mouse anti-human **CD44** antibody (AB6124) purchased from Abcam, and used at the concentration of 1:100.

- Rabbit anti- human **CXCR4** antibody (AB2074) purchased from Abcam, and used at the concentration of 1:100.

- Rabbit anti- human **CX3CR1** (AB8021) antibody purchased from Abcam, and used at the concentration of 1:100.

- **MicroBeads conjugated goat anti-mouse** IgG antibody (11033) purchased from Dynal; Invitrogen, Carlsbad CA, USA.

- **Cy3-conjugated goat anti rabbit** antibody (111-165-003) was purchased from Jakson Immunoresearch, West Baltimore, Pike, USA, and used at the concentration of 1:50.

- **Cy5-conjugated donkey anti mouse** antibody (715-175-150) purchased from Jackson Immunoresearch and used at the concentration of 1:50.

- **Cy3-conjugated goat anti-mouse** antibody (115-165-003) purchased from ackson Immunoresearch and used at the concentration of 1:50.

- **FITC-conjugated goat anti mouse** antibody (115-095-003) purchased from Jackson Immunoresearch and used at the concentration of 1:50.

- **FITC-conjugated goat anti rabbit** antibody (111-095-003) purchased from Jackson Immunoresearch and used at the concentration of 1:50.

2.8 Other reagents

Dapi: 4',6'-diamidino-2-phenylindole dihydrochloride hydrate was purchased from Sigma-Aldrich.

FITC-labeled lectin Wheat Germ Agglutinin (WGA) was purchased from Vector Lab., Burlingame, CA, USA, and used at the concentration of 1:400.

Human IGF-I Quantikyne ELISA Kit purchased from R&D Systems Inc., Minneapolis, MN, USA.

Lympholyte-H purchased from Cedarlane; Ontario, Canada, and used at the concentration of 1.077 g/ml.

In Situ Cell Death Detection Kit, Fluorescein was purchased from Roche.

Milliplex MAP purchased from Millipore, Billerica, MA, USA.

PKH-26: Red Fluorescent Cell Linker Kit for general cell membrane labeling was purchased from Sigma-Aldrich.

Rhodamine-labelled Lectin Lens Culinaris Agglutinin (LCA) was purchased from Vector Laboratories Inc., and used at the final concentration of 25 μg/ml.

RosetteSep purchased from StemCell Technologies; Vancouver, Canada.

Search Light proteome array, a multiplexed sandwich ELISA (Pierce-Endogen, Illinois, USA).

Vectastain ABC kit purchased from Vector Laboratories, Burlingame, CA, USA.

2.9 Disposable material

LiHeparinzed capillary pipettes, Hirschmann Laborgerate, Eberstadt, Germany.

Polyethylene labelled-cone shaped capsules purchased from Electron Microscopy Sciences.

Reflotron Urea test strips purchased from Roche Diagnostics GmbH, Mannheim, Germany.

2.10 Instruments

Bioplex 200 Suspension Array System purchased from Bio-Rad, Hercules, CA, USA.

Confocal laser-scanning microscope LS 510 Meta; Zeiss, Jena, Germany.

Cytofluorimeters FACSCanto II was purchased from Becton Dickinson,

BD Bioscience, Milan, Italy.

DynalBeads apparatus purchased from Dynal; Invitrogen.

Electron microscope Morgagni 268D was purchased from Philips, Bmo, Czech Republic.

Real time-PCR: TaqMan ABI 7300 Sequence Detection System (PE Applied Biosystems, Monza, Italy).

Reflotron analyser purchased from Roche, Basel, Switzerland .

Ultramicrotome purchased from LKB Instruments, Milan, Italy.

Nanodrop purchased from Celbio, Milan, Italy.

2.11 RNA isolation

Total RNA (Trizol® Method)

Trizol® reagent was purchased as a ready-to-use solution (GIBCO-Invitrogen). It is an improvement to the single-step RNA isolation Methods, developed by Chomczynski and Sacchi (Chomczynski & Sacchi, 1987) and consists of phenol and GITC (guanidine isothiocyanate).

Chloroform was purchased from MERCK, Darmstad, Germany.

Isopropyl alcohol was purchased from Carlo Erba Reagenti

2.12 DNase digestion of total RNA

The residual amount of DNA remaining after total RNA extraction/isolation was removed by digestion of the total RNA sample with DNase.

		final concentration
RNA	(?) µl	(10 µg)
RNase-free DNase 10U/µl	1 µl	10 U
DNase digestion buffer 10X	10 µl	1 x *
RNase Inhibitor 20 U/µl	1 µl	20 U
Distilled water to the final volume of 100 µl		

Total volume	100 µl	
# Stop Solution		10 µl

(?)Volume that depends on the initial RNA concentration

***RQ1 RNase-Free DNase** (Promega, Madison, USA) cointains RNase-free DNase, RNase Inhibitor DNase digestion buffer 10X (400 mM Tris-HCl pH 8.0, 100 mM $MgSO_4$, 10 mM $CaCl_2$). Enzyme storage buffer is composed of 10 mM HEPES pH 7.5, 50% glycerol v/v, 10mM $CaCl_2$ and 10 mM $MgCl_2$).

 # Stop Solution 20mM EGTA.

To precipitate RNA		final concentration
Distilled water	90 µl	

Sodium acetate (3 M)	20 µl	3 mM
Ethanol	500 µl	
	---	
total volume	610 µl	

2.13 RT-PCR

A DNA thermal cycler RT-PCR was used to carry out reactions.

RT reaction		final concentration in 20 µl
RNA	? µl	2 µg
*dNTPs (10 mM)	1 µl	0.5 mM
# RT primer (50 ng/ml)	2 µl	5 ng/µl (=100 ng)
Distilled water to the final volume of 10 µl		

Total volume	10 µl	

*RT buffer 10 X	2 µl	1 X
*MgCl2 (25 mM)	2 µl	2.5 µM
*DDT (0.1 mM)	2 µl	10 µM
*RNase inhibitor (40 U/µl)	1 µl	40 U
Distilled water	3 µl	

Total volume	20 µl	

(?)Volume that depends on the initial RNA concentration

§ Reverse Transcriptase (50 U/1 µl)	1 µl	50U

*SUPERSCRIPT ™ First-Strand Synthesis System for RT-PCR (Gibco-Invitrogen) included: RT buffer 10 X (200 mM Tris-Cl pH8.4; 500 mM KCl); 25 mM $MgCl_2$; dNTP MIX (10 mM each dATP, dCTP, dGTP, dTTP); DTT (0.1 M); #Random hexamers (50 ng/µl); RNase OUT™ Recombinant Ribonuclease Inhibitor (40 units/µl); § Superscript ™ II RNaseH- Reverse Trancriptase (50 units/µl), Gibco-Invitrogen.

2.14 Real time RT-PCR (SYBR green methodology)

		Target genes	**GAPDH**
	Volume	Final in the reaction	
SYBR Green PCR Master Mix 2X *	12.5 µl	1x	1x
Reverse primer	2.5 µl	300 nM	50 nM
Forward primer	2.5 µl	300 nM	50 nM
double distilled water	5 µl		
template from RT reaction	2.5 µl	(1:10)	(1:100)
	----------		
	25 µl		

* SYBR Green PCR Master Mix contains SYBR Green 1 Dye, AmpliTaq Gold DNA Polymerase, dNTPs with dUTP and optimised buffer components. It is supplied at a 2X concentration by Applied Biosystems, Foster City, CA, USA.

CHAPTER 3

METHODS

Methods for *in vivo* and *in vitro* experiments with hCB-MSCs

3.1 Isolation and characterization of hCB-MSCs

Human cord blood mesenchymal stem cells (hCB-MSCs) were kindly given by Dr. Lorenza Lazzari of the "Cell factory" at Fondazione IRCCS Ospedale Maggiore Policlinico, Magiagalli and Regina Elena, Milan, Italy. Briefly, human cord blood (CB) was collected after informed consent of the mother from full-term newborns and isolation of MSCs was performed within 12 hours. Cord blood was centrifuged, plasma discarded and UCB mononuclear cells were obtained by negative immunodepletion of CD3+, CD14+, CD19+, CD38+, CD66b+, and glycophorin A+ cells using a commercially available kit (RosetteSep; Materials, section 2.8) following manufacturer's instructions. Then the cells were laid on density gradient Lympholyte-H (Materials, section 2.8) and, following centrifugation, the low-density cell fraction was collected. After washing, cells were seeded at $1x10^6$ cells/cm^2 in the presence of "growth medium" (Materials, section 2.3). Medium was changed every 2-3 days, cells were detached using trypsin 0.25%/EDTA 50 μM (Materials, section 2.3) when subconfluent (80%) and split 1:3. This technique allows reaching a 54% of isolation efficiency.

CB-derived cells obtained as described above were studied in order to verify their mesenchymal potential to differentiate towards

osteoblasts, adipocytes and chondroblasts.

Adipogenesis: at confluence hCB-MSCs were incubated with human MSC Adipogenic Induction and Maintenance Media (Materials, section 2.3) replaced every 2-3 days, for 3 weeks. Oil Red O (Materials, section 2.5) incubated for 25 minutes at room temperature was used to detect the accumulation of lipid droplets in the vacuoles.

Osteogenesis: hCB-MSCs were grown for 2-3 weeks with human MSC Osteogenic Medium (Materials, section 2.3) replaced every 3-4 days. Subsequently the cells were washed with PBS and fixed in 10% formalin (Materials, section 2.5) for 20 minutes at room temperature. The presence of calcium rich hydroxyapatite of the extracellular matrix was assessed incubating the cells with 2% w/v Alizarin Red S (Materials, section 2.5) solution for 20 minutes. A digital camera acquired images of mineral deposits.

Chondrogenesis: hCB-MSCs were centrifuged to form a pellet and cultured in differentiation chondrogenic medium (0.5 ml) with TGFβ (Materials, section 2.3) for 2 weeks. Cell clump was fixed in paraformaldehyde (Materials, section 2.5) and stained with Alcian Blue (Materials, section 2.5) to detect proteoglycans.

Human CB-MSCs were characterized by FACS analysis. Three independent evaluations of a pool of three different donors were performed. Stem cells ware incubated with "blocking buffer" (Materials, section 2.6) to block nonspecific sites for 15 minutes at 4°C. Cells were permeabilized with "permeabilizing solution" (0.1% Triton

X-100, Materials, section 2.6) for 5 minutes at 4°C. Then, hCB-MSCs were incubated with conjugated mouse-anti human antibodies: CD45-PC7, CD34-PE, CD146-FITC, CD90-PE, CD44-FITC, VE-Cadherin-FITC, alpha SMA-FITC, NG2-PE, CD105-PE, CD73-PE, CXCR4-APC, CD56-PE, LNGFR-PE, HLA class I-FITC or HLA class II (Materials, section 2.7), for 30 minutes at 4°C.

Additional samples were stained with the primary unconjugated mouse-anti human antibodies: CK3/12, CK19, BB9 and SSEA4 followed by FITC-conjugated and PE-conjugated goat-anti-mouse antibodies (Materials, section 2.7). Isotype immunoglobulins IgG1 PE-FITC, IgG1 PC7, and IgG1 APC (Materials, section 2.7) were used as negative controls. Subsequently, cells were rinsed in PBS 1X, centrifuged and the pellet was suspended in 500 μl of PBS 1X. Human CB-MSCs were analysed by flow cytometer.

3.2 Murine model of acute kidney injury

NOD-SCID female mice (Materials, section 2.1) two months of age at the start of the experiments were used. Animal care and treatment were conducted in conformity with the Institutional guidelines that are in compliance with national (D.L. n.116, G.U., suppl 40, 18 Febbraio 1992, Circolare No. 8, G.U., 14 Luglio 1994) and international laws and policies (EEC Council Directive 86/609, OJL 358, Dec 1987; NIH Guide

for the Care and Use of Laboratory Animals, U.S. National Research Council, 1996). Animals were housed in a constant temperature room (22-24 °C) with a 12-hour dark 12-hour light cycle and fed a standard diet.

3.2.1 Cisplatin preparation and injection

AKI was induced in female mice by subcutaneous injection of cis-diamminedichloroplatinum (cisplatin, Sigma-Aldrich) (Materials, section 2.5). To test the effect of hCB-MSCs, cisplatin was administered to mice, based on their weight, at a concentration (chosen by preliminary experiments) of 12.7 mg/kg. Cisplatin was freshly prepared as a stock solution of 1 mg/1 ml and dissolved in 0.9% sterile saline solution that was pre-warmed to 37°C. Cisplatin dissolved easily in saline as indicated by the disappearance of the yellow powder. Importantly, cisplatin needs to be protected from light and contact with metal (i.e aluminium) should be avoided.

To facilitate injection, mice were anesthetized for a few minutes in a container containing Isofluorane (Materials, section 2.5). A total volume of 400 μl was subcutaneously injected into female mice by using 1 ml syringe (needle 30Gx1/2").

3.3 Cell administration

3.3.1 Human CB-MSC administration

Human CB-MSCs were administered to NOD-SCID female mice one day after receiving cisplatin. Cells were suspended in 500 µl of sterile saline. Before injection, mice were exposed to an infrared lamp to induce vasodilatation and facilitate injection into the tail vein. To investigate the effect of hCB-MSCs, female NOD-SCID mice were divided into two groups and intravenously (i.v.) injected as follows: group 1, saline (n=12); group 2, hCB-MSCs (5x 10^5 cells/mouse) (n=11). Mice were sacrificed at 4 days after cisplatin and kidney samples were used for histology and immunohistochemistry evaluations. For survival studies seven animals for each groups (saline and hCB-MSCs) were used.

By additional experiments, we compared the effect of hCB-MSCs with that of human bone marrow (BM)-MSCs on renal function (at 4 days) and animal survival. Human BM-MSCs (Materials, sections 2.2 and 2.3) were isolated as previously described (Morigi *et al.*, 2008; Capelli *et al.*, 2007). Mice were divided into three groups and i.v. injected 24 h after cisplatin as follows: group 1, saline (n=8); group 2, hCB-MSCs (5x10^5 cells/mouse) (n=10); group 3, hBM-MSCs (5x10^5 cells/mouse) (n=10).

3.3.2 Human fibroblast administration

To better explain the specificity of stem cell effect, we intravenously injected human fibroblast (Materials, sections 2.2 and 2.3) ($5x10^5$ cells/mouse) in mice 24 hours after cisplatin administration (n=9), in comparison with mice given saline (n=10). Three mice treated with human fibroblast and four saline-treated mice were sacrificed at 4 days to assess renal function and histology. The remaining mice were followed during time for survival studies. Normal mice served as controls

3.4 Renal function measurement

To assess renal function, we measured blood urea nitrogen (BUN). Mice were bled from the retro-orbital plexus while they were anesthetized with Isofluorane. By means of disposable LiHeparinzed capillary pipettes (Materials, section 2.9), 32 μl blood was collected from the venous retro-orbital plexus. Blood was applied to test strips and BUN was read by a Reflotron analyser (Materials, section 2.10) in 180 seconds. BUN levels exceeding 30 mg/dl were considered abnormal (normal range in our laboratory: 14-29 mg/dl).

Blood samples for BUN determination were collected at day 0 (basal BUN) and day 4, after cisplatin injection in mice administered with saline or receiving stem cells.

3.5 Sacrifice and tissue collection

Mice were sacrificed by exposure to CO_2 at 4 days after cisplatin or 24 h after cell administration. Kidneys were weighed and in order to take samples representative of the different structural components of the kidney, sections were cut in the axial coronal plane. Depending on the type of procedure that would have been applied (light microscopy, electron microscopy, immunohistochemistry), samples were differently fixed as described in each specific chapter.

Kidney samples were also taken from mice (n=3), which survived 40 days after hCB-MSC injection to assess the possible presence of abnormal phenotype.

3.6 Renal morphology

3.6.1 Light microscopy

Immediately after collection, kidney fragments were fixed overnight in Duboscq-Brazil solution (Materials, section 2.6) and then dehydrated by ascending concentrations of ethanol (50, 70, 90, 100% for 5 minutes each). Once dehydrated, samples were dipped in toluene (Materials, section 2.5) for 1 hour, transferred to stainless steel base moulds and then paraffin (Materials, section 2.5) was added to cover the sample, subsequently incubated at 60°C for 2 hours. During this

period of time paraffin can infiltrate the sample. Samples were then placed at room temperature to allow paraffin to solidify and embed the sample. A microtome was used to cut 3 μm thickness slices, which were placed at room temperature on glass slides. The sections were deparaffinised in toluene (a paraffin solvent) for 20 minutes and then rehydrated in decreasing concentrations of ethanol: (100% for 10 minutes followed by 90, 70, 50% for 5 minutes each) and water. In order to study renal morphology, samples were stained with haematoxylin and eosin (Materials, section 2.5). Glass slides were immersed in haematoxylin for 10 minutes followed by two quick rinses in distilled water and then in tap water for 5 minutes. Eosin was then added for 3 minutes. After rinsing in water, samples were immersed in 100% ethanol followed by toluene and then mounted with Eukitt (Materials, section 2.5).

To identify the basement membrane we stained the glass slides with periodic acid-Schiff's reagent (PAS-stain) (Materials, section 2.5). Samples were deparaffinized as already described, incubated for 10 minutes with 1% periodic acid and were then washed under tap water for three minutes followed by a rapid wash in distilled water. Slides were stained with Schiff's reagent for 35 minutes and immersed three times for 5 minutes each in sodium hyposulphite (Materials, section 2.5), rinsed in tap water for 5 minutes, and then in distilled water for another 5 minutes. Samples were then immersed in 100% ethanol followed by toluene and then mounted.

Slides were scored for the following changes: luminal hyaline casts, tubular cell degenerative changes (cytoplasmic vacuolisation, swelling, cell flattening, PAS-positive droplets, nuclear fragmentation, cell debris) and cell loss (denudation of the tubular basement membrane). Non-overlapping fields of the entire section (up to 28 fields for each mouse) were analysed at high magnification using a 40x objective (high power field, HPF). Lesions were focal in distribution and the scores ranged from 0 to 3+ as follows: 0, no changes; 1+, very occasional tubular profiles (usually < 3/section and < 2/HPF) affected by lesions; 2+, more evident lesions affecting a minor percentage of tubules in each affected area; 3+, lesions in most tubules within affected areas. Sections were analysed in a single-blind fashion. Renal histology pictures were acquired and representative images are shown in the Results.

3.6.2 Electron microscopy

Small fragments of kidney tissue, not more than 0.5-1 mm thickness, were fixed for 4 h in 2.5% glutaraldehyde in 0.1 M cacodylate buffer, pH 7.4 (Materials, section 2.6) and washed repeatedly in the same buffer in order to stabilize the sample and prevent degradation. Specimens were post-fixed in 1% OsO_4 (Materials, section 2.6) for 1 hour. This step confers stability during the following steps of dehydration and embedding and provides electron contrast. Specimens were dehydrated through ascending grades of alcohol: 10% for 10

minutes, 50% and 70% for 10 minutes each, 90% and 100% for 15 minutes each. Samples were then placed in propylene oxide (1,2-epoxypropane) (Materials, section 2.5), a fluid miscible with both alcohol and epoxy resin, and embedded in Epon resin (Materials, section 2.6) overnight at room temperature that maintains the resin in a liquid state to better infiltrate the sample. Polyethylene labelled-cone shaped capsules (Materials, section 2.9) containing freshly prepared resin was used to contain the samples. Tissue fragments were placed at the tip of the truncated cone that was filled with embedding thermosetting synthetic resins. After 3 days during which time the samples were incubated at 60°C to allow polymerisation and solidification of the resin, the blocks of resin were cut by ultramicrotome (Materials, section 2.10). Ultrathin sections were stained with uranyl acetate and lead citrate and examined using a Philips Morgagni electron microscope (Methods, section 2.10) by Dr. Daniela Rottoli.

3.7 PKH-26 staining

To study intrarenal localization of stem cells, we labelled before injection, the cells with a red fluorescence cell linker (PKH-26) (Materials, section 2.8) as follows. A single cell suspension, obtained after stem cell detachment with Trypsin, was washed once using

medium without serum. After centrifugation at 400xg for 5 minutes, the cells were incubated with 1 ml of Diluent C and then with 1 ml of 2X Dye Solution (4 μM) for 5 minutes with periodic mixing. An equal volume (2ml) of serum was added for 1 minute to stop the staining. After centrifugation at 400xg for 5 minutes, the cells were resuspended in complete medium and centrifuged at 400xg for 5 minutes, then the cells were washed 2 more time with serum free medium. Labelling efficacy was assessed to be >98% and viability evaluated by Trypan blue (Materials, section 2.5) exclusion was >96%. For *in vivo* experiments the PKH-26 positive cells were resuspended in saline (500 μl/mouse) and intravenously injected.

3.7.1 Quantification of PKH-26 labelled hCB-MSCs

After 4 days, mice were sacrificed and kidney samples were fixed in 4% paraformaldehyde (Materials, section 2.5) overnight at 4°C, then infiltrated with 30% sucrose/phosphate buffer saline (PBS), embedded in Tissue-Tek OCT Compound (Materials, section 2.5) and frozen in liquid nitrogen. Eight-micrometer-thick sections were stored at -80°C. Sections were fixed 10 minutes in acetone (Materials, section 2.5) and incubated for 10 minutes at room temperature with FITC-labelled lectin Wheat Germ Agglutinin (WGA, Materials, section 2.8), which binds membrane glycoproteins and sialic acid and was used to better identify tubular structure. Nuclei were stained with 4',6'-diamidino-2-phenylindole dihydrochloride hydrate for 15 minutes at room

temperature (DAPI, Materials, section 2.8). Slides were analysed for PKH-26 positive cells. A number of twenty sections/mouse (n=4 mice) were analyzed and PKH-26 positive cells were counted. Data were expressed as number of PKH-26 positive cells/10^5 renal cells. The engraftment of hCB-MSCs-PKH-26 positive was also evaluated at 4 days in other organs as liver, lung and spleen. Tissue samples were fixed as above and sections stained with DAPI. Six sections /mouse (n=3 mice) were analysed for each organ, and PKH-26 positive cells were counted.

In order to confirm the human origin of hCB-MSCs, the stem cells were also identified for their positivity to the human nuclear antigen (HNA). Sections were fixed 10 minutes in acetone and then treated with "permeabilized solution" containing Triton 0.5% (Materials, section 2.6) for 10 minutes at room temperature. After washing in PBS 1X (Materials, section 2.6), sections were treated with "blocking buffer" (Materials, section 2.6) for 15 minutes at room temperature, followed by incubation overnight with mouse anti-human HNA antibody (Materials, section 2.7) at 4°C. Subsequently, kidney samples were treated with an anti-mouse Cy3 antibody for 1 hour at room temperature as secondary antibody. Renal structure was evidenced by staining the sections with FITC-WGA lectin for 10 minutes, while nuclei were stained with DAPI for 15 minutes at room temperature.

Fluorescence was examined by an inverted confocal laser-scanning microscope (Materials, section 2.10).

3.8 Immunohistochemistry

3.8.1 Oxidative damage

To determine protein nitration of tyrosine residues, paraffin kidney sections (3 μm) were fixed with methanol and incubated with 30% H_2O_2 for 30 minutes at room temperature. Then sections were treated in citrate buffer (Materials, section 2.6) 10 mmol/L (pH 6.0) at boiling temperature for 20 minutes, followed by incubation with citrate buffer (20 minutes) at room temperature to enhance the reactivity of antibodies to antigens. Subsequently slides were treated with "permeabilizing solution" (0.3% Triton X-100) (Materials, section 2.6) for 15 minutes and "blocking buffer" (Materials, section 2.6) for 30 minutes at room temperature. Then sections were incubated with rabbit polyclonal anti-nitrotyrosine (Materials, section 2.7), followed by biotinylated goat anti-rabbit antibody (Materials, section 2.7). Signal was developed using Vectastain ABC kit (Materials, section 2.8) and DAB reagents (Materials, section 2.6). Negative controls were performed omitting the primary antibody. At least 30-40 non-overlapping sequential fields (n= 4 mice for each group) were analyzed. Each section was scored for intensity (absent, faint, moderate, intense: 0 through 3).

3.8.2 Apoptosis

Apoptosis was measured by a terminal transferase-mediated dUTP nick-end labelling (TUNEL) assay using an in situ cell death detection kit (Materials, section 2.8). Sections fixed in PLP (Materials, section 2.6) were treated in citrate buffer 10 mmol/L (pH 6.0) at boiling temperature for 20 minutes, followed by incubation with citrate buffer (20 minutes) at room temperature to enhance the reactivity of antibodies to antigens. To block nonspecific sites, sections were treated with "blocking buffer" for 15 minutes at room temperature and then incubated for 80 minutes at 37°C with TUNEL reaction mixture, that should be prepared immediately before use. The TUNEL reaction mixture was prepared add 50 µl of Enzyme Solution to 450 µl of Label Solution. As negative controls PLP-fixed slides were incubated only with Label Solution, while as positive controls, slides were treated with DNase I recombinant for 20 minutes at 37°C. Subsequently, sections were rinsed in PBS 1X and then counterstained with Rhodamine-labelled lectin Lens Culinaris Agglutinin (LCA, Materials, section 2.8) and DAPI for 15 minutes. Slides were mounted with mounting medium and analysed by confocal microscopy. To identify the anti-apoptotic effect of hCB-MSCs (ten fields/mouse; n=5 mice for each group) apoptotic nuclei and DAPI-positive cells per field were counted and the results were expressed as TUNEL positive cells/10^3 cells.

3.8.3 Akt

To evaluate the effect of stem cells on the activation of the pro-survival factor Akt, kidney samples were directly embedded in Tissue-Tek OCT Compound, frozen in liquid nitrogen, and stored at -80°C. Three-micrometer-thick sections of control, cisplatin-treated mice and cisplatin mice injected with PKH26-labeled hAFS cells, were fixed 10 minutes in acetone at 4°C. The antigen retrieval was performed in citrate buffer at boiling temperature for 20 minutes, followed by incubation with citrate buffer (20 minutes) at room temperature. To block nonspecific sites, sections were treated with "blocking buffer" for 30 minutes at room temperature, followed by incubation overnight with rabbit anti-phosphorylated Akt (Ser 473) antibody (Materials, section 2.7) at 4°C. Subsequently, kidney samples were treated with goat anti rabbit-Cy3 antibody (Materials, section 2.7) for 1 hour at room temperature. Renal structure was stained with FITC-WGA lectin for 10 minutes, while nuclei with DAPI for 15 minutes at room temperature. Fluorescence was examined by an inverted confocal laser-scanning microscope.

Thirty fields per mouse (n=3 mice for each group) were analyzed and phosphorylated-Akt positive tubules were counted. Data were expressed as percentage of phosphorylated-Akt positive tubules per field.

3.8.4 Proliferation

The contribution of hCB-MSCs in the proliferation of tubular cells was evaluated by using an antibody identifying the proliferating cell nuclear antigen (PCNA) (Materials, section 2.7) as followed. Sections fixed in Dubosq-Brazil were deparaffinized and dehydrated. To obtain an adequate signal with PCNA antibody, the sections were microwaved twice for 10 min in citrate buffer, and incubated for 30 min with 0.3% H_2O_2 in methanol to quench endogenous peroxidases. To block nonspecific sites, sections were treated with 2% normal sheep serum and 1% BSA for 30 min at room temperature. Then the sections were incubated overnight with anti-PCNA antibody (Materials, section 2.7) at 4°C. After rinsing with PBS 1X, sections were incubated with secondary antibody biotinylated sheep anti-mouse IgG (Materials, section 2.7), for 30 min at room temperature. PCNA signal was developed by Vectastain ABC kit using 3,3′ diaminobenzidine (DAB) as substrate. Nuclei were counterstained with Harris hematoxylin. Evaluation was performed by counting PCNA positive cells in tubular profiles in at least 15 high power field (HPF, x400)/section (n=6 mice for each group).

3.9 PCR and PCR-based techniques

These experiments were performed in collaboration with Dr. Lorena Longaretti of the "Gene Therapy unit" at the "Mario Negri" Institute for Pharmacological Research, Bergamo, Italy.

3.9.1 Preparation of total RNA

In order to isolate total RNA, Trizol® reagent (Materials, section 2.11) was used. Trizol® reagent consists of a ready-to-use solution of phenol and GITC (Guanidine isothiocyanate). While disrupting cells and dissolving cell components, this solution has the function of maintaining the integrity of RNA. This method is an improvement to the single-step RNA isolation method originally developed by Chomczynski and Sacchi (Chomczynski & Sacchi, 1987). RNA was prepared by following the manufacturer's instructions.

Frozen kidney samples of cisplatin-mice given saline or hCB-MSCs were lysed with Trizol® reagent under a fumehood (1 ml/10 cm^2). With the aim of separating the solution into an aqueous phase and an organic phase, 0.2 volumes (200 µl per 1ml Trizol) of chloroform were added. Chloroform (Materials, section 2.11) was incubated for 2-5 minutes at room temperature followed by centrifugation (12000 g, 15 minutes, 4°C). Centrifugation separates the aqueous phase of the solution from the organic phase. Following centrifugation, RNA remained in the upper aqueous phase and this was carefully removed and transferred to

a new tube. In order to precipitate RNA, isopropyl alcohol (Materials, section 2.11) was added to the recovered aqueous phase (500 µl isopropyl alcohol per 1 ml Trizol) and incubated for 10 minutes at room temperature. Following centrifugation for 15 min at 4°C at 12000 g, a gel-like pellet formed on the side and bottom of the tube and this was washed with 75% ice-cold ethanol (1 ml EtOH/ml Trizol). Ethanol at this concentration removed the excess of the remaining isopropyl alcohol and partially rehydrated the RNA pellet. After centrifuging at 7500 g, for 5 minutes, at 4°C, RNA was allowed to air dry prior to resuspension in sterile water (about 20 µl, depending on the size of the pellet). RNA concentration was determined spectrophotometrically by Nanodrop (Materials, section 2.10). The calculation of the concentration of the nucleic acid in the sample was obtained by reading at a wavelength 260 nm. By using the formula here reported, we can easily calculate the µg/ml of RNA in the sample since 40 µg/ml of single-stranded RNA approximately corresponds to an OD of 1:

RNA (µg/µl) = OD 260nm x 40 x dilution (i.e. 100 =100 µl / 1µl)/1000

To evaluate the purity of nucleic acid we can observe the ratio between the readings at 260 nm and 280 nm (OD260/OD280 = nucleic acid and proteins/proteins) providing an estimation of the purity. The optimum value is between 1.8 and 2 (for RT-PCR it is better to have 2-2.1). If there is contamination of proteins the value will be lower, and the accuracy of the RNA quantisation will be impaired. In addition to

control for phenol contamination, a reading at 320 nm is performed and it should be equal to the blank.

3.9.2 DNA digestion of total RNA

For certain RNA applications that are sensitive to very small amounts of DNA, further DNA removal may be necessary. Indeed, in these cases, digestion with the enzyme DNase can remove the small residual amounts of DNA remaining after total RNA isolation. Total RNA (10 μg) was treated with RNase-free DNase (10 U DNase/10 μg RNA) in the presence of RNase Inhibitor (2 U/μg of RNA) in a final volume of 100 ml with nuclease free water following the manufacturer's instructions (Materials, section 2.12). Samples were digested for 1 hour at 37°C and then the reaction was blocked by incubation (10 minutes at 65 °C) with Stop Solution (Materials, section 2.12) (10 μl, same volume of the enzyme) containing 20 mM EGTA (pH 8.0) that blocks enzyme activity. At the end of incubation, RNA is precipitated by sodium acetate 3M pH 5.2 (1/10 of the volume) (Materials, section 2.12) and 100% ethanol and centrifuged at 13800 rpm for 30 minutes at 4°C. After washing with 70% ethanol (500 μl), air-drying for 5 minutes on ice and centrifuging for 10 minutes, the pellet was resuspended in 10 μl of sterile water.

A second quantification of the RNA was then performed by a spectrophotometer, as already described (Methods, section 3.23).

3.9.3 Preparation of cDNA by RT-PCR

The purified RNA was reverse transcribed into cDNA. We prepared a solution containing 2 μg RNA, dNTPs, random examer primers and sterile water to a final volume of 10 μl/sample (Materials, section 2.13). This solution was incubated in the thermal cycler for 5 minutes at 65°C, quickly spun and put at 4 °C for primer annealing/hybridization. The following reagents were mixed and incubated for 2 minutes at 25°C: RT-buffer, Mg^{2+}, DDT and RNase OUT (Materials, section 2.13). Samples to be retro-transcribed were added with Reverse Transcriptase (Materials, section 2.13). Negative controls, needed to verify if there was a genomic contaminant, consisted of samples that had no enzyme added. Reaction was allowed to take place at 25 °C for 10 minutes in the thermal cycler followed by 50 minutes at 42°C to start retro-transcription, 15 minutes at 70°C to terminate elongation. Finally samples were transferred to 4°C to stop the reaction.

3.9.4 Real time PCR for HGF gene

The cDNA obtained by RT-PCR was amplified by real-time PCR. Real-time PCR was performed by TaqMan ABI 7300 Real Time PCR System and PCR amplification reaction were by SYBR Green methodology with all the reagents supplied directly from Applied Biosystems and performed following the manufacturer's instructions as described in Materials, section 2.14. Template from RT reaction was mixed with SYBR Green PCR Master Mix and with forward primers

and reverse for human HGF or glyceraldehyde-3-phosphate dehydrogenase (GAPDH) (Materials, section 2.14). The primer sequence design was achieved by using the "Primer Express" dedicated software (Applied Biosystems) and were as follows:

HGF primers:

Forward: 5'-TCAAATGCCAGCCTTGGAA-3'

Reverse: 5'- GCAAAAAGCTGTGTTCATGGG-3'

GAPDH primers:

Forward: 5'-TCATCCCTGCATCCACTGGT-3'

Reverse: 5'-CTGGGATGACCTTGCCCAC-3'

After an initial hold of 2 minutes at 50°C and 10 minutes at 95°C, the samples were cycled 40 times at 95°C for 15 seconds and 60°C for 60 seconds. The comparative Ct method normalizes the number of target gene copies to a housekeeping gene as GAPDH (ΔCt). Gene expression was then evaluated by the quantification of cDNA corresponding with the target gene relative to a calibrator sample serving as a physiologic reference (mouse with vehicle, ΔΔCt). On the basis of exponential amplification of target gene as well as calibrator, the amount of amplified molecules at the threshold cycle is given by: $2^{-\Delta\Delta Ct}$.

The identity of the amplification product was ensured by primer specificity for the HGF sequence, the presence of a single dissociation curve at a constant T melting, and the lack of genomic DNA contamination or primer dimers in the RT $^-$ samples.

3.10 *In vitro* experiments

3.10.1 Cells and cell culture

HK2. Immortalized adult human proximal tubular cell line (HK-2) was purchased from ATCC (Materials, section 2.2). Originally, the HK-2 cell line has been established by the group of Dr. Ryan (Ryan *et al.*, 1994) from normal adult male kidney unsuitable for transplantation. Firstly, cortical proximal tubular segments were isolated by microdissection and digestion with collagenase. The digested tissue was centrifuged after passing through a steel sieve. The pellet was then added to a 31% Percoll and viable proximal tubular cells (PTCs) were recovered at the bottom of the tube after centrifugation. Once obtained, PTCs were transferred in a tissue culture flask and maintained in selected medium until approximately 2 weeks to obtain the confluence. Secondly, in order to establish long-term culture, the cells were exposed for 48 hours to a replication-defective recombinant retrovirus containing the human papilloma virus (HPV) 16 E6/E7 genes. At molecular level, E6 binds to p53 inducing its degradation, and E7 inactivates the retinobloastoma tumor-suppressor gene product, p105-Rb. The elimination of these two negative regulators of the cell proliferation allowed for the development of the immortalized cell line. Transfected cells were then enzymatically detached, re-plated in flasks and growing cell clones were isolated. Only the clone, named HK-2, was grown for more than 30 passages for almost one year and has been characterized.

HK-2 cells showed cuboidal morphology and dome formation, numerous surface projections consistent with microvilli and junctional complexes resembling those observed in primary cultured proximal tubular epithelial cells (PTECs). HK-2 cells stained positive for typical brush border membrane (BBM)-associated enzymes (alkaline and acid phosphatase, gamma glutamyltranspeptidase and leucine amidopeptidase), for cytokeratin and vimentin -intermediate cytoskeletal filaments characteristic of epithelial cells- and they also express $\alpha 3\beta 1$ integrin with a pericellular pattern. The HK-2 cells did not express factor VIII, CALLA endopeptidase or 6.19 antigen, markers for endothelial cells, fibroblasts and adipocytes, respectively.

This cell line maintained functional characteristics similar to the primary PTECs, such as adenilate cyclase activity in response to parathyroid hormone (PTH) and Na^+-dependent glucose uptake, suggesting that some receptor-mediated hormonal responses as well as sugar transport mechanisms are preserved.

In our laboratory, HK-2 cells were maintained in culture following the conditions allowing the maintenance of the described proximal tubular cell phenotype.

Medium. "Growth medium" (Materials, section 2.3).

Cell density. For routine cell culturing, HK-2 cells were seeded at the dilution of 1:2 (1:3 in the week-end) and maintained at 37°C in a 5% CO_2 humidified atmosphere. The cells were maintained at sub-confluence. The

cells were subcultured every second day by using trypsin/EDTA (Materials, section 2.3) for 1 minute at room temperature.

Viability: Each time HK2 were detached, we evaluated the cell viability by Trypan blue. An aliquot of solution containing cells (20 µl) was mixed with the same volume of 2% Trypan blue solution. After a few seconds, the cells were seeded on Burker's chamber (Methods, Section 3.26) in the space within the glass of the chamber and the coverslip. Live (white) and dead (blue) cells were counted.

Cell storage. HK-2 cells were preserved for long-term storage in liquid nitrogen. Cell pellets were suspended in FCS plus 7.5% DMSO (Materials, section 2.5) in cryovials. To guarantee a gradual freezing, the vials were left in isopropanol-filled containers overnight at -80°C and then transferred to liquid nitrogen tanks for storage.

Thawing frozen cells. The cells were thawed rapidly by placing the vial in a water bath at 37°C with a gentle agitation. The cells were then slowly resuspended in 9 ml of complete medium and DMSO traces were remove by centrifugation at 1200 rpm for 7 minutes.

hCB-MSCs. Human cord blood mesenchymal stem cells were kindly supplied from Dr. Lazzari as already described in Materials, section 2.2. Cells were maintained in culture in "growth medium" (Materials, section 2.3) then they were detached and used for *in vivo* and *in vitro* experiments.

Cell storage. hCB-MSCs were preserved for long-term storage in liquid nitrogen. Cell pellets were suspended in "growth medium" plus 10%

DMSO in cryovials. To guarantee a gradual freezing, the vials were left in isopropanol-filled containers overnight at -80°C and then transferred to liquid nitrogen tanks for storage.

Thawing frozen cells. The cells were thawed rapidly by placing the vial in a water bath at 37°C with a gentle agitation. The cells were then slowly resuspended in 9 ml of complete medium and DMSO traces were remove by centrifugation at 1200 rpm for 7 minutes.

3.10.2 Indirect co-culture experiments

For the experiments, HK-2 cells were seeded on 6-well transwell plates at the concentration of $46x10^3$ cells/cm^2 (day -1). The day after (day 0), HK2 that were about 70-80% confluent, have been washed with PBS 1X and incubated with 8 μM of cis-platinum (II)-diamine dichloride (cisplatin) (Materials, section 2.5) in pre-warmed "test medium"(Materials, section 2.3). Cisplatin was incubated for 6 hours and then was removed followed by rinsing with PBS 1X. After drug withdrawal, hCB-MSCs ($5x10^4$ cells/well) were seeded on the top of the semipermeable Transwell polycarbonate tissue culture inserts (0.4 μm, diameter). Cell supernatants obtained by cisplatin-treated HK-2 cells alone or in co-culture with hCB-MSCs were collected at 24-72 hours after cisplatin.

3.10.3 Proteome assay

These experiments were performed in collaboration with Dr. Lazzari's group. Growth factors and inflammatory cytokines produced by

indirect co-culture experiments were quantified by Search Light proteome array (Materials, section 2.8) in conditioned cell supernatants. Supernatants were analysed by Human Angiogenesis Array 1 (HGF, FGF, HB-EGF, VEGF) and the Human Inflammatory Cytokine 1 (IL-1b and TNFa) following manufacturer's instructions. ArrayVisionTM Software for data acquisition and management was used following manufacturer's instructions. In addition, serum levels of HGF were evaluated in cisplatin-mice given saline (n=10 mice) or hCB-MSCs (n=10 mice) at 4 day using the same multiplexed sandwich ELISA.

3.11 Statistics

The results are expressed as mean ± SE. Statistical analysis was performed using ANOVA followed by Tukey Cicchetti test for multiple comparisons, non parametric Kruskal-Wallis test or log-rank test, as appropriate. The Wilcoxon- based method was used to determine the significance of differences between independent groups. Statistical significance level was defined as $p<0.05$.

Methods for *in vivo* and *in vitro* experiments with hAFS cells

3.12 Isolation and characterization of hAFS cells

Human amniotic fluid stem (hAFS) cells were kindly given by Dr. Paolo De Coppi of the "Stem Cell Processing Laboratory, Clinic of Paediatric Oncohematology" at University of Padova, Padova, Italy. The isolation was performed as previously described (De Coppi *et al.*, 2007). Briefly, back up samples of human amniocentesis were collected from consenting volunteer donors, according to guidelines from the Azienda Ospedaliera Padova (protocol number 451P/32887). The cellular content of the AF samples was pelleted by centrifugation, washed in PBS 1x and subjected to immunoselection. The cells were incubated with a mouse monoclonal antibody anti-CD117 (c-Kit, Materials, section 2.7) followed by goat anti-mouse IgG MicroBeads (Materials, section 2.7) and then selected on a DynalBeads apparatus (Materials, section 2.10). After immunoselection, c-Kit positive cells were seeded in "growth medium" (Materials, section 2.3). Human AFS cells were subcultured at a dilution of 1:4 to 1:8 and expanded up to 70% of confluence. All the *in vitro* and *in vivo* experiments were performed with hAFS cells between passages 6-8.

Differentiation of human AFS cells (2-7th passage) toward adipocytes and osteocytes was obtained by exposing cells to specific inductive media. ***Adipogenesis:*** cells were seeded at the density of 3,000 cells/cm^2 and were cultured with "inductive media" with adipogenic supplements (Materials,

section 2.3). Medium was replaced every 2-3 days, for 3 weeks. Oil Red O (Materials, section 2.5) incubated for 25 minutes at room temperature was used to detect the accumulation of lipid droplets in the vacuoles.

Osteogenesis: cells were seeded at the density of 3,000 cells/cm^2 and were cultured with "inductive media" with osteogenic supplements (Materials, section 2.3). Medium was replaced every 2-3 days, for 3 weeks. Von Kossa (Materials, section 2.5) staining was used to detect calcium deposition.

Immunophenotype of hAFS cells was evaluated by FACs analysis. Five independent evaluations of a pool of three different donors were performed. Stem cells were incubated with "blocking buffer" to block nonspecific sites for 15 minutes at 4°C. Then, hAFS cells were incubated with conjugated anti-human antibodies: CD29 FITC, CD44 FITC, CD73 PE, CD90 FITC, CD105 PE, CD80 FITC, CD86 PE, Oct-4 FITC, SSEA-4 FITC, HLA-ABC FITC or HLA-DR PE (Materials, section 2.7) for 30 minutes at 4°C. Subsequently, cells were rinsed in PBS 1X, centrifuged and the pellet was suspended in 500 μl of PBS 1X. Human AFS cells were analysed by flow cytometer.

3.13 Murine model of acute kidney injury

Murine model of acute kidney injury was induced in NOD-SCID female mice by subcutaneous injection of cisplatin (Ebewe; Materials,

section 2.5) described above (see section 3.2).

To test the effect of hAFS cells, we used a cisplatin already diluted, commonly used in patients undergoing chemotherapy, at a concentration of 15.5 mg/Kg. To facilitate injection, mice were anesthetized for a few minutes in a container containing Isofluorane (Materials, section 2.5). A total volume of 400 μl was subcutaneously injected into female mice by using 1 ml syringe (needle 30Gx1/2").

3.14 Stem cell administration

To test the effect of hAFS cells, female NOD-SCID mice were divided into two groups and 24 h after cisplatin were intravenously injected as follows: group 1, saline (n=11); group 2, hAFS cells (5x 10^5 cells/mouse) (n=11). Mice were sacrificed at 4 days after cisplatin and kidneys used for histology and immunohistochemistry. Normal mice served as controls (n=11).

To assess survival, cisplatin-treated mice given saline (n=7) and cisplatin-treated mice infused with hAFS cells (5x10^5 cells/mouse) (n=9) were used. By additional experiments the effect of hAFS cell infusion (5x10^5 cells/mouse) on survival of mice with AKI, was compared with that of hBM-MSCs (5x10^5 cells/mouse) and saline (n=6 animals for each group).

In addition, we compared the effect of hAFS cells with that of hAFS cells pre-conditioned with GDNF (100 ng/ml for 24 h Materials, section

2.4) before injection. Twenty-four hours after cisplatin, mice were divided into three groups and i.v. injected as follows: group 1, saline (n=9); group 2, hAFS cells ($5x10^5$ cells/mouse) (n=10); group 3, GDNF pre-conditioned hAFS cells ($5x10^5$ cells/mouse) (n=10). Animals were sacrificed at 4 days after cisplatin. For cell engraftment experiments, female mice were divided as follow (n=3 animals/group): control mice injected with hAFS cells untreated (group 4) or treated with GDNF (group 5), cisplatin-mice infused with hAFS cells untreated (group 6) or treated with GDNF (group 7). The animals were sacrificed 24 h after cell injection.

3.15 Renal function measurement

Blood samples for blood urea nitrogen (BUN) determination were collected as previously describe (section 3.4).

3.16 Sacrifice and tissue collection

Mice were sacrificed by exposure to CO_2 at 4 days after cisplatin or 24 h after cell administration. Kidneys were weighed and sections were cut in the axial coronal plane. Depending on the type of procedure that would have been applied (light microscopy, electron microscopy, immunohistochemistry), samples were differently fixed as described in each specific chapter.

3.17 Renal morphology

3.17.1 Light microscopy

As described in section 3.6.1, kidney samples were fixed in Duboscq-Brazil and paraffin-sections were stained with hematoxylin and eosin, or periodic acid-Schiff's reagent (PAS). Luminal hyaline casts and tubular necrosis (denudation of tubular basement membrane) were assessed as reported in section 3.6.1 in non-overlapping fields (up to 28 for each section) (40x, high power field, HPF).

3.17.2 Electron microscopy

Fragments of kidney tissue were fixed for 4 h in 2.5% glutaraldehyde in 0.1 M cacodylate buffer, pH 7.4, and washed repeatedly in the same buffer. After post-fixation in 1% OsO_4, specimens were dehydrated through ascending grades of alcohol and embedded in Epon resin. Ultrathin sections were stained with uranyl acetate and lead citrate and examined using a Philips Morgagni electron microscope by Dr. Daniela Rottoli and Dr. Mauro Abbate, Laboratory of Experimental Models of Kidney Disease, "Mario Negri" Institute, Bergamo. For more details, see section 3.6.2.

3.18 PKH-26 staining

To study intrarenal localization of stem cells, we labelled before injection, the cells with PKH-26 (Materials, section 2.8) as described in section 3.7. For *in vivo* experiments the PKH-26 positive cells were resuspended in saline (500 µl/mouse) and intravenously injected.

3.18.1 Quantification of hAFS-PKH-26 positive cells

Human AFS cells, untreated or pre-conditioned with GDNF, were labeled with PKH-26. At different time points, hAFS cell-treated mice were sacrificed and kidney samples were fixed in 4% paraformaldehyde (Materials, section 2.5) overnight at 4°C, and embedded in OCT. Frozen kidney sections were stained with FITC-WGA lectin and DAPI. Ten to twenty sections/mouse (n=3-6 animals for each time point) were analyzed. Data are expressed as number of PKH-26 cells per 10^5 renal cells. The percentage of hAFS cells in tubular and peritubular areas was calculated as number of PKH-26 positive cells in each compartment per total PKH-26 cells. Human AFS cell engraftment in other organs as lung, liver, heart and spleen was also evaluated in control and cisplatin-treated mice (n=3). Nuclei were stained with DAPI.

To identify the human origin of hAFS cells, frozen kidney sections of cisplatin mice injected with PKH26-labeled hAFS cells, were stained with the anti-human CD105 antibody. Sections were fixed 10 minutes in acetone and then treated with "permeabilized solution" containing Triton 0.5% (Materials, section 2.6) for 10 minutes at room temperature. After washing in PBS 1X, sections were treated with "blocking buffer" (Materials, section 2.6) for 15 minutes at room temperature, followed by incubation overnight with mouse anti-human CD105 antibody (Materials, section 2.7) at 4°C. Subsequently, kidney samples were treated with an anti-mouse Cy5 antibody for 1 hour at room temperature as secondary antibody. Renal structure was evidenced by staining the sections with

FITC-WGA lectin for 10 minutes, while nuclei were stained with DAPI for 15 minutes at room temperature.

3.19 Immunohistochemistry

3.19.1 Apoptosis

Apoptosis was measured by TUNEL assay using an in situ cell detection kit (Materials, section 2.8) as previously described (see section 3.8.2), followed by counterstaining with Rhodamine-labeled lectin Lens Culinaris Agglutinin (Materials, section 2.8) and DAPI (Materials, section 2.8) for 15 minutes. Slides were mounted with mounting medium (Materials, section 2.5) and analysed by confocal microscopy. To identify the anti-apoptotic effect and hAFS cells, apoptotic nuclei and DAPI-positive cells per field (ten fields/mouse; n=3 mice for each group) were counted and the results were expressed as TUNEL positive cells/10^3 cells.

3.19.2 Akt

Using the same procedure described in section 3.8.3, frozen kidney sections were fixed in acetone, incubated with anti-phosphorylated (p)Akt (Ser 473) antibody (Materials, section 2.7) followed by goat anti rabbit-Cy3. Slides were counterstained with FITC-WGA lectin and DAPI. Fifteen fields/mouse (n=3 mice for each group) were analysed and pAkt positive tubules were counted and expressed as percentage of positive tubules/field.

3.19.3 Proliferation

Proliferation of tubular cells induced by hAFS cells, was immunohistochemically identified by labeling with a monoclonal antibody against the cell-cycle associated protein Ki67 (Materials, section 2.7) as follows. Sections fixed in 4% paraformaldehyde (Materials, section 2.5) overnight at 4°C, and subsequently embedded in Tissue-Tek OCT Compound, were treated with citrate buffer 10 mmol/L (pH 6.0) at boiling temperature for 20 minutes, followed by incubation with citrate buffer (20 minutes) at room temperature. Then, sections were incubated with "blocking buffer" for 30 minutes at room temperature, followed by incubation overnight with mouse anti-Ki-67 antibody (Materials, section 2.7) at 4°C. Cy3-conjugated goat anti-mouse antibody was used for 1 hour at room temperature as secondary antibody. Slides were counterstained with FITC-WGA lectin and nuclei were visualized by DAPI. Evaluation of Ki-67 positive cells in tubular profiles was performed in at least 10 HPF/section (n =3 mice for each group).

3.20 *In vitro* experiments

3.20.1 Cells and cell culture

Human AFS cells. Human amniotic fluid stem cells were kindly supplied from Dr. De Coppi as already described in Materials, section 2.2. Cells were maintained in culture in "growth medium" (Materials, section 2.3) seeded on special dishes (Optilux™) then they were detached by

Trypsin (Materials, section 2.5) and used for *in vivo* and *in vitro* experiments.

Cell storage. Human AFS cells were preserved for long-term storage in liquid nitrogen. Cell pellets were suspended in "growth medium" plus 10% DMSO in cryovials. To guarantee a gradual freezing, the vials were left in isopropanol-filled containers overnight at -80°C and then transferred to liquid nitrogen tanks for storage.

Thawing frozen cells. The cells were thawed rapidly by placing the vial in a water bath at 37°C with a gentle agitation. The cells were then slowly resuspended in 9 ml of complete medium and DMSO traces were remove by centrifugation at 1200 rpm for 7 minutes.

3.20.2 Wound-healing assay

To study hAFS cell motility, confluent hAFS cells seeded on Optilux™ were cultured in "growth medium" for 24 hours with or without 100 ng/ml GDNF (Materials, section 2.4). After 24 hours, hAFS cells were scratched with a 200-µl pipette tip to create an artificial wound. Cells were washed with PBS1X to remove cell debris and fresh "growth medium" with or without GDNF was added. Images of wounded monolayer were obtained after 7 hours.

3.20.3 Cell viability assay

In order to study the capacity of hAFS to survive in a toxic environment, hAFS cells seeded 29.000/cm^2, were exposed to "growth

medium" alone or GDNF 100 ng/ml for 24 hours and then incubated with H_2O_2 (Materials, section 2.5) 200 mM for 24 hours. Morphology was analysed by light microscopy and then cells were detached by trypsin and counted after Trypan blue staining. Data were expressed as percentage of viable cells over the total number of untreated control cells (n=3 experiments).

3.20.4 FACs analysis

Human AFS cells treated or not with GDNF 100 ng/ml for 24 hours, were detached by trypsin and a small aliquot was counted. After centrifuging at 1200 rpm for 10 minutes, the pellet was incubated with "blocking buffer" for 15 minutes at 4°C. Cells were centrifuged and then suspended in 500 µl of mouse anti-CD44 or rabbit anti-CXCR4 or rabbit anti-CX3CR1 antibodies (Materials, section 2.7) for 30 minutes at 4°C. Then the cells were incubated with goat anti-mouse or goat anti-rabbit FITC secondary antibodies as appropriate for 30 minutes at 4°C. Cells were rinsed in PBS 1X and centrifuged. The pellet was suspended in 500 µl of PBS 1X and cells were analysed by flow cytometer (Materials, section 2.10).

3.20.5 Measurement of cytokines and growth factors.

These experiments were performed in collaboration with Dr. Aline Fabricio of Veneto Oncology Institute (IOV), Padova, Italy. Commercially-

available human multiplex kits (Milliplex MAP; Materials, section 2.8) were used to quantify the production of Interleukin (IL)-6 and IL-10, as well as vascular endothelial growth factor (VEGF), fibroblast growth factor 2 (FGF-2), hepatocyte growth factor (HGF) and stromal cell-derived factor-1 (SDF-1+β), in conditioned media of hAFS cells untreated or treated for 48 h with GDNF 100 ng/ml (n=3 experiments). IGF-1 was measured using Human IGF-I Quantikyne ELISA Kit (Materials, section 2.8). IL-6, IL-10 and VEGF were measured using the MILLIPLEX MAP Human Magnetic Cytokine/Chemokine I Panel - 3 Plex Kit (Materials, section 2.8). FGF-2, HGF and SDF-1 were measured using the MILLIPLEX MAP Human Magnetic Circulating Cancer Biomarker Panel - 3 Plex Kit (Materials, section 2.8). Multi-analyte profiling was performed on the Bioplex 200 Suspension Array System (Materials, section 2.10). All samples were coded for a blinded analysis, and each sample concentration was determined in duplicate. Data were processed with Bio-Plex Manager 5.0 software. Results were expressed as pg/ml/10^6 hAFS cells. Assay sensitivities (minimum detectable levels + 2 SD) were: IL-6, 0.2 pg/ml; IL-10, 0.5 pg/ml, VEGF < 5.8 pg/ml, HGF, 6.8 pg/ml; FGF-2, 3.2 pg/ml, SDF1, 33.9 pg/ml; IGF-1, from 7 to 56 pg/ml. The percentage of augmentation of IL-6, VEGF and SDF-1 production in GDNF-treated over untreated hAFS cells was also calculated as [GDNF/hAFS cells] – [hAFS cells]/ [hAFS cells] x 100.

3.21 Statistics

The results are expressed as mean ± SE. Statistical analysis was performed using ANOVA followed by Tukey Cicchetti test for multiple comparisons or Bonferroni post-hoc analysis, and unpaired t test using Sigmaplot software, version 11.0 (Systat Software, Inc. Chicago, IL, USA). Non-parametric Kruskal-Wallis test or Kaplan-Meier analysis and Log-Rank test were applied, as appropriate. Statistical significance was defined as $p<0.05$.

Principles of the main techniques and instruments

3.22 Flow cytometer

Flow cytometry is a technique used for counting, examining and sorting microscopic particles suspended in a stream of fluid. In the flow cytometer any suspended particle or cell from 0.2-150 micrometers in size is suitable for analysis. This instrument allows simultaneous multiparametric analysis of the physical and/or chemical characteristics of single cells flowing through an optical/electronic detection apparatus. The properties measured include a particle's relative size, relative granularity or internal complexity, and relative fluorescence intensity. These characteristics are determined using an optical-to-electronic coupling system that records how the cell or particle scatters incident laser light and emits fluorescence. A flow cytometer is made up of three main systems: fluidics, optics, and electronics. The fluidics system transports particles in a stream to the laser beam for interrogation. For optimal illumination, the stream transporting the particles should be positioned in the centre of the laser beam. The flow of sheath fluid accelerates the particles and restricts them to the centre of the sample core. In addition, only one cell or particle should move through the laser beam at a given moment. To accomplish this, the sample is injected into a stream of sheath fluid within a flow chamber, that in a benchtop cytometer, is called flow cell whereas in a stream-in-air cytometer is called nozzle tip. Laser light of a single

frequency hits the stream of fluid. The optic system consists of lasers to illuminate the particles in the sample stream and optical filters to direct the resulting light signals to the appropriate detectors. A number of detectors are aimed at the point where the stream passes through the light beam; one in line with the light beam (forward scatter or FSC) and several perpendicular to it (side scatter or SSC). Each suspended particle passing through the beam scatters the light in some way, and fluorescent chemicals in the particle may be excited into emitting light at a lower frequency than the light source. This combination of scattered and fluorescent light is picked up by the detectors, and by analysing fluctuations in brightness at each detector (one for each fluorescent emission peak) it is possible to deduce various indications about the physical and chemical structure of each individual particle. FSC correlates with the cell volume and is proportional to cell-surface area or size. FSC is a measurement of the most diffracted light and is detected just off the axis of the incident laser beam in the forward direction by a photodiode. FSC provides a suitable method of detecting particles greater than a given size independent of their fluorescence and is therefore often used in immunophenotyping to trigger signal processing. SSC depends on the inner complexity of the particle (i.e. shape of the nucleus, the amount and type of cytoplasmic granules or the membrane roughness). SSC is a measurement of mostly refracted and reflected light that occurs at any interface within the cell where there is a change in the refractive index. SSC is collected at approximately 90 degrees to the laser beam by a

collection lens and then redirected by a beam splitter to the appropriate detector. Correlated measurements of FSC and SSC can allow for differentiation of cell types in a heterogeneous cell population.

A fluorescent compound absorbs light energy over a range of wavelengths that is characteristic for that compound. The absorption of light causes an electron in the fluorescent compound to be raised to a higher energy level. The excited electron quickly decays to its ground state, emitting the excess energy as a photon of light. This transition of energy is called fluorescence. The range over which a fluorescent compound can be excited is termed its absorption spectrum. The range of emitted wavelengths for a particular compound is termed its emission spectrum. The argon ion laser is commonly used in flow cytometry because the 488-nm light that it emits excites more that one fluorochrome. One of these fluorochromes is fluorescein isothiocyanate (FITC). In the absorption spectrum of FITC the 488-nm line is close to the maximum absorption of FITC. If the fluorochrome was excited by another wavelength within its absorption spectrum, light emission of the same spectrum would occur but it would not be of the same intensity. More than one fluorochrome can be used simultaneously if each is excited at 488 nm and if the peak emission wavelengths are not extremely close to each other. When a fluorescent dye is conjugated to a monoclonal antibody, it can be used to identify a particular cell type based on the individual antigenic cell markers of the cell.

The optical system consists of excitation optics and collection optics.

The excitation optics consist of the laser and lenses that are used to shape and focus the laser beam. The collection optics consist of a collection lens to collect light emitted from the particle-laser beam interaction and a system of optical mirrors and filters to address specified wavelengths of the collected light to designated optical detectors. The detected light signals are converted by an electronic system into electronic pulses that can be processed by the computer.

3.23 PCR based techniques

PCR

Polymerase chain reaction (PCR) is a method to create copies of specific fragments of DNA. PCR rapidly amplifies a single DNA molecule into many billions of copies. PCR is based on the enzymatic amplification of short DNA sequences (oligonucleotides) that are flanked by two "primers" (forward and reverse) defining the region to be amplified. Primers prime synthesis of the complementary DNA sequence by DNA polymerase. If primers are negligently designed, there may occur some unwanted structures. These can be prevented using specific programs, which calculate the possibility of those structures to form. One of this kind of structure is the hairpin structure. This happens when the primers 3'end and 5'end pairs, or the other end pairs with the body. Another structure is primer dimers where the primers bind themselves. There may

also be non-specific products because of false adhesion of primers. This can occur if few bases are wrong or temperature of annealing (T_a) is too low. The chain reaction is a three-step process: denaturation, hybridization or annealing, and extension that are repeated over several cycles (Figure 3.1). At each cycle of the process, the number of copies is doubled. Denaturation is the process during which two strands separate from each other. Denaturation is carried on by heating up at a specific melting temperature, T_m (usually 95°C) that depends on the length of the primers (the longer the higher) and the number of guanine and cytosine bases (the more the higher temperature). During the denaturation, the double strand melts opening to single stranded DNA and all enzymatic reactions stop (for example: the extension from a previous cycle). After denaturation of the double stranded DNA (or RNA/cDNA from RT reaction), the primers are allowed to anneal to their 100% complementary sequence (one primer each strand) by lowering the temperature (down to T_a of the primers). T_a depends on the concentration of primers and on the composition of the oligonucleotide and is generally set about 5°C below T_m of the primers, T_m being the temperature at which 50% of the primer and its complementary sequence are present in a duplex DNA molecule. The elongation step involves the enzyme polymerase that derives from the bacterium *Thermus acquaticus* since this polymerase is heat-stable. Taq DNA polymerase performs the polymerisation reaction downstream of both primers. To allow exponential amplification of the target sequence comprised within the primers, these three steps "Denaturation-Annealing-Elongation" are

then repeated for a number of times (cycles), at the end of one cycle, the region between the two primers has been copied once, producing two copies of the original sequence region. During PCR, the amount of product initially increases exponentially, but then the rate slows and eventually plateaus. Because a heat resistant polymerase is used, the reaction can be repeated continuously without addition of more enzymes. The reaction is carried out in a computer-regulated heating block, a thermal cycler, that permits rapid, controlled heating and cooling.

RT-PCR

RNA cannot serve as template for PCR, so first it must be reverse transcribed into cDNA and then amplified by PCR. The technique involves the reverse transcription of an RNA molecule to a complementary DNA strand (1st strand cDNA) and is known as RT-PCR.

In the RT reaction the choice of reverse transcriptase enzyme (i.e. MMLV-RT or SuperScriptII RT) used to synthesize cDNA is important since enzymatic properties such as temperature optima, divalent ion requirement, specificity and sensitivity, can vary. The RNA is reverse transcribed in the presence of RT primers. Priming affects the size and specificity of the cDNA produced.

There are three types of primers that may be used for reverse transcription:

- **Oligo(dT)$_{12-18}$**, which binds to the endogenous poly(A) tail at the 3′ end of mammalian mRNA. This primer often produces a full-length cDNA;

- **Random hexanucleotides,** which bind to mRNA at a variety of complementary sites and lead to partial length (short) cDNAs. Random hexanucleotides may be ideal for overcoming the difficulties presented by extensive secondary structure in the template. These primers may also transcribe more efficiently 5′ regions of the mRNA;
- **Specifc oligonucleotide primers,** which selectively prime the mRNA of interest;

The RT reaction is carried out by reverse transcriptase enzyme for 45–60 min at 37-42°C. Reactions are kept either at 4°C or at -20°C until further use.

Real time RT- PCR

Real-time reverse transcriptase (RT) polymerase chain reaction (PCR) is a widely specific, sensitive and reproducible used method to quantify the initial amount of the template (Real Time PCR). Two important findings made possible the discovery of real-time PCR: First, the Taq polymerase has, apart from its polymerase activity, a 5′-3′ exonuclease activity. Second, dual labelled fluorogenic oligonucleotide probes have been created which emit fluorescence upon cleavage. The first real-time PCR created, the TaqMan assay, combines these two principles. The method is based on the 5'-3' exonuclease activity of the Taq DNA polymerase, which results in the cleavage of fluorescent dye-labelled probes during PCR. The TaqMan® probe has a fluorescent dye usually on the 5′ base called reporter dye (R), and a quenching dye (Q) typically at its

3′ base. While the probe is intact, the close proximity of the reporter and quencher prevents emission of any fluorescence (Figure 3.2). During reaction, TaqMan® probe bound to the template is cleaved by the TaqMan DNA polymerase 5' exonuclease activity and its degradation frees the reporter dye from the quenching activity. Fluorescence emitted by the reporter dye increases in each cycle proportionally to probe cleavage that, in turn, is proportional to the amount of formed PCR product (amplicon production, the amplified target sequence). The cleavage occurs only in the case the probe is annealed to the target therefore the origin of the detected fluorescence is specific amplification. At each PCR cycle, we can monitor the accumulation of amplified products by detecting the increase of reporter dye fluorescence. In real time RT-PCR, the amplicon formation is observed as the reaction goes on and during each PCR cycle with a continuous observation and not at the end of the reaction like in conventional PCR methods.

Reactions are characterized by the point in time during cycling when amplification of a PCR product is first detected rather than the amount of PCR product accumulated after a fixed number of cycles. The higher the starting copy number of the target sequence, the sooner a significant increase of fluorescence is detectable. A representative amplification plot, that is the plot of fluorescence signal against cycle number is shown in Figure 3.3. Initially, during the first cycles of amplification the fluorescence signal does not change much (baseline for amplification plot). An increase of fluorescence above the baseline indicates the detection of

accumulated PCR product. A fixed fluorescence threshold can be set above the baseline. The threshold cycle (Ct) is the cycle at which exceeds the chosen fluorescence and the plot of the log of initial target copy number for a set of standards versus Ct is a straight line. Ct values are very reproducible in replicates when the threshold is picked in the exponential phase of PCR. Indeed, in the exponential phase, reaction components are not limiting and replicate reactions exhibit uniform and reproducible results. As the reaction components become limiting, the rate of target amplification decreases until a plateau is reached and there is no more increase (or little increase) in PCR product. On the other hand, the amount of PCR product observed at the end of the reaction is very sensitive to slight variations in the reaction components. In order to quantify the amount of target in unknown samples, Cts are measured and a standard curve is needed to determine a starting copy number. In each quantitative PCR method, specific errors are introduced due to minor differences in starting amount of RNA differences in efficiency of cDNA synthesis and PCR amplification Therefore, a reliable quantitative RT-PCR method requires correction of these experimental variations. At the present, this is most often performed by normalization to a housekeeping gene. However, the choice of the most suitable gene should be made for each experimental condition. In particular, the housekeeping gene should not be modulated in the experimental setting. For this reason GADPH, β-actin or ribosomal RNA (rRNA) (i.e. 18S rRNA) are used as housekeeping,

indeed their expression is less likely to vary under conditions that change the levels of mRNA expression.

Because the 18S rRNA does not have a poly-A tail, cDNA synthesis using oligo-dT should not be used if such a transcript will be used as a normalizer. Normalization is performed by subtracting, for each reaction, the Ct value of the housekeeping gene, that is expected to be higher expressed than the target, from the Ct value of the gene of interest obtaining the "Delta Ct" or "ΔCt".

ΔCt = Ct(target) - Ct (normalizer)

For comparison among the samples and for relative gene expression comparisons, the ΔCt value of each experimental sample is compared to the ΔCt value of the control sample. The comparative "DeltaDeltaCt" calculation is:

ΔΔCt = ΔCt (experimental sample) - ΔCt (sample control)

The fold induction/reduction value is then determined by the following formula:

Fold difference = $(2^{-\Delta\Delta Ct})$.

SYBR Green methodology. As the real time RT-PCR has become more used, other methodologies have been developed to directly measure PCR

product accumulation by fluorescence emission. For example, minor groove binding dyes, such as SYBR Green 1. SYBR Green 1 is a non-sequence specific fluorescent agent method that is based on double-stranded DNA binding dye chemistry (Figure 3.4). Since SYBR Green 1 does not bind to single stranded DNA and it is possible to quantify amplicon production. When in solution, SYBR Green exhibits little fluorescence but upon binding to double-stranded DNA it emits a strong fluorescent signal. During the amplification process, it is possible that a non-specific amplification takes place or that primer-dimer complexes are formed and in these cases a fluorescent signal may account for non-specific amplification. Therefore, to verify the specificity of the PCR reaction, follow-up assays have been developed: identification of the melting point and the dissociation curve. Moreover, negative controls are included as well: No Amplification Controls (NAC, a minus-reverse transcriptase control) and No Template Controls (NTC, a minus sample control). In optimised conditions, a sharp peak at the melting temperature of the amplicon should be obtained, and the NAC and NTC should not generate significant fluorescent signal indicating that the products are specific, and that SYBR Green fluorescence is a direct measure of accumulation of the product of interest. In the presence of a dissociation curve with series of peaks it cannot be discriminated between specific and non-specific reaction products.

3.24 Microscopy

3.24.1 Transmission electron microscopy

The transmission electron microscope is a type of microscope that uses beam of electrons to observe the specimen. The beam of electrons, emitted by a high voltage electron emitter situated at the top of the microscope column, pass through the sample and through a series of magnifying magnetic lenses, to finally reach the viewing screen where they are ultimately focused. To change the magnification and focal point of the image, different lenses can be used; the contrast and resolution of the image can be changed as well by operating through apertures-holes on the microscope column. The electron beam size that passes through the microscope column can be limited by one of these accesses. Another aperture serves to condense and maintain the coherence of the electron beam (condenser aperture). The objective aperture controls image contrast and is located below the sample just after the objective lens. In the column, a very high vacuum is created in order to reduce the electron beam interactions with air. Energy produced by an electric source (~2500K) superheats a tungsten wire that emits electrons. Liquid nitrogen is used to cool down the column for easier removal of water vapour. Electrons are sent down the microscope column, across the sample, lenses, and apertures. The lenses are magnetic coils that, set on a specific electron wavelength, focus and direct the electron beam. As it passes through the lens (three primary lenses) the electron beam is split. The topmost lens is

the objective and it magnifies and focuses the image. Then there is the intermediate lens that controls the magnification of the image and the diffraction pattern. Finally, the projector lens that focuses and projects the image onto the imaging surface. The image can be visualized on a screen: where fewer electrons were transmitted through the sample, in thicker or denser zones, the image shows dark areas whereas areas where the sample was thinner or less dense more electrons are transmitted through and the image appears more light. The power of resolution of electron microscopy depends on the lens-systems and on sample preparation method. Usually, in modern microscopes the resolution power ranges from 0.2 - 0.3 nm and magnify up to 180,000x.

3.24.2 Light microscopy

A microscope is an instrument that allows observation of objects that are too small to be seen by the naked eye. In order to visualise objects, the light microscope uses light and magnifying lenses. Most microscopes in current use are known as compound microscopes, where a magnified image of an object is produced by the objective lens, and this image is magnified by a second lens system, the ocular, for viewing. Thus, final magnification of the microscope depends on the magnifying power of the objective lens times the magnifying power of the ocular lens. Objective magnification powers range from 4x to 100x whereas ocular magnification ranges are typically 8x -12x. As a result, a standard microscope provides a final magnification range of 40x up to 1000x. Each objective lens consists of

six or more pieces of glass that combine to produce a clear image of an object. The use of lenses with a spatial curvature on their surface allows correcting spatial aberration due to the interaction of light with the glass (refraction). The objective lenses in most microscopes are achromatic, but for high resolution imaging with white light it is preferable to use totally corrected apochromatic lenses or fluorite lenses.

The light is an essential factor in producing good image. It should be bright and uniform across the field. The best way to illuminate the specimen is to use another lens, the condenser. The condenser sits directly beneath the specimen and focuses the light beam and maximizes the intensity and controls the uniformity of illumination. The condenser diaphragms, allows for an increase in contrast. After passing through the specimen on the stage the light enters the objective.

The fine detailed observation requires an imaging system capable of providing spatial details across a small distance. Resolution is defined as the ability to distinguish two objects as separate entities. Resolution is best when the distance separating the two tiny objects is small. Resolution depends on wavelength of the light, and the light gathering power of the objective (numerical aperture, NA) and condenser lenses.

3.25 Immunofluorescence technique and confocal microscopy

Immunofluorescence is the labeling of antigens with fluorescent dyes. This technique is often used to visualize subcellular distribution of biomolecules of interest. Immunofluorescent labeled samples are studied using a fluorescence microscope or by confocal microscopy.

Most commonly, immunofluorescence employs two sets of antibodies: a primary antibody is used against the antigen of interest; a subsequent, secondary, dye-coupled antibody is introduced that recognizes the primary antibody. In this fashion, several primary antibodies recognizing various antigens but sharing a common constant region may be recognized by a single dye-coupled antibody. Typically this is done by using antibodies made in different species. This allows re-use of the difficult-to-make dye-coupled antibodies in multiple experiments. In some cases, it is advantageous to use primary antibodies directly labelled with a fluorophore. This direct labelling decreases the number of steps in the staining procedure and, more importantly, often avoids cross-reactivity and high background problems.

A *fluorescence microscope* is a light microscope used to study properties of organic or inorganic substances using fluorescence and phosphorescence instead of, or in addition to, reflection and absorption. In most cases, a component of interest in the specimen is specifically labeled with a fluorescent molecule called a fluorophore. The specimen is

illuminated with light of a specific wavelength (or wavelengths), which is absorbed by the fluorophores, causing them to emit longer wavelengths of light (of a different color than the absorbed light). The illumination light is separated from the much weaker emitted fluorescence through the use of an emission filter. Typical components of a fluorescence microscope are the light source (Xenon or Mercury arc-discharge lamp), the excitation filter, the dichroic mirror (or dichromatic beamsplitter), and the emission filter (Figure 3.5 A). The filters and the dichroic are chosen to match the spectral excitation and emission characteristics of the fluorophore used to label the specimen.

The *confocal microscope* is an optical imaging technique used to increase micrograph contrast and/or to reconstruct three-dimensional images by using a spatial pinhole to eliminate out-of-focus light or flare in specimens that are thicker than the focal plane (Figure 3.5 B). The principle of confocal imaging was patented by Marvin Minsky in 1957. In a conventional (i.e., wide-field) fluorescence microscope, the entire specimen is flooded in light from a light source. Due to the conservation of light intensity transportation, all parts of specimen throughout the optical path will be excited and the fluorescence detected by a photodetector or a camera. In contrast, a confocal microscope uses point illumination and a pinhole in an optically conjugate plane in front of the detector to eliminate out-of-focus information. Only the light within the focal plane can be detected, so the image quality is much better than that of wide-field images. As only one point is illuminated at a time in confocal microscopy,

2D or 3D imaging requires scanning over a regular raster (i.e. a rectangular pattern of parallel scanning lines) in the specimen. The thickness of the focal plane is defined mostly by the square of the numerical aperture of the objective lens, and also by the optical properties of the specimen and the ambient index of refraction.

3.26 Haemocytometer

The most practical method for routine determination of the number of cells that are in suspension is a direct count on a haemocytometer. Burker's chamber is a counting chamber that has been modified to a final single block of glass. This haemocytometer contains two chambers, each of which is divided into 9 squares of 1 mm^2 (Figure 3.6). In use, a cover glass is supported 0.1 mm above the ruled areas. Thus, when the chamber is filled, the volume of cell suspension over each square is 0.1 mm^3, $1x10^{-4}$ cm^3 or about $1x10^{-4}$ ml. Therefore, the number of cells per 1 ml is calculated by multiplying the number of cells counted in the square by 10^4. The total cell number of the original cell suspension can be obtained by multiplying by the volume in ml and by the appropriate dilution factor.

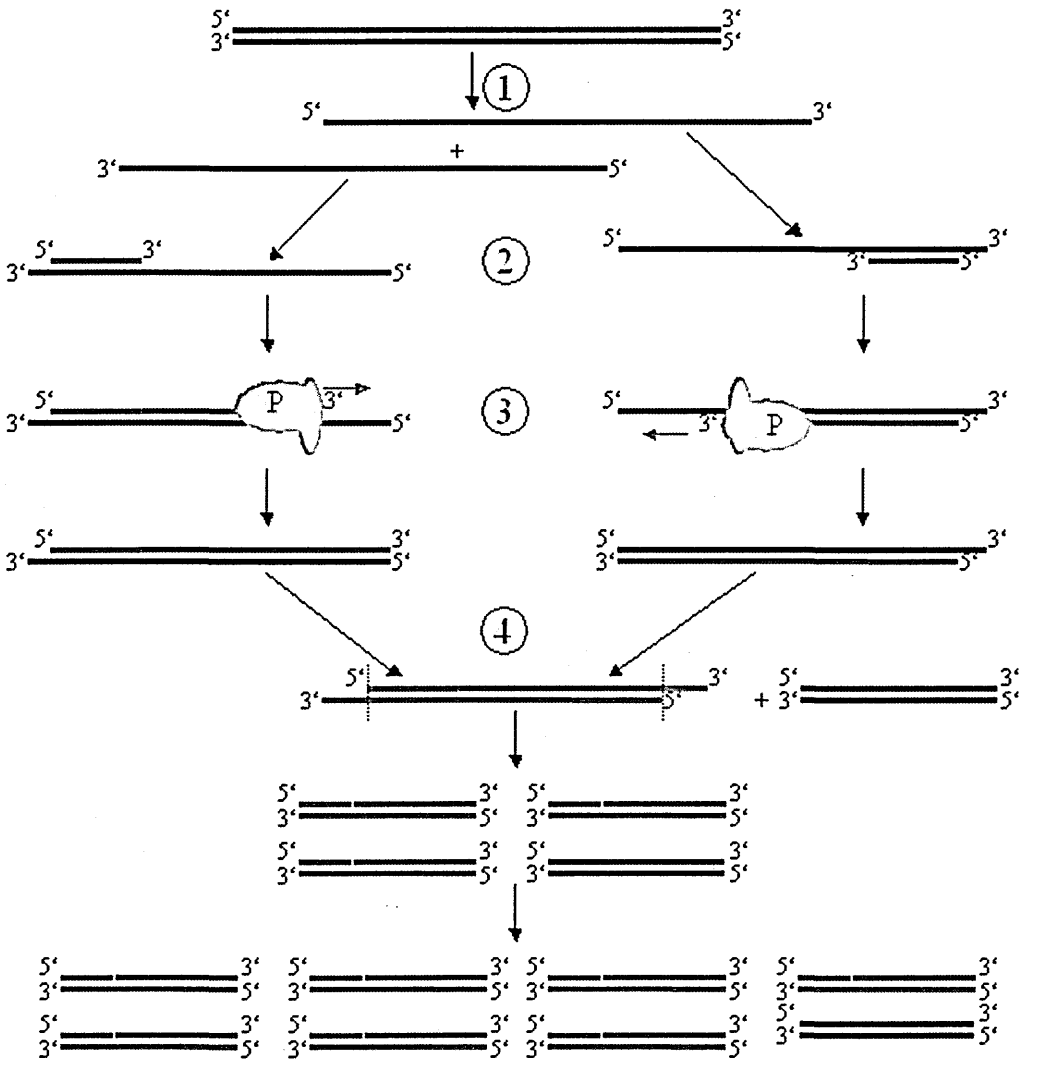

Figure 3.1 *Schematic drawing of the PCR cycle*
(1) Denaturation; (2) Hybridization; (3) Extension by Polymerase (P); (4) The first cycle is complete. The two resulting DNA strands make up the template DNA for the next cycle, thus doubling the amount of DNA duplicated for each new cycle.

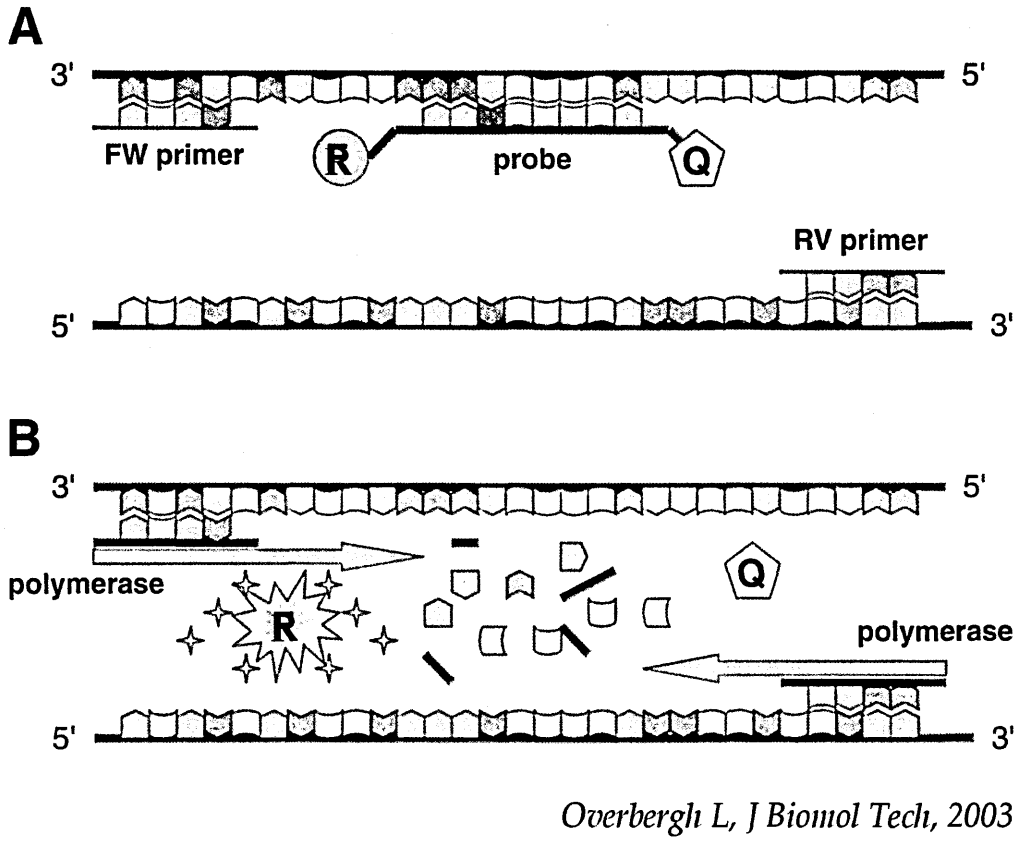

Figure 3.2 *Schematic representation of the TaqMan principle*

(A) Annealing of primers and probe to the target gene. The probe is still intact and fluorescence emission does not occur. **(B)** Extension phase of the PCR reaction. The probe is cleaved by the 5'-3' exonuclease activity of the Taq polymerase, allowing fluorescence emission. FW, forward; RV, reverse; R, reporter dye; Q, quencher dye.

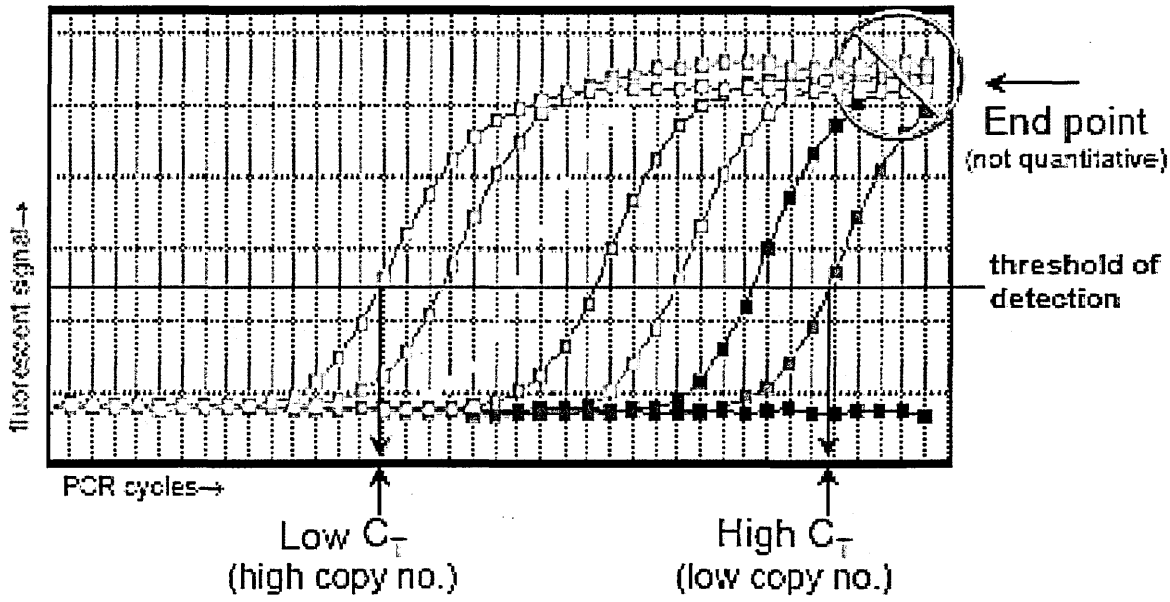

Figure 3.3 *Real time RT-PCR amplification plot*

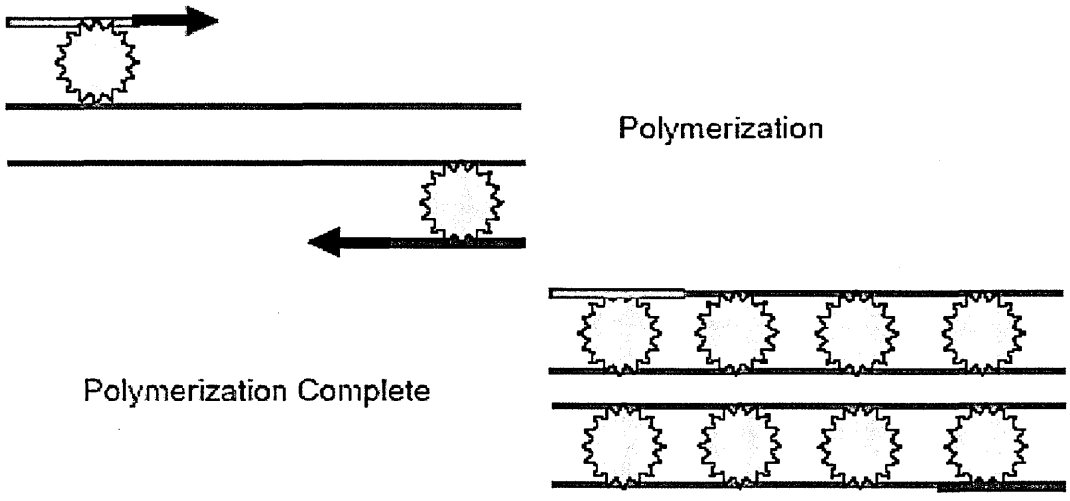

Figure 3.4 *SYBR Green dye assay chemistry*
SYBR Green does not bind to single stranded DNA. It is a minor groove binding dye and emits strong fluorescence signal upon binding to double-stranded DNA.

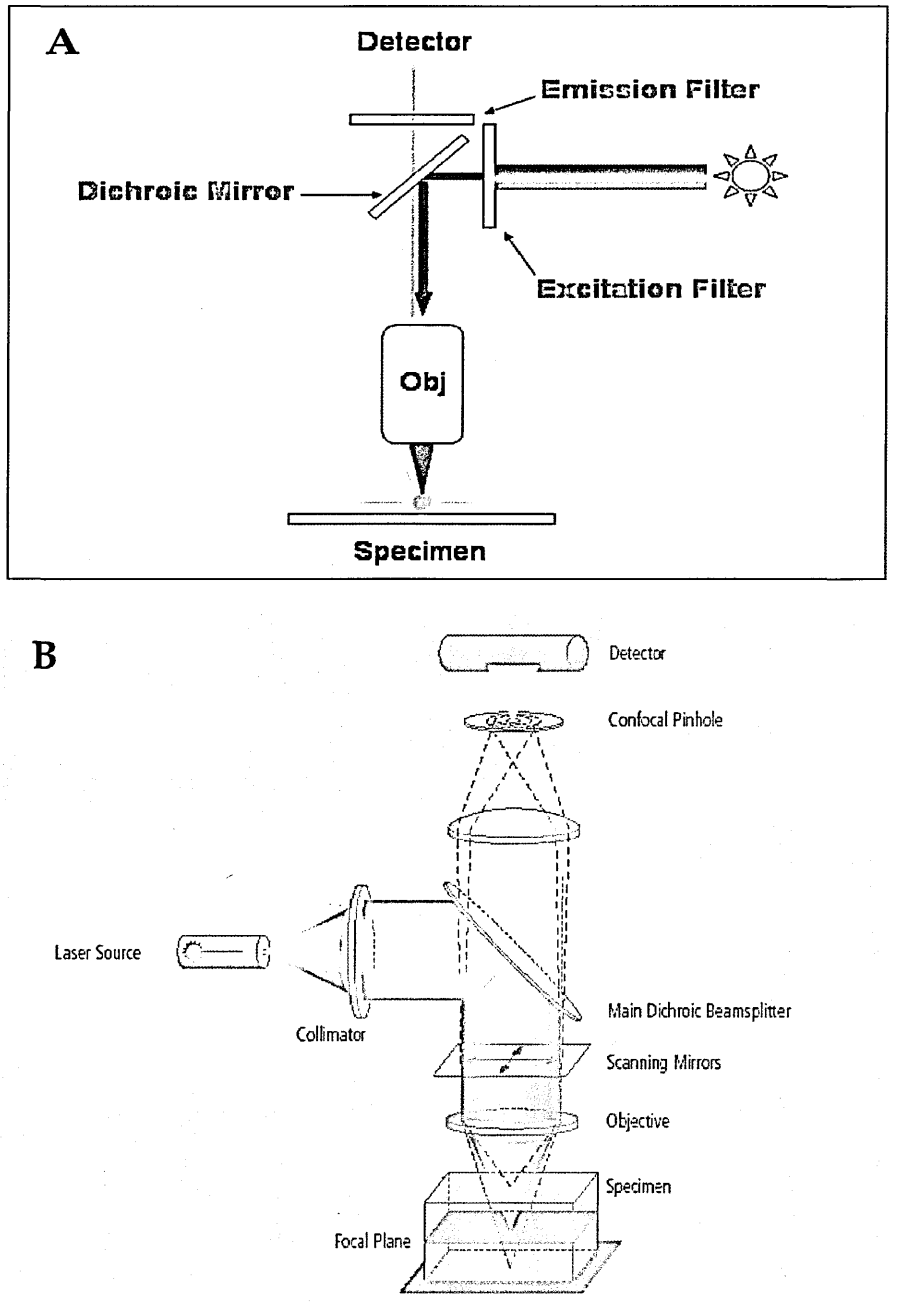

Figure 3.5 *Schematic representation of a fluorescent (A) and a laser scanning (B) microscope*

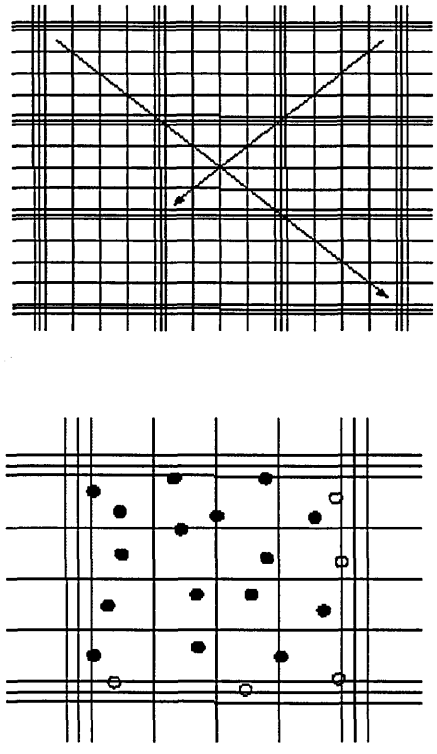

Figure 3.6 *Schematic representation of the Burker's chamber grid*

RESULTS

CHAPTER 4

RENOPROTECTIVE EFFECT OF HUMAN CORD BLOOD-MESENCHYMAL STEM CELLS IN EXPERIMENTAL MODEL OF ACUTE KIDNEY INJURY

4.1 Introduction

Acute kidney injury (AKI) is a common and costly complication of critical illness associated with adverse clinical outcomes. Recent studies have demonstrated that the incidence of AKI varies between 15% and 80% in the intensive care unit (ICU) (James Seminar *et al.,* 2011) and the mortality, associated with this syndrome, has remained unchanged worldwide during the past 30 years (Shah *et al.,* 2006). To accelerate renal regeneration and to improve survival, several pharmacological strategies have been approached. However, translational research efforts have yielded disappointing results (Thadhani *et al.,* 1996; Kelly *et al.,* 2000; Grino *et al.,* 1994; Haug *et al.,* 1993). In the attempt to create innovative interventions for the cure of AKI, recent studies have tested stem cell-based treatment to repair acutely damaged organs by virtue of stem cell's peculiar properties of tropism and regenerative capability (Aejaz *et al.,* 2007; Daley *et al.,* 2008; Lindvall *et al.,* 2006; Laflamme *et al.,* 2005; Little *et al.,* 2006; Morigi *et al.,* 2006). In this context, mesenchymal stem cells (MSCs) represent an attractive tool because of their beneficial effects on tissue repair in experimental models of myocardial infarction (Nagaya *et al.,* 2004; Tang *et al.,* 2006), neurologic disease (Lindvall *et al.,* 2006; Torrente *et al.,* 2008) and more recently, in experimental acute kidney injury {Morigi *et al.,* 2004; Imberti *et al.,* 2007; Morigi *et al.,* 2008; Herrera *et al.,* 2004). MSCs were originally isolated from bone marrow (BM) (Pittinger *et al.,* 1999; Bianco *et al.,* 2008), but similar cell

populations have been found to be harboured in other tissues including umbilical cord blood, placenta, adipose tissue, peripheral blood, dermal connective tissue, deciduous teeth, dermis and skeletal muscle (Liu *et al.*, 2009). Studies by our group have documented that murine (Morigi *et al.*, 2004; Imberti *et al.*, 2007) and human (Morigi *et al.*, 2008) MSCs of bone marrow origin infused in mice with cisplatin-induced AKI promoted renal functional and structural recovery by stimulating renal resident cells to proliferate, via local release of the growth factor IGF-1 (Imberti *et al.*, 2007). Consistently, studies in the ischemia/reperfusion rat model have documented that BM-MSCs were beneficial via paracrine production of mitogenic, anti-apoptotic and vasculotropic factors (Togel *et al.*, 2005; Togel *et al.*, 2007). To date, the most common source of MSCs has been the bone marrow, but collection of bone marrow from the patient is an invasive procedure and, in addition, it has been demonstrated that the number, differentiation potential and life span of these stem cells decline with age (D'ippolito *et al.*, 1999). Therefore, the search for alternative sources of MSCs in the clinical perspective to cure AKI is of significant value. Recent studies have identified cord blood (CB) as an alternative reservoir, readily available and extremely rich of stem and progenitor cells (Flynn *et al.*, 2007; Sanchez-Ramos *et al.*, 2006; Erices *et al.*, 2000; Lee O *et al.*, 2004). Some studies have documented that human cord blood mesenchymal stem cells (hCB-MSCs) possess morphological characteristics, immunophenotypic markers and differentiation ability similar to hBM-

MSCs {Kern *et al.*, 2006; Panepucci *et al.*, 2004; Wagner *et al.*, 2005). With regard to the gene expression profile, the two MSC lineages share all of the most expressed transcripts, but hCB-MSCs express higher levels of genes involved in matrix remodelling and angiogenesis while hBM-MSCs express genes related to osteogenesis {Panepucci *et al.*, 2004). Human CB-MSCs also deserve attention for their capability to synthesize growth factors (Flynn *et al.*, 2007; Wagner *et al.*, 2005; Liu *et al.*, 2005) with anti-apoptotic and regenerative effects on renal tubular cells, the key target of AKI. Early clinical evidence documented safety and efficacy of CB progenitor cell infusion in humans for the treatment of haematological (Edwards *et al.*, 2007; Pinto *et al.*, 2008; Locatelli *et al.*, 2008) and neurological disorders (Sanchez-Ramos *et al.*, 2006; Escolar *et al.*, 2005) and Buerger's disease (Kim *et al.*, 2006). So based on these evidences the aim of this study was to investigate whether hCB-MSCs could ameliorate acute renal dysfunction and attenuate tubular injury. To this aim, we set up an acute kidney injury model in immunodeficient mice, by using cisplatin, an anti-tumour drug accompanied by a high incidence of nephrotoxicity (Arany *et al.*, 2003).

4.2 Murine model of acute kidney injury

In order to evaluate the renoprotective effect of CB-MSCs of human origin, we set up an experimental model of AKI induced by

cisplatin in immunodeficient NOD-SCID mice. Renal function, assessed as blood urea nitrogen (BUN), and body weight were evaluated at different time intervals from cisplatin treatment. Previous experiments (Morigi *et al.*, 2008) indicated that subcutaneous injection of cisplatin (12.7 mg/kg) resulted in a significant increase in serum BUN at 2-3 days, which peaked at 4-5 days and stabilized at high values until animal death (Table 1). In parallel, animals lost weight starting at 1 day from cisplatin treatment. Mice also invariably died within 5-7 days after receiving cisplatin (Table 1).

Renal injury was assessed by histological analysis. By light microscopy, no significant changes were detectable in the kidney taken 1 day after cisplatin injection, the time at which hCB-MSCs were infused. Focal and severe tubular changes were observed at day 4 (Figure 4.1 *b*). Changes in proximal tubules were revealed by the loss of brush border, cytoplasmic vacuolization, flattening and loss of the epithelial cells, PAS-positive droplets, nuclear fragmentation and luminal debris. Hyaline casts and cell loss were prominent. The most damaged tubules displayed areas of apparent denudation of the tubular basement membranes (Figure 4.1 *b*). Histology of kidney control mice is shown in Figure 4.1 *a*.

Electron microscopy analysis of all cisplatin treated mice revealed at day 1 after cisplatin, mitochondrial swelling, loss of brush border, and myelin figures in tubular epithelial cells. Necrotic epithelial cells with detachment from the underlying basement membrane were

prominent in kidneys taken at day 4 after cisplatin injection (Figure 4.2 *b* and *c*). Moreover, we observe peritubular capillary changes consisting of endothelial cell swelling, cytoplasmic vacuolisation, nuclear degeneration and detachment occasionally associated with polymorphonuclear (PMN) cell infiltration (Figure 4.2 *c*).

4.3 Characterization of human cord blood-mesenchymal stem cells

Eighty human cord blood (CB) units were processed and 54% generated MSC cultures. Human CB-MSCs isolated by lineage-depletion represented 1-2% of the initial cell population and grew up to 10 passages maintaining their typically spindle-shaped morphology (Figure 4.3 *a*). The ability of hCB-MSCs to differentiate into osteocytes and chondrocytes, after exposure to appropriate inductive media, was observed by the extended area of mineralization and by secretion of cartilage-specific proteoglycans (Figure 4.3 *b* and *c*). At variance, hCB-MSCs were not able to differentiate into adipocytes as also previously described {Kern *et al.*, 2006; Manca *et al.*, 2008; Rebelatto *et al.*, 2008).

The expression of cell-surface antigens was evaluated by flow cytometry on all hCB-MSC cultures. As shown in Table 2, human CB-MSCs expressed mesenchymal stem cells markers as CD105, CD44, CD90, CD73, SSEA4 and HLA class I, while were weakly positive for CD56, desmin, CK3/12, CK19, BB9 and negative for HLA class II,

LNGFR and VE-Cadherin. These cells also expressed CD146, alpha SMA (Table 2) but not CD34, CD45 and NG2, which altogether characterize a multipotent adult stem cell population consistent with a perivascular/pericyte-like phenotype (Crisan *et al.*, 2008).

By RT-PCR analysis we observed that human CB-MSCs expressed some genes as RUNX1 and OCT4 that characterize the undifferentiated stem cell state (Figure 4.4), while the cells were negative for PPAR-2, VE-Cadherin, ABCG2, REX1, FGF4, hTERT, SOX2, PAX7 and renal genes such as PAX2 and GATA3.

4.4 Human cord blood-mesenchymal stem cells protect cisplatin-treated mice from renal impairment

With the aim to study the renoprotective effect of hCB-MSCs, we injected $5x10^5$ cells into the tail vain of immunodeficient mice with AKI induced by cisplatin. We infused saline or hCB-MSCs in NOD-SCID mice, one day after cisplatin treatment, when tubular ultrastructural changes were already present. As reported in Figure 4.5, hCB-MSC treatment strongly protected renal function at 3 and 4 days, as reflected by the significant lower BUN values (hCB-MSCs 3d, 39.90±6.23 mg/dl and hCB-MSCs 4d, 50.83±8.09 mg/dl) in respect to cisplatin-treated mice injected with saline (saline 3d, 98.60±6.83 mg/dl and saline 4d, 124.46±4.71 mg/dl).

Subsequently, we studied whether renal function improvement induced by hCB-MSC treatment, was associated with the preservation of renal structure. Renal histology of mice with cisplatin-induced AKI on day 4, showed focal and severe tubular damage, characterized by tubules affected by necrosis and luminal casts (Figure 4.1*b* and Table 3). Conversely, in kidneys of cisplatin-mice injected with human CB-MSCs, we observed an evident attenuation of renal tubular damage, as reflected by the significant reduction of necrotic tubules and casts (Figure 4.6 *a* and Table 3). Electron microscopy analysis at 4 days of kidneys of cisplatin-mice that received hCB-MSCs showed much less severe ultrastructural changes in proximal tubules and in peritubular capillaries (Figure 4.6 *b*).

Kunter et al. documented in a progressive model of mesangioproliferative nephritis, a long-term maldifferentiation of rat BM-MSCs into glomerular adipocytes. In order to exclude this side effect, we investigated in the renal tissue of cisplatin mice, whether hCB-MSCs were able to give rise to cell types of non-renal origin or adipocytes. (Kunter *et al.*, 2007). Histological analysis of renal tissue of cisplatin-mice at 40 days, revealed no sign of abnormal phenotype.

4.5 Localization of human cord blood-mesenchymal stem cells in cisplatin-treated mice

To better explain the therapeutic effect of hCB-MSCs on renal tissue damaged by cisplatin, we evaluated whether the renoprotection was associated with recruitment of the injected stem cells into the renal parenchyma. For this purpose, hCB-MSCs were labelled, before their *in vivo* infusion, with a red fluorescence cell membrane linker, PKH-26. Sections of renal tissue of cisplatin-treated mice at 4 days were analysed, and the frequency of PKH-26-positive cells averaged 2 ±0.4 /10^5 renal cells. Labelled hCB-MSCs were predominantly localized in peritubular areas (Figure 4.7 *a*), and only few cells were found in the context of tubular epithelium and glomeruli. The percentage (expressed as number of PKH-26 cells per total PKH-26 cells) in each compartment of PKH-26 positive CB-MSCs, averaged 83±11% in peritubular areas, 5±5% in tubules, and 12±12% in glomeruli. The human origin and the ability of hCB-MSCs to engraft the damaged tissue were further confirmed by the positive staining for the human nuclear antigen HNA, in murine renal tissue (Figure 4.7 *b*).

We evaluated whether hCB-MSCs were able to engraft other organs, as liver, lung and spleen. Analysis of sections of these tissues, showed rare or absent PKH-26 positive hCB-MSCs suggesting a local recruitment of stem cells through renotroprism at site of injury.

4.6 Human cord blood-mesenchymal stem cells prolong survival of cisplatin-treated mice

The high responsiveness of NOD-SCID mice to cisplatin toxicity, allowed us to test whether hCB-MSC treatment could affect survival, the key clinical outcome in AKI. As shown in Figure 4.8, 14% of cisplatin-mice given saline was alive at 7 days, but all mice died within 9 days (Figure 4.8). Human CB-MSC infusion remarkably prolonged animal survival ($p<0.001$), indeed at 9 days, when all mice died in the saline group, 86% of cisplatin-mice injected with hCB-MSCs were alive. The percentage of living animals given hCB-MSCs remained unchanged until 14 days, when the experiment was stopped.

We previously described in the same experimental model (Morigi *et al.*, 2008), the effect of hBM-MSCs on lifespan of AKI mice. As shown in Table 4, we compared hCB-MSC efficacy to decrease animal mortality, with that of hBM-MSCs. Infusion of hCB-MSCs improved animal survival to a more significant extent than hBM-MSCs in respect to cisplatin mice given saline (hCB-MSCs, $p<0.004$ and hBM-MSCs, $p<0.05$ vs untreated cisplatin mice). By comparing renal function of mice infused with hCB-MSCs or hBM-MSCs, we found that serum BUN levels in cisplatin-mice treated with hCB-MSCs at 4 days were lower than those found in hBM-MSC-treated mice although a statistical significance was not achieved (hCB-MSCs, 58±7 and hBM-MSCs, 76±8

vs saline, 122±7 mg/dl; hCB-MSCs, $p<0.01$ and hBM-MSCs, $p<0.01$ vs saline).

4.7 Human cord blood-mesenchymal stem cells prevent cisplatin-induced tubular damage and apoptosis

Oxidative damage, play a central role in cisplatin-induced renal injury because cisplatin generates active oxygen species such superoxide anion and hydroxyl radicals and stimulates renal lipid peroxidation (Matsushima *et al.*, 1998). To assess oxidative damage we used nitrotyrosine staining because peroxynitrite, the reaction product of nitric oxide and superoxide anion, has been taken as key oxidant species involved in the direct nitration of tyrosine residues causing protein oxidation (Viappiani *et al.*, 2006). As shown in Figure 4.9, cisplatin-mice with AKI exhibited at 4 days a high expression of nitrotyrosine in tubules of both the cortex and the medulla, in respect to control mice (Figure 4.9, Table 5). An evident reduction of nitrotyrosine staining within the tubules were detected in hCB-MSC transplant recipients (Figure 4.9, Table 5), indicating that human stem cells protect renal tissue from oxidative damage.

In vitro and *in vivo* models of cisplatin–induced toxicity, have demonstrated that apoptosis is partially responsible for tubular cell loss (Bonegio *et al.*, 2002); therefore, we have studied whether hCB-MSC

treatment could exert an anti-apoptotic action on renal cells in mice with AKI. Cells positive for TUNEL staining were quantified in kidney sections at day 4 by confocal laser scanning microscopy. In normal control kidneys, a low number of apoptotic cells were detected, while in renal tissues of mice treated with cisplatin we observed a significant increase ($p<0.01$) in the number of TUNEL-positive cells (Figure 4.10 *a*). Human CB-MSC infusion significantly ($p<0.01$) reduced apoptotic cells, compared to cisplatin-mice given saline (Figure 4.10 *a*), suggesting an anti-apoptotic effect of the stem cell therapy in mice with AKI. Representative images of kidney sections demonstrating TUNEL-positive cells are shown in Figure 4.10 *b,c* and *d*.

4.8 Human cord blood-mesenchymal stem cells induce Akt phosphorylation leading to tubular cell proliferation in cisplatin-treated mice

Based on the evidence that the serine-threonine kinase Akt is a key enzyme involved in survival signals (Datta *et al.*, 1999), we performed experiments to study whether the renoprotective effect of hCB-MSCs was mediated by an activation of Akt, represented by Akt phosphorylation (pAkt). Kidney sections of cisplatin-mice with AKI at 4 days, showed a decrease of tubular phosphorylation of Akt in respect to control animals (Figure 4.11 *a*). Human CB-MSC treatment significantly

increased the number of tubuli positive for pAkt at 4 days in respect to cisplatin-mice given saline (Figure 4.11 *a*), suggesting a role of stem cells in the activation of prosurvival pathways.

The effect of engrafted hCB-MSCs on tubular cell regeneration was explored by analysing the proliferation marker PCNA (proliferating cell nuclear antigen) in cisplatin-treated mice. The quantification of PCNA positive cells on renal tissues is shown in Figure 4.12. In normal control kidneys at 4 days, low number of PCNA positive cells was detected, reflecting a low level of tubular cell regeneration. In cisplatin-mice with AKI, the number of PCNA positive cells, slightly increased as compared to controls, indicating a spontaneous weak induction of the reparative process. The treatment with hCB-MSCs strongly induced the DNA synthesis suggesting a powerful induction of tissue recovery ($p<0.01$ vs control and $p<0.05$ vs saline).

4.9 *In vitro* expression of growth factors and cytokines by human cord-blood mesenchymal stem cells

In order to better explain the capability of hCB-MSCs to create a pro-regenerative environment able to promote tissue repair, we performed *in vitro* experiments, by co-culturing hCB-MSCs with cisplatin-treated proximal tubular cells (HK-2 cells) in a transwell

system for 24 h. We focussed on the production of growth factors with vasculotropic, anti-apoptotic and renoprotective effect as FGF, HB-EGF, VEGF and HGF. In particular, we observed that HGF significantly ($p<0.05$) increased in the supernatants of co-cultured cells with respect to those of damaged HK-2 cells (FGF: 2-, HB-EGF: 7-, VEGF: 5- and HGF: 12- fold increase). Given the robust expression of HGF observed in *in vitro* experiments, we further studied the expression of this growth factor *in vivo*. The serum levels of HGF at 4 days in cisplatin-mice receiving hCB-MSCs, were significantly increased in respect to mice given saline (hCB-MSCs, 779±120 vs saline, 382±63 pg/ml, $p<0.05$). In parallel, kidneys of animals treated with human CB-MSCs showed a significant up-regulation of HGF mRNA expression at 4 days (hCB-MSCs, 1.8±0.1 fold increase vs saline, 1±0.03, $p<0.0001$).

Inflammatory cytokines produced by renal parenchymal cells, as IL-1β and TNFα, are responsible of cisplatin-induced renal toxicity (Ramesh *et al.*, 2002; Zhang *et al.*, 2007). To determine whether hCB-MSC ability to create a regenerative environment, is also due to anti-inflammatory properties, proximal tubular cells pre-exposed to cisplatin were co-cultured with human CB-MSCs for different time intervals. We observed at 24 and 72h, a significant increase of the release of IL-1β and TNFα by proximal tubular cells exposed to cisplatin, as shown in Figure 4.13. Human CB-MSCs added to the co-culture system, significantly inhibited the cytokine production during

time (Figure 4.13), showing a modulator effect of stem cells on the production of inflammatory cytokines.

4.10 Conclusions

With the purpose to study the effect of hCB-MSCs, we first of all set up a model of acute kidney injury induced by the nephrotoxic drug, cisplatin. The results presented in Chapter 4 of this thesis can be summarized as follows. We found that:

- Injection of hCB-MSCs ameliorated both renal function and tubular cell injury prolonging animal survival.
- Transplanted hCB-MSCs localized in peritubular area acting though a paracrine mechanism.
- Human CB-MSCs markedly inhibited oxidative stress, apoptosis and inflammation, activating the pro-survival factor Akt and inducing proliferation of renal tubular cells.
- Human CB-MSCs produced a large amount of regenerative growth factors, inhibiting the release of inflammatory cytokines produced by damaged proximal tubular cells.

4.11 Discussion

Mesenchymal stem cells have been most widely used in experimental models because of their plasticity, paracrine action and immunologic properties (Caldas *et al.,* 2011). The most common and studied source of MSCs has been the bone marrow. We previously documented the renoprotective effect of human bone marrow derived-mesenchymal stem cells in the treatment of experimental AKI (Morigi *et al.,* 2008). Data also demonstrated that stem cell transplantation could prolong animal survival and identified a suitable stem cell population for the possible use in future studies of cell therapy for human AKI (Morigi *et al.,* 2008). However, aspirating bone marrow from the patients is an invasive procedure and it has been demonstrated that the number, the efficacy and the plasticity of these stem cells decrease with age of the donor (D'Ippolito *et al.,* 1999). Therefore, the search for alternative sources of MSCs easily accessible is of significant value. Recent researches have revealed that cord blood is an alternative and extremely rich reservoir of stem cells with mesenchymal stem cell phenotype (Flynn *et al.,* 2007; Sanchez-Ramos *et al.,* 2006; Erices *et al.,* 2000; Lee *et al.,* 2004). As cell therapy, MSCs of cord blood origin may be helpful in patients for whom the availability of autologous functional stem cells is limited, as patients treated with chemotherapy, which could compromise the availability of mesenchymal cells in bone marrow (Perry, 1969). Moreover, hCB-MSCs have many advantages

partly related to the immaturity of newborn cells compared with adult stem cells and their being prone to escape immune rejection (Sanchez Ramos *et al.*, 2006; Pinto *et al.*, 2008; Locatelli *et al.*, 2008). For these reasons, human umbilical cord blood in the last years has been 'banked' and used as a source of marrow repopulating stem cells in patients with bone marrow deficit or inborn errors of metabolism (Sanchez Ramos *et al.*, 2006; Pinto F *et al.*, 2008; Locatelli *et al.*, 2008; Escolar *et al.*, 2005) resulting safe and efficacious. On this basis, we studied the capability of hCB-MSCs to regenerate the kidney in acute kidney injury.

We observed that hCB-MSCs expressed typical markers of mesenchymal stem cells, also expressed by hBM-MSCs. Moreover, we documented absence of adipogenic differentiation by hCB-MSCs (Kern *et al.*, 2006; Manca *et al.*, 2008; Rebellato *et al.*, 2008), while no differences in the osteogenic and chondrogenic differentiation capacity were detected between hBM-MSCs and CB-MSCs.

The transplantation of hCB-MSCs attenuated severe epithelial cell injury and improved renal function. Moreover, the present study shows for the first time, evidence that hCB-MSCs remarkably prolong animal survival to a more significant extent than hBM-MSCs.

Subsequently, once established the capacity of hCB-MSCs to repair renal injury, we then addressed the mechanisms possibly implicated in the renal reparative processes. Functional protection by hCB-MSCs can be the consequence of the capacity of stem cells to engraft the damaged kidney. Consistent with this possibility, the

present data documented that hCB-MSCs were able to reach and survive in kidneys of NOD-SCID mice with AKI. We observed that in the renal tissue of cisplatin mice, hCB-MSCs almost exclusively localized in the peritubular areas and not in the context of the tubular epithelial lining, excluding that hCB-MSCs acted by transdifferentiation into proximal tubular cells. Rare or no cells were found in other organs including liver, lung and spleen. These data support the hypothesis that hCB-MSCs act through a paracrine effect once engrafted in the damaged kidney. This may happen via the local release of soluble factors (Imberti *et al.*, 2007; Togel *et al.*, 2005; Togel *et al.*, 2007) and/or via the stimulation of target cells to produce growth factors with regenerative potential for renal cells. In this respect, some studies have documented that hCB-MSCs in culture constitutively produce pro-survival, anti-inflammatory and mitogenic proteins (Liu *et al.*, 2005; Kogler *et al.*, 2005). Of interest, we have observed that growth factors as FGF, HB-EGF, VEGF, and particularly HGF, produced by hCB-MSCs in co-culture with cisplatin-damaged tubular cells, create a regenerative environment for tubular repair. We assume that the combination of several growth factors, locally produced by hCB-MSCs, could act in concert to create a proregenerative environment, in a more effective way than any single growth factor treatment.

Another significant finding of the present thesis was the identification of intracellular pathways of reno-protection conferred by hCB-MSCs. Oxidative damage induced by ROS and cell apoptosis, is

consequence of renal tubular toxicity of cisplatin. Previous studies have demonstrated the favourable effect of anti-oxidants and ROS scavengers, in limiting programmed cell death (Lieberthal *et al.*, 1996) and reducing tubular cell oxidative damage. Our data, that demonstrate an improvement of oxidative damage and cell apoptosis induced by hCB-MSC treatment, are consistent with idea that growth factors as HGF prevent oxidative stress in damaged tissues through their ability of normalizing anti-oxidant enzyme activity and mitochondrial function. (Garcia-Fernandez *et al.*, 2008; Okada *et al.*, 2004; Li *et al.*, 2006; Ueda H 2001, 41}. On the other hand, the above growth factor together with VEGF have also the ability to activate the pro-survival factor Akt (Kumar *et al.*, 200), a kinase that plays a critical role as mediator of the phosphoinositide-3 kinase (PI3K)-survival signals (Datta *et al.*, 1999). Phosphorylated Akt counteracts cell apoptosis by phosphorylating and inhibiting the pro-apoptotic member of the Bcl-2 family, Bad (Zha *et al.*, 1996) and the mitochondrial caspase-9 (Yang *et al.*, 2001; Zhou *et al.*, 2000). Recent findings have documented that blockade of PI3K-γ-Akt pathway markedly accelerated renal tubular cell apoptosis and death leading to poor prognosis for mice with cisplatin–induced AKI (Kuwana *et al.*, 2008). Our data confirmed the relevance of Akt in renal repair, showing that phosphorylation of Akt markedly decreased at 4 days, the time point with higher tubular damage and apoptosis, in renal tissue of cisplatin-mice. Conversely, treatment with hCB-MSCs, significantly increased pAkt positive tubuli

and possibly activated downstream targets known to modulate cell proliferation and survival (Datta *et al.*, 1999). All these protective effects were associated with a marked induction of proximal tubular cell proliferation as evidenced by the high number of cells positive for PCNA staining, after hCB-MSC injection.

Finally, we explored *in vitro*, the possible anti-inflammatory action of hCB-MSCs. Previous study in experimental and human AKI, have described an up-regulation of TNF-α and IL-1 β that are considered crucial in cisplatin-induced nephrotoxicity, as they act synergistically to stimulate the production of other cytokines and chemokines (Ramesh *et al.*, 2002; Zhang *et al.*, 2007; Devarajan *et al.*, 2006). Moreover, some researches have described an over-expression of E-selectin and ICAM-1, induced by TNF-α and IL-1 β, which promote inflammatory leukocyte migration (Takada *et al.*, 1997). Here, we have documented the anti-inflammatory effect of hCB-MSCs co-cultured with proximal tubular cells damaged by cisplatin, which enhanced the production of these pro-inflammatory cytokines. We observed a marked reduction of TNF-α and IL-1 β when hCB-MSCs were co-cultured with proximal tubular cell damaged by cisplatin.

In summary, our findings indicate that hCB-MSCs promote kidney regeneration and prolong animal survival when transplanted in a mouse model of AKI. These effects seem to be mediated by a paracrine action of hCB-MSCs on tubular cells, which are able to proliferate as a result of activation of pro-survival and anti-apoptotic

pathways. In the context of regenerative medicine, hCB-MSCs could be considered an option for autologous transplantation in human with AKI.

Table 4.1: Time course of body weight, BUN and survival in NOD-SCID mice injected with cisplatin

	0	1	2	3	4	5	7 days
Body Weight (g)	21±0.6	20±0.4	18±0.4	16±0.8	16±0.6	15±1	dead
BUN (mg/dl)	25±0.6	26±0.9	46±12	81±10	*123±19	*132±9	dead
Survival (%)	100	100	100	100	100	60	0

Data for body weight and BUN are expressed as mean ± SE (n=5).
*$p<0.01$ vs day 0 (ANOVA, followed by Tukey Cicchetti test)
BUN: blood urea nitrogen.

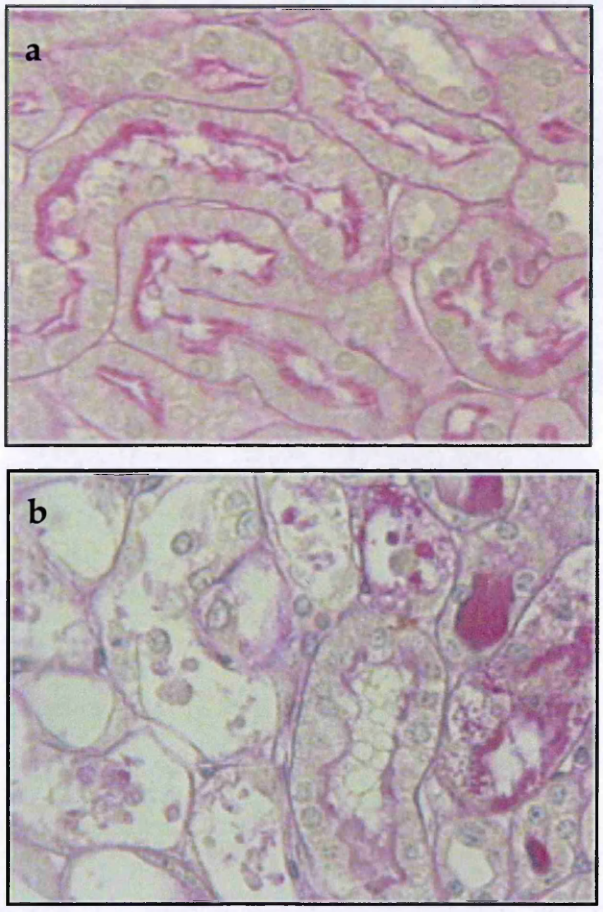

Figure 4.1: Renal histology of NOD-SCID control mice (a) or cisplatin-treated mice sacrificed after 4 days (b). Original Magnification, x400.

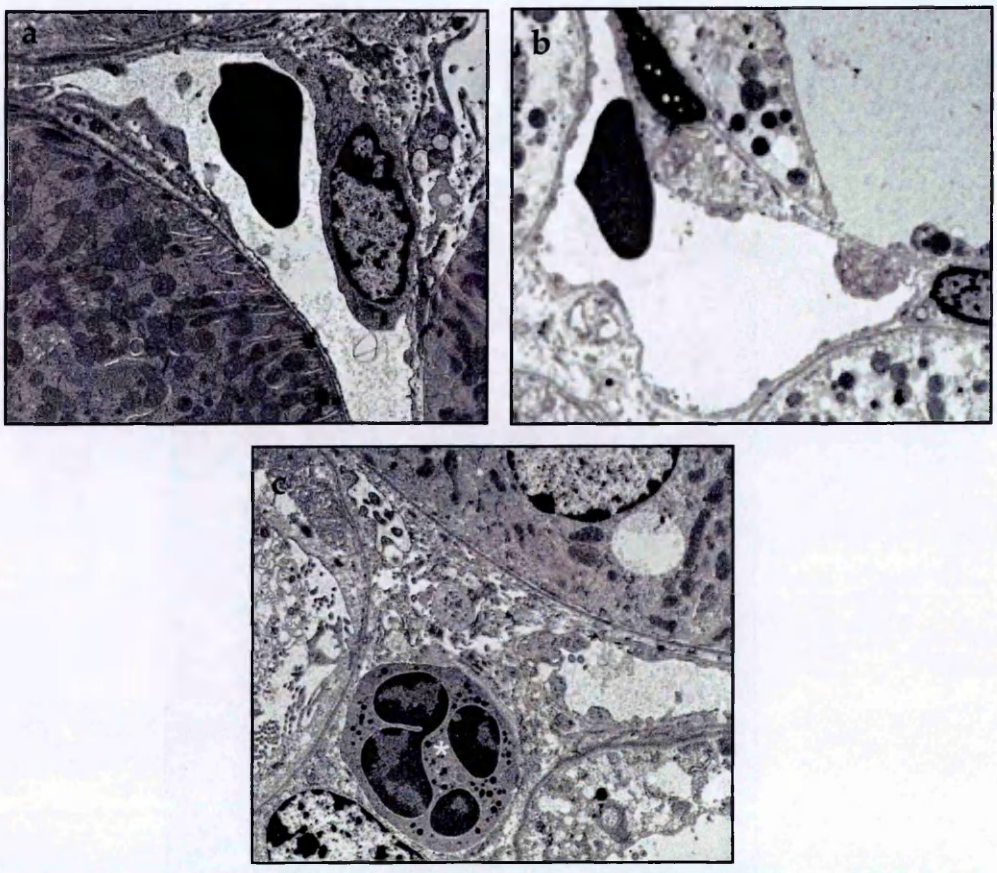

Figure 4.2: Ultrastructural changes in NOD-SCID mice 4 days after cisplatin injection.

(a) Ultrastructural analysis of normal proximal tubular cells. (b, c) Ultrastructural changes of tubular epithelium and peritubular capillaries in mice given saline at 4 days after cisplatin treatment. Note the presence of PMN cell infiltration (*) in cisplatin mice at 4 days (c) . Original magnification, X2,800.
PMN: polymorfonuclear.

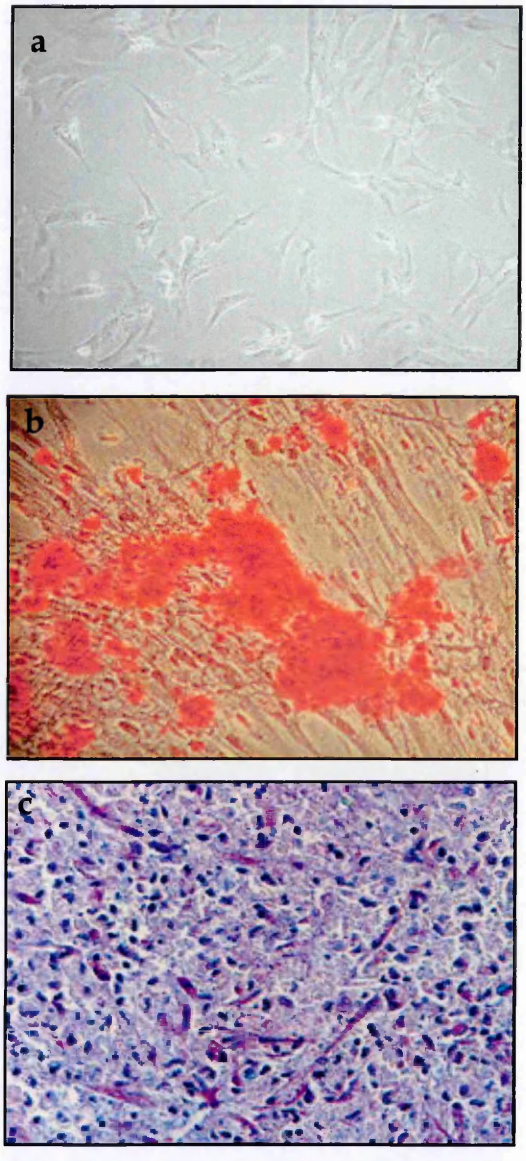

Figure 4.3: Human CB-MSC morphology and differentiation

(a) Representative image of hCB-MSCs with typical spindle shape morphology. Original magnification, x10. (b) Differentiation of hCB-MSCs toward osteocytes evidenced by Alizarin Red staining. (c) Proteoglycans stained by Alcian Blue reveals chondrogenic potential of hCB-MSCs. Original magnification, x20.

Table 4.2: Immunophenotype of hCB-MSCs

Antigens	Percentage of fluorescent cells
CD105	55.3 ± 37.3
CD44	62.8 ± 35.1
CD90	90.4 ± 6.9
CD73	98.8 ± 1.9
SSEA4	3.9 ± 4.1
HLA cl I	96.6 ± 2.9
CD146	35 ± 18.1
α SMA	53.5 ± 19.6
CD56	2.1 ± 1.4
DESMIN	0.4 ± 0.3
CK3/12	1 ± 0.7
CK19	2.6 ± 1.7
BB9	0.2 ± 0.1

Data are expressed as mean ± SD
hCB-MSCs: human cord blood mesenchymal stem cells.

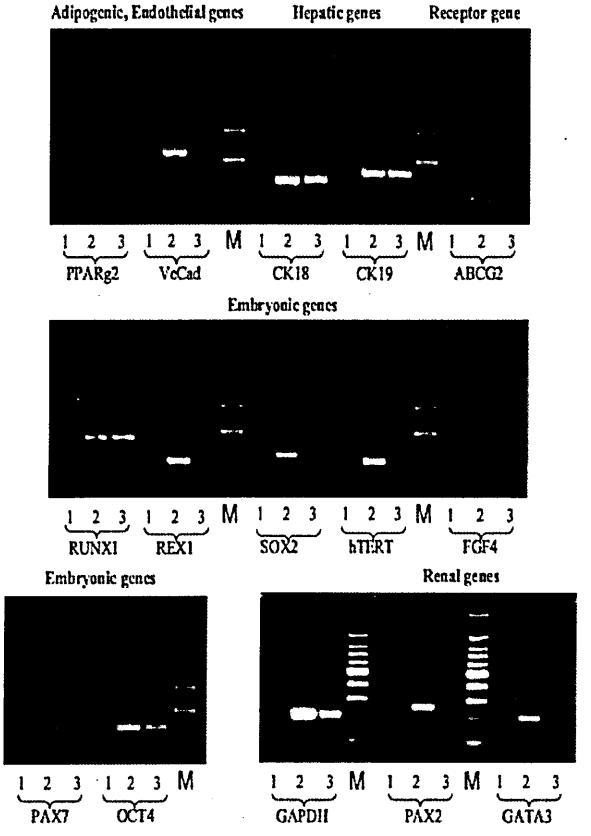

Figure 4.4: Molecular profile of hCB-MSCs.

Human CB-MSCs were characterized for the expression of several adipogenic, endothelial, hepatic, receptor, embryonic and renal genes. lane1: negative control; lane 2: positive control; lane 3 hCB-MSCs; lane M: marker

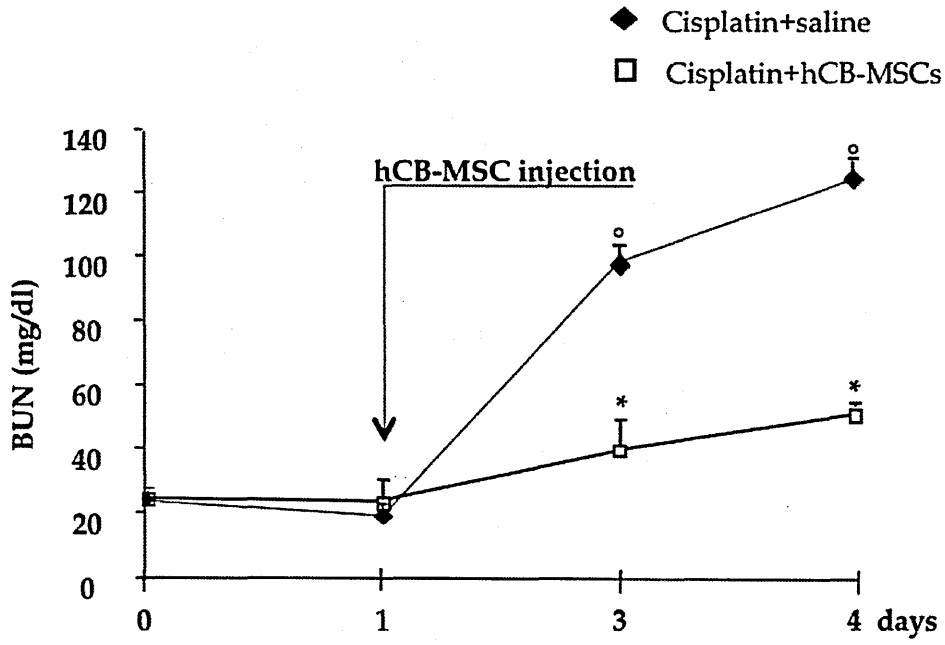

Figure 4.5: Effect of hCB-MSCs treatment in NOD-SCID mice with AKI

Cisplatin was administered to female NOD-SCID mice. Impairment of renal function was observed in cisplatin treated-mice injected with saline (◆ n=12). Human CB-MSCs treatment protected cisplatin treated-mice from renal damage (□ n=11). °$p<0.01$ vs day 0 (basal); *$p<0.01$ vs cisplatin+saline at the same time (ANOVA, followed by Tukey Cicchetti test)

Table 4.3: Effect of hCB-MSCs on renal histological changes at 4 days

	Casts (n casts/HPF)	**Tubular Necrosis** (n necrotic tubuli/HPF)
Control (n=5)	0	0
Cisplatin+saline (n=12)	2.98±0.8	1.79±0.4
Cisplatin+hCB-MSCs (n=11)	0.13 ±0.04*	0.09 ±0.03*

Data are mean ± SE. * $p<0.01$ vs Cisplatin+saline (Wilcoxon-Mann-Whitney test)
HPF: high-power field
hCB-MSCs: human cord blood mesenchymal stem cells.

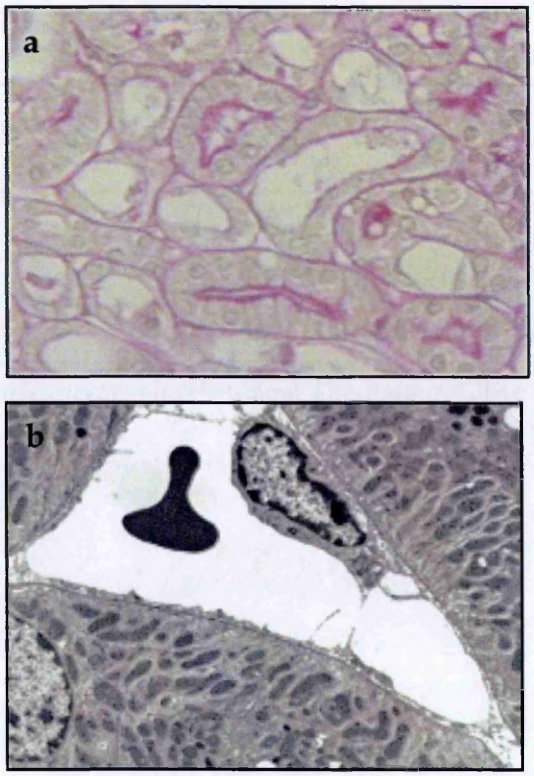

Figure 4.6: Human CB-MSC infusion protects mice with AKI from tubular injury.

(a) Renal histology of cisplatin-treated mice receiving hCB-MSCs at 4 days. Original Magnification, x400. (b) In cisplatin-treated mice injected with hCB-MSCs, at 4 days, tubular cell and peritubular capillary injury is markedly attenuated. Original Magnification, x2800.

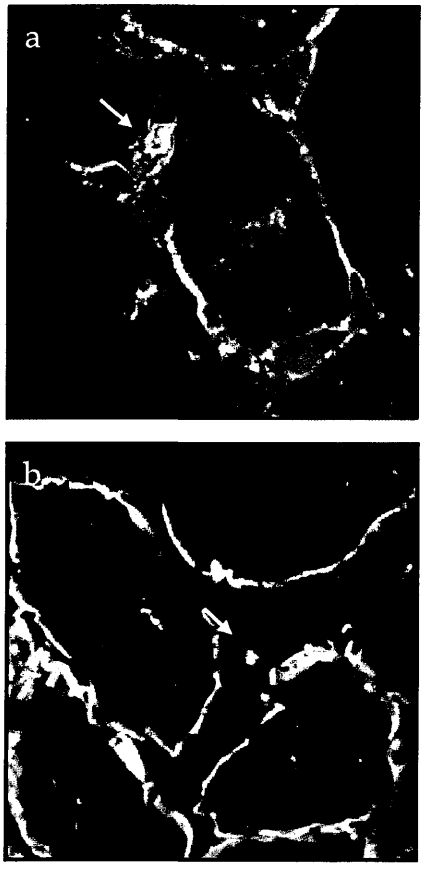

Figure 4.7: Localization of hCB-MSCs in renal tissue.

(a) Representative micrograph of kidney tissue from cisplatin-treated mouse injected with PKH-26-labeled hCB-MSCs at 4 days. PKH-26 fluorescent hCB-MSCs were predominantly localized in peritubular area (arrow). Original magnification, x630.
(b) Representative micrograph of hCB-MSCs in a kidney section of cisplatin-mouse at 4 days stained for human antigen HNA (red). Original magnification, x630.

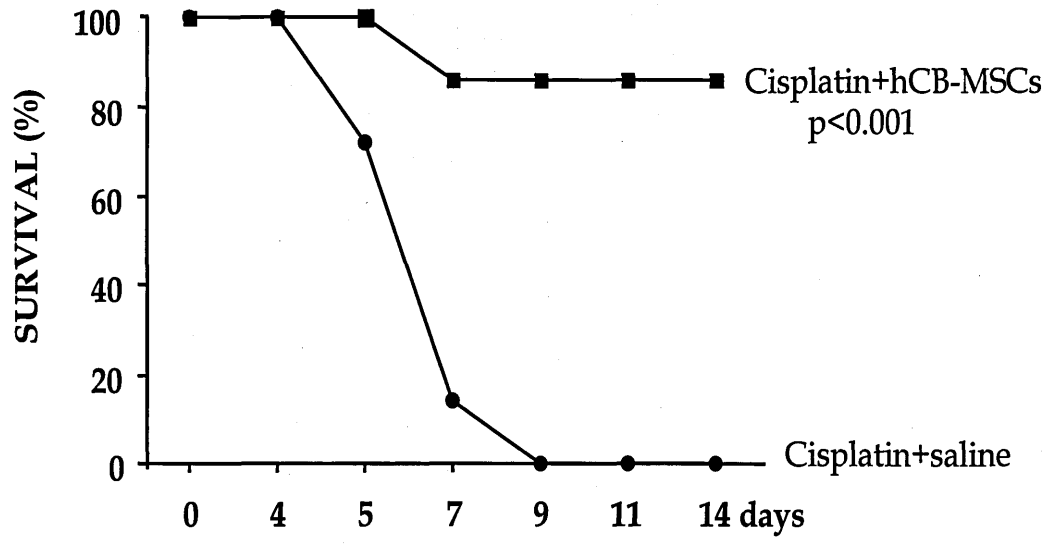

Figure 4.8: Human CB-MSC treatment prolongs survival in mice with AKI.

All mice receiving saline (n=7) died within 9 days. At this time, 86% of NOD-SCID mice given hCB-MSCs (n=7) survived. $p<0.001$ vs Cisplatin+saline (Log Rank test)

Table 4.4: Comparison between hCB-MSCs and hBM-MSCs on survival of cisplatin-treated mice

	SURVIVAL (%)					
	0d	**4d**	**5d**	**7d**	**9d**	**14d**
Cisplatin+saline (n=8)	100	100	50	0	0	0
Cisplatin+hCB-MSCs (n=10)	100	100	100	80	70	70*
Cisplatin+hBM-MSCs (n=10)	100	100	90	30	30	30**

**p<0.004 hCB-MSCs vs Cisplatin+saline;
*p<0.05 hBM-MSCs vs Cisplatin+saline (Kaplan-Meier analysis and Log-Rank Test)
hCB-MSCs, human cord blood mesenchymal stem cells
hBM-MSCs, human bone marrow mesenchymal stem cells

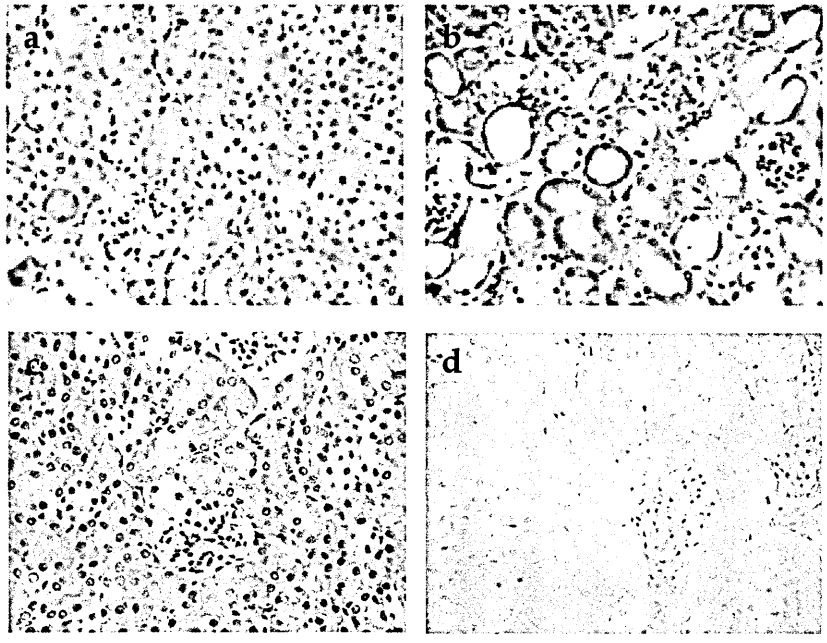

Figure 4.9: Human CB-MSC treatment reduces renal oxidative damage in mice with AKI at 4 days.

Representative images of nitrotyrosine staining (dark brown), a marker of peroxynitrite, in renal tissue of control (a) and cisplatin-mice receiving saline (b) or hCB-MSCs (c). Representative image of negative control (d). Original magnification 400x.

Table 4.5: Effect of hCB-MSCs on nitrotyrosine expression

	Tubuli of Cortex (score)	**Tubuli of Medulla** (score)
Control (n=4)	0.60±0.06	0.39±0.03
Cisplatin+saline (n=4)	1.69±0.10°	1.29±0.08°
Cisplatin+hCB-MSCs (n=4)	0.98±0.21*°	0.54±0.11*

Data are mean ± SE. * $p<0.05$ vs Cisplatin+saline; ° $p<0.05$ vs Control (Kruskal Wallis test).
hCB-MSCs, human cord blood mesenchymal stem cells.

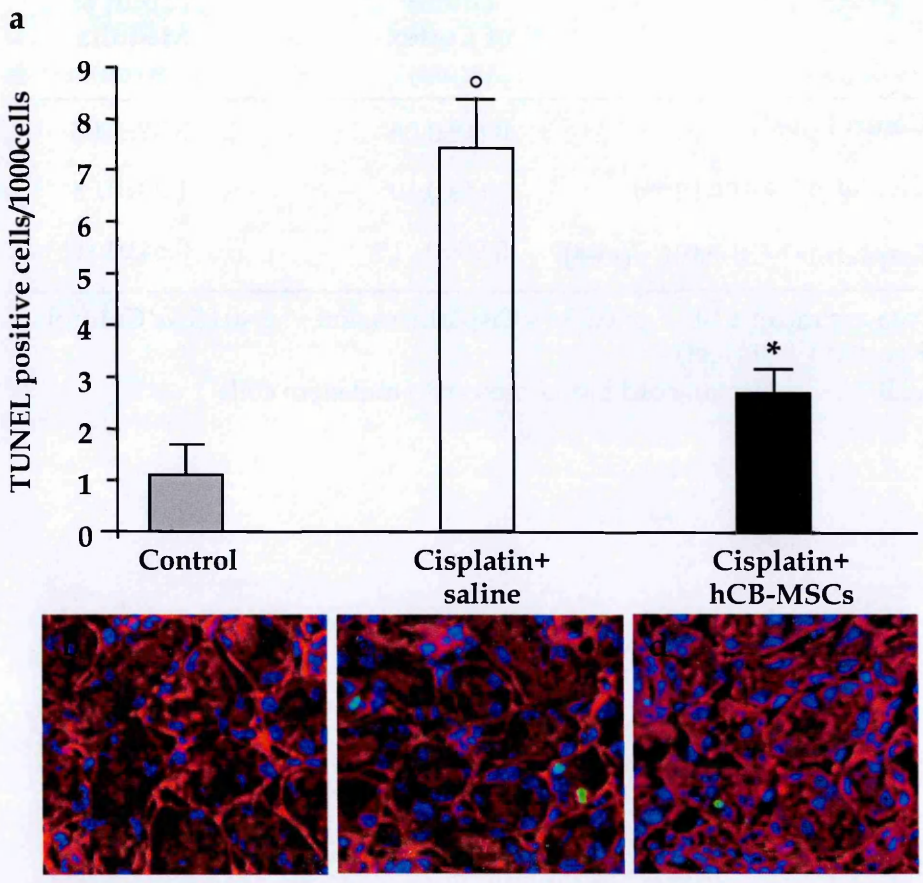

Figure 4.10: Human CB-MSC treatment reduces tubular cell apoptosis in mice with AKI at 4 days.

(a) TUNEL positive cells quantified in kidney sections of control mice (n=5), cisplatin-treated mice given saline (n=5) or hCB-MSCs (n=5). °$p<0.01$ vs Control; *$p<0.01$ vs cisplatin+saline (ANOVA, followed by Tukey Cicchetti test). (b-d) Representative images of kidney sections labelled with TUNEL (green), rhodamine-labeled lectin LCA (red) and DAPI (blue). Original magnification 630X.

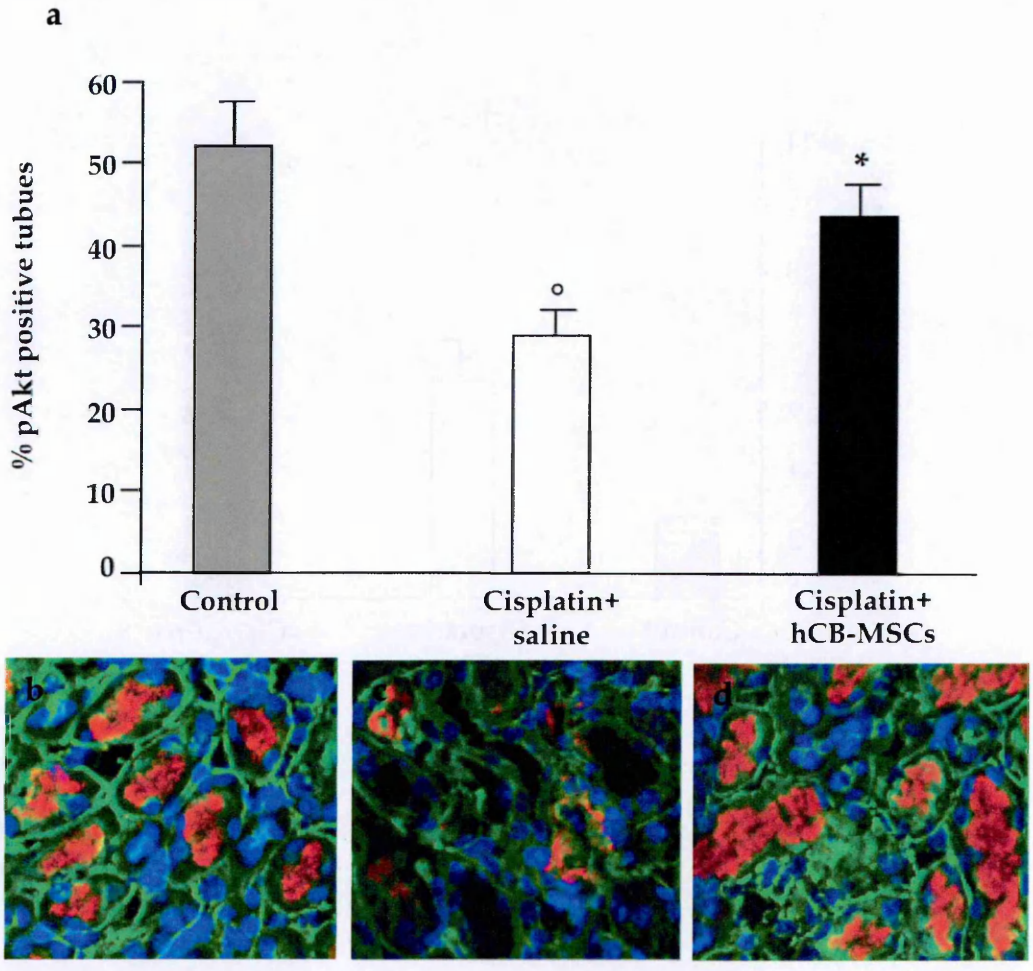

Figure 4.11: Human CB-MSC treatment enhances Akt phosphorylation in mice with AKI at 4 days.

(a) Percentage of pAkt positive tubules in control mice (n=3), cisplatin-treated mice receiving saline (n=3) or hCB-MSCs (n=3). °p<0.01 vs control; *p<0.01 vs cisplatin +saline (ANOVA, followed by Tukey Cicchetti test). (b-d)Representative images of p-Akt staining (red) with FITC-labelled lectin WGA (green) and DAPI (blue) in kidney sections of control, cisplatin-mice given saline or hCB-MSCs. Original magnification 630X.

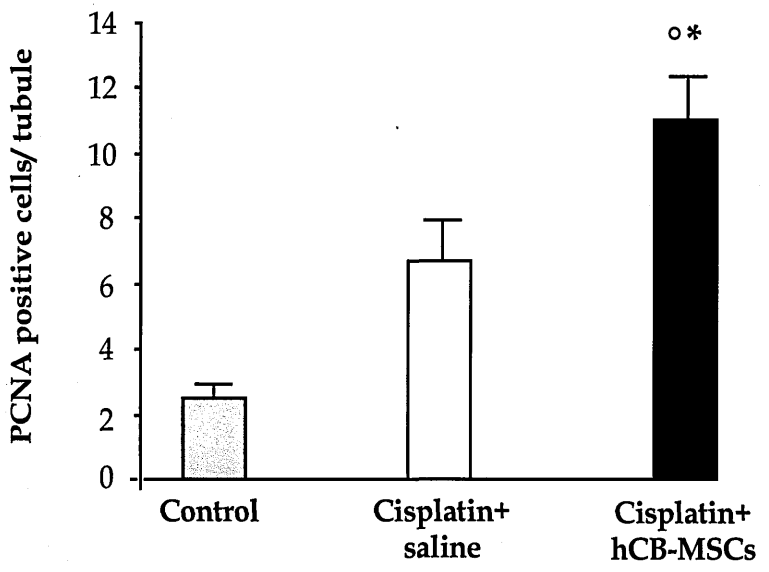

Figure 4.12: Effect of hCB-MSCs at 4 days on tubular cell regeneration after cisplatin

Quantification of PCNA-positive tubular cells.°$p<0.01$ vs control; *$p<0.05$ vs cisplatin +saline (ANOVA, followed by Tukey Cicchetti test). Control (n=6), Cisplatin+saline (n=6), Cisplatin+hCB-MSCs (n=6).

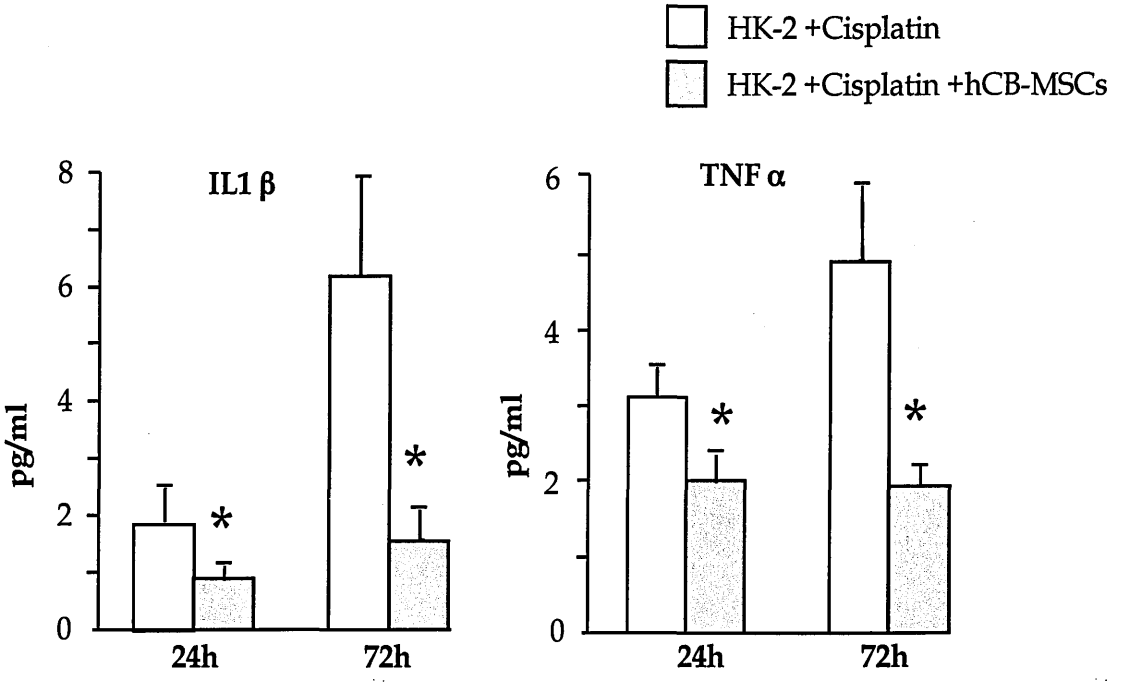

Figure 4.13: Anti-inflammatory effect of hCB-MSCs.

HK2 were incubated with cisplatin (8 μM) for 6 hours and after drug withdrawal, were co-cultured with hCB-MSCs for 24-72 hours.*$p<0.05$ vs HK-2 cells +cisplatin (unpaired t test). The experiments were performed in triplicate and repeated 3 times.

CHAPTER 5

HUMAN AMNIOTIC FLUID STEM CELLS FOR THE TREATMENT OF ACUTE KIDNEY INJURY IN MICE

5.1 Introduction

Stem cell transplantation has been proposed as innovative and efficacious strategy for the treatment of acute organ injury (Choi *et al.*, 2011; Shimada *et al.*, 2011; Morigi *et al.*, 2006; Iwatani *et al.*,2010). In this context, mesenchymal stem cells (MSCs) represent an attractive tool because of their regenerative effects in experimental model of myocardial infarction (Nagaya *et al.*, 2004), in experimental acute kidney injury (Morigi *et al.*, 2008; Herrera *et al.*, 2004) and in neurologic disease like multiple sclerosis, amyotrophic lateral sclerosis and Parkinson (Torrente *et al.*, 2008). The most common source of MSCs is the bone marrow (BM). Our group has documented that transplanting either murine or human BM-MSCs in mice with AKI improved tubular injury and ameliorated renal function through local release of growth factors as IGF-1. All resulted in such a protective effect by prolonging animal survival (Morigi *et al.*, 2004; Imberti *et al.*, 2007, Morigi *et al.*, 2008). Moreover, an alternative source of MSCs it has been identified in the cord blood (CB) (Flynn *et al.*,2007; Sanchez-Ramos *et al.*, 2006; Erices *et al.*, 2000; Lee *et al.*, 2009). Human CB-MSCs share with human BM-MSCs morphological characteristics, immunophenotypic markers and differentiation ability (Kern *et al.*, 2006; Panepucci *et al.*, 2004; Wagner *et al.*, 2005). Human CB-MSCs also displayed renoprotection, which resulted in prolonged animal survival as compared to hBM-MSCs (Morigi *et al.*, 2010).

Possible restrictions to using human BM and CB-MSCs may rest on both their limited capacity to grow in culture and difficulties to isolate enough cells from different cord blood samples. Finally, the capacity of MSCs to differentiate toward renal phenotype during kidney repair seems to be very confined (Togel *et al.*, 2005; Morigi *et al.*, 2008; Duffield *et al.*, 2005). Alternative sources of stem cells with higher plasticity would add value to the employment of cell therapy in terms of supporting tissue regeneration via direct cell replacement.

Embryonic stem cells are the most plastic stem cell population with unlimited capacity for self-renewal, however their employment is limited by ethical and safety issues (Hyun *et al.*, 2010; Odorico *et al.*, 2001). Similarly, induced-pluripotent stem cells derived from de-differentiation of somatic cells, still have limitations in regard to their clinical applicability because of teratogenic potential (Takahashi *et al.*, 2006).

On the other hand, in the last 10 years, the placenta, the fetal membranes (i.e. amnion and chorion) and amniotic fluid have also been extensively investigated as a non-controversial source of stem cells with multilineage differentiation potential and immunomodulatory properties (De Coppi *et al.*, 2007; Cananzi *et al.*, 2009). In particular, in the amniotic fluid, a population of stem cells with intermediate characteristics between embryonic and adult stem cells has been isolated (De Coppi *et al., 2007*). Indeed, human amniotic fluid stem (hAFS) cells, immunoisolated for c-Kit, express embryonic and

mesenchymal stem cell markers including Oct-4 and SSEA-4, CD29, CD44, CD73, CD90 and CD105 (De Coppi *et al., 2007*). Human AFS cells can be readily expanded and reach 250 population doubling - characteristics of embryonic cells- while at the same time retaining stable telomerase length and normal karyotype between early and late passages (De Coppi *et al., 2007*). Clonal hAFS cell lines can differentiate into cells of the three embryonic germ layers and possess advantageous behaviours including the feeder independence and non-tumorigenicity at late passages, when injected into immunodeficient mice (De Coppi *et al., 2007*). For all these reasons, hAFS cells with high differentiation potential would be extremely valuable for cell therapy.

Because of the recent identification of hAFS cells few papers, exploring their differentiation potential, have been published. However, some studies have documented the capacity of hAFS cells to integrate and differentiate into damaged tissues. In an experimental model of naphthalene-induced lung damage, hAFS cells integrate in bronchio-alveolar position and differentiate into Clara cells (Carraro *et al.,* 2008). Long-term experiments, up to 7 months, excluded tumor formation arising from hAFS cells (Carraro *et al.,* 2008). Murine and human AFS cells displayed strong hematopoietic potential in sub-lethally irradiated RAG-1 deficient mice (Ditadi *et al.,*2009). Recently, hAFS cells showed high ability to differentiate into cardiomyocytes in rats with infarcted myocardium (Tsuji *et al.,* 2010). Moreover, GFP-transfected hAFS cells incorporated into primordial kidney structures

and expressed the early renal markers ZO-1, glial cell line-derived neurotrophic factor (GDNF) and claudin thus contributing to the development of renal vesicles, C- and S-shaped bodies (Perin *et al.*, 2007).

Based on these evidences, the aim of this chapter is to study the potential of hAFS cells to regenerate renal tissue and to prolong survival of mice with cisplatin-induced AKI. Considering the plasticity of hAFS cells, we have investigated whether these cells afford protection through differentiation into renal cells or through local paracrine effect.

Moreover, we evaluated whether preconditioning of hAFS cells with a factor able to enhance their migration, engraftment and survival could maximize the regenerative potential of a stem cell-based therapy.

5.2 Isolation and characterization of human amniotic fluid stem cells

Human AFS cells were isolated from human amniocentesis specimens by immunoselection of cells positive to c-kit (CD117) as previously described (De Coppi *et al.*, 2007). As shown in Figure 5.1 *a*, amniotic fluid cells, seeded immediately after amniocentesis, displayed different morphologies, whereas after immunoselection for c-kit (Figure 5.1 *b*), hAFS cells presented a small oval shape. Immunofluorescence

analysis of hAFS cells, at first passage, showed positivity for HLA-ABC, SSEA4 and Vimentin (Figure 5.2 *a-c*).

Immunophenotype of hAFS cells were evaluated by FACs analysis. As shown in Table1, hAFS cells stably expressed CD29, CD44 and stromal cell markers as CD90, CD105 and CD73 at 4^{th} and 8^{th} passage (Table 1). The expression of c-kit was progressively lost after passaging whereas human AFS cells expressed embryonic stem cell markers Oct-4 and SSEA-4 after 8 passages of culture (Table 1). Human AFS cells also expressed HLA-ABC but not HLA-DR (Table 1), suggesting a low immunogenicity profile. This was further confirmed by absence of detectable CD80 and CD86 (data not shown). The ability of human AFS cells to differentiate into osteocytes and adipocytes, upon incubation with the appropriate inductive media, was observed by the extended area of mineralization and by lipid droplet formation (Figure 5.3 *a* and *b*).

5.3 Therapeutic effect of human amniotic fluid stem cells

In order to evaluate whether hAFS cells could exert a renoprotective effect, we set up an immunodeficient mouse model of cisplatin-induced AKI (see section 4.2). We observed that immunodeficient NOD-SCID mice injected with cisplatin developed renal function impairment characterized by high serum levels of BUN

starting at 3 days after disease induction (basal, 23.1±1; 24 h, 24.4±1 and 3 days, 98.7±9 mg/dl) that further increased at 4 days (133±4 mg/dl). By light microscopy, no structural changes were found in kidneys at 24 h after cisplatin injection, the time of hAFS cell administration (Figure 5.4 *b*). Conversely, ultrastructural analysis at 24 h revealed focal changes consisting of swelling of mitochondria, loss of brush border, and myelin figures in tubular epithelial cells (Figure 5.5 *b*), as previously described (see section 4.2).

After identifying an experimental model of AKI suitable to test the effect of hAFS, we injected saline or stem cells ($5x10^5$ cells) into the tail vein of NOD-SCID mice, one day after cisplatin treatment. As reported in Figure 5.6, hAFS significantly decrease ($p<0.01$) BUN levels at 4 days, as compared to cisplatin-treated mice given saline. Subsequently, we studied whether renal function improvement reflected an equally preserved renal structure. At 4 days, renal histology of cisplatin-treated mice showed focal and severe tubular cell degenerative alterations (Table 2, Figure 5.7 *a*) including nuclear fragmentation, loss of tubular epithelium and hyaline casts. Extended areas of necrosis affected the injured tubules (Table 2). Human AFS cells markedly attenuated renal tubular damage, as reflected by the significant reduction ($p<0.01$) of necrotic tubules and casts (Table 2, Figure 5.7 *b*).

5.4 Distribution of human amniotic fluid stem cells

To study whether the renoprotective effect of hAFS cells was associated with their localization into renal parenchyma of cisplatin-treated mice, we labelled hAFS cells with PKH-26, a red fluorescence cell membrane linker before injection. As shown in Table 3, 24 h after PKH26-labeled-hAFS cell infusion, we quantified 2.9±0.2 cells/10^5 renal cells in the injured renal tissue. The frequency declined during time as assessed at 4 and 31 days (0.9±0.3 and 0.2±0.2 PKH-26+ cells/10^5 renal cells, respectively). The localization of PKH-26 labelled hAFS cells into the renal parenchyma was mainly in peritubular areas (Table 3, Figure 5.8 *a*) and rarely within tubular epithelium, suggesting a differentiation-independent mechanism of action. To further confirm the human origin of PKH-26-labeled hAFS cells and the ability of these stem cells to engraft the damaged kidney, we co-stained kidney sections with anti-human CD105 antibody (Figure 5.8 *b* and *c*).

In support of the concept that hAFS cells contributed to renal regeneration via a paracrine action and not through differentiation toward tubular cell phenotype, we performed immunofluorescence studies. Kidney sections of cisplatin mice treated with hAFS cells at 31 days were incubated with human markers of epithelial tubular cells as cytokeratin and aquaporin-1. The results indicated that hAFS cells do not acquire renal phenotype in the long-term (Figure 5.9).

The fate of human AFS cells in cisplatin-mice was also evaluated in liver, heart, spleen and lung at different times. As shown in Table 4, we didn't find at 24h hAFS cells in organs other than kidney. At 4 days, no hAFS cells were detected in liver, heart and spleen, while few PKH-26 positive cells were found in the lung (Table 4). In control animals infused with hAFS cells, no engraftment was observed in the kidney and in the other organs at 24h.

5.5 Human amniotic fluid stem cell treatment inhibits apoptosis

In vitro and *in vivo* models of cisplatin-induced toxicity have demonstrated that renal tubular cells die by apoptosis. (Bonegio *et al.*, 2002). Based on this evidence, we have studied whether hAFS cell transplantation could exert an anti-apoptotic effect on renal cells in mice with AKI. Apoptotic cells, evaluated as TUNEL positive cells, were quantified in kidney sections at day 4 by confocal laser scanning microscopy. As reported in Figure 5.10, kidney sections of control mice shown few apoptotic cells, while in renal tissue of cisplatin mice, we observed in damaged tubuli a significant increase ($p<0.01$) in the number of apoptotic TUNEL-positive cells (Figure 5.10 *a,c*). Infusion of hAFS cells led to a significant ($p<0.01$) decrease of TUNEL-labelled cells in respect to cisplatin-mice given saline (Figure 5.10 *a,d*), indicating their anti-apoptotic activity.

5.6 Human amniotic fluid stem cells activate pro-survival pathways, leading to renal regeneration

The serine-threonine kinase Akt is a mediator of survival signals that activates mitogenic pathways and counteracts apoptosis, through the phosphorylation of multiple substrates (Datta *et al.*, 1999; Chang *et al.*, 2003). Starting from this evidence, we studied whether the renoprotective effect of hAFS cells could pass through the activation of Akt, represented by its phosphorylation. As indicated in Figure 5.11, kidney sections of control mice showed a high number of tubuli positive for phosphorylated (p) Akt, while in mice with AKI the expression of phosphorylated (p) Akt declined at 4 days (Figure 5.11 *a,c*). Treatment with hAFS cells significantly ($p<0.01$) increased the number of tubules positive for pAkt (Figure 5.11 *a,d*) suggesting a role of stem cells as activators of pro-survival pathways.

All these protective effects resulted in the induction of tubular cell proliferation that reflected renal regeneration. We used the nuclear marker of cycling cells, Ki-67, to quantify the number of proliferating cells. In section 4.8 we used PCNA as marker of proliferation, but given that PCNA has a role in DNA replication but also in DNA repair, we prefered to use a marker strictly associate with cell proliferation. Ki-67 is a protein present during all active phase of the cell cycle (G1, S, G2) but is absent in resting cells (G0) (Scholzen *et al.* 2000). In control mice at 4 days, we observed weak spontaneous tubular cell regeneration, while

in cisplatin mice the number of proliferating cells decreased (control, 5±1.5 and saline 2±0.4 Ki-67+ cells/HPF). Human AFS cell treatment significantly ($p<0.01$) increased the number of Ki-67 positive cells in respect to cisplatin mice (hAFS cells, 16±1.3 Ki-67+ cells/HPF).

5.7 Human amniotic fluid stem cells prolong survival of mice with AKI

Survival is the key clinical outcome in AKI, so based on the high sensitivity of NOD-SCID mice to cisplatin toxicity we investigated whether hAFS cell treatment could exert a protective effect also on survival. As shown in Figure 5.12, NOD-SCID mice with AKI started dying from day 5 and all animals receiving saline died within day 7 (Figure 5.12) with high BUN levels (≥140 mg/dl). Infusion of hAFS cells significantly ($p<0.005$) increased the lifespan of mice with AKI. All animals receiving hAFS cells were alive at 5 days, 56% of animal survived at 7 days and 33% of animals were still alive at the end of the study at 31 days.

In the same experimental model, we also compared the ability of hBM-MSCs and hAFS cells to prolong animal survival. As shown in Table 5, survival of cisplatin-mice treated with hAFS cells or hBM-MSCs was prolonged in respect to mice receiving saline ($p<0.009$). The

effect on animal lifespan observed with hAFS cells and hBM-MSCs was comparable (Table 5).

5.8 Human amniotic fluid stem cells preconditioned with GDNF enhance their regenerative potential

Glial cell line-derived neurotrophic factor (GDNF), a member of the transforming growth factor family, is known to be a survival factor of dopaminergic and noradrenergic neurons and spinal motoneurons (Sariola *et al.*, 2003). Moreover, recently, GDNF has been described to be necessary for migration and/or survival of renal resident MSCs (Shi *et al.*, 2008). In the attempt to enhance the therapeutic potential of hAFS cell treatment, we tested the effect of hAFS cells pre-exposed to GDNF.

First, we evaluated whether hAFS cells preconditioned with GDNF for 24 h before their *in vivo* infusion, exhibited an increased capacity to engraft and survive in the damaged renal tissue in respect to untreated hAFS cells. At 24 h, we observed in the renal tissue, a higher number of GDNF-treated hAFS cells compare to unstimulated cells (GDNF/hAFS 24h, 4.9±0.3 vs hAFS 24h, 2.9±0.2/10^5 renal cells, $p<0.05$), suggesting a role of GDNF in stem cell migration. Moreover, we observed at 4 days that GDNF-treated hAFS cells were present in the renal tissue to a more significant extent than untreated hAFS cells (GDNF/hAFS 4 days, 3.6±0.5 vs hAFS 4 days, 0.9±0.3/10^5 renal cells, $p<0.01$). Both cell populations were predominantly localized in

peritubular areas (Figure 5.13 *a* and *b*). When infused in control NOD-SCID mice, preconditioned hAFS cells did not migrate in the kidney and in the other organs.

Subsequently, we studied whether GDNF-increased capacity of hAFS cells to migrate and survive in damaged renal tissue, was accompanied by an even greater effect on renal function and renal structure. As shown in Figure 5.14, GDNF-treated hAFS cells further ameliorated BUN levels of AKI mice compared to untreated cells (Figure 5.14). Moreover, tubular alterations like casts and tubular necrosis were significantly ($p<0.01$) reduced in cisplatin-mice transplanted with GDNF-treated hAFS cells in respect to AKI mice receiving untreated hAFS cells (Figure 5.15). The increased protective effect of GDNF-treated hAFS cells on renal function and structure was accompanied by a markedly enhancement of hAFS cell ability to induce tubular cell proliferation (Figure 5.16 *a-d*).

5.9 GDNF improves *in vitro* human amniotic fluid stem cell motility, chemokines/adhesive receptors and survival

Starting from evidence reported in literature (Shi *et al.*, 2008) and from our *in vivo* results, we studied the mechanisms underlying the protective effect induced by GDNF-treated cells in AKI mice. Using a

wound healing assay, we tested whether GDNF incubation for 24 h could enhance hAFS cell motility. As shown in Figure 5.17, hAFS cells treated with GDNF rapidly reduced the surface area of the wound at 7 h in respect to untreated cells (Figure 5.17 *a* and *b*). In support of this result, we evaluated whether GDNF treatment could enhance the surface expression of receptors known to be involved in cell mobilization and engraftment within damaged tissue (Herrera *et al.*, 2007; Shi *et al.*, 2007, 897; Ji *et al.*, 2004). As shown by flow cytometry histograms, hAFS cells constitutively expressed CD44, CXCR4 and CX3CR1 receptors, which were markedly enhanced by pre-conditioning with GDNF (Figure 5.18).

Next, to evaluate whether GDNF treatment could enhance hAFS cell survival in an oxidative environment like damaged tissue, we studied the effect of GDNF on hAFS cells exposed to hydrogen peroxide-induced cytotoxicity. Hydrogen peroxide (200 mM for 24 h) significantly reduced hAFS cell viability in respect to untreated cells (45.8±2% vs 95.2±0.7%, $p<0.05$). GDNF markedly ($p<0.05$) decreased hAFS cell susceptibility to hydrogen peroxide (72.9±5.7%).

5.10 Human amniotic fluid stem cell production of pro-regenerative factors

The potential of hAFS cells to create a pro-regenerative microenvironment was investigated by studying hAFS cell production of factors with mitogenic and prosurvival activities, comparing with that produced by GDNF-treated hAFS cells. By multi-analyte profiling assay, we observed that hAFS cells released in 48 h conditioned medium considerable amounts of IL-6, VEGF, SDF-1 and IGF-1 (350.3±16.8, 369.2±4.6, 469.3±10.1 and 61±1 pg/ml/10^6 cells, respectively). The levels of IL-10, FGF-2 and HGF were below the detection limits. When hAFS cells were exposed to GDNF, a markedly increased production of IL-6, VEGF and SDF-1 was detected (416.4±5.5, 493.7±19.8 and 618.7±31.8 pg/ml/10^6 cells). At variance, IGF-1 secreted by GDNF preconditioned cells was not increased (67±7 pg/ml/10^6 cells). In Figure 5.19 is shown the percentage of IL-6, VEGF and SDF-1 production by GDNF-treated hAFS cells compared to untreated cells.

5.11 Conclusions

The results presented in Chapter 5 of this thesis, can be summarized as follows. We observed that:

- Transplantation of hAFS cells ameliorated renal function and tubular structure prolonging animal survival.
- Mechanisms underlying tissue repair by hAFS cells operate through local activation of paracrine signals rather than cell differentiation.
- Human AFS cells blocked apoptosis activating pro-survival pathways.
- Preconditioning of stem cells with GDNF before their *in vivo* injection can enhance hAFS cell tropism and survival in damaged tissue, improving their regenerative capacity.

5.12 Discussion

Many stem cell populations (e.g. embryonic, adult and fetal stem cells) have been described and characterized to date. All of them show advantages and disadvantages, and seem to be possible candidates for cell therapy. However, the search of an easily accessible source of stem cells with high plasticity and without ethical concerns would add value to the employment of cell therapy in terms of supporting tissue regeneration.

Recently, human amniotic fluid has been identified as a source of multipotent stem cell population with remarkable plasticity, high expansion potential and a low risk for tumor development (De Coppi *et al.*, 2007; Carraro *et al.*, 2008). Some papers have explored the

differentiation potential of human AFS cells, highlighting the capacity of these stem cells to differentiate towards cardiac, neural, and pulmonary lineages (Bollini *et al.*, 2011; Tsai *et al.*, 2006, 545; Carraro *et al.*, 2008).

In the present study, we tested whether hAFS cells were able to trigger a regenerative process in a model of cisplatin-induced acute kidney injury. Recent evidence documented the efficacy of hAFS cells in a mouse model of AKI induced by glycerol. Human AFS cells were injected into the renal cortex of nu/nu mice, 2 h after intramuscular glycerol injection when the damage in the kidney has not yet been established (Perin *et al.*, 2010). Furthermore, Hauser et al. demonstrated in the same experimental model of glycerol-induced rhabdomyolysis, that hAFS improve renal regeneration, but at a comparable extent as hBM-MSCs (Hauser *et al.*, 2010). However, in both studies no data on animal survival, a critical outcome of AKI, were provided. Here, we have documented in NOD/SCID mice with established cisplatin-induced AKI, that hAFS cell treatment ameliorated tubular damage and limited renal function impairment prolonging animal lifespan. We compared the effect of hAFS cells and hBM-MSCs on survival of mice with AKI, and we obtained a comparable result between hAFS cells and hBM-MSCs but lower than that previously reported for human CB-MSCs (Morigi *et al.*, 2010).

Another significant finding of the present thesis regards the capacity of hAFS cells to accelerate renal recovery in mice with AKI

through a differentiation-independent mechanism. Indeed, we observed that, upon infusion, hAFS cells specifically engrafted the damaged kidney and predominantly localized in peritubular compartment rather than within the tubular epithelium, without differentiating in renal cells. This result is in contrast with the capacity of hAFS cells to develop and differentiate into de novo kidney structure when injected into kidney rudiments (Perin *et al.*, 2007). Moreover, when hAFS cells were infused into damaged renal parenchyma of adult mice with AKI, their renal differentiation capacity was modest (Perin *et al.*, 2010). These observations would suggest that only an embryonic microenvironment is able to create the appropriate condition for driving hAFS cells toward renal commitment. In our model, the regenerative effect of hAFS cells on damaged kidney was mediated through a local paracrine action due to the secretion of cytokines and growth factors with mitogenic and pro-survival effects like IL-6, VEGF, SDF-1 and IGF-1 that were found in the conditioned medium of hAFS cells.

Subsequently, once established the capacity of hAFS cells to induce renal regeneration, we studied the mechanisms involved in this reparative process. We previously demonstrated that renal toxicity induced by cisplatin was due to an increase of tubular oxidative damage responsible for cell apoptosis and reduction of the prosurvival factor Akt (Morigi *et al.*, 2010). Moreover, Kuwana et al. have observed that blocking PI3Kγ-Akt pathway, tubular cell apoptosis and necrosis

were markedly accelerated, leading to a worse prognosis of cisplatin-treated mice (Kuwana *et al.*, 2008). Here, we have documented that treatment with hAFS cells significantly reduced tubular cell apoptosis in respect to cisplatin-mice given saline. The capability of hAFS cells to create a regenerative environment was supported by the increased tubular expression of pAkt and proliferation at 4 days, the time point at which untreated mice exhibited higher tubular injury and apoptosis.

Another significant point of the present thesis has been to study an additional way to maximize hAFS cell regenerative potential by preconditioning of cells before their *in vivo* injection. Data are already available that gene modification (Hagiwara *et al.*, 2008; Mangi *et al.*, 2003) or stem cell preconditioning with growth factors, cytokines, hypoxia or other factors (Shi *et al.*, 2008; Mias *et al.*, 2008; Schmidt *et al.*, 2006; Hung *et al.*, 2007) can optimize *in vitro* and *in vivo* stem cell migration, engraftment, survival and efficacy. Here, we focussed on GDNF, a growth factor known to be a survival factor of dopaminergic and noradrenergic neurons and spinal motoneurons (Sariola *et al.*, 2003), besides being necessary for migration and/or survival of renal resident MSCs as recently described (Shi *et al.*, 2008). Moreover, GDNF is known to participate to early nephrogenesis (Constantini *et al.*, 2006) and to induce adult stem cells toward renal commitment (Yokoo *et al.*, 2005). Based on these evidences, we preconditioned hAFS cells with GDNF. We observed an increase of hAFS cell migration and homing in damaged kidney and a reduction of their susceptibility to the hypoxic

environment, as reflected by the high number of GDNF-treated hAFS cells engrafting the renal tissue at 24 h that was also stably detectable at 4 days. However, GDNF exposure did not commit hAFS cells toward renal phenotype, as supported by cell engraftment limited to the peritubular site. The increased engraftment and survival of preconditioned hAFS cells into the injured tissue, was associated with further amelioration of renal function, tubular injury and proliferation.

In vitro experiments allowed to batter explain the mechanisms underlying the protective effect of GDNF on hAFS cells. We observed that GDNF enhanced the motility of cultured hAFS cells, up-regulated the expression of surface receptors involved in chemotaxis and homing and increased the constitutive production of mitogenic and angiogenic factors. Moreover, enhanced survival of GDNF-treated hAFS cells, in response to a toxic concentration of hydrogen peroxide, suggests that GDNF can activate stem cell cytoprotective and anti-oxidant pathways capable to protect hAFS cells from oxidative stress occurring in damaged tissue.

In summary, our findings indicate that amniotic fluid could be considered a new potential stem cell source for organ regeneration. The renoprotective effect of hAFS cells seems to be mediated by local activation of paracrine signals rather than cell differentiation. A new approach to enhance hAFS cell tropism and survival in damaged tissue has been proposed by preconditioning of stem cells with GDNF before their in vivo use.

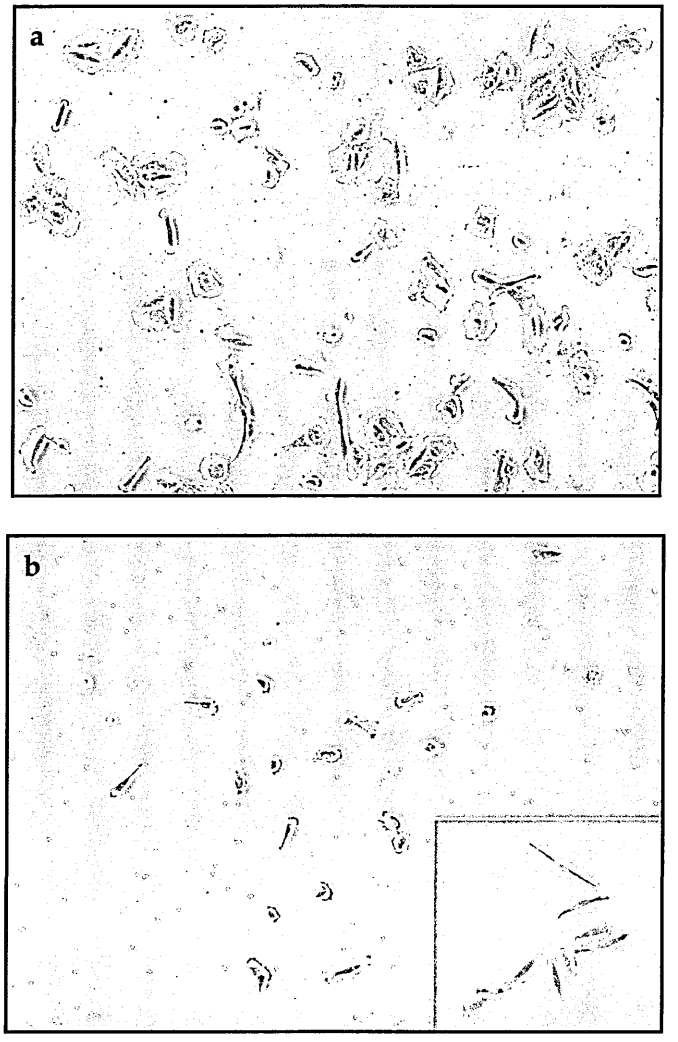

Figure 5.1: Morphology of human AFS cells.

(a) Phenotypic appearance of the amniotic sample after amniocentesis: cells show different shape and volume. Original magnification 20X. (b) Human AFS cells after 5 days of selection for c-kit, receptor of the Stem Cell Factor (SCF). Selected cells showed a characteristic morphology: small oval shape that during maturation in culture becomes bigger. Original magnification 20X; inset 40X.

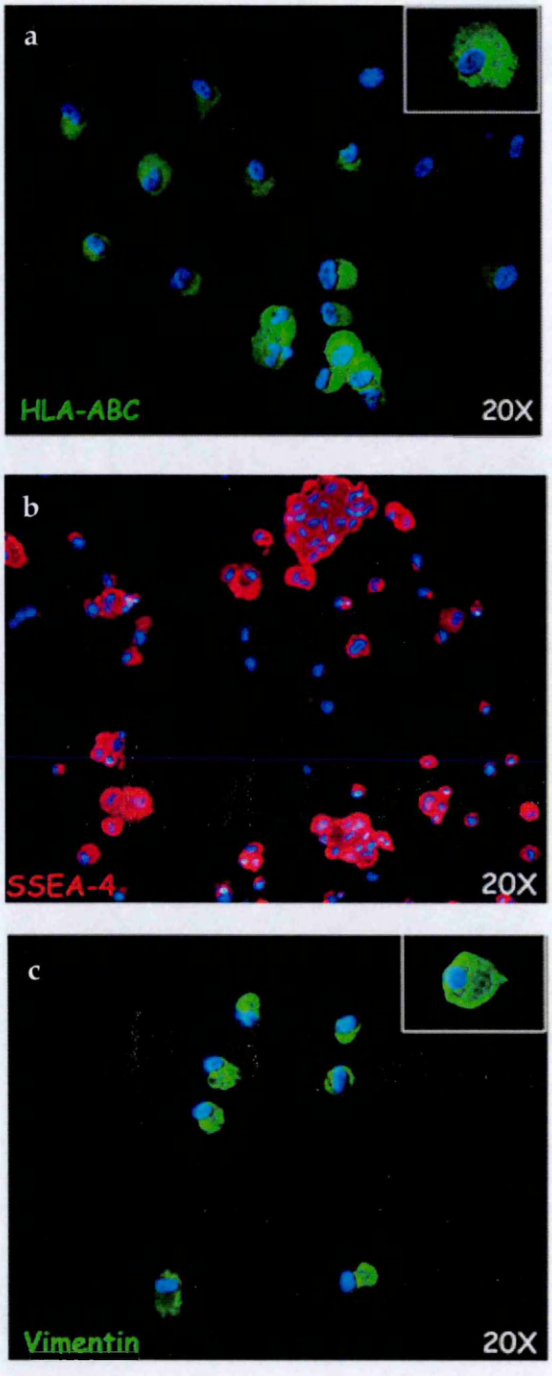

Figure 5.2: Immunophenotype of human AFS cells.

Representative images of hAFS cells (first passage) showing positive staining for HLA-ABC (a), SSEA-4(b) and vimentin (c). Original magnification 20X.

Table 5.1: Phenotypic analysis of hAFS ckit+ cells

Antibody	P4	P8
CD29	99.95%	82.94%
CD44	99.81%	82.77%
CD90	90.55%	77.51%
CD105	99.27%	90.70%
CD73	99.85%	95.80%
CD117	4.41%	2.10%
OCT4	69.50%	50.50%
SSEA-4	38.26%	33.21%
HLA-ABC	42.50%	28.01%
HLA-DR	0.58%	0.12%

Standard deviation was ≤ 10%

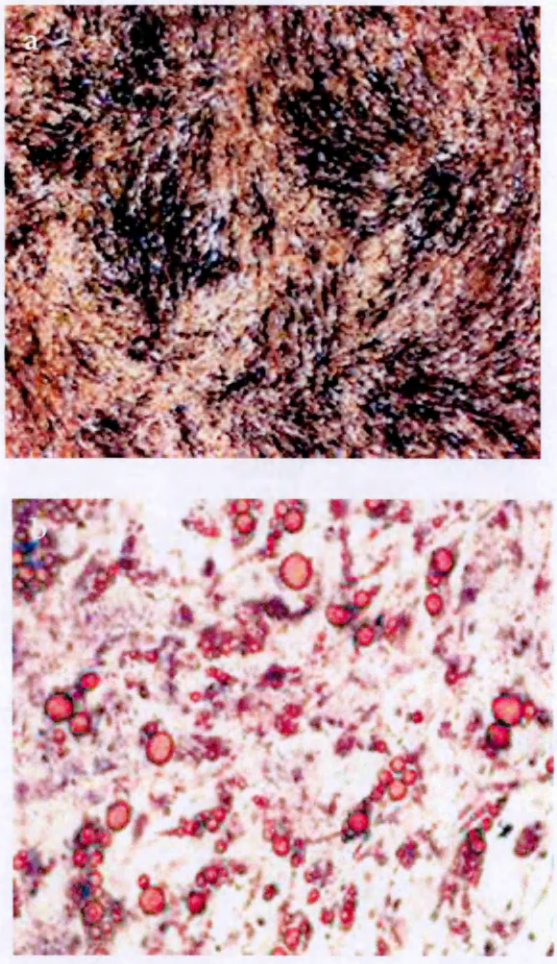

Figure 5.3: Differentiation of human AFS cells

(a) Osteogenic differentiation of hAFS cells was evidenced by Von Kossa staining with area of mineralization. (b) Adipogenic differentiation of hAFS cells was visualized by Oil Red O staining. Original magnification 20X.

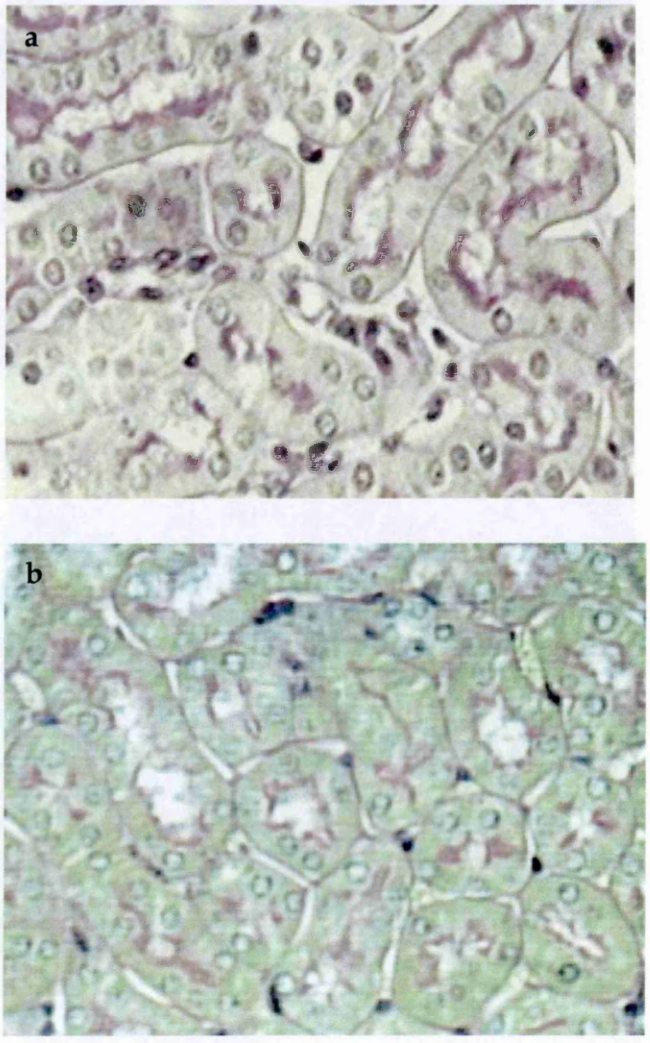

Figure 5.4: Representative light micrographs of PAS-stained-sections of kidneys taken from a control mouse (a) or from mice at 24 h (b, the time of hAFS cell infusion). Original magnification 400X.

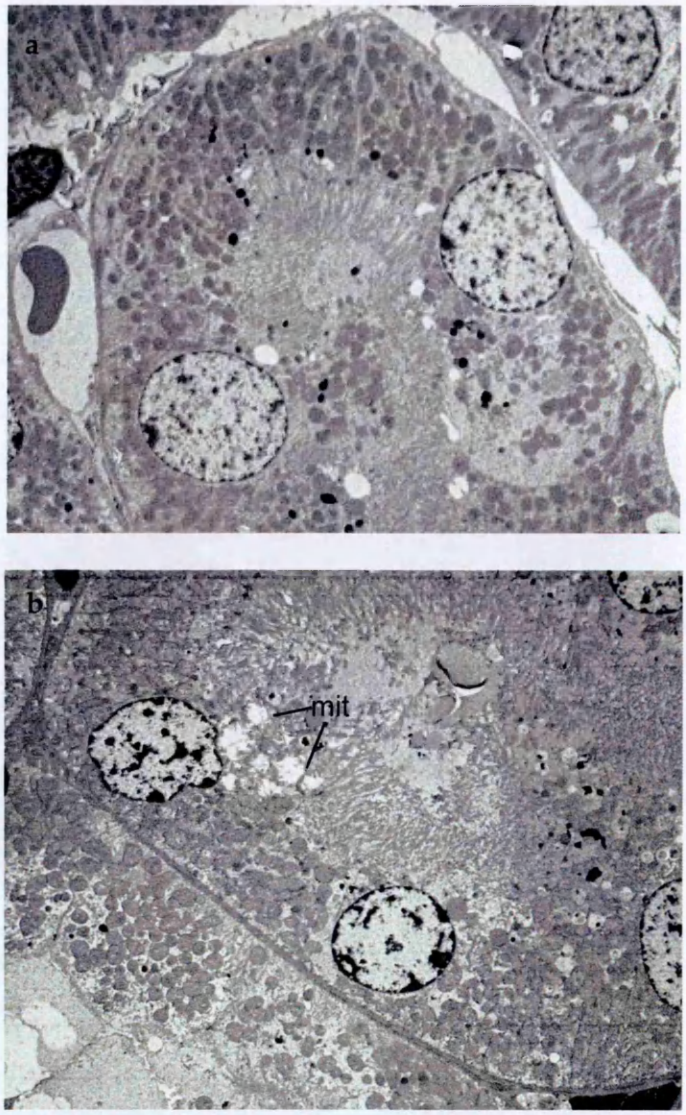

Figure 5.5: Ultrastructural changes in NOD-SCID mice 1 day after cisplatin injection

Electron micrographs of sections of proximal tubuli from a control mouse kidney (a) and a 24h cisplatin-treated mouse (b), showing cisplatin-induced mitochondrial swelling (mit) and loss of brush border. Original magnification 2,500X.

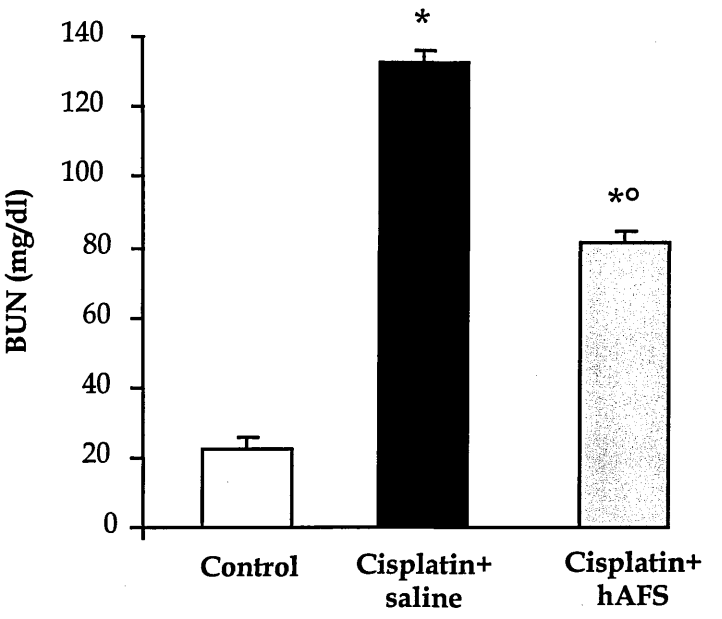

Figure 5.6: Effect of human AFS cells on renal function impairment

Renal function, assessed as BUN, in control (n=11) and in cisplatin-treated mice given saline (n=11) or hAFS cells (n=11) at 4 days. Data are mean±SE. *p<0.01 vs Control; °p<0.01 vs Cisplatin+saline (ANOVA, followed by Tukey Cicchetti test).

Table5.2: Effect of hAFS cells on renal histology of AKI mice at 4 days

	Casts (n/HPF)	**Tubular Necrosis** (n/HPF)
Control (n=6)	0	0
Cispltin+saline (n=6)	8.6±1.2*	5.2±0.8*
Cisplatin+hAFS (n=6)	2.1±0.8°	2.1±0.8°

hAFS cells, human amniotic fluid stem cells.
Data are mean±SE
HPF: high-power field
*$p<0.01$ vs Control; °$p<0.01$ vs Cisplatin+saline (Kruskal Wallis test)

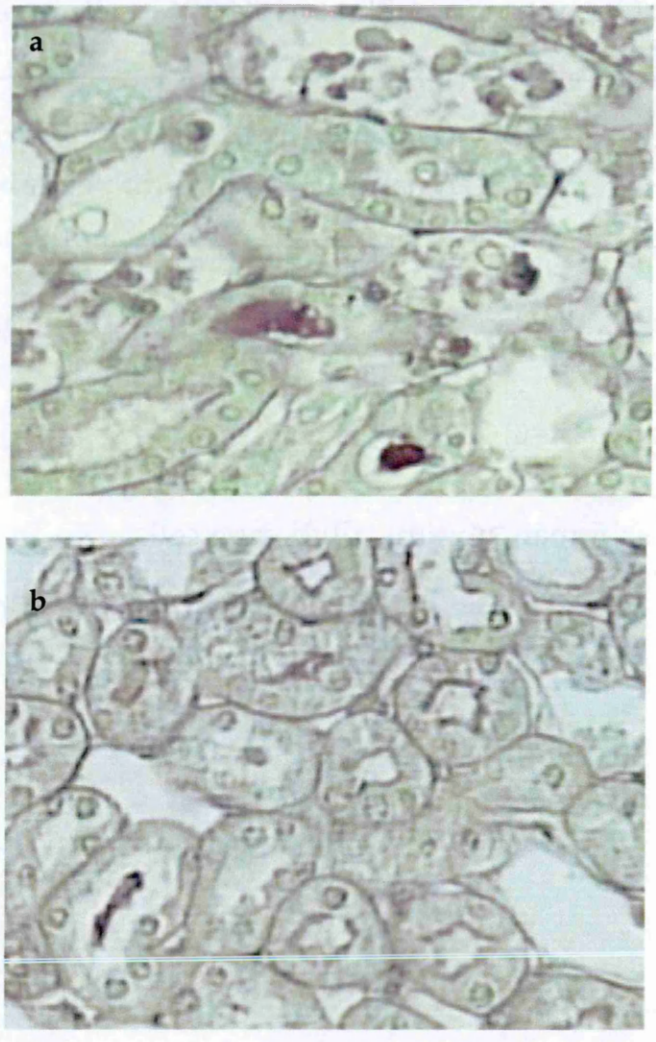

Figure 5.7: Human AFS cell infusion protects NOD-SCID mice with AKI from tubular injury

Renal histology at 4 days of cisplatin-treated mice receiving saline (a) or hAFS cells (b). Original magnification 400x.

Table 5.3: Quantification of hAFS PKH-26+ cells in renal tissue of cisplatin mice.

	hAFS cells/10^5 renal cells	**% hAFS cells in peritubular areas**
hAFS 24h (n=3)	2.9±0.2°	93±4%
hAFS 4 days (n=6)	0.9±0.3	90±7%

hAFS cells, human amniotic fluid stem cells.
Data are mean±SE
*p<0.05 vs hAFS 24h; °p<0.01 vs hAFS 4gg (Mann-Whitney test)

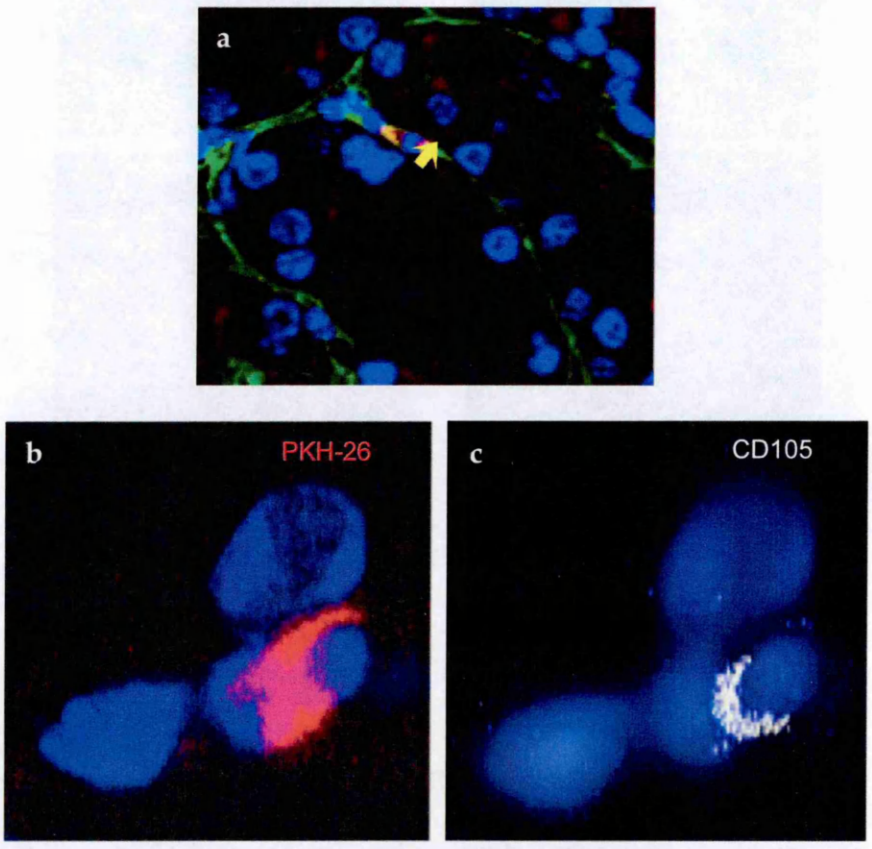

Figure 5.8: Human AFS cells engraft the kidney in cisplatin mice.

(a) Representative micrograph of kidney tissue from cisplatin-treated mouse injected with PKH-26 labeled hAFS cells (red) at 4 days. Human AFS PKH-26+ cells were localized in peritubular area. Original magnification 630X. The sections were stained with FITC-labeled lectin WGA (green), and DAPI for nuclei (blue). (b) Representative images of hAFS cells co-stained with PKH-26 (red) and (c) human antigen CD105 (white). Nuclei were stained with DAPI (blue). Original magnification 630X.

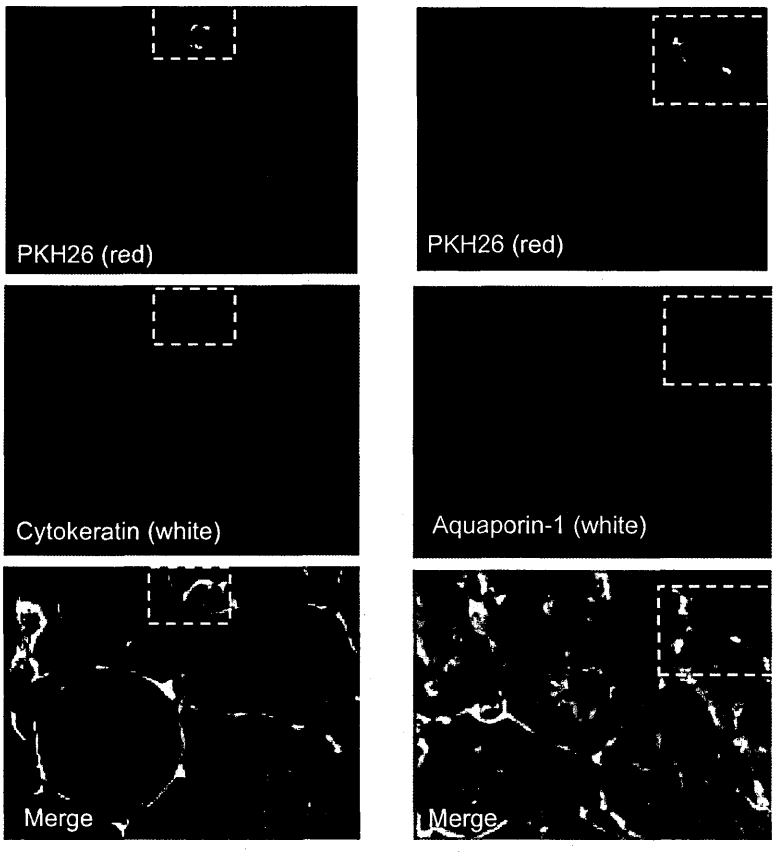

Figure 5.9: Human AFS cells don't differentiate towards a renal phenotype.

Frozen kidney sections were incubated overnight at 4°C with anti-human cytokeratin (1:100) or with anti-human aquaporin-1 (1:50) antibodies. Then sections were incubated with secondary antibody, donkey anti-mouse Cy5 and goat anti rabbit Cy5 (1:50), respectively. Slides were counterstained with FITC-labeled lectin WGA (green) and nuclei were stained with DAPI (blue).

Table 5.4: Quantification of hAFS PKH-26+ cells in different organs of cisplatin-mice with AKI

	PKH-26+ cells/10^5 cells			
	liver	**lung**	**heart**	**spleen**
hAFS 24h (n=3)	0	0	0	0
hAFS 4 days (n=3)	0	0.8 ±0.1	0	0

hAFS, human amniotic fluid stem cells.
Data are mean±SE

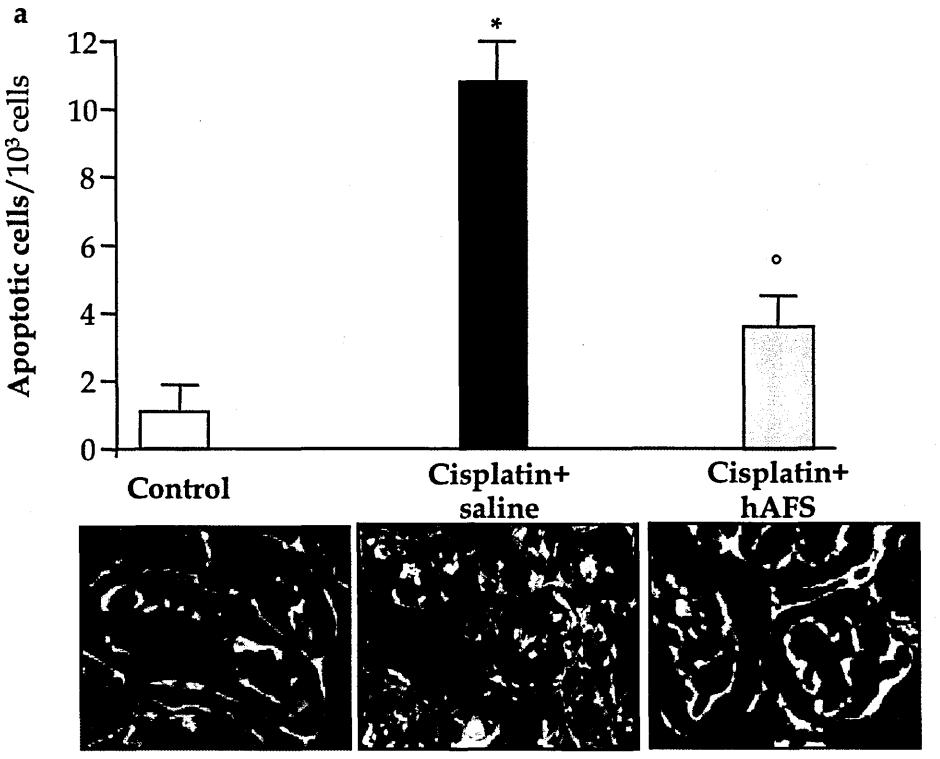

Figure 5.10: Human AFS cell treatment reduces tubular cell apoptosis in mice with AKI at 4 days.

(a) TUNEL positive cells quantified in kidney sections of control mice (n=3), cisplatin-treated mice given saline (n=3) or hAFS cells (n=3). *$p<0.01$ vs Control; °$p<0.01$ vs Cisplatin+saline (ANOVA followed Tukey Cicchetti test). (b-d) Representative images of apoptotic tubular cells labeled with TUNEL (green), rhodamine-labeled lectin LCA (red) and DAPI (blue) in kidney sections of control mice, cisplatin-mice given saline or hAFS cells. Original magnification 630X

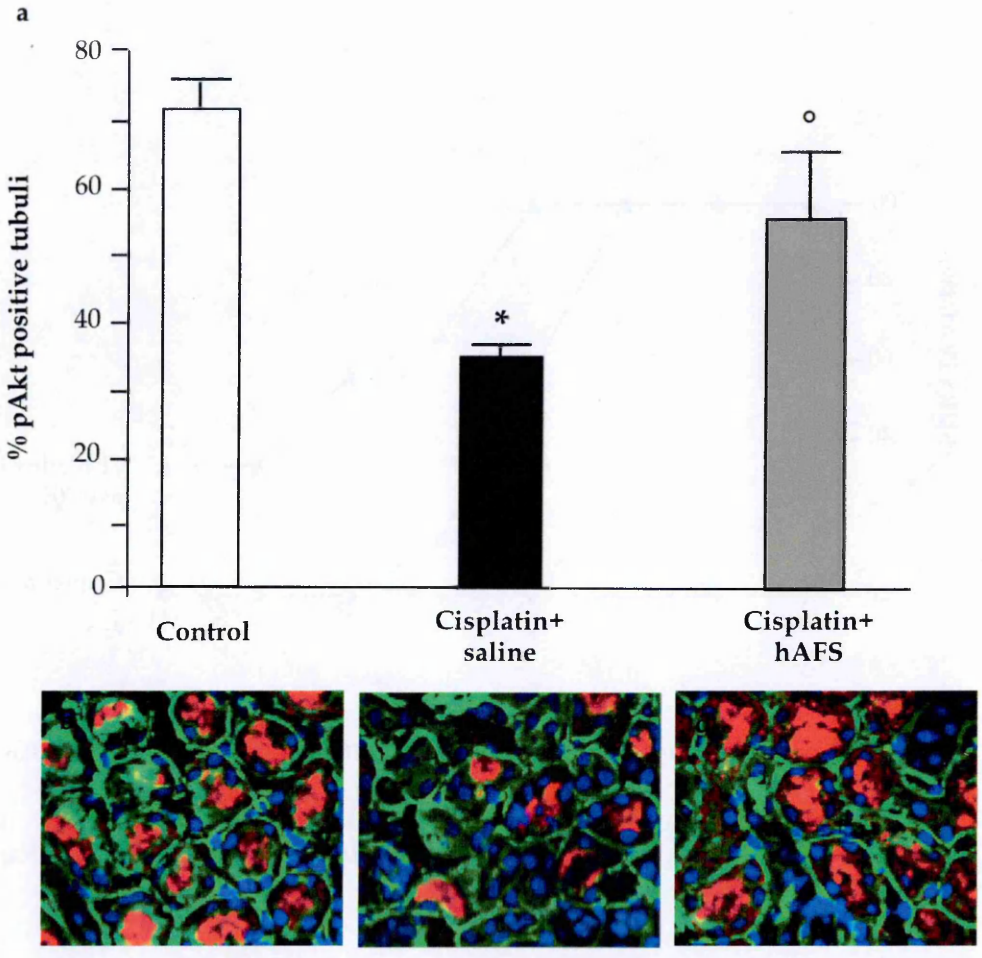

Figure 5.11: Human AFS cells enhance Akt phosphorylation in mice with AKI at 4 days.

(a) Percentage of pAkt positive tubules in control mice (n=3), cisplatin-treated mice receiving saline (n=3) or hAFS cells (n=3). *$p<0.01$ vs Control; °$p<0.01$ vs Cisplatin+saline (ANOVA followed Tukey Cicchetti test). (b-d) Representative images of pAkt staining (red) with FITC-labeled lectin WGA (green) and DAPI (blue) in kidney sections of control, cisplatin-mice given saline or hAFS cells. Original magnification 630X.

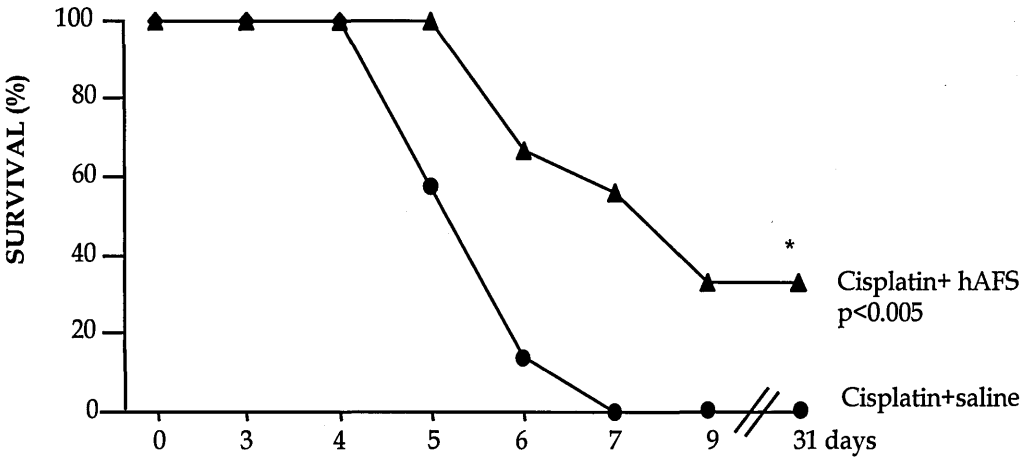

Figure 5.12: Human AFS cell treatment prolongs survival in mice with AKI.

At 7 days all mice receiving saline died (n=9), while 56% of NOD-SCID mice given hAFS cells (n=7) survived. *p<0.005 vs Cisplatin+saline (Log Rank Test).

Table 5.5: Comparison between hAFS cells and hBM-MSCs on survival of cisplatin-mice with AKI.

	Survival (%)			
	0 day	**5 days**	**7 days**	**31 days**
Cisplatin+saline (n=6)	100	50	0	0
Cisplatin+ hAFS (n=6)	100	100	50	33*
Cisplatin+ hBM-MSCs (n=6)	100	83	33	33*

hAFS, human amniotic fluid stem cells.
hBM-MSCs, human bone marrow mesenchymal stem cells
*$p<0.009$ vs Cisplatin+saline. (Kaplan-Meier analysis and Log-Rank test).

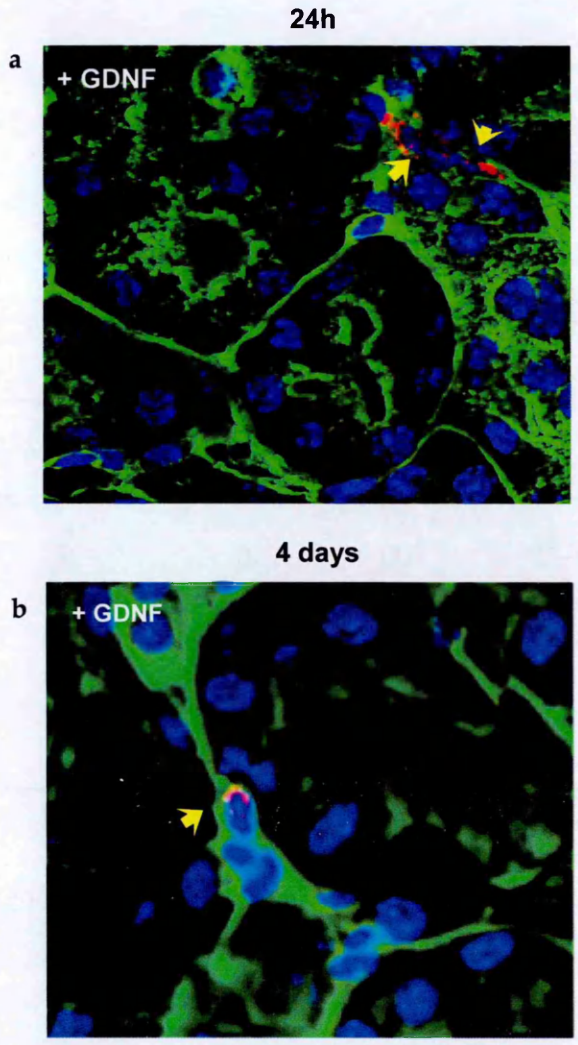

Figure 5.13: Localization of hAFS cells preconditioned with GDNF

Representative micrographs of kidney tissue from cisplatin-mice injected with PKH-26-labelled hAFS cells preconditioned with GDNF at 24h (a) and 4 days (b). The sections were stained with FITC-labeled lectin WGA (green), and DAPI for nuclei (blue). PKH-26 fluorescent cells (red) were localized in peritubular area (arrow). Original magnification 630X.

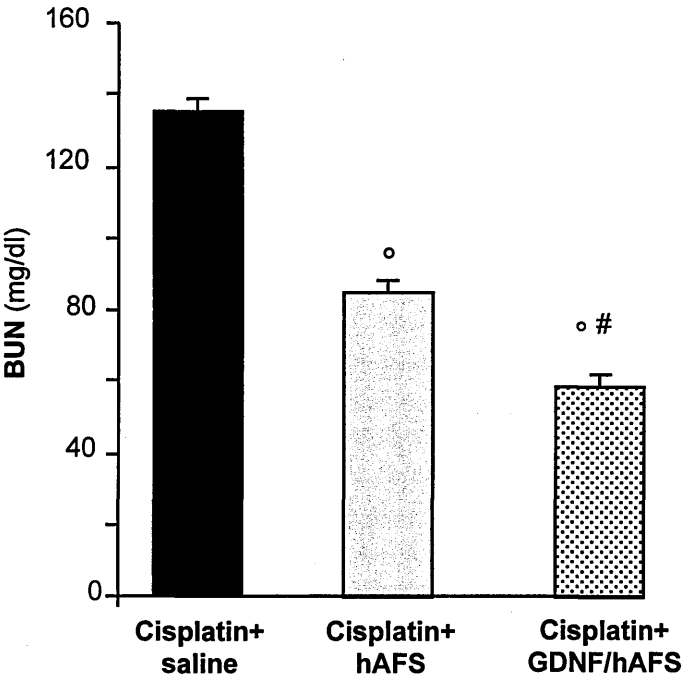

Figure 5.14: Preconditioning with GDNF increases renoprotection of hAFS cells in mice with AKI.

Renal function, measured as BUN, in cisplatin-treated mice given saline (n=9), untreated hAFS cells (n=10) or GDNF-preconditioned hAFS cells (n=10) at 4 days. Data are mean±SE. °$p<0.01$ vs Cisplatin+saline; #$p<0.05$ vs Cisplatin+hAFS cells (ANOVA followed by Tackey Cicchetti test).

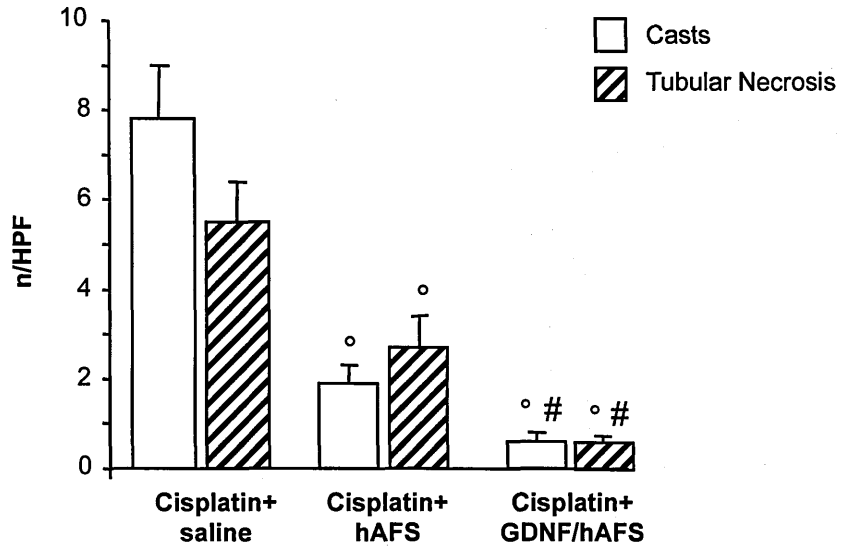

Figure 5.15: GDNF-preconditioned hAFS cells ameliorate renal structure in mice with AKI at 4 days

Histological changes in kidneys from cisplatin-treated mice receiving saline (n=6), untreated hAFS cells (n=6) or GDNF-preconditoned hAFS cells (n=6) at 4 days. Data are mean±SE. °p<0.01 vs Cisplatin+saline; #p<0.01 vs Cisplatin+ hAFS cells (Kruskal-Wallis test).

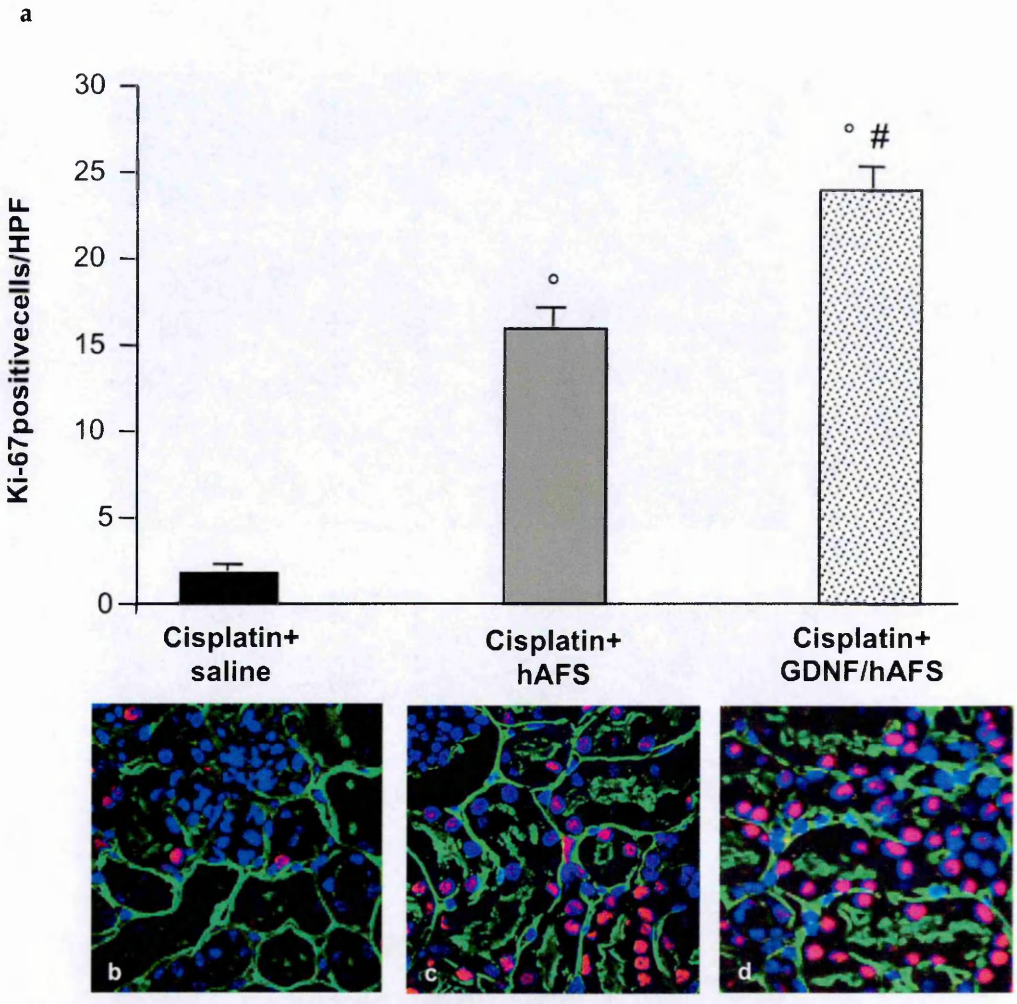

Figure 5.16: Preconditioning with GDNF enhances the ability of hAFS cells to induce tubular cell regeneration

(a) Quantification of Ki-67 positive tubular cells at 4 days after cisplatin treatment in mice receiving saline (n=3), hAFS (n=3) and GDNF/hAFS (n=3). Data are mean±SE. °$p<0.01$ vs Cisplatin+saline; #$p<0.01$ vs Cisplatin+ hAFS cells (ANOVA followed by Tukey Cicchetti test).
(b-d) Representative images of Ki-67 positive tubular cells (red) co-stained with FITC-labelled lectin WGA (green) and DAPI (blue) in kidney sections of cisplatin-mice given saline, untreated hAFS cells or GDNF-preconditioned hAFS cells. Original magnification 630X.

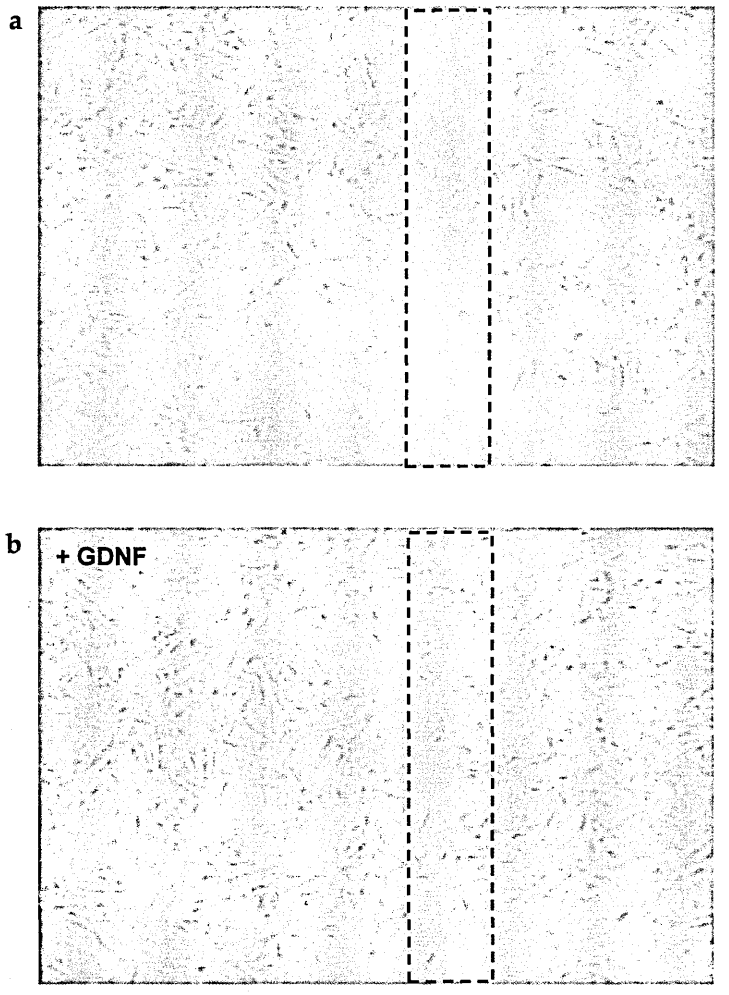

Figure 5.17: GDNF increases *in vitro* hAFS cell motility

Representative micrographs of scratch-wound-closure assays in hAFS cells untreated (a) or treated for 24 h with GDNF (100 ng/ml) (b). Preconditioned hAFS cells with GDNF showed a more rapid capacity to cover the wound area after 7 h in respect to untreated hAFS cells.

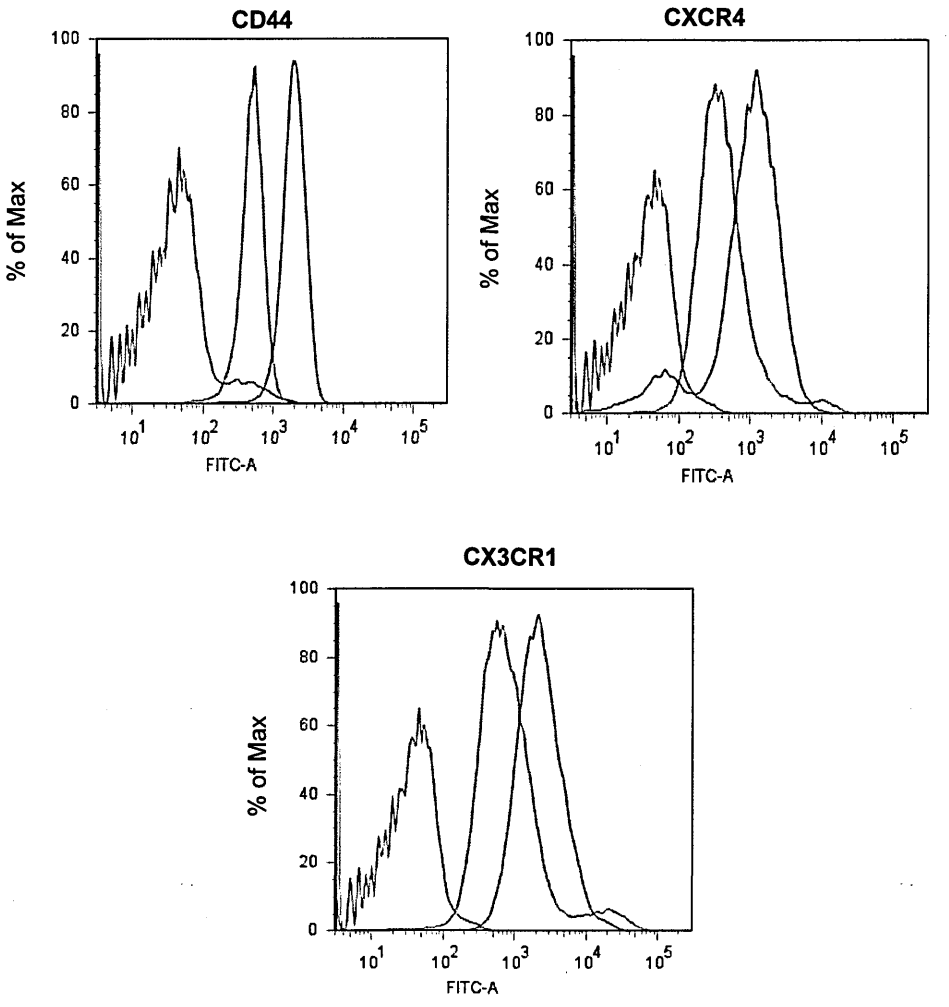

Figure 5.18: GDNF increases *in vitro* hAFS expression of CD44, CXCR4 and CX3CR1 receptors

Representative fluorescence histograms show the expression of CD44, CXCR4 and CX3CR1 in untreated hAFS cells (green) and GDNF-conditioned hAFS cells (blue) by FACs. The negative controls are shown as red line.

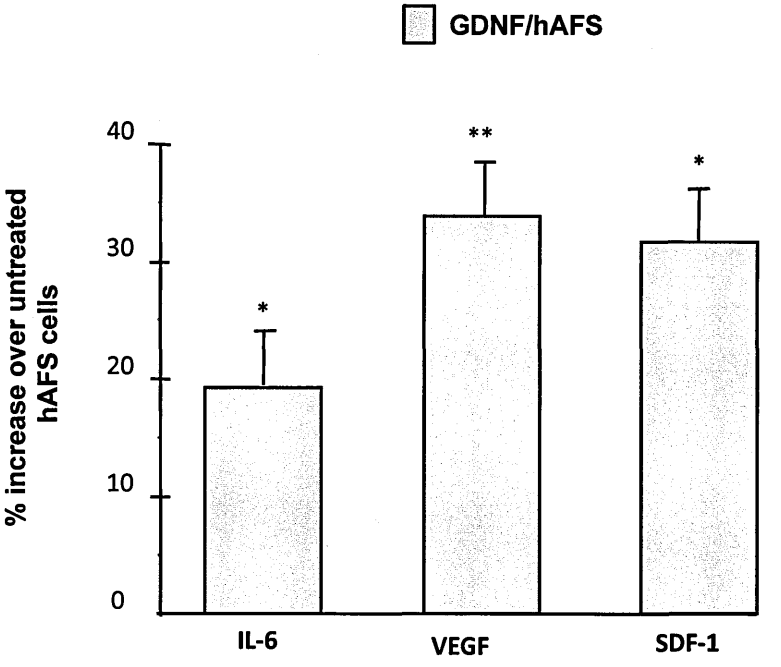

Figure 5.19: GDNF increases *in vitro* hAFS production of pro-regenerative factors

Percentage of increased production of IL-6, VEGF and SDF-1 by hAFS cells treated with GDNF (GDNF/hAFS) for 48 h in respect to untreated hAFS cells. *$p<0.05$ and **$p<0.01$ vs untreated hAFS cells (unpaired t test). The experiments were performed in triplicate and repeated 3 times.

CHAPTER 6

GENERAL DISCUSSION

In the last decade, several studies have widely demonstrated the important role of stem cells, not only in the physiological cell turnover, but also in the repair of the damaged tissues. These discoveries have opened a new branch of medicine. Where the traditional medicine has not been able to offer therapeutic opportunities, stem cells used as vehicles, have represented a great challenge that has lead to profound effects on regenerative medicine. Despite this, therapeutic applications of stem cells to injured organs are still largely a matter of experimental investigation in order to prove the real efficacy and safety of such approaches.

Organs, like kidney, showing minimal cell turnover and limited capacity for self-repair after injury, could benefit from the stem cell treatment. Following damage, renal tubular cells have capacity to regenerate, although regeneration is limited by the extent of the injury and the number of surviving cells. Cell therapy, based on the used of stem cells, could represent a valid alternative to pharmacological therapies, that up to now are characterized by poor success rates. Therefore, we decided to address our efforts to investigating the possibility that stem cells could help in regenerating the kidney after AKI. In particular, we focused on the possible therapeutic effect of stem cells isolated from fetal tissues in order to bypass the limits of adult stem cells.

In the last years, several researches focused on the renoprotective effect of BM-MSCs, given their paracrine, anti-inflammatory and

immunomodulatory properties. In particular our group have demonstrated that the intravenous administration of BM-MSCs in mice with AKI induced by cisplatin, protected renal function and structure through the local release of anti-apoptotic and mitogenic growth factors, like IGF-1 (Morigi *et al.*, 2004, Imberti *et al.*, 2007). Although bone marrow represents the first identified tissue source of MSCs, harvesting these stem cells is invasive and their number, frequency, differentiation potential, and life span decline with the age of the donor. Therefore, in the clinical perspective to cure AKI, the search for new sources of MSCs, is of significant value. It has been reported that stem cells with similar surface expression patterns of MSCs can be isolated from alternative sources as umbilical cord blood, placenta, adipose tissue, amniotic fluid, peripheral blood, and other tissues (Liu *et al.*, 2009).

Since the first successful transplantation of umbilical cord blood in 1988, the cord blood has proved a fetal rich source of stem cells, and in particular of mesenchymal stem cells with morphological characteristics, immunophenotypic markers and differentiation ability similar to BM-MSCs (Kern *et al.*, 2006; Panepucci *et al.*, 2004; Wagner *et al.*, 2005). Moreover, unlike the invasive harvesting of bone marrow, the collection of cord blood is relatively simple and lacks of risks to mother or infant and of ethical barrier. Early clinical evidence documented both safety and efficacy of CB progenitors cell infusion in humans for the treatment of haematological (Pinto *et al.*, 2008; Locatelli *et al.*, 2008),

neurological disorders (Sanchez-Ramos *et al.*, 2006; Escolar *et al.*, 2005) and Burger's disease (Kim *et al.*, 2006). Furthermore, for future therapies it will be possible to use the established cord blood bank to construct a cord blood-MSC bank network system. Altogether, these findings prompted us to investigate whether hCB-MSCs could represent a new option to cure AKI. We chose to induce acute kidney injury, treating immunodeficient (NOD-SCID) mice with the cytotoxic drug cisplatin. This compound is one of the most effective for the treatment of several solid tumours; unfortunately, its administration is associated with severe nephrotoxicity in 10-15% of patients (Madias *et al.*, 1978). In this model of AKI, we transplanted hCB-MSCs 1 day after cisplatin treatment, when an ultrastructural damage was already present, and we observed that stem cells were able to ameliorate renal function and structure compared to cisplatin-mice treated with saline. Another significant finding of the present study regards the capacity of this population of stem cells to affect the critical outcome of AKI, the survival. The renoprotective effect of hCB-MSCs was so strong that these stem cells were able to prolong animal survival to a more significant extent than that observed in cisplatin mice treated with hBM-MSCs. The reasons for this difference still remain to be elucidated. A possible explanation may rest on the evidence of the immaturity of hCB-MSCs that could produce large amount of growth factors that are more active in the mitogenic and pro-survival pathways than that produced by hBM-MSCs. Moreover, the fetal nature of these stem cells

makes them more prone to escape immune rejection than adult stem cells.

The positive effect of hCB-MSCs was due to their renotropic capacity that allows them to home to injured kidney, following the inflammatory cytokines released from the damaged renal cells. Indeed, we observed hCB-MSCs exclusively localized in the peritubular areas and not in the context of the tubular epithelial lining, excluding the transdifferentiation into renal cells. These data are in support of a paracrine action of hCB-MSCs once engrafted in the damaged kidney, as already described for BM-derived stem cells in experimental AKI by other and our laboratories (Imberti *et al.*, 2007; Togel *et al.*, 2005; Togel *et al.*, 2007). Relevant to the former interpretation are data that hCB-MSCs in culture constitutively produce pro-survival, anti-inflammatory and mitogenic proteins (Liu *et al.*, 2005; Kogler *et al.*, 2005) as also demonstrated by our *in vitro* experiments, showing a remarkable amounts of growth factors as FGF, HB-EGF, VEGF and HGF produced by hCB-MSCs in co-cultured with cisplatin -damaged tubular cells.

In this study, we observed that the differentiative capacity of hCB-MSCs toward renal phenotype during kidney repair seems to be very confined. Therefore, the sources of stem cells with higher plasticity would add value to the employment of cell therapy in terms of supporting tissue regeneration via a differentiation-mechanism. To this purpose, we tested the effect of hAFS cells in a cisplatin-induced AKI model. In the last 10 years, the amniotic fluid, obtained from

amniocentesis, has been extensively studied as a non-controversial source of a population of stem cells with intermediate characteristics between embryonic and adult stem cells (De Coppi *et al.*, 2007). Human AFS cells, immunoisolated for c-Kit, express embryonic and mesenchymal stem cell markers, can be readily expanded and possess immunomodulatory properties (De Coppi *et al.*, 2007; Cananzi *et al.*, 2009). Moreover, hAFS cells show potential to differentiate into hematopoietic, neurogenic, osteogenic, chondrogenic, adipogenic, renal, hepatic and various other lineages (In't Anker *et al.*, 2003; Tsai *et al.*, 2004, 1450; Bossolasco *et al.*, 2006; Kim *et al*, 2007; De Coppi *et al.*, 2007; Prusa *et al.*, 2004; Rehni *et al.*, 2007; Kolambkar *et al.*, 2007; Orciani *et al.*, 2008; Rosner *et al.*, 2011, 1). Therefore, based on the high plasticity of this stem cell population, we investigated whether hAFS cells afford protection through differentiation into renal cells or through local paracrine effect. The injection of hAFS cells in NOD-SCID mice with cisplatin-induced AKI showed a partial renoprotective effect. Indeed, BUN values were higher than those observed in control animals. Partial renoprotective effect of hAFS cells became complete when hAFS cells were preconditioned with GDNF, suggesting a contribution of this growth factor in the enhancement of the therapeutic effect of these stem cells. Moreover, comparing the efficacy of hAFS cells with that of hBM-MSCs, we observed that the effect on animal lifespan observed with hAFS cells and hBM-MSCs was comparable.

One possibility of the partial therapeutic effect of hAFS cells could be their lower renotropic capacity. Indeed, hAFS cells engrafted the injured kidney of cisplatin mice with a low frequency. GDNF pre-conditioning increased the number of hAFS cells homing the damaged tissue, because, as we observed in *in vitro* experiments, GDNF was able to enhance the surface expression of receptors known to be involved in cell mobilization and engraftment within damaged tissue. As reported in literature for MSCs (Shi *et al.*, 2008), also in this case GDNF was necessary to enhance migration and/or survival of hAFS cells.

It is widely demonstrated that MSCs facilitate kidney regeneration predominantly through a differentiation-independent mechanism characterized by the delivering of growth factors and cytokines to the site of the injury. The same occurred for hAFS cells, even if, given the high plastic capacity of these stem cells, we would expect to observe a differentiation-dependent mechanism of action. Our results differ from the recent study of Perin et al. (Perin *et al.*, 2010), who showed that $1x10^6$ hAFS cells directly injected into the renal tissue of nu/nu mice with AKI were able to differentiate, contributing to kidney regeneration. This discrepancy may depend on the amount of cells transplanted and the route of administration.

To date MSCs isolated from bone marrow are the favoured population of stem cells in the clinical practice. However, for future application in humans, we have to consider that, since acute kidney injury is a sudden phenomenon and there is possibility of donor site

morbidity, there is no chance of using the patient's own MSCs because it takes too long to isolate and *in vitro* expand the MSCs. It means that there is need to use populations of allogeneic stem cells, which, however, may pose the significant problem of immune response. As fetal cells, hCB-MSCs and hAFS cells, might have an immunoprivileged status, as they likely possess mechanism to avoid destruction by the maternal immune system during development (Betz, 2010). Moreover, given the extensive self-renewal capacity in respect to hBM-MSCs, hCB-MSCs and hAFS cells represent ideal sources for cell banking and allogeneic transplantation. As allogeneic cell sources, hCB-MSCs and hAFS cells may raise the issue of a possible adverse reaction or ultimate rejection by the recipient. However, both populations of stem cells, similarly to BM-MSCs, expressed MHC I but not MHC II and are negative for costimulatory molecules as CD80, CD86, CD40 and CD40 ligands, which are mainly expressed on antigen presenting cells and tissue cells (Wang *et al.*, 2009; Moorefield *et al.*, 2011). Moreover, hCB-MSCs were not able to induce allogeneic peripheral blood mononuclear cell (PBMC) proliferation and can suppress *in vitro* the function of mature dendritic cells (Wang *et al.*, 2009). Human AFS cells, through the release of soluble factors, inhibited lymphocyte activation, suppressing inflammatory responses *in vitro* (Moorefield *et al.*, 2011).

In conclusion, this study suggests a therapeutic effect of foetal stem cells in a model of AKI, through a local paracrine mechanism of action rather then cell differentiation. In the future, the safety and

efficacy of hCB-MSCs and hAFS cells should be investigated in the prospective of the clinical use of these new potential stem cell sources for organ regeneration. Moreover, starting from the data obtained in this thesis, future studies should study how stem cells can communicate with adult or progenitor cells in order to maintain the integrity of renal structure. The sharing of proteins and mRNA through exosomes and microvesicles will be the next step to better clarify the mechanism of communication between cells.

CHRONIC KIDNEY DISEASE

CHAPTER 7

INTRODUCTION

7.1 Non-communicable diseases

The end of the 20th century was characterised by significant demographic changes, particularly prominent in the developing nations. This has been the result of different factors including advances in medical practice and technology related to communicable disease, reduction of nutritional deficiency disorders, economic improvement and development of public health programmes. Life expectancy has lengthened, increasing the exposure to the risk factors of non-communicable diseases, (NCDs) like tobacco use, unhealthy diet, lack of physical activity and alcohol abuse (Codreanu *et al.*, 2006). To date NCDs are the largest cause of death in the world, and cardiovascular disease, cancer, chronic lung disease, and diabetes mellitus are considered NCDs (Perico *et al.*, 2012). Actually, the prevalence of these chronic diseases is projected to increase over the next decades. According to WHO, the worldwide number of patients with diabetes in 2000 was estimated to be 171 million, in 2030 will be estimated 366 million (Wild *et al.*, 2004).

In all countries, the increased burden of NCDs is also an ever-growing economic cost. For example, it has been anticipated that in the United States, cardiovascular disease and diabetes together cost $750 billion annually (Narayan *et al.*, 2010). As observed by the World Economic Forum's 2009 report, NCDs are among the most severe threats to global economic development.

7.1.1 Chronic kidney disease

Chronic kidney disease (CKD) is a key determinant of the poor health outcome for major NCDs. CKD is a general term for heterogeneous disorders that affect the structure and function of the kidney but also include some complications such as hypertension, anemia, malnutrition, bone and mineral disorders, and neuropathy as well as increased risk of cardiovascular disease. The definition of CKD is based on the presence of kidney damage (ie. albuminuria) or decreased kidney function (ie. glomerular filtration rate [GFR] below 60 ml/min per 1.73 m^2) for 3 months. Because of the central role of GFR in the pathophysiology of complications, the disease is classified into five stages on the basis of GFR: >90 ml/min per 1.73 m^2 (stage 1), 60-89 ml/min per 1.73 m^2 (stage 2), 35-59 ml/min per 1.73 m^2 (stage 3), 15-29 ml/min per 1.73 m^2 (stage 4), less then 15 ml/min per 1.73 m^2 (stage 5). The U.K. National Institute of Health and Clinical Excellence (NICE) has modified in 2008 the KDOQI CKD classification by subdividing CKD stage 3 into 3A and 3B, estimated GFR of 45 to 59 ml/min per 1.73 m^2 and 30 to 44 ml/min per 1.73 m^2, respectively. The NICE CKD guidelines also stipulated that the suffix p be added to the stages in proteinuric patients (National Kidney Foundation, 2002; Vassalotti *et al.*, 2007; Stevens *et al.*, 2009).

CKD is a worldwide threat to public health, but the true dimension of this problem is not fully appreciated. On potential outcome of CKD is end-stage renal disease (ESRD), requiring costly

renal replacement therapy, which consists primarily of kidney transplantation, haemodialysis and peritoneal dialysis. In developed countries, ESRD is a major cost for health-care system, with annual growth of dialysis programs ranging between 6% and 12% over the past two decades and continuing to grow (Couser *et al.*, 2011).

Approximately 2 million people are currently treated with renal replacement therapy (RRT), but this likely represents less than 10% of those who need (Eggers, 2011). More than 90% of these individuals live in industrialized countries, while available RRT in developing countries is scarce, and null in underdeveloped areas. Indeed, 112 countries, with a combined population of over 600 million people, cannot afford renal replacement at all-resulting in the death of over 1 million people annually from untreated kidney failure (Couser *et al.*, 2011).

The most obvious social effect of CKD is the enormous financial cost and loss of productivity associated with advanced kidney disease. Many developed nations spend more than 2-3% of their annual health-care budget to provide treatment for ESRD, while the population with ESRD represents approximately 0.02-0.03% of the total population (Couser *et al.*, 2011).

According to the 2010 US Renal Data System Annual Data Report, the leading causes of CKD leading to kidney failure in the United States are diabetes, hypertension and glomerulonephritis (Collins *et al.*, 2009). A conceptual model for the course of CKD has been identified (Figure 7.1). This model describes, how the kidney disease tends to worsen over

time through a sequence of risk factors like susceptibility, initiation, progression factors and end-stage factors. Susceptibility factors can be genetic, developmental or demographic factors. Initiation factors are conditions that can cause kidney damage, as diabetes, hypertension and autoimmune diseases. Progression factors include elevate blood pressure, higher level of proteinuria, poor glycemic control in diabetes, and smoking, while end-stage factors influence the risk for the development of adverse outcome in patients with kidney failure. Once established, CKD progression is influence by a number of non-modifiable and modifiable risk factors (Taal *et al.*, 2008). The non-modifiable progression risk factors include age; gender: the ESRD occurs more frequently in men than in women; race: the incidence and prevalence of diabetic and hypertensive CKD are higher in African and Hispanic Americans compared with Caucasians (Traver-Carr *et al.*, 2002); and genetics: recent technologic advancements in genome-wide association studies are likely to uncover new CKD susceptibility genes. The modifiable progression risk factors include systemic hypertension, proteinuria and metabolic factors. Moreover, cigarette smoking, alcohol consumption and drug use can influence the progression of CKD (Floege J *et al.*, 2010).

The progression of CKD is associated with the appearance of progressive scarring that lead to loss of kidney function and ESRD. Scarring is characterized by loss of intrinsic renal cells and their replacement with fibrous tissue made of collagenous extracellular

matrix (ECM) that affects the glomeruli (glomerulosclerosis), tubules and interstitium (tubulointerstitial fibrosis), and vessels (vascular sclerosis) (Floege J *et al.*, 2010). This fibrotic process is preceded by kidney cell loss through apoptosis or necrosis, phenotypic changes towards embryonic phenotype (epithelial-mesenchymal transition), and proliferation of myofibroblasts with subsequent increased ECM synthesis.

In the past decades, ample evidence from clinical trials and meta-analysis has shown the efficacy of several treatments for CKD, to reduce risk of progression to ESRD. These treatments are based on the control of hypertension with inhibitors of the rennin-angiotensin system which slowing the progression of diabetic and non-diabetic CKD (Remuzzi *et al.*, 2002). In addition, lifestyle intervention (wight loss, smoking cessation), tight diabetes control, and treatment of other cardiovascular risk factors as dyslipidemia are associated with a slow progression to ESRD (Couser *et al.*, 2011).

7.2 Adriamycin toxicity

In literature different experimental model of CKD are described. In this study, we chosen ADR-induced nephropathy as it is universally considered the prototypical experimental model of human primary focal segmental glomerulosclerosis (FSGS). So, in this animal model we

studied the effect of bone marrow derived mesenchymal stem cells. This section of the introduction focuses on features of adriamycin nephrotoxicity and goes deeper inside the mechanisms underlying toxicity.

7.2.1 Metabolism of adriamycin

Adriamycin (ADR; doxorubicin) is an anthracycline antibiotic, a class of anti-tumour drugs used for the treatment of solid tumors including breast cancer and childhood leukemias (Lee V *et al.*, 2011). Unfortunately, this broadly successful antineoplastic agent has also been shown to be cardiotoxic and nephrotoxic (Berthiaume *et al.*, 2007; Bertani *et al.*, 1982).

Detailed pharmacokinetic studies have been performed in human and animals. Adriamycin is not significantly metabolized; indeed, it is rapidly cleared from the plasma after intravenous administration, deposited in the tissue, and slowly excreted into urine and bile. Adriamycin accumulates mainly in the kidney but also in liver, heart and small intestine (Lee V *et al.*, 2011).

Different mechanisms have been proposed for the cytostatic and cytotoxic action of ADR, including intercalation into DNA, inhibition of topoisomerase II, free radical formation and lipid peroxidation (Figure 7.2). Cells in the S phase of the cell cycle appear to be most sensitive to the cytotoxic action of ADR, the antibiotic inhibits both cellular DNA and RNA synthesis, presumably by binding to nucleic acid (Gewirtz,

1999; Momparler *et al.*, 1976). Intercalation of ADR into DNA inhibits the progression of the topoisomerase II, which is a nuclear enzyme that regulates the overwinding or underwinding of DNA and it is essential for cell replication. ADR stabilizes the topoisomerase II complex preventing the DNA double helix from being resealed and thereby stopping the process of replication (Gewirtz, 1999; Bodley *et al.*, 1989).

Another toxic effect of ADR is due to the capacity of this antibiotic to form free radicals. The quinone structure permits ADR to act as an electron acceptor. The addition of free electron, converts the quinone to semiquinone free radicals, which may induce DNA damage or form superoxides, hydroxyl radicals and peroxides if they interact with molecular oxygen (Gewirtz, 1999). There is further evidence for free-radical generation due to the formation of complexes between ADR and iron formation with consequent induction of DNA damage or lipid peroxidation (Gewirtz, 1999; Eliot *et al.*, 1984; Gianni *et al.*, 1985). All these cytotoxic and cytostatic effect of ADR, result in the induction of apoptotic cell death, which is the final cellular response to upstream events such as inhibition of topoisomerase II (Gewirtz, 1999; Ling *et al.*, 1993).

7.2.2 Pathophysiology of ADR-induced nephropathy

ADR-induced nephropathy in rats is universally considered to be the prototypical experimental model of human primary focal segmental glomerulosclerosis (FSGS). In both experimental models and affected

humans, the podocytes are the site of the initial injury in the development of FSGS (Pippin *et al.*, 2009). Adriamycin exerts oxidative damage on cell structure through a direct reduction to a semiquinone radical or by producing ROS via the xanthine oxidase system. The ROS-mediated injury is associated with down-regulation and shift in polarity of α-3 and α-5 integrin expression, key molecules for maintenance of podocyte shape and adhesion. Changes in these integrins, may underlie podocyte foot process fusion and alteration in the cell-cell and cell-matrix interactions, with consequent podocyte loss (Fogo, 2003; Pippin *et al.*, 2009).

The loss of podocytes has been linked to an altered expression of numerous factors, as vascular endothelial growth factor and its receptors, which decreasing in glomerular endothelial cells cause adverse effects on capillary growth and permselectivity. All resulted in the formation of segmental glomerulosclerosis, followed by global sclerosis and interstitial fibrosis (Fogo, 2003; Pippin *et al.*, 2009). The tubulointerstitial fibrosis is strongly linked to macrophage infiltration and ongoing proteinuria.

7.3 Stem cell therapy in chronic kidney disease

As discussed in section 1.3, kidney has an intrinsic capacity to undergo repair after acute damage, and this is best illustrated by the capacity of tubular cells to replace damaged ones. The same does not occur in chronic kidney disease. This is probably due to the complexity of the chronic kidney damage, which involves different populations of renal cells. Moreover, glomeruli have rather limited capacity for repair and once the damage has reached a certain point, the ability to recuperate from the injury is compromised and may primarily dependent on extrarenal cellular sources. Several studies have shown that bone marrow treatment may lead to improvement of renal function in several diseases, including IgA nephropathy and Alport's syndrome. Imasawa and co-workers showed in a mouse model of spontaneous presentation of IgA nephropathy an amelioration of disease after bone marrow transplantation from an unaffected donor (Imasawa *et al.*, 1999). Whole BM transplantation has been reported to induce a significant improvement in renal function and histological damage in the collagen4α3 defective model of Alport syndrome (Sugimoto *et al.*, 2006; Prodromini *et al.*, 2006). These positive results are also accompanied by conflicting findings. Using chimeric mice transplanted with enhanced green fluorescent protein (EGFP)-expressing BM, Li *et al.* have demonstrated that BM may also act as a source of α-SMA-positive interstitial myofibroblasts, which have been shown to participate in the

production of extracellular matrix in renal fibrosis (Li *et al.*, 2007).

Accumulating evidence suggests that MSCs are efficacious in acute kidney injury. Conversely stem cells in models of CKD is a new area of investigation with many open questions as whether CKD, which has different many causes, has a complex pathophysiology and is associated with different segments of the nephron, can be repaired by using stem cell treatment (Table 1). In a mouse model of Alport syndrome, Ninichuk and coworkers have observed that multiple intravenous injections of MSCs reduced interstitial renal fibrosis but not glomerulosclerosis, and also had no effect on functional and physiological parameters as proteinuria (Ninichuk *et al.*, 2006). In the rat remnant kidney model (5/6 nephrectomy), Semedo *et al.* have observed that a single injection of MSCs was sufficient to reduce interstitial fibrosis and glomerulosclerosis. However, functional restoration was only temporary achieved with a single dose of MSCs, while frequent and continuous MSC treatments effectively ameliorated renal functional parameters (Semedo *et al.*, Dec 2009). Conflicting results were also observed in an Adriamycin model of nephropathy. Magnasco and co-workers have observed the protective effect of MSCs on adriamycin-damaged podocytes in vitro. However, *in vivo* experiments showed that MSCs failed to ameliorate proteinuria and progression of renal failure (Magnasco *et al.*, 2008).

In order to identify a most adequate method to deliver MSCs, Cavaglieri *et al.* have tested the effect of subcapsular injection of MSCs

in the rat remnant kidney model. The Authors observed a migration of these cells into renal parenchyma, resulting in a significant reduction of albuminuria and serum creatinine and glomerulosclerosis. These results could suggest that locally implanted MSCs into the kidney could represent an effective route for MSC delivery (Cavaglieri *et al.*, 2009).

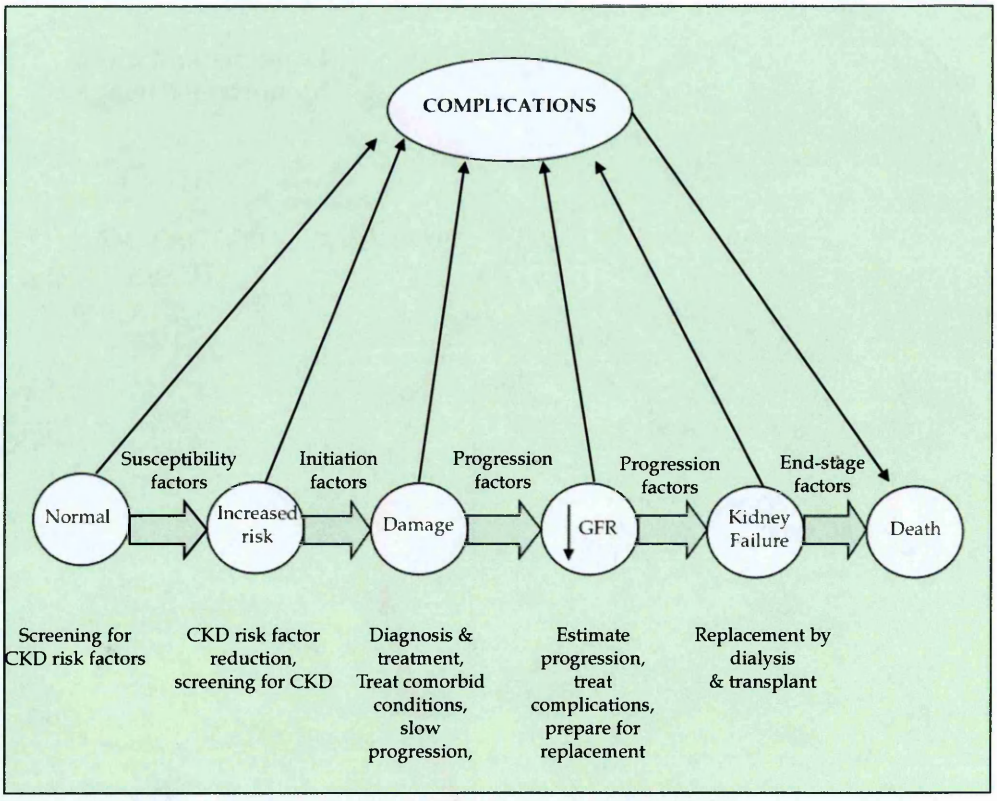

Figure 7.1: Conceptual model for chronic kidney disease (Modified from Levey A. et al., 2009)

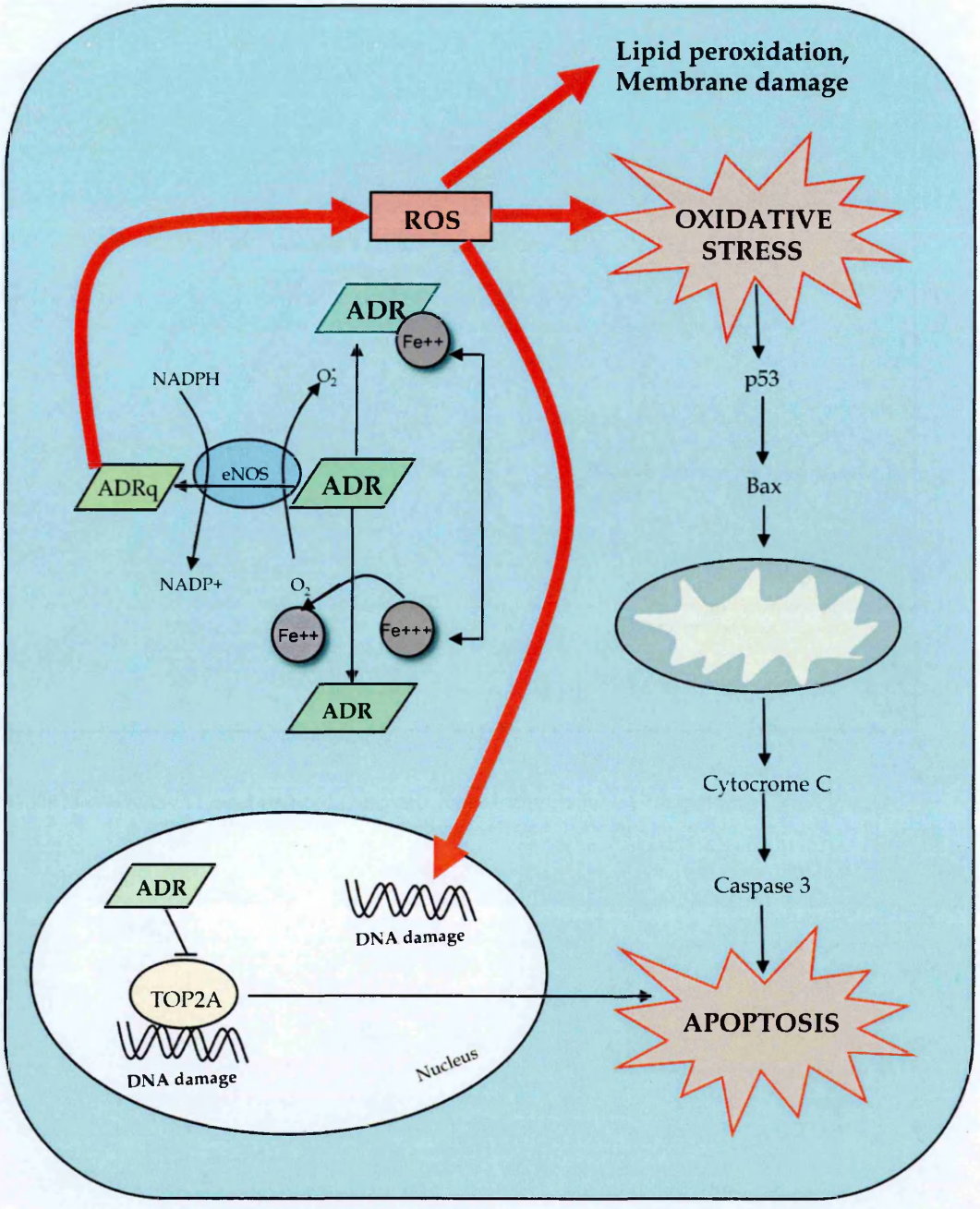

Figure 7.2: Main biological effects of Adriamycin (ADR))

Table 7.1. Summary of studies using mesenchymal stem cells (MSCs) isolated from bone marrow to treat chronic kidney disease

Reference	Model	Number and Cell Type	Functional Outcome	Delivery Method	Histology
Ninichuk *et al.*, 2006	COL4A3 KO	MSC (1×10^6)	No change in renal function	Tail vein	↓ Interstitial fibrosis
Kunter et al., 2006	Anti-Thy1.1 (GN)	MSC (2×10^6)	Improved renal function and decreased proteinuria	Intra-arterially	↓ Glomerulosclerosis
Choi *et al.*, 2009	5/6 nephrectomy	MSC (1×10^6)	No change in creatinine and decreased proteinuria	Tail vein	↓ Glomerulosclerosis
Cavaglieri *et al.*, 2009	5/6 nephrectomy	MSC (2×10^6)	Increased albuminuria and serum creatinine	Subcapsule	↓ Glomerulosclerosis
Semedo *et al.*, 2009	5/6 nephrectomy	MSC (2×10^5)	Amelioration of renal function	Tail vein	↓ Lymphocytic infiltration, ↓Interstitial fibrosis, ↓Glomerulosclerosis
Prodromidi *et al.*, 2006	COL4A3 KO	MSC (5×10^5)	No amelioration of renal function	Tail vein	No improvement in glomerular histology and interstitial fibrosis

7.4 Aim of the study

Given the extensive amount of literature related to the renoprotective effect of BM-MSCs in experimental model of AKI, we wanted to test the possible therapeutic effect of this population of stem cells in an experimental model of CKD. In a model of spontaneously progressive glomerular injury, we have previously shown that podocyte loss, abnormal migration, and proliferation of glomerular parietal epithelial progenitor cells contributed to the formation of synechiae and crescentic lesions. Here, we have aimed to investigate whether a similar sequence of events could be extended to rats with adriamycin (ADR)-induced nephropathy. Moreover, we wanted to evaluate the regenerative potential of BM-MSCs on glomerular resident cells as progenitor cells. Another important goal of this study was to clarify *in vitro* the mechanisms underlying the renoprotective effect of this population of stem cells. We have investigated which kind of regenerative pathways are activated or blocked by BM-MSCs.

CHAPTER 8

MATERIALS

8.1 Mice and Rats

C57BL6/J male mice and Lewis male rats were purchased from Charles River Italia s.p.a., Calco, Italy.

8.2 Cells

Rat MSCs. Rat mesenchymal stem cells were isolated from bone marrow of 2 month-old male Lewis rats.

Murine MSCs. Murine mesenchymal stem cells were isolated from bone marrow of 2 month-old male C57BL6/J.

Murine Podocytes. Immortalized mouse podocyte line was kindly given by Dr. Peter Mundel of "Department of Medicine" at Mount Sinai School of Medicine, New York, USA.

8.3 Media, supplements and cell culture reagents

Penicillin-Streptomycin, liquid containing 10,000 units of penicillin and 10,000 µg of streptomycin, GIBCO-Invitrogen, S. Giuliano Milanese (MI), Italy, was used at 1% (1ml/100ml).

L-Glutamine-200 mM, liquid, GIBCO-Invitrogen.

"Isolation medium" for rat MSCs

Alpha-MEM, GIBCO-Invitrogen.

+ 1% penicillin -streptomycin

+ 2% Foetal Calf Serum (FCS), selected lot. Euroclone.

+ 2 mM L-Glutamine, GIBCO-Invitrogen.

"Growth medium" for rat MSCs

Alpha-MEM, GIBCO-Invitrogen.

+ 1% penicillin -streptomycin

+ 20% Foetal Calf Serum (FCS), selected lot. Euroclone.

+ 2 mM L-Glutamine, GIBCO-Invitrogen.

"Inductive medium" for rats MSCs

Alpha-MEM, GIBCO-Invitrogen.

+ 1% penicillin -streptomycin

+ 20% Foetal Calf Serum (FCS), selected lot. Euroclone.

+ 2 mM L-Glutamine, GIBCO-Invitrogen.

Adipogenic supplements:

5 μg/ml insulin, Sigma-Aldrich, St Louis, MO, USA.

+ 10-6 M dexamethasone, Sigma-Aldrich.

+ 0.5 μM isobutylmethylxanthine, Sigma-Aldrich.

+ 50 μM indomethacin, Sigma-Aldrich.

Osteogenic supplements:

10 mM β-glycero-phosphate, Sigma-Aldrich.

+ 0.2mM ascorbic acid 2-phosphate, Sigma-Aldrich.

+ 10^{-8} M dexamethasone, Sigma-Aldrich.

"Growth medium" for podocytes

RPMI 1640, Sigma-Aldrich

+ 1% penicillin -streptomycin

+ 10% FCS, GIBCO-Invitrogen

+ 2 mM L-Glutamine, GIBCO-Invitrogen

+ 10 U/ml recombinant murine γ-interferon (permissive conditions), Peprotech, Rocky Hill, NJ, USA.

"Isolation medium" for murine MSCs

DMEM, Sigma-Aldrich

+ 1% penicillin -streptomycin, GIBCO-Invitrogen.

+ 2% Foetal Calf Serum (FCS), selected lot from Euroclone.

+ 2 mM L-Glutamine, GIBCO-Invitrogen.

"Growth medium" for murine MSCs

DMEM, Sigma-Aldrich

+ 1% penicillin -streptomycin

+ 20% Foetal Calf Serum (FCS), selected lot. Euroclone.

+ 2 mM L-Glutamine, GIBCO-Invitrogen.

"Test medium" (for *in vitro* experiments)

RPMI, Sigma-Aldrich

+ 2 mM L-Glutamine, GIBCO-Invitrogen

+ 10% FCS, GIBCO-Invitrogen

+ 1% penicillin -streptomycin, GIBCO-Invitrogen

Trypsin

Trypsin for MSCs: 0.25% Trypsin-EDTA (1X) in Hanks' Balanced Salt and phenol red was purchased from GIBCO-Invitrogen.

Trypsin for podocytes: 0.5% Trypsin-EDTA (10X) was purchased from GIBCO-Invitrogen.

8.4 Growth factors

Recombinant mouse VEGF-A was purchased from Immunotools, Germany.

8.5 Chemicals

Adriamycin (ADR) was purchased from Pfeizer Italia s.r.l, Latina, Italy.

Alizarin Red S (sodium alizarin sulfonate) was purchased from Sigma-Aldrich. 2% Solution was prepared by dissolving the powder in

distilled water. Solution was stirred and centrifuged at 4000 rpm for 10 minutes. The supernatant was collected and filtered. pH was adjusted at 4.1 with 0.5% ammonium hydroxide.

Coomassie brilliant blue dye was purchased from Sigma-Aldrich.

Ethanol was purchased from Carlo Erba, Milan, Italy.

Formalin solution, ready to use was purchased from Bio-Optica.

Harris haematoxylin and eosin was purchased from Bio-Optica, Milan, Italy.

Isofluorane was purchased from Abbot.

Mounting medium was purchased from DakoCytomation, Glostrup, Denmark.

Oil Red O was purchased from Sigma-Aldrich. We prepared a 0.5% solution in methanol. Solution was stirred and centrifuged at 4000 rpm for 10 minutes. The supernatant was collected and filtered.

Orthophosphoric acid was purchased from Merck, Milan, Italy.

Paraffin, Bioplast Plus, was purchased from Bio Optica.

Paraformaldehyde was purchased from Electron Microscopy Sciences (Hatfield, PA, USA). In order to prepare a 4% solution, we diluted 8% aqueous solution in PBS 2X under a fume hood.

Periodic acid, Diapath, Martinengo, Bergamo, Italy

Schiff's reagent, Kaltek srl, Padova, Italy

Streptavidin-alkaline phosphatase conjugated was purchased from Roche Diagnostic and used at final concentration of 1:50.

Toluene was purchased from Sigma-Aldrich.

Trypan blue (4% solution) was purchased from Sigma-Aldrich. This solution was diluted 1:2 with saline and filtered (0.4 μm filters).

8.6 Buffers and solutions

"Blocking buffer "

Bovine serum albumin (BSA) (Sigma-Aldrich) was added to PBS to obtain a final BSA concentration of 1%. The solution was maintained on ice for few minutes to facilitate albumin solubilisation. The solution was then filtered with a 0.2 μm sterile filter.

"Buffer" for immunodepletion

PBS 1X have been added with:

EDTA 2 mM

BSA 0.5%

The solution was then filtered with a 0.4 μm filter.

Citrate buffer 10% concentrated pH 6.0, was diluted 1:10 in PBS 1X and was purchased from DiaPath .

3,3'-diaminobenzidine (DAB)

One tablet of DAB was put into 25 ml of distilled water. Solution was mixed and 6.5 μl of 30% H_2O_2 was added.

DAB was purchased from Merck.

Duboscq-Brazil solution ready to use, was purchased from DiaPath, Martinengo (BG), Italy.

Fast Red

One tablet was dissolved into 2 ml of 0.1 M TRIS-HCl (pH 8.2) and then filtered with a 0.45 μm filter. It was purchased from Roche.

Paraformaldehyde-lysine-periodate (PLP) fixative

Solution A: 8% paraformaldehyde, purchased from Electron Microscopy Sciences (Hatfield, PA, USA).

Solution B: 0.05 M Phosphate buffer Stock (pH 7.4)

- Dissolve 0.69 gr of Sodium Phosphate Monobasic Monohydrate in 100 ml of dH_20 (solution I)

-Dissolve 4.45 gr of Sodium Phosphate in 500 ml of dH_20 (solution II)

- Add 95 ml of solution I and 405 ml of solution II.

Solution C:

-Dissolve 9.13 gr of L-Lysine (Sigma-Aldrich) and 1.425 gr of Sodium m-Periodate (Sigma-Aldrich) in 500 ml of Solution B.

Solution D: PLP fixative

- Add 10 ml of solution A and 30 ml of solution C

"Permeabilizing solution"

TRITON X100 was purchased from Sigma-Aldrich and was diluted to a

final concentration of 0.5% in PBS 1X.

Phosphate buffer saline (PBS) 10X (for cell culture and immunohistochemistry) was purchased from Ambion-Invitrogen. Finally, PBS 1X is prepared diluting 1:10 PBS 10X in water.

Vector Red substrate, Vector Laboratories Inc.

One tablet was dissolved (and kept in the dark) in 2 ml of TRIS-HCl immediately before using and filtered with a 0.45 μm filter.

8.7 Materials and buffers for Western blotting

30% acrylamide/bis solutions, liquid, 99.9% pure acrylamide and bis-acrylamide at the concentration of 30%, crosslinker ratio 37.5:1, purchased from Bio-Rad.

Ammonium persulfate $(NH_4)_2S_2O_8$ (APS), powder, purchased from Sigma-Aldrich. A 10% stock solution was prepared in water.

Bio-Rad protein assay reagent, purchased from Bio-Rad.

Bicinchoninic acid assay, purchased from Thermo Scientific, Rockford, IL, USA.

Filter paper 3MM, purchased from Whatman.

Glycine, 0.2% Glycine solution was prepared by dissolving 0.2 g glycine in PBS 2X. Glycine was purchased from Sigma-Aldrich.

Halt protease inhibitor cocktail, purchased from Thermo Scientific.

Hyperfilm™ ECL, high performance chemiluminescent film, purchased from Amersham Biosciences.

N,N,N',N'-tetramethylethylenediamine (TEMED), liquid, purchased from Sigma-Aldrich.

Non fat dry milk, purchased from Sigma-Aldrich.

Phenylmethylsulfonyl fluoride (PMSF), powder, purchased from Sigma-Aldrich. A stock solution (200 mM) was prepared in isopropyl alcohol.

Protran® Nitrocellulose membrane, purchased from Whatman.

SeeBlue® Plus2 Pre-stained Standard, purchased from GIBCO-Invitrogen. It contains eight blue-dyed and two with contrasting colours providing easier band identification.

Sodium dodecyl sulfate (SDS), liquid, purchased from Sigma-Aldrich.

Sodium orthovanadate (Na_3VO_4), powder, purchased by Sigma-Aldrich. A stock solution of 1 mM was constituted in distilled water and adjusted to pH 10. To ensure the presence of monomers, the solution was boiled until translucent and the pH readjusted.

Supersignal west pico chemiluminescent substrate working solution: chemiluminescent detection system composed by luminol/enhancer solution and stable peroxidase solution, was purchased from Pierce, Rockford, Illinois, USA.

Supersignal chemiluminescent substrate purchased from GE Healthcare, UK

Tris-HCl was purchased from Sigma-Aldrich. A solution of 50mM was prepared by solubilising 0.3028 g TRIS-HCl into 50 ml of distilled water. The pH was adjusted to 8.

Tween 20, purchased from Sigma-Aldrich.

X-ray Developer and Fixer solutions, purchased from Kodak Industry.

- Rabbit anti mouse **Akt** antibody, purchased from Cell Signaling Technology, Danvers, MA, USA, and used at the concentration of 1:1000.

- Rabbit anti mouse **p-Akt** Ser473 antibody, purchased from Cell Signaling Technology, and used at the concentration of 1:1000.

- **Horseradish peroxidase (HRP) conjugated goat anti rabbit** antibody was purchased from Sigma-Aldrich, and used at the concentration of 1:4000.

- Goat anti rat anti-**$VEGF_{164}$** antibody was purchased from R&D System and used at the final concentration of 1:200.

- Mouse anti rat **α-tubulin** antibody was purchased from Sigma-Aldrich and used at the final concentration of 1:4000.

- **Horseradish peroxidase (HRP) conjugated rabbit anti goat** antibody was purchased from Sigma-Aldrich, and used at the concentration of 1:20000.

- **Horseradish peroxidase (HRP) conjugated goat anti mause** antibody was purchased from Sigma-Aldrich, and used at the concentration of 1:20000.

Scraping buffer

A cold solution of PBS 1X containing 2 mM EDTA (Sigma-Aldrich) and the protease inhibitor phenylmethylsulfonyl fluoride PMSF (1 mM) was used to mechanically detach the cells using a scraper.

Lysis buffer

For frozen kidney section, lysis buffer was composed by 50 mM Tris-HCl (pH 8; Sigma-Aldrich), 150 mM NaCl (Merck), 1% Triton X-100, 0.5% Sodium deoxycholate, 0.1% SDS) containing the Halt protease inhibitor cocktail (Thermo Scientific, Rockford, IL, USA) at the final concentration of 1X.

For podocytes, lysis buffer was composed by 20 mM Tris-HCl (pH 7.5), 1%Triton X-100, 25 mM NaCl, 1.5 mM EDTA, 50 mM NaF and 15 mM $Na_4P_2O_7$ containing protease inhibitor (Complete, Roche Diagnostic).

Sample Buffer 3X

Sample buffer 3X was composed by Tris-HCl 0.24 M at pH 6.8, 6% SDS (Sigma-Aldrich), 15% β-mercaptoethanol (Merck), 30% glycerol (Fischer Scientific), 0.03% bromophenol blue (Sigma-Aldrich) in water.

TANK buffer 10X

TANK buffer was composed by 250 mM Tris base (Sigma-Aldrich) and 2M glycine (Sigma-Aldrich) in water.

8.8 Antibodies

For all antibodies, preliminary experiments were performed following manufacturer's suggestions in order to identify the most appropriate concentration.

- Rabbit anti-**Wilm´s tumor 1** (SC-192), purchased from Santa Cruz Biotechnology, Santa Cruz, CA, USA. Final concentration: 2 μg/ml.
- Mouse anti-**Nestin** (611658), purchased from BD Biosciences, Milan, Italy. Final concentration: 1:100.
- Rabbit anti-**CD2AP** (SC-9137), purchased from Santa Cruz Biotechnology, Santa Cruz, CA, USA. Final concentration: 0.2 μg/ml.
- Goat anti-**Nephrin** (SC-32530), purchased from Santa Cruz Biotechnology, Santa Cruz. Final concentration: 0.2 μg/ml.
- Rabbit anti-**claudin1** (PA5-13332), purchased from Thermo Scientific, Rockford, IL, USA. Undiluted.
- Mouse anti-**NCAM** (5B8), purchased from Developmental Studies Hybridoma Bank, University of Iowa, USA. Final concentration: 1:2.
- Mouse anti-rat endothelial cell antigen (**RECA-1;** MCA970R),

purchased from AbD Serotec, Kidlington, Oxford, UK. Final concentration 1:100.

- Monoclonal anti rat monocytes/macrophages (**ED-1;** MAB1435) antibody, purchased from Chemicon. Final concentration 1:100.

- Goat anti-rat **VEGF** antibody (AF564) was purchased from R&D Systems and used at the final concentration of 1:10.

- **Biotinilated-horse anti-goat** IgG antibody (BA-9500) purchased from Vector Labs and used at the concentration of 1:150.

- **Cy3-conjugated goat anti rabbit IgG** (111-165-003), purchased from Jackson ImmunoResearch Laboratories and used at final concentration of 1:50.

- **FITC-conjugated goat anti mouse IgG** (115-095-003), purchased from Jackson ImmunoResearch Laboratories and used at final concentration of 1:50.

- **FITC-conjugated rabbit anti goat IgG** (305-095-003), purchased from Jackson ImmunoResearch Laboratories and used at final concentration of 1:50.

- **Cy3-conjugated donkey anti mouse IgG** (715-165-150), purchased from Jackson ImmunoResearch Laboratories and used at final concentration of 1:50.

- **Cy5-conjugated donkey anti mouse IgG** (715-175-150), purchased from Jackson ImmunoResearch Laboratories and used at final concentration of 1:50.

- **Biotinylated sheep anti-mouse IgG** (AP302B), purchased from

Chemicon and used at final concentration of 1:50.

For immunodepletion of murine MSCs:

-Rat anti-mouse **CD45** antibody (550539), purchased from Beckton Dickinson and used at a concentration of 0.2 μg/10^6 cells diluted in buffer.

- **MACS goat anti-rat IgG magnetic microbeads** (130-048-501), purchased from Miltenyi Biotec.

For in vitro experiments:

- **Functional blocking anti-VEGF** antibody (AF471) was purchased from R&D System and used at final concentration of 10 μg/ml.

- Mouse anti-**cytochrome C** antibody (556432) was purchased from BD Biosciences and diluted 1:100 in blocking buffer.

- Rabbit anti-**cleaved caspase-3** antibody (9661) was purchased from Cell Signaling (Beverly, MA, USA) and used at the final concentration of 1:400.

- FITC-conjugated **donkey anti rabbit** antibody (711-095-152) purchased from Jackson ImmunoResearch Laboratories and used at final concentration of 1:50.

8.9 Other reagents

Collagenase IV was purchased from Worthington Biochemical Corporation, Lakewood, NJ, USA.

Collagen Rat Tail Type I was purchased from BD Biosciences. It was used at the final concentration of 0.1 mg/ml.

Dapi: 4′,6′-diamidino-2-phenylindole dihydrochloride hydrate was purchased from Sigma-Aldrich.

FITC-labeled lectin Wheat Germ Agglutinin (WGA) was purchased from Vector Lab., Burlingame, CA, USA. Final concentration 1/400.

Hoechst 33258 was purchased from Sigma-Aldrich.

In Situ Cell Death Detection Kit (TUNEL), Fluorescein was purchased from Roche.

Nanoparticles: negative poly-methyl-methacrylate (PMMA)-based nanoparticles of 200nM (200-) was kindly provided by Dr. Davide Moscatelli, Politecnico di Milano, Italy.

PKH-26: Red Fluorescent Cell Linker Kit for general cell membrane labeling was purchased from Sigma-Aldrich.

Rhodamine-labelled Lectin Lens Culinaris Agglutinin (LCA) was purchased from Vector Laboratories Inc., and used at the final concentration of 25 μg/ml.

Vectastain ABC kit purchased from Vector Laboratories, Burlingame, CA, USA.

8.10 Disposable material

Sterile filters: 100 μm nylon mesh, purchased from BD Biosciences, Bedford, MA, USA

8.11 Instruments

Confocal laser-scanning microscope LS 510 Meta; Zeiss, Jena, Germany.

FACS Canto II Becton Dickinson, BD Bioscience, Milan, Italy.

MACS Separator: Miltenyi Biotec, Bergisch Gladbach, Germany.

Reflotron analyser purchased from Roche, Basel, Switzerland .

CHAPTER 9

METHODS

Methods for *in vivo* studies

9.1 Isolation and characterization of rat MSCs

Rat MSCs were obtained from bone marrow (BM) of 2 month-old male Lewis rats (Materials, section 8.2). Rats were sacrificed by exposure to CO2 for a few minutes. Under a laminar flow hood, femurs and tibias were aseptically removed from the posterior legs by using sterilized surgical instruments. BM was flushed from the shaft of each bone by using a syringe filled with "Isolation medium" (Materials, section 8.3). Each bone was washed twice with 2 ml of medium. BM obtained from each rat was collected in different tubes and maintained on ice. Tubes were centrifuged at 1200 rpm for 10 min at 4 °C and then the pellet was suspended by using a 2 ml pipette in a volume of 2 ml alpha-MEM serum-free. Several passages into pipette were needed in order to disaggregate bone marrow and to obtain a single cell suspension. Eight ml of medium were added and cells were dissociated by aspirating through a syringe needle (21Gx1 9/16"). Thereafter, the cell suspension was filtered through a 100-µm sterile nylon mesh filter (Materials, section 8.10) to eliminate bone fragments and to produce a single cell suspension. Cells were counted by a haemocytometer and cells obtained from one rat (4 bones) have been seeded in complete medium onto one flask (75 cm^2), left to adhere for 24 hours and maintained at 37 °C in a CO_2 incubator with 5% CO_2.

Mesenchymal stem cells (MSCs) were recovered from BM by their tendency to tightly adhere to plastic culture dishes. After 24 hours, non-adhered cells have been transferred to a new flask and left to adhere for other 48 hours. After 48 hours, all the flasks have been washed with PBS 1X to remove unadhered cells (mainly haematopoietic cells). Adhered MSCs have been added with freshly prepared "growth medium" (Materials, section 8.3) that was changed every three days. After 2 to 3 weeks, subconfluent cells were detached by adding 500 µl trypsin-EDTA (Materials, section 8.3) and by incubating for 2 minutes at 37°C. Trypsin was blocked by addition of 5 ml "growth medium". Detached MSCs were combined, counted by haemocytometer and stored in liquid nitrogen for in vivo experiments. The MSCs preparation used for the *in vivo* experiments derived from a pool of MSCs obtained by bone marrow collected from 12 Lewis rats.

BM-derived cells obtained by plastic adhesion, as described above, were studied in order to verify their mesenchymal potential to differentiate towards adipocytes and osteoblasts. MSCs were grown to confluence and the growth medium was replaced with the "Inductive medium" (Materials, section 8.3) supplemented with specific differentiation reagents (Materials, section 8.3).

Adipogenesis: cells were incubated for 3 weeks with "Inductive medium" plus adipogenic supplements. Adipogenic differentiation was visualized by phase contrast microscopy by the presence of highly

refractive intracellular lipid vacuoles during this period of time in which the cells can differentiate and images were acquired by a digital camera. To further confirm the accumulation of lipid droplets in these vacuoles, cells were rinsed with PBS 1X, fixed with 10% formalin (Materials, section 8.5) and incubated with Oil Red O for 25 minutes at room temperature (Materials, section 8.5). After extensive rinsing with PBS 1X, cells were observed under phase contrast microscopy and images were acquired by a digital camera.

***Osteogenesis*:** MSCs were fed twice a week for three weeks with "Inductive medium" plus osteogenic supplements. The cells were then washed with PBS 1X and fixed in 10% formalin for 20 minutes at room temperature. Fixed cells were rinsed with PBS 1X and stained for 20 minutes with 2% w/v Alizarin Red S solution (Materials, section 8.5) to evaluate the presence of calcium rich hydroxyapatite of the extracellular matrix. Images of mineral deposits were acquired by a digital camera.

9.2 Rat model of adriamycin-induced nephropathy

Male Lewis rats (Materials, section 8.1), with initial body weights of 200-250 g, were used. Animal care and treatment were in accordance with institutional guidelines in compliance with national (D.L. n.116, G.U., suppl 40, 18 February 1992, Circolare No. 8, G.U., 14 July 1994) and international laws and policies (EEC Council Directive 86/609, OJL

358, Dec 1987; NIH Guide for the Care and Use of Laboratory Animals, U.S. National Research Council, 1996). Animal studies were submitted to and approved by the Institutional Animal Care and Use Committee of "Mario Negri" Institute, Milan, Italy. Animals were housed in a constant temperature room with a 12-hour dark 12-hour light cycle and fed a standard diet.

9.2.1 Adriamycin preparation and injection

CKD was induced by a single dose of adriamycin (ADR; Materials, section 8.5) by tail-vein infusion. To test the effect of rat MSCs, ADR was administered to rats based on their weight, at a concentration (chosen by preliminary experiments) of 5 mg/kg. We used an ADR already diluted, commonly used in patients undergoing chemotherapy. To facilitate the injection, rats were anesthetized for a few minutes in a container containing Isofluorane (Materials, section 8.5). A total volume of 500 μl of ADR was intravenously injected by using 1 ml syringe (needle 30Gx1/2").

9.3 Rat MSC administration

Rat MSCs were administered to Lewis rats 36, 60 hours, 3, 5, 7, 14, and 21 days after receiving ADR. Cells were suspended in 500 μl of

sterile saline. Before injection, rats were exposed to an infrared lamp to induce vasodilatation and facilitate injection into the tail vain. To study the effect of rat MSCs, Lewis rats were intravenously (i.v.) injected with saline (n=16), or MSCs (2×10^6 cells) (n=16) at different times after ADR in order to ensure the presence of MSCs in the kidney during time. Before injection, MSCs were labeled with PKH-26 red fluorescence cell linker (Materials, section 8.9). In selected experiments, ADR-treated rats (n=3) were injected with MSCs labeled with polymeric large nanoparticles (fluoNP; Materials, section 8.9). Six normal rats injected with saline, served as controls. Twenty-four-hour urine samples were collected using metabolic cages, and proteinuria was determined by the Coomassie protein assay (Materials, section 8.5). Serum creatinine was measured by the Reflotron test (Materials, section 8.11). Rats were sacrificed at 3, 9, 16 and 30 days after ADR, and kidneys were removed for histology and immunohistochemistry analysis.

9.4 Renal function measurement

To assess renal function, we measured total urinary protein excretion rate by using the Coomassie brilliant blue dye-binding assay. Coomassie brilliant blue (50 mg; Materials, section 8.5) was dissolved in 50 ml orthophosphoric acid 99% 16 M (Materials, section 8.5) and 46.7 ml absolute ethanol (Materials, section 8.5) then diluted to 1 L with

water. The solution was filtered through Whatman paper and stored in dark-colour glass bottles, maintaining rigorous cleanliness. The half-life of the solution is several weeks, but refiltering may be required if precipitation of dye occurs. The assay was performed in plastic cuvettes. Coomassie brilliant blue dye-reagent (2 ml) was added to 50 μl of urine samples. In each evaluation 1 sample of water alone and 3 samples with bovine serum albumin (BSA) at known concentrations (50, 100 and 200 μg/ml) were included to obtained the standard curve. Samples were always assayed in triplicate. The colour development is essentially complete at 5 minutes and remains stable for a period of 2 hours. The absorbance at 578 nm was measured at the spectrophotometer. The concentration of proteins present in the samples of interest was obtained taking into account the absorbance values derived from the standard curve in which the BSA concentrations were known.

9.5 Sacrifice and tissue collection

Rats were sacrificed by exposure to CO_2 at 3, 9, 16 and 30 days after ADR. Kidneys were weighed and in order to take samples representative of the different structural components of the kidney, sections were cut in the axial coronal plane. Depending on the type of

procedure that would have been applied (light microscopy, electron microscopy, immunohistochemistry), samples were differently fixed as described in each specific chapter.

9.6 Renal morphology

Procedure for light microscopy was the same described in chapter 3, section 3.6.1.

At least 15-20 glomeruli were examined for each rat, and the extent of synechiae was expressed by giving a score from 0 to 4 related on the percentage of glomerular tuft occupied by the lesions (0: no lesions; 1: lesions affecting <25% of the glomerulus; 2: lesions affecting >25 to 50% of the glomerulus, 3: lesions affecting >50 to 75% of the glomerulus, 4: lesions affecting >75 to 100% of the glomerulus). Data were expressed as percentage of glomeruli with different degree of lesions (synechiae and more extensive adhesions). To evaluate the extent of glomerular sclerosis, an average of 35 glomeruli was examined and data were expressed as glomerular sclerosis index. Each glomerulus was scored according to the extension of sclerotic changes as follows: 0 = absence of sclerosis; 1 = sclerotic changes affecting less than 25% of glomerular tuft area; 2 and 3 = lesions affecting >25 to 50% and >50 to 75% of the tuft, and 4 = lesions exceeding 75% of the tuft. The indices for glomerulosclerosis was calculated by using the following formula:

$GS= (1 \times n_1)+ (2 \times n_2)+ (3 \times n_3)+ (4 \times n_4)/ n_0+ n_1+ n_2+ n_3+ n_4$

Where nx = number of glomeruli in each grade of glomerulosclerosis (Davis *et al.*, 2004). The same pathologist, who was unaware of the nature of the experimental groups, analyzed all renal biopsies.

9.7 Staining and quantification of labelled MSCs

9.7.1 PKH-26 labelling

To study intrarenal localization of stem cells, rat MSCs were labelled with PKH-26 (Materials, section 8.9) before injection into ADR-treated rats, as previously described (see chapter 3, section 3.7). After staining, PKH-26 positive cells were resuspended in saline (500 µl/rat) and intravenously injected.

At different times, rats were sacrificed and kidney samples were fixed in paraformaldehyde-lysine-periodate (PLP) (Materials, section 8.6) overnight at 4°C then infiltrated with 30% sucrose/phosphate buffer saline (PBS), embedded in Tissue-Tek OCT Compound and frozen in liquid nitrogen. Eight-micrometer-thick sections were stored at -80°C. Sections were fixed 10 minutes in acetone and incubated for 10 minutes at room temperature with FITC-labeled lectin Wheat Germ Agglutinin (WGA, Materials, section 8.9). Nuclei were stained with DAPI for 15 minutes at room temperature (Materials, section 8.9). Slides

were analysed for PKH-26 positive cells. Data were expressed as number of PKH-26 positive cells/10^5 renal cells. A number of 9 sections/rat (n=3 rats) were analyzed and PKH-26 positive cells were counted.

9.7.2 Nanoparticles staining

These experiments were performed in collaboration with the group of Dr. Paolo Bigini, Laboratory of Biochemistry and Protein Chemistry at "Mario Negri" Institute for Pharmacological Research. The presence of MSCs into the damaged kidney was also evaluated by tracking MSCs with polymeric 200 nm large nanoparticles (fluoNP, Materials, section 8.9) (Lazzari *et al.*, 2012) in which the dye rhodamine-B was covalently bounded to the polymer to avoid the risk of leakage of the fluorescent compound once injected in animals. Briefly, MSCs were incubated for 72 hours with polymeric nanoparticles (35 μg/ml). At the end of the incubation, MSCs were resuspended in sterile saline and injected into the tail vein of ADR-treated rats (n=3). To verify the efficiency of the labeling, a small aliquot of MSCs was fixed with 4% paraformaldehyde in PBS, co-stained with Hoechst 33258 (Materials, section 8.9) and visualized with Confocal laser-scanning microscope LS 510 Meta (Materials, section 8.11). FACS analysis was used to quantify the number of fluoNP-labeld MSCs in the kidneys of ADR-treated rats sacrificed at 3 days. Kidneys were minced and digested with collagenase IV (300U/ml, Materials, section 8.9) for 45 min at 37°C. The

cell suspension was filtered through a 100-μm sterile filter, washed with PBS 1X and red emission for nanoparticles was analyzed by using BD FACSCanto II (Materials, section 8.11). Kidneys isolated from ADR-treated rats that did not receive fluoNP-labeled MSCs were used as negative control. The threshold used for the negative control was set at 2%.

9.8 Immunohistochemistry

9.8.1 Immunofluorescence

For all immunofluorescence experiments, sections (3-μm) from PLP-fixed kidney specimens were fixed 10 minutes in acetone at 4°C. The antigen retrieval was performed in citrate buffer (Materials, section 8.6) 10 mmol/L (pH 6.0) at boiling temperature for 20 minutes, followed by incubation with citrate buffer (20 minutes) at room temperature to enhance the reactivity of antibodies to antigens. To block nonspecific sites, sections were treated with "blocking buffer" (Materials, section 8.6) for 30 minutes at room temperature and then incubated with the following primary antibodies.

WT1. Sections were incubated overnight with rabbit anti-Wilm´s tumor 1 antibody (Materials, section 8.8) at 4°C. Subsequently, kidney samples were treated with goat anti rabbit-Cy3 antibody (Materials, section 8.8) for 1 hour at room temperature. Renal structure was stained with FITC-

WGA lectin for 10 minutes (Materials, section 8.9), while nuclei with DAPI for 15 minutes at room temperature.

In some experiments, some sections were co-incubated with anti-WT1 and anti-nestin antibodies.

Nestin. Slides were incubated overnight with mouse anti-nestin antibody (Materials, section 8.8) at 4°C. Subsequently, kidney samples were treated with goat anti mouse-FITC antibody for 1 hour at room temperature. Nuclei were stained with DAPI for 15 minutes. In some experiments, some sections were co-incubated with anti-claudin1 antibody.

CD2AP. PLP-fixed kidney sections, were incubated with rabbit anti-CD2AP antibody (Materials, section 8.8) at 4°C. Subsequently, kidney samples were treated with goat anti rabbit-Cy3 antibody for 1 hour at room temperature.

Nephrin. Slides were incubated overnight with goat anti-nephrin antibody (Materials, section 8.8) at 4°C. Subsequently, kidney samples were treated with rabbit anti goat-FITC antibody for 1 hour at room temperature.

Claudin1. Sections were incubated overnight with rabbit anti-claudin1 antibody (Materials, section 8.8) at 4°C. Subsequently, kidney samples were treated with goat anti rabbit-Cy3 antibody for 1 hour at room temperature. Then, slides were co-incubated with anti-nestin antibody.

NCAM. PLP-fixed kidney sections, were incubated overnight with mouse anti-NCAM antibody (Materials, section 8.8) at 4°C and then

treated with donkey anti mouse-Cy3 antibody for 1 hour at room temperature.

RECA-1. Slides were incubated 2 hours at room temperature with mouse anti-rat endothelial cell antigen (RECA-1) antibody (Materials, section 8.8) at 4°C and then treated with donkey anti mouse-Cy5 antibody for 1 hour at room temperature.

After each step, slides were washed with PBS 1X (two times for 5 minutes) and finally mounted with the mounting medium DAKO (Materials, section 8.5). Double and triple fluorescence labeling were analyzed by an inverted confocal laser-scanning microscope (Materials, section 8.11). Glomerular expression of the podocyte-associated proteins nephrin, CD2AP and nestin was estimated by calculating the proportion of area occupied by the staining within each glomerulus, using NIH image J software and a Mac OS PC (Apple computer, Cupertino, CA, USA). At least 30 randomly chosen glomeruli per section were analyzed.

9.8.2. Differentiative potential of MSCs

To evaluate whether MSCs acquired a podocyte phenotype, some PLP-fixed kidney sections (twenty sections/ rat, n=3) from ADR-treated rats injected with PKH-26 labeled MSCs (day 16) were stained with anti-WT1 antibody. Slides were fixed 10 minutes in acetone at 4°C, followed by boiling in citrate buffer (Materials, section 8.6) 10 mmol/L (pH 6.0) for 20 minutes and then incubation with citrate buffer (20

minutes) at room temperature. To block nonspecific sites, sections were treated with "blocking buffer" (Materials, section 8.6) for 30 minutes at room temperature and then incubated overnight with mouse anti-Wilm´s tumor 1 antibody (Materials, section 8.8) at 4°C. Subsequently, kidney samples were treated with donkey anti mouse-Cy5 antibody (Materials, section 8.8) for 1 hour at room temperature. Renal structure was stained with FITC-WGA lectin for 10 minutes, while nuclei with DAPI for 15 minutes at room temperature. After each step, slides were washed with PBS 1X (two times for 5 minutes) and finally mounted with the mounting medium DAKO (Materials, section 8.5). Fluorescence was analyzed by an inverted confocal laser-scanning microscope (Materials, section 8.11).

9.8.3 ED-1 staining

Renal tissue was fixed overnight in Dubosq Brazil, dehydrated in alcohol, and embedded in paraffin. ED1 staining was detected by alkaline phosphatase-Fast Red technique. Microwave and citrate buffer treatment was performed to increase the reactivity of antibody to antigen. The sections were blocked " blocking buffer" (Materials, section 8.6), and incubated overnight at 4°C with monoclonal anti rat monocytes/macrophages (ED-1) (Materials, section 8.8). After washing in PBS 1X, slides were incubated with biotinylated sheep anti-mouse IgG (Materials, section 8.8) for 30 minutes at room temperature. Then the sections were incubated with streptavidin-alkaline phosphatase

conjugated (Materials, section 8.5) for 30 min at room temperature. After washing in PBS 1X, Fast Red substrate (Materials, section 8.5) was applied for 5 min at room temperature. The sections were counterstained with Harris haematoxylin (Materials, section 8.5). Negative controls were obtained by omitting the primary antibody. ED1-labeled cells were counted in at least 30 randomly selected high-power microscopic fields (x400) per each animal.

9.8.4 VEGF staining

For the immunohistochemical detection of VEGF, kidneys were fixed in Dubosq-Brazil (Materials, section 8.6) and then embedded in paraffin. Three μm sections were deparaffinized and after washing with PBS 1X, endogenous peroxidases was inactivated by incubation in 3% H_2O_2 in methanol for 30 minutes. Slides were treated with "blocking buffer" (Materials, section 8.6) and then incubated with goat anti-rat VEGF antibody (Materials, section 8.8) overnight at 4°C followed by biotinylated-horse anti-goat IgG antibody (Materials, section 8.8) for 1 hour. Sections were incubated for 30-min with avidin-biotin complex solution (ABC) (Materials, section 8.9), and the staining was visualized using diaminobenzidine (DAB) (Materials, section 8.6).

Intensity of glomerular VEGF signal was graded on a scale of 0 to 3 (0, no staining; 1, weak staining, 2, staining of moderate intensity; 3, strong staining). Negative controls were obtained by omitting the primary antibody on adjacent sections.

9.8.5 Apoptosis

Apoptosis was detected by enzymatic labelling of DNA strand breaks using a terminal deoxynucleotidyl transferase-mediated deoxyuridine triphosphate nick end-labelling (TUNEL) assay (Materials, section 8.9). PLP-fixed sections were treated in citrate buffer 10 mmol/L (pH 6.0) at boiling temperature for 20 minutes, followed by incubation with citrate buffer (20 minutes) at room temperature to enhance the reactivity of antibodies to antigens. To block nonspecific sites, sections were treated with "blocking buffer" for 15 minutes at room temperature and then incubated for 80 minutes at 37°C with TUNEL reaction mixture, that was prepared add 50 μl of Enzyme Solution to 450 μl of Label Solution. As negative controls PLP-fixed slides were incubated only with Label Solution, while as positive controls slides were treated with DNase I recombinant for 20 minutes at 37°C. Subsequently, sections were rinsed in PBS 1X and then counterstained with Rhodamine-labeled lectin Lens Culinaris Agglutinin (LCA, Materials, section 8.9) and DAPI for 15 minutes. Podocytes were identified by WT-1 staining, as described above. Triple fluorescence labeling was analyzed by an inverted confocal laser-scanning microscope, and 30 random images for each sample were acquired.

9.9 Morphometrical analysis

Glomerular podocytes were identified as cells positive for WT1, as described above (see section 9.8.1). Using fluorescence microscopy with appropriate filters, images of single wavelength will be acquired, and digitally merged. In the merged image, podocytes will be then identified and counted.

Estimation of glomerular volume (VG) was performed using a computer-based image analysis system (Mac OS 09, Apple Computer, Cupertino CA). Histological sections of fluorescein WGA-labeled glomeruli were digitized from the fluorescence microscope and stored on 696 x 520 pixel images. Exact enlargement in μm/pixel of digital images was calculated from images of a reference grid digitized at the same resolution. The outline of the minimal polygon around the glomerular tuft area was manually traced, and its surface area automatically measured, in the same glomeruli examined for counting WT1-positive cells in each tissue section. Mean value of VG will be then calculated using the formula

$$V_G = (\beta/k)(A_m)^{3/2}$$

where k = 1.01 is a size distribution coefficient, and β = 1.38 is the shape coefficient for spheres, which is the assumed shape of glomeruli.

The estimation of the average number of podocytes per glomerulus (NP) was determined by the stereological method of particle density

proposed by Weibel (Weibel, 1979). Briefly, the volume density of the podocytes (NV) in glomerular tuft volume is estimated as $N_V = N_A/\overline{D}$ where NA, the podocyte nuclear profile area density, is estimated by the ratio between the numbers of podocyte nuclear profiles and the glomerular profile area in each glomerulus. $\overline{D}$ is the average diameter of podocyte nuclei that we estimate from major and minor axis of cell nuclear sections. To calculate $\overline{D}$ the average volume of podocyte nuclei ($\overline{V}$) is first calculated based on the assumption that podocyte nuclei have an ellipsoidal shape. The average diameter of an equivalent sphere having the same volume of the ellipsoid is then determined. The mean number of podocytes per glomerular tuft (NP) is calculated for each animal by multiplying podocyte volume density NV in the capillary tuft by the mean value of VG previously calculated.

Volume density (Vv) of glomerular endothelial cells was estimated as area density occupied by RECA-1 staining. Twenty renal sections per rat were digitalized using an inverted confocal laser microscopy (original magnification, x630). Each image (512x512 pixels) was digitally overlapped with an orthogonal grid composed of 2500 points (ImageJ; NIH, Bethesda, MD, USA). The volume density (Vv) of endothelial cells was calculated as the ratio of the number of grid points hitting RECA-1 staining to the total number of grid points falling into the total area occupied by the glomerulus.

9.10 Western blot analysis

These experiments were performed in collaboration with Dr. Cristina Zanchi Laboratory of Pathophysiology of Experimental Renal Disease and Interaction with other Organ systems at "Mario Negri" Institute for Pharmacological Research, Bergamo, Italy. Frozen kidney tissues were homogenized in lysis buffer (50 mM Tris-HCl (pH 8), 150 mM NaCl, 1% Triton X-100, 0.5% Sodium deoxycholate, 0.1% SDS) containing the Halt protease inhibitor cocktail (Materials, section 8.7). Protein concentration was determined using the bicinchoninic acid assay (Materials, section 8.7) following the manufacturer's instructions. The samples (50 μg) were resolved on 7-15% SDS-polyacrylamide gel (Materials, section 8.7) and transferred to nitrocellulose membrane. After blocking, membranes were incubated 4°C overnight with anti-$VEGF_{164}$ antibody (Materials, section 8.7) or anti-α-tubulin antibody (Materials, section 8.7) and with an appropriate secondary antibody (Materials, section 8.7). Protein bands were detected by supersignal chemiluminescent substrate (Materials, section 8.7) and quantified using NIH Image J software. The amount of VEGF protein was calculated relative to the level of α-tubulin.

Methods for *in vitro* studies

9.11 Cells and cell culture

Murine podocytes. Immortalized mouse podocyte line was kindly given by Dr. Peter Mundel (Materials, section 8.2). The group of Dr. Mundel has originally isolated murine podocytes (Mundel *et al.*, 1997) using standard procedures and grown in medium at 37°C on collagen-I (Materials, section 8.9) coated dishes as previously described (Mundel *et al.*, May 1997).

Medium. "Growth medium" (Materials, Section 8.3).

Cell density. For routine cell culturing, murine podocytes were seeded on collagen-I coated dishes at the dilution of 1:6 (1:8 in the week-end) and maintained at 33°C in a 5% CO_2 humidified atmosphere. The cells were sub-cultured every second day by using trypsin (Materials, section 8.3) for 1 minute at room temperature. In order to perform *in vitro* experiments, murine podocytes (23000 cells/cm^2) were induced to differentiate along podocyte lineages by shifting them to 37°C for 14 days and culturing in "growth medium" without γ-interferon.

Cell storage. Murine podocytes were preserved for long-term storage in liquid nitrogen. Cell pellets were suspended in FCS plus 7.5% DMSO in cryovials. To guarantee a gradual freezing, the vials were left in isopropanol-filled containers overnight at -80°C and then transferred to liquid nitrogen tanks for storage.

Thawing frozen cells. The cells were thawed rapidly by placing the vial in a water bath at 37°C with a gentle agitation. The cells were then slowly resuspended in 9 ml of complete medium and DMSO traces were remove by centrifugation at 1200 rpm for 7 minutes.

MSCs. Murine MSCs were obtained from BM of 2-month-old male C57BL6/J mice with the same procedure used for isolation of rat MSCs (see section 9.1). Briefly, BM was flushed from the shaft of the bone by using the "isolation medium" (Materials, section 8.3), and filtered through a 100 μm sterile filter. Filtered BM cells were plated in the "growth medium" (Materials, section 8.3) and allowed to adhere for 24 hours. After 2 to 3 weeks, subconfluent (80%-90%) cells were detached by trypsin-EDTA (Materials, section 8.3), immunodepleted and used for *in vitro* experiments (23000 cells/cm^2).

9.12 Depletion of CD45 positive cells from mesenchymal stem cell preparation

Murine MSCs were immunodepleted of CD45 positive cells. MSCs grown for two weeks, as described in methods, section 9.11, were trypsinized counted and incubated in "Buffer" for immunodepletion (Materials, section 8.6) for 15 minutes. After centrifuging, cells were

incubated at 4°C for 20 min with a rat anti-mouse CD45 antibody (Materials, section 8.8), at a concentration of 0.2 μg/10^6 cells diluted in buffer. After washing with buffer, the pellet was suspended in 80 μl of buffer per 10^7 total cells plus 20 μl of MACS goat anti-rat IgG magnetic microbeads (Materials, section 8.8), and incubated for 15 minutes. By passage on LS columns assembled on a MACS separator (Materials, section 8.11), cells were magnetically sorted by exposure to a magnetic field. Before adding cells, columns were filled and washed with "buffer" for immunodepletion. Cells that did not express the CD45 (CD45$^-$ MSCs) antigen were eluted from the column, collected after washing the columns several times, and used for *in vitro* experiments.

9.13 Co-culture experiments

For co-culture experiments, podocytes were seeded in growth medium with γ-interferon, at the concentration of 23x10^3 cells/cm^2 and 14 days later were incubated with RPMI plus 10% FCS (test medium) (Materials, section 8.3) alone or in the presence of 1.5 μM ADR (Materials, section 8.5) for 6 hours. After drug withdrawal, podocytes were incubated with test medium or with MSCs at the density of 23x10^3 cells/cm^2 (1:1) for 72 hours, and then total viable cells were counted by Trypan blue dye exclusion (Materials, section 8.5). Number of adherent podocytes was obtained by counting total viable cells in co-culture

subtracted of MSC number. The percentage of viable podocytes in each sample was calculated versus control podocytes imposed as 100%. The role of VEGF was studied by adding to ADR-treated podocytes co-cultured with MSCs, functional blocking anti-VEGF antibody (Materials, section 8.8) for 72 hours. In additional samples, exogenous recombinant mouse VEGF-A (Materials, section 8.4) was added to podocytes treated with ADR.

9.14 Apoptosis assay

Apoptosis was assessed by studying the expression of cytocrome C at 3, 15 and 24 hours after ADR incubation. Cells, seeded on glass slides, were treated with "permeabilized solution" containing Triton 0.5% (Materials, section 8.6) for 5 minutes at room temperature. After washing in PBS 1X (Materials, section 8.6), sections were treated with blocking buffer (Materials, section 8.6) for 30 minutes at room temperature, followed by incubation 1 hour with anti-cytochrome C antibody (Materials, section 8.8) at room temperature. Subsequently, cells were treated with goat anti mouse-FITC antibody for 1 hour at room temperature as secondary antibody. Nuclei were counter-stained with DAPI and slides were mounted with the mounting medium. Apoptotic podocytes were expressed as percentage of cells with cytocrome C in the cell cytosol/total cells.

Apoptosis was also evaluated by assessment of cleaved caspase-3 at 3 and 15 hours after ADR incubation. Cells were detached with Trypsin/EDTA, centrifuged and resuspended in the "permeabilized solution" for 5 minutes at room temperature. Then, after rinsed in PBS 1X the cells were centrifuged, incubated with "blocking buffer" for 15 minutes at 4°C and then incubated with anti-cleaved caspase-3 antibody (Materials, section 8.8), followed by donkey anti rabbit-FITC antibody Cells were analyzed by FACS at 488 nm excitation, green emission for cleaved caspase-3. Data were expressed as percentage of apoptotic cells.

9.15 Western blot analysis

The expression of Akt and pAkt was studied in control podocytes exposed to medium, in ADR-treated podocytes incubated with medium, exogenous VEGF-A (40 ng/ml) or with MSC-conditioned medium (24-hour conditioned medium) for 72 hours. Podocytes were lysed with lysis buffer (20 mM Tris-HCl (pH 7.5), 1%Triton X-100, 25 mM NaCl, 1.5 mM EDTA, 50 mM NaF and 15 mM $Na_4P_2O_7$) containing protease inhibitor (Materials, section 8.7). Protein lysates were separated on 10% polyacrylamide gel by SDS-PAGE (Materials, section 8.7) and transferred to nitrocellulose membrane. After blocking, membranes were incubated overnight with primary antibodies against

Akt or p-Akt Ser473 (Materials, section 8.8) and with an appropriate secondary antibody (Materials, section 8.8). Protein bands were detected by supersignal chemiluminescent substrate (Materials, section 8.7).

9.16 Statistical analysis

Results are expressed as means ±SE. Data were analyzed by non-parametric Mann-Whitney test or Kruskal-Wallis test for multiple comparisons followed by Ryan's procedure, or by Anova test coupled with Bonferroni post-hoc analysis, as appropriate. The statistical significance level was defined as $P<0.05$.

Principles of the main techniques and instruments

9.17 Flow cytometer

See Chapter 3, section 22.

9.18 MACS cell separation system

MACS technology is based on MACS microbeads, magnets and columns. Microbeads are tiny superparamagnetic particles of approximately 50 nanometers in diameter. They are composed of biodegradable matrix, and it is therefore not necessary to remove them after the separation process. Usually, microbeads do not alter structure, function or activity status of labelled cells and are not known to interfere with subsequent experiments. Cell separation takes place within the columns that retain magnetically labelled cells. When columns are placed in a MACS separator, the column matrix provides a magnetic field strong enough to retain cells labelled with minimal amounts of magnetic material. Therefore, microbeads used for labelling the cells can be so small and only a few are needed to separate a cell. The magnetically labelled cells are separated over a column placed in a separator. They are retained on the column, while unlabeled cells pass through. These cells can be collected as the unlabeled fraction. We have

used LS columns that are useful for the isolation of up to 10^8 magnetically labelled cells. Up to $2x10^9$ total cells can be processed. The column matrix is composed of ferromagnetic spheres, which are covered with a cell-friendly plastic coating allowing fast and gentle selection of cells. The columns are packed in a sterile way and can be used to separate eukaryotic cells, bacteria, viruses, or subcellular material less than 30 μm in size.

For obtaining lineage negative MSCs ($CD45^-$), we have performed a negative selection. It means that the non-target cells (lineage positive cells and CD45 positive cells) are magnetically labelled and eliminated from the starting mixture of cells. With this strategy, the target cells remain non-magnetical (or "untouched"). Single depletion can remove nearly all of the magnetically labelled cells, resulting in a very pure fraction of unlabeled cells. By this procedure, first non-target cells are recognized by labeling with specific antibodies (i.e rat anti-CD45), and then magnetical microbeads, able to target the antibody (beads coated with anti-rat IgG) are added. Cells labelled with MACS are the non-target cells and are retained on MACS column.

9.19 Western blotting

Western blotting is a method to detect a specific protein in a given sample of tissue homogenate or cell extract. It uses gel electrophoresis to separate native or denaturated proteins by the length of the polypeptide (denaturing conditions) or by 3-D structure of the protein (native/non-denaturing conditions).

Sample preparation

Sample may be taken from the whole tissue or from cell culture that should be first broken down mechanically with a blender or by sonication. The latter acts by applying ultrasound energy to disrupt cell membrane and release cellular content. In laboratory, it usually performed by using an ultrasonic bath or an ultrasonic probe. Detergents, salts, and buffers may be employed to encourage lysis of cells and to solubilize proteins whereas protease inhibitors are often added to prevent the digestion of the sample by it own enzymes.

Protein concentration detection

Protein concentration was determined by using the Bio-Rad protein assay reagent (Materials, section 8.7). First, a series of BSA serial

solutions of known concentrations were prepared starting from a stock solution of 10 mg/ml as follows:

BSA final concentration

10 µl of 10 mg/ml	+ 10 µl of H_2O	5 mg/ml
15 µl of 5 mg/ml	+ 15 µl of H_2O	2.5 mg/ml
21 µl of 2.5 mg/ml	+ 9 µl of H_2O	1.75 mg/ml
15 µl of 1.75 mg/ml	+ 6 µl of H_2O	1.25 mg/ml
15 µl of 1.25 mg/ml	+ 5 µl of H_2O	0.938 mg/ml
10 µl of 0.938 mg/ml	+ 5 µl of H_2O	0.625 mg/ml
10 µl of 0.625 mg/ml	+ 10 µl of H_2O	0.312 mg/ml

Then, 200 µl of Bio-Rad dye reagent diluted 1/5 was added to a 96-multiwell plate followed by the addition of the above described BSA dilutions or samples (2 µl). The absorbance was read at the wavelength of 620 nm using a spectrophotometer. The standard curve, created by plotting the absorbance versus the concentration of each standard, was used to calculate the concentration for an unknown sample given its absorbance.

Gel electrophoresis

The most common type of gel electrophoresis employs polyacrylamide gels and buffer containing sodium dodecyl sulphate

(SDS) (Materials, section 8.7). The SDS polyacrylamide gel electrophoresis (SDS-PAGE) maintains polypeptides in a denatured state once they have been treated with strong reducing agents to remove secondary and tertiary structure (e.g. S-S disulphide bonds to SH and SH) and thus allows separation of proteins by their molecular weight. Sampled proteins become covered in the negatively charged SDS and move to the positively charged electrode through the acrylamide mesh of the gel. Smaller proteins migrate faster through this mesh and the proteins are thus separated according to the size. Polyacrylamide gels are composed of chains of polymerized acrylamide that are cross-linked by a bifunctional agent such as N,N'-methylenebisacrylamide. Polyacrylamide gels form as a result of polymerization of the monomeric acrylamide into polymeric polyacrylamide chains with cross-linking of the chains by bisacrylamide. The polymerization reaction is initiated by addition of ammonium persulfate (Materials, section 8.7) and accelerated by addition of TEMED (Materials, section 8.7), which catalyzes the formation of the free radicals from ammonium persulfate.

The effective range of separation of SDS-polyacrylamide gels depends on the concentration of polyacrylamide used to cast the gel and the amount of cross-linking formed from bisacrylamide that add rigidity and tensile strength to the gel and form pores through which the SDS-polypeptide complexes must pass. When samples are loaded into wells in the gel, one line is usually reserved for a marker or ladder,

a commercially available mixture of proteins having defined molecular weights, typically stained so as to form visible, coloured bands. By using a marker of known molecular weight, it is possible to estimate the molecular weight of the polypeptide chain(s).

The most common buffer system used for protein electrophoresis is the Tris-glycine buffer system (Materials, section 8.7), where glycine is the trailing ion. During electrophoresis, a sharp zone, usually visible as change of refractive index, forms a boundary between the slower trailing ion (glycine) and the faster leading ion (chloride). When the protein sample is applied in a stacking gel, in which proteins can move faster than the trailing ion, the proteins stack up between the leading and trailing ion fronts. Once the proteins enter the higher percentage separating gel, they are passed by trailing ion, and separation of the proteins begins based on their mobility through the pores of the separating gel. Thus, freed from the moving boundary, the SDS-polypeptide complexes move through the resolving gel in a zone of uniform voltage and pH and are separated according to size by sieving. When voltage is applied along the gel, proteins migrate into it at different speeds. These different rates of advancement (different electrophoretic mobilities) separate into bands within each lane.

Electroblotting

Electroblotting is a method applied to transfer proteins onto a membrane (generally PVDF or nitrocellulose) after gel electrophoresis.

The proteins can then be analyzed using specific antibodies. This technique relies upon a current and a transfer buffer solution to drive proteins onto a membrane. Following electrophoresis a standard tank or semi-dry blotting transfer system is set-up. A stack is put together in the following order from cathode to anode: sponge | three sheets of filter paper soaked in transfer buffer | gel | PVDF or nitrocellulose membrane | three sheets of filter paper soaked in transfer buffer | sponge. The membrane is located between the gel and the anode, as the current and sample will be moving in that direction.

Protein binding is based upon hydrophobic interactions, as well as charged interactions between the membrane and protein.

Protein detection

Since the membrane has been chosen for its ability to bind protein, and both antibodies and the target are proteins, steps must be taken to prevent interactions between the membrane and the antibody used for detection of the target protein. Blocking of non-specific binding is achieved by placing the membrane in a dilute solution of protein - typically bovine serum albumin (BSA) or non-fat dry milk-(Materials, section 8.7) in the presence of a detergent such as 0.1% Tween 20 (Materials, section 8.7). Proteins in the dilute solution attach to the membrane in all places where the target proteins have not attached. Thus, when the antibody is added, it can only attach to the binding sites of the specific target protein.

To detect target protein, the membrane is "probed" with a primary antibody specific for the protein of interest. After blocking, a dilute solution of primary antibody is incubated with the membrane under gentle agitation. The solution is comprised of buffered saline solution with a small percentage of detergent, and sometimes with BSA. After rinsing the membrane to remove unbound primary antibody, the membrane is exposed to another antibody, directed at a species-specific portion of the primary antibody. This secondary antibody is usually linked to biotin or to a reported enzyme such as alkaline phosphatase or horseradish peroxidase. Most commonly, a horseradish peroxidase-linked secondary is used in conjunction with a chemiluminescent agent, and the reaction product produces luminescence in proportion to the amount of protein. Chemiluminescent detection methods depend on incubation of the western blot with a substrate that will luminesce when exposed to the reporter on the secondary antibody. A sensitive sheet of photographic film is placed against the membrane, and exposure to the light from the reaction creates an image of the antibodies bound to the blot. The image is analysed by densitometry, which evaluates the relative amount of protein staining and quantifies the results in terms of optical density.

9.20 Microscopy

9.20.1 Light microscopy

See Chapter 3, section 3.24.

9.21 Immunofluorescence technique and confocal microscopy

See Chapter 3, section 3.25.

9.22 Haemocytometer

See Chapter 3, section 3.26.

RESULTS

CHAPTER 10

BONE MARROW-MESENCHYMAL STEM CELL THERAPY PRESERVES GLOMERULAR PODOCYTES AND PROGENITOR CELLS IN ADRIAMYCIN-INDUCED NEPHROPATHY

10.1 Introduction

Chronic kidney disease (CKD) is a worldwide threat to public health, with an estimated prevalence of 11% of the adult population in Western industrialized nations (Hallan *et al.*, 2006), but the true dimension of this problem is not fully appreciated. Approximately, over 2 million people are currently treated with renal replacement therapy (RRT), which consist primarily of kidney transplantation, haemodialysis and peritoneal dialysis (Remuzzi *et al.*, 2006; Couser *et al.*, 2011). More than 90% of these individuals live in industrialized countries, while in developing countries, available RRT is scarce, and null in underdeveloped areas (Remuzzi *et al.*, 2006). Moreover, in the next decade, the cost for dialysis will become unbearable even in the most developed countries (Just *et al.*, 2008).

Although considerable gains have been obtained in retarding progression of CKD by renin-angiotensin system blockade in a significant proportion of patients, the therapeutic goal of arresting CKD progression to end-stage renal disease remains unfulfilled. At this purpose, stem cell-based therapy exploiting stem cell peculiar properties of renal tropism and regenerative capability, may also contribute to kidney repair and could represent an innovative strategy as cure for CKD.

In this contest, bone marrow-derived mesenchymal stem cells (BM-MSCs) are a source of multipotent cells having the potential of tissue regeneration in experimental models of myocardial infarction (Laflamme *et al.*, 2005; Nagaya *et al.*, 2004; Tang *et al.*, 2006), neurological disease (Torrente *et al.*, 2008) and acute kidney injury (Morigi *et al.*, 2004; Imberti B *et al.*, 2007; Morigi *et al.*, 2008; Herrera *et al.*, 2004). We showed that infusion of murine (Morigi *et al.*, 2004; Imberti *et al.*, 2007) and human BM-MSCs (Morigi *et al.*, 2008) in mice with acute kidney injury decreased renal tubular injury and ameliorated renal function impairment reducing animal mortality. The mechanism underlying renoprotection was due to a paracrine action of these stem cells, with production of regenerative, prosurvival, anti-apoptotic and angiogenic factors including IGF-1 and VEGF (Imberti *et al.*, 2007; Togel *et al.*, 2005; Togel *et al.*, 2007).

In experimental models of acute kidney injury, the renoprotective effect of BM-MSCs is well established, unfortunately, the therapeutic potential of these stem cells in animal models of chronic nephropathies has not been completely demonstrated so far. In literature there are reported some conflicting results. Ninichuk *et al.* have observed that BM-MSC treatment improved interstitial fibrosis and loss of peritubular capillaries, but it failed to prevent the progression of CKD in mice with Alport disease (Ninichuk *et al.*, 2006). Infusion of MSCs in rats with 5/6 nephrectomy partially preserved renal function and attenuated

glomerulosclerosis (Cavaglieri *et al.*, 2009) and interstitial fibrosis (Semedo *et al.*, 2009). Early treatment with MSCs blunted glomerulosclerosis in adriamycin model of nephropathy, while it failed to modify proteinuria and progression of renal failure (Magnasco *et al.*, 2008).

So based on these evidences the aim of this study was to investigate whether BM-MSCs could ameliorate renal function and glomerular architecture in a model of chronic kidney disease. To this aim, we set up a model of adriamycin-induced nephropathy and we evaluated if treatment of nephrotic rats with ex-vivo expanded bone marrow-derived MSCs, a cell source of pro-survival and angiogenic factors, had regenerative effects on cells of distinct glomerular compartments as podocytes, parietal epithelial cells (PECs) and endothelial cells.

10.2 Model of ADR nephropathy

In order to evaluate the renoprotective effect of BM-MSCs, we set up an experimental model of nephropathy induced by adriamycin (ADR) in rats. Renal function assessed as proteinuria, was evaluated at different time points from ADR treatment.

Since podocytes are target of injury in a variety of kidney diseases, we evaluated whether podocyte number was reduced following ADR treatment. Using WT-1, a podocyte-specific marker that localizes in nuclei, we observed a decrease in the number of podocytes in ADR-treated rats in respect to control rats (Figure 10.1 *a* and *b*). By morphometric analysis a significant decrease in the number of WT-1-positive cells was observed after ADR injection, starting from 3 days, with respect to control rats (ADR, day 3: 129.57±3.56; day 9: 127.01±2.83; day 16: 122.84±5.37 vs control, 221.99±5.66 podocytes/glomerulus, $p<0.01$). Podocyte loss in response to ADR was confirmed by immunostaining with nestin, a specific marker of podocytes (glomerular area percentage: ADR, day 3: 10.25±4.16% vs control, 16.00± 0.75%, $P<0.01$). Loss of podocytes, was coupled to slit diaphragm protein alterations including nephrin and CD2AP. We observed that nephrin, a key component of the slit diaphragm, which functions to maintain slit pore integrity and renal filtration capacity (Tryggvason *et al.*, 2001), was reduced and the staining was discontinuous (glomerular area percentage: ADR, day 9: 1.69±0.05 vs control 10.84±0.41%, $p<0.05$) (Figure 10.2 *a* and *b*). Also CD2AP, a protein associated to nephrin (Shih *et al.*, 2001), shown a decreased expression in ADR-treated rats in respect to control (Figure 10.2 *c* and *d*) (glomerular area percentage: ADR, day 9: 2.85±0.43 vs control, 15.06± 0.23%, $p<0.05$).

Since the cytotoxic and cytostatic effect of ADR results in the induction of apoptotic cell death, we observed whether the loss of podocytes observed starting from 3 days, was due to apoptosis. Using double-staining for TUNEL and WT-1, we observed in the renal tissue of ADR-rats given saline, a high number of apoptotic podocytes, at variance with kidneys from control rats where no apoptotic podocytes were detected (ADR, day 3: 17.8±0.54; day 9: 16.79±0.78; day 16: 15.34±0.61 vs control 0 TUNEL/WT-1 positive podocytes/glomerulus).

As a consequence of ADR-induced podocyte injury, we observed starting from 16 days, glomerular adhesions of the capillary tuft to the Bowman's capsule (synechiae), followed by crescents-like lesions at 30 days (Figure 10.3 a and b). The phenotype of cells contributing to early lesions of ADR-treated rats was then assessed by studying the expression of claudin1, an intercellular tight junction protein constitutively expressed by all glomerular parietal epithelial cells (PECs) lining the Bowman's capsule (Ohse et al., 2008) and of nestin, a marker of podocytes (Perry et al., 2007). As shown in Figure 10.4, co-staining of claudin1 and nestin revealed that PECs and podocytes both participated to the formation of early cellular bridges at 16 days (Figure 10.4 a and b). At the same time, parietal progenitor cells expressing the metanephric mesenchymal marker NCAM (Metsuyanim et al., 2009; Bard et al., 2002), contributed to the formation of the early lesions (Figure 10.5 a and b). With time (30 days), multilayers of cells

accumulated at the site of synechiae resulting in more severe crescentic-like lesions (Figure 10.3 c and d).

All resulted in a mild degree of glomerulosclerosis characterized by accumulation of the extracellular matrix material and obliteration of the capillary filter. We observed glomerulosclerosis starting from 16 days after ADR, which became more evident at 30 days (glomerulosclerosis index, control rats: 0; ADR, day 16: 0.15±0.06; day 30: 0.39±0.09).

10.3 Characterization of mesenchymal stem cells isolated from bone marrow

MSCs were obtained from bone marrow of 2 month-old male Lewis rats. After 2 to 3 weeks, subconfluent cells were detached and used for *in vivo* experiments. The ability of BM-MSCs to differentiate into adipocytes and osteocytes, after exposure to appropriate inductive media, was observed by lipid droplet formation and by extended area of mineralization (Figure 10.6 *a* and *b*).

10.4 Localization of bone marrow-mesenchymal stem cells

Because of the severity of the disease, we decided to maintain a constant number of BM-MSCs in the kidney during the study. At this purpose, repeated infusions of MSCs were applied to ADR-treated rats. To assess the ability of MSCs to engraft the kidney in response to injury, we labelled before *in vivo* injection MSCs with PKH-26, a red fluorescent membrane dye. We found that the frequency of PKH-26 positive-MSCs homing the kidney averaged 4.33±0.38, 4.85±0.43 and 5.73±2.85 cells/10^5 renal cells, respectively, at day 3, 9 and 16 after ADR, as assessed 15 hours after MSC injection. Thirty-four % of PKH-26-labeled MSCs were found in the glomeruli at 3 days (Figure 10.7 *a*), but the amount of MSCs localized in the glomeruli declined over time. The labeled MSCs localized in the glomeruli did not show positivity for the podocyte marker WT-1 (Figure 10.7 *b*). Moreover, FACS analysis of dissociated renal tissue of ADR-treated rats receiving MSCs labeled with another tracer, rhodamine-B-conjugated nanoparticles, was also performed. Kidney samples of ADR- rats receiving fluoNP-labeled MSCs, showed 1.6±0.2% positive cells for rhodamine B-fluoNP above the negative control set at 2%.

10.5 Effect of bone marrow mesenchymal stem cells on renal function parameters in ADR-treated rats

With the aim to study the renoprotective effect of BM-MSCs, we performed repeated injection of MSCs into the tail vain of ADR-treated rats, starting 36 hours after ADR treatment. As reported in Figure 10.8, rats injected with a single dose of 5mg/kg ADR exhibited proteinuria within 6 days (133±8 vs basal, 19±1 mg/day, $p<0.01$). Proteinuria progressively increased during time averaging 1004±33 mg/day at day 30 in ADR-rats given saline. Unfortunately, the repeated infusions of MSCs did not affect the development of proteinuria at any time of the study (Figure 10.8).

In parallel, we observed that serum creatinine levels tended to increase during time in ADR-rats given saline in respect to controls, although a statistical significance was not achieved (ADR, day 9: 0.60± 0.09; day 16: 0.73±0.01, day 30: 0.86±0.02 versus controls: 0.58±0.01mg/dl). Serum creatinine levels, of ADR-rats that received MSC therapy, were not different from those of rats given saline (ADR+MSC, day 16: 0.80±0.03; day 30: 0.81±0.06 mg/dl).

10.6 Bone marrow mesenchymal stem cell treatment preserves glomerular architecture

As noted by the set up of ADR-induced nephropathy, the targets of ADR toxicity are podocytes, so we focus on the effect of BM-MSCs on podocyte loss. As shown in Figure 10.9, repeated injections of BM-MSCs, significantly limited ($p<0.01$) podocyte depletion. Indeed, at day 3, 9 and 16, we observed a higher number of podocytes per glomerulus in the group of ADR-treated rats receiving MSCs as compared to saline (Figure 10.9). The preservation of podocyte number was also confirmed by nestin expression (glomerular area percentage: ADR+MSCs, day 3: 18.19±2.6%, $P<0.01$ vs ADR). Associated with limited podocytes depletion, we observed at day 9 in ADR-treated rats receiving MSCs, a partial, although, significant preservation of both nephrin and CD2AP expression as compared to ADR-rats given saline (nephrin, glomerular area percentage: ADR+MSC, 3.81±0.34%, $P<0.05$ vs saline; CD2AP, glomerular area percentage: ADR+MSC, 5.24±0.24%, $p<0.05$ vs saline).

In vivo and *in vitro* model of ADR-induced toxicity (Magnasco *et al.*, 2008) have demonstrated that podocytes depletion is due to an induction of apoptotic pathway, therefore we have investigated whether BM-MSCs were able to exert an anti-apoptotic effect. As shown in Figure 10.10, BM-MSCs infusions, significantly ($p<0.01$) reduced apoptotic podocytes, as indicated by the lower number of TUNEL+ WT1+ podocytes in renal

tissue of MSC-treated rats compare to ADR-rats given saline, at the corresponding times (Figure 10.10).

Protective effect of BM-MSCs on podocytes depletion resulted in a significant reduction of glomerular podocyte-PEC bridges. We observed in ADR-rats given saline a significant ($p<0.01$) increase of percentage of glomeruli with area occupied by more than 50% adhesions of the tuft to the Bowman's capsule (Figure 10.11). In ADR-rats receiving BM-MSCs, the percentage of glomeruli with area occupied by more than 50% adhesions of the tuft to the Bowman's capsule was significantly lower than that observed in rats given saline (Figure 10.11). In control animals, no glomeruli with adhesions more than 50% were found (Figure 10.11).

In the set up model, we observed in ADR-rats given saline, that NCAM positive cells contributed to the formation of early synechiae (Figure 10.12). Following MSC injections, the distribution of NCAM positive progenitor cells was restored along the Bowman's capsule to a pattern similar to controls (Figure 10.12).

Since BM-MSCs were able to restore glomerular architecture, we tested whether BM-MSCs treatment could exert a protective effect on glomerulosclerosis, a serious outcome of ADR nephropathy. As shown in Figure 10.13, ADR-rats given saline revealed at 30 days sclerotic lesions which were significantly reduced ($p<0.01$) in ADR-rats treated with BM-MSCs (Figure 10.13).

10.7 Role of bone marrow mesenchymal stem cells on glomerular VEGF level and endothelial cell damage

Looking for factors possibly involved in MSC-mediated renoprotection in ADR-rats, we focused on VEGF, highly produced by rat MSCs (Figliuzzi *et al.*, 2009) and known to exert pro-survival and angiogenic activity (Togel *et al.*, 2007; Togel *et al.*, 2009). As shown in Figure 10.14, glomeruli of ADR-rats given saline showed, starting from 3 days, a decrease of VEGF staining in respect to control rats. Infusions with BM-MSCs, significantly ($p<0.05$) enhanced glomerular VEGF expression at days 9 and 16. Consistently, Western blot experiments performed in renal tissue of all the experimental groups showed that at days 9 and 16, MSC treatment almost normalized renal levels of VEGF protein (Figure 10.15).

In parallel, we observed that BM-MSC infusions translated into preservation of glomerular endothelial cells. By morphometric analysis of the glomerular endothelium labelled with RECA, a marker of rat endothelial cells, we observed a marked reduction in volume density (Vv) of endothelial cells in ADR-treated rats given saline compared with control rats (Figure 10.16). The degree of microvessel rarefaction was significantly reduced in glomeruli of ADR-rats infused with MSCs versus glomeruli of ADR-rats given saline, confirming a key role of VEGF on glomerular endothelial cell integrity and function.

10.8 Anti-inflammatory effect of bone marrow derived mesenchymal stem cells

Consistent with the data reported in literature, we observed in the glomeruli of ADR rats given saline, an increased number of ED1-positive monocytes/macrophages as compared to control rats (ADR, day 9: 4.31±0.22; day 16: 4.78±0.23 vs control 1.11±0.14 ED-1+ cells/glomerulus, $p<0.05$). ADR-rats treated with BM-MSCs, showed a significant ($p<0.05$) reduction of glomerular cell infiltrates with respect to ADR-rats given saline (ADR+MSC, day 9: 1.87±0.06; day 16: 2.78±0.31 ED-1+ cells/glomerulus), suggesting a marked anti-inflammatory effect of BM-MSCs.

10.9 Bone marrow mesenchymal stem cells protect podocytes from adriamycin-induced toxicity via VEGF: *in vitro* studies

In order to better explain the capability of BM-MSCs to exert protective effects on podocytes, we performed *in vitro* experiments using a co-culture system whereby BM-MSCs were in co-culture with podocytes pre-treated with ADR. Murine differentiated podocytes were exposed for 6 hours to ADR, and 72 hours after drug withdrawal, cell

count was performed. As shown in Figure 10.17 exposure to ADR significantly ($P<0.01$) reduced the number of viable podocytes compared to control podocytes (Figure 10.17). Co-culture of damaged podocytes with murine BM-MSCs completely prevented podocyte loss caused by ADR ($p<0.01$) (Figure 10.17). BM-MSCs seeded alone did not proliferate.

Since BM-MSCs produce high levels of VEGF (Figliuzzi *et al.*, 2009) that, as shown by our *in vivo* results, played important role on glomerular endothelial integrity, we tested in the co-culture system the contribution of VEGF in MSC-induced podocyte survival. Using a specific antibody against VEGF, we observed, an abrogation of BM-MSC protective effects on ADR-treated podocytes (Figure 10.18). In order to provide further evidence on the role of VEGF, we added exogenous VEGF to ADR-treated podocytes, and we observed that VEGF was able to prevent cell loss at a similar extent as MSCs did (Figure 10.18).

To study whether MSCs could counteract podocyte apoptosis induced by ADR, we evaluated the expression of cytochrome C (Cyt C), a marker of intrinsic apoptosis when released from mitochondria into the cell cytosol (Lebrecht *et al.*, 2004; Gewirtz *et al.*, 1999; Park *et al.*, 2002; Brooks *et al.*, 2009). As shown in Figure 10.19, we found that ADR caused apoptosis in a high number of podocytes at 3, 15 and 24 hours ($p<0.01$ vs control podocytes) after ADR (Figure 10.19). BM-MSCs co-

cultured with ADR-treated podocytes, significantly ($p<0.01$) reduced the percentage of apoptotic podocytes at all times considered (Figure 10.19). The anti-apoptotic effect exerted by MSCs was abrogated by the addition of a specific functional blocking anti-VEGF antibody to the co-culture system, while using exogenous VEGF on damaged podocytes, we observed a percentage of apoptotic cells comparable to that observed with BM-MSCs (Figure 10.19 and 10.20). The anti-apoptotic activity of MSCs was further confirmed by evaluating cleaved caspase-3 in cells exposed to ADR at different times. ADR-treated podocytes exposed to MSCs showed a significant ($P<0.01$) decrease in the percentage of cells positive for cleaved caspase-3 at 3 hours (control podocytes: 4.7±0.4; ADR: 15.3±2.1 and ADR+MSCs: 6.0±0.7 % apoptotic cells) and at 15 hours (ADR: 26.0± 1.0 and ADR+MSCs: 8.7±1.1 % apoptotic cells) in respect to ADR-treated podocytes exposed to medium alone. Exposure to VEGF markedly reduced the percentage of apoptotic cells in response to ADR at 3 hours (10.5±2.6%) and at 15 hours (8.0±1.4%, $P<0.01$ vs ADR).

The serine threonine kinase Akt is a critical factor in the regulation of pro-survival signals (Datta *et al.*, 1999). By Western blot analysis, in control podocytes, we observed a constitutively expression of the phosphorylated form of Akt (pAkt), while in ADR-damaged podocytes, we reported a markedly reduction of pAkt (Figure 10.21). Conversely, addition of exogenous VEGF and conditioned medium from BM-MSCs

markedly stimulated activation/phosphorylation of Akt in podocytes 72 hours after ADR incubation (Figure 10.21).

Since the intracellular serine/threonine protein kinase integrin-linked kinase (ILK), plays an important role in mediating podocyte adhesion to matrix, migration and survival (Yang *et al.*, 2005; Dai *et al.*, 2006), we investigated whether changes in ILK expression in ADR-treated podocytes were restored by BM-MSCs. As shown in Figure 10.22, damaged podocytes exhibited a marked redistribution and decrease of ILK staining with respect to control cells. When ADR-treated podocytes were co-cultured with BM-MSCs the granular pattern of ILK was almost normalized (Figure 10.22).

10.10 Conclusions

In order to study the effect of BM-MSCs in a model of chronic kidney disease, we set up a model of nephropathy induced by ADR. The results presented in this Chapter, can be summarized as follows. We found that:

- Early podocyte injury and subsequent chaotic migration of parietal epithelial progenitor cells lead to crescents-like lesions and glomerulosclerosis in ADR nephropathy.

- Repeated injections of BM-MSCs, created a glomerular pro-regenerative environment able to restored glomerular architecture, limiting podocyte and endothelial dysfunction and moderating progenitor cell activation.
- The protective effect of BM-MSCs could be due to VEGF, produced by large amount from BM-MSCs, which acts limiting podocyte apoptosis, endothelial rarefaction and inducing podocyte survival.

10.11 Discussion

Several studies have suggested the therapeutic effect of BM-MSCs in experimental model of acute kidney injury (Morigi *et al.*, 2004; Imberti *et al.*, 2007; Morigi *et al.*, 2008; Herrera *et al.*, 2004), unfortunately, only limited data are available on the role of BM-MSCs in models of chronic kidney disease. In this contest, we studied the capability of BM-MSCs to promote renal repair in a rat model of adriamycin-induced nephropathy, analysing the ability of these stem cells to regenerate different cellular components of glomeruli.

First of all, we characterized the model of adriamycin-induced nephropathy. We observed starting at 3 days, podocyte loss due to ADR-induced apoptosis, accompanied by slit diaphragm protein alterations. Moreover, for the first time, we demonstrated that podocyte

depletion was followed by intercellular bridges between nestin+ podocytes and claudin1+ PECs and by more extensive areas of adhesions between the Bowman's capsule and the tuft. More importantly, claudin1+ PECs present at the adhesion sites expressed also the metanephric mesenchymal marker NCAM (Metsuyanim *et al.*, 2009; Bard *et al.*, 2002). The presence of NCAM+ cells in such lesions implied that progenitor cells of parietal origin, in response to ADR-induced podocyte damage, acquired a migratory phenotype and invaded the glomerular tuft participating to the formation of crescents-like lesions and glomerular sclerosis. In human adult kidney, along the Bowman's capsule, has been identified a hierarchical population of progenitor cells organized in a precise sequence, that contributed to the turnover of senesced or injured podocytes (Ronconi *et al.*, 2009). However, in glomerular disease in response to a severe podocyte damage an aberrant repair may take place, with an excessive proliferative response of renal progenitor cells from the Bowman's capsule, that contribute to hyperplastic lesions of podocytopathies and crescentic glomerulonephritis (Smeets *et al.*, 2009; Lasagni *et al.*, 2010). In adult rat kidney, we recently provided the evidence for the presence of renal progenitor cells along the Bowman's capsule by showing that the stemness markers NCAM and CD24 (Challen *et al.*, 2004; Ronconi *et al.*, 2009)} were expressed by the large majority of claudin1+ PECs (Benigni *et al.*, 2011). In the MWF rat model characterized by

spontaneous podocyte loss, extracapillary crescents and glomerulosclerosis, a high percentage of claudin1+ PECs expressing NCAM, and to a lesser extent WT1+ podocytes were found in hyperplastic lesions during disease progression, suggesting that renal injury in this model could be the consequence of progenitor cell dysfunction (Benigni *et al.*, 2011).

Subsequently, once characterized the damage induced by adriamycin, we addressed the capacity of BM-MSCs to induce renal repair. We showed that repeated BM-MSC injections limited podocyte depletion by exerting a remarkable anti-apoptotic effect, and partially restored nephrin and CD2AP expression. The protective effect of BM-MSCs on podocyte dysfunction and loss resulted in a significant reduction of adhesions between PECs and podocytes, with the re-establishment of a normal localization of NCAM+ PECs along the Bowman's capsule. Thus, stem cell therapy by reducing podocyte injury and progenitor cell activation, ameliorated glomerular architecture and prevented glomerular sclerotic lesions. The fact that BM-MSC treatment failed to reduce proteinuria in ADR-rats could be ascribed to the limited recovery of the slit diaphragm proteins in the preserved podocytes.

We than studied the mechanisms underlying the BM-MSC-mediated glomerular protection in ADR-rats. VEGF, a factor that critically regulates and maintains podocyte and glomerular endothelial cell integrity and function {Sugimoto *et al.*, 2003; Eremina *et al.*, 2003), is

highly produced *in vitro* and *in vivo* by rat BM-MSCs (Figliuzzi *et al.*, 2009; Togel *et al.*, 2007) and by podocytes (Eremina *et al.*, 2003; Eremina *et al.*, 2006; Guan *et al.*, 2006). So, based on these evidences, we investigated whether the positive BM-MSC effect on glomerular compartments was possibly mediated by VEGF. We observed in ADR-treated rats a reduction of glomerular VEGF staining with consequent loss of endothelial integrity. These results were consistent with studies that documented that alterations in VEGF expression were associated with glomerular diseases (Kim *et al.*, 2000; Ostendorf *et al.*, 1999; Eremina *et al.*, 2003). BM-MSC treatment recovered glomerular VEGF levels restoring endothelial integrity as confirmed by a significant limitation of capillary rarefaction in ADR rats infused with BM-MSCs.

It is plausible to hypothesize that BM-MSCs homing the glomeruli could locally release VEGF that acting on podocytes would activate pro-survival pathways that render podocytes again metabolically active to synthesize great amount of the pro-regenerative growth factor itself. That VEGF may exert a beneficial effect on podocytes is supported also by data showing that nephrin and CD2AP -target proteins regulated by VEGF (Sugimoto *et al.*, 2003; Guan *et al.*, 2006) - were partially preserved in renal tissues of BM-MSC-treated animals.

Finally, the regenerative effect of BM-MSC-derived VEGF on ADR-damaged podocytes was explored in *in vitro* studies. In agreement with the *in vivo* data, BM-MSCs significantly enhanced viability and

limited apoptosis of podocytes in response to ADR. A neutralizing anti-VEGF antibody markedly abrogated such a prosurvival effect, thereby indicating a cytoprotective action of BM-MSC-derived VEGF on podocytes. The hypothesis that VEGF could activate pro-survival pathways in ADR-treated podocytes was confirmed by our finding that showed activation/ phosphorylation of Akt, a key factor in the regulation of pro-survival signals, in ADR-treated podocytes exposed to BM-MSC-conditioned medium or directly to exogenous VEGF. Similarly, previous studies showed that VEGF induced the activation of Akt signalling pathway in several cell types, thus reducing apoptosis (Foster *et al.*, 2005, F48-57; Cai *et al.*, 2003; Gerber *et al.*, 1998).

Consistent with the view that alterations of ILK expression -an important intracellular kinase regulating cell binding and migration- are associated with podocyte dysfunction (Dai *et al.*, 2006) here we found that ILK protein distribution was partially restored when ADR-injured podocytes were co-cultured with MSCs.

In summary, our findings indicate that early podocyte injury and subsequent chaotic migration of parietal epithelial progenitor cells lead to crescents-like lesions and glomerulosclerosis in ADR nephropathy. Treatment with BM-MSCs creates a glomerular pro-regenerative environment possibly via VEGF, and restores glomerular architecture by limiting podocyte and endothelial dysfunction and by moderating progenitor cell activation.

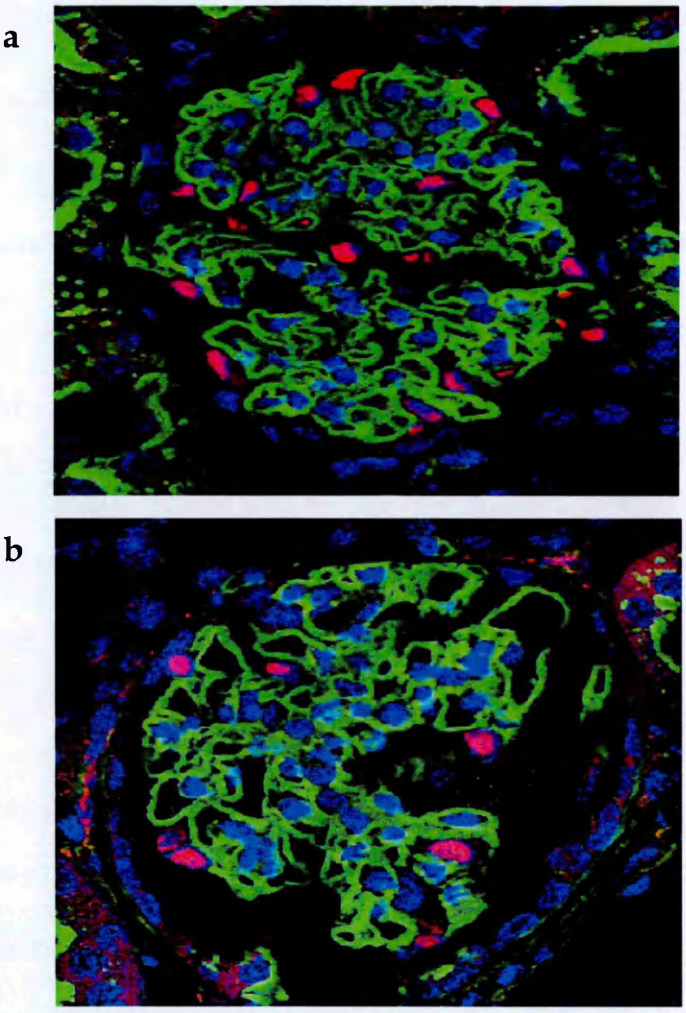

Figure 10.1 : Adriamycin causes loss of podocytes

Representative micrographs of renal sections from (a) control and (b) ADR-treated rats showing podocytes (WT-1 positive nuclei in red), glomerular capillaries (lectin, green) and cell nuclei (DAPI in blue). Original magnification, x400.

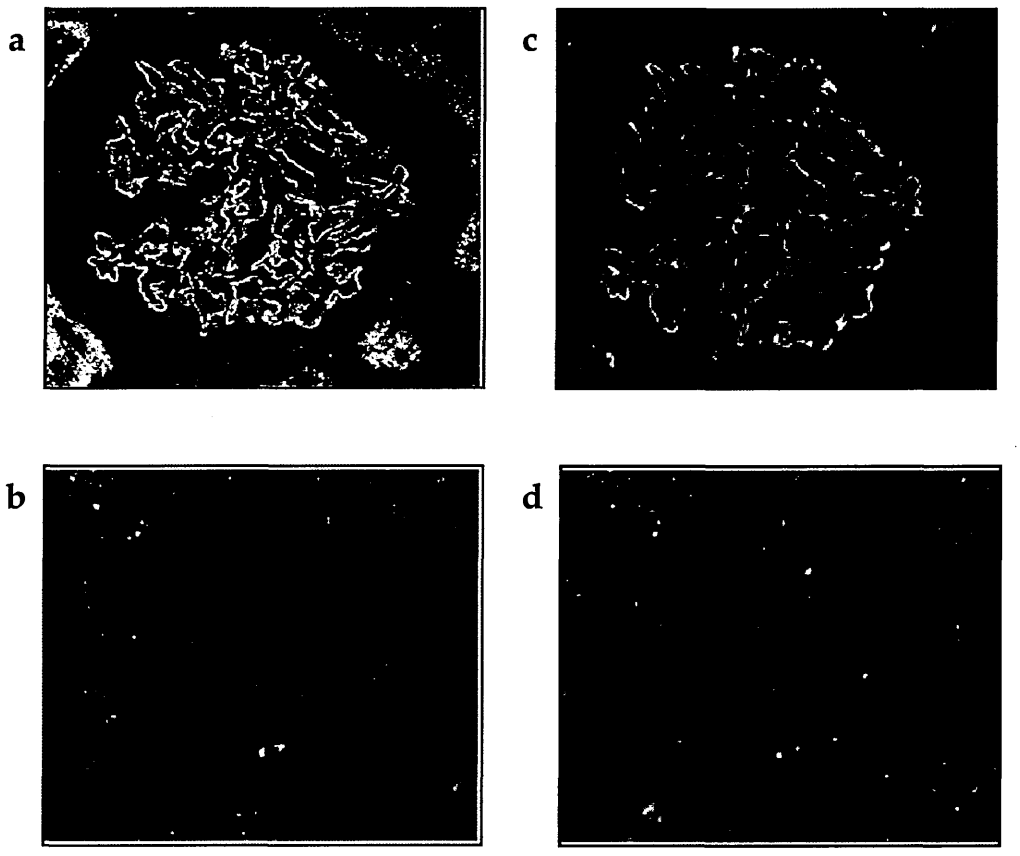

Figure 10.2: Adriamycin reduces the expression of the podocyte-associated proteins nephrin and CD2AP

Representative images of renal sections showing nephrin (green; a,b) and CD2AP (red; c,d) expression in glomeruli from control (a, c) and ADR-rats (b, d). Original magnification, x400.

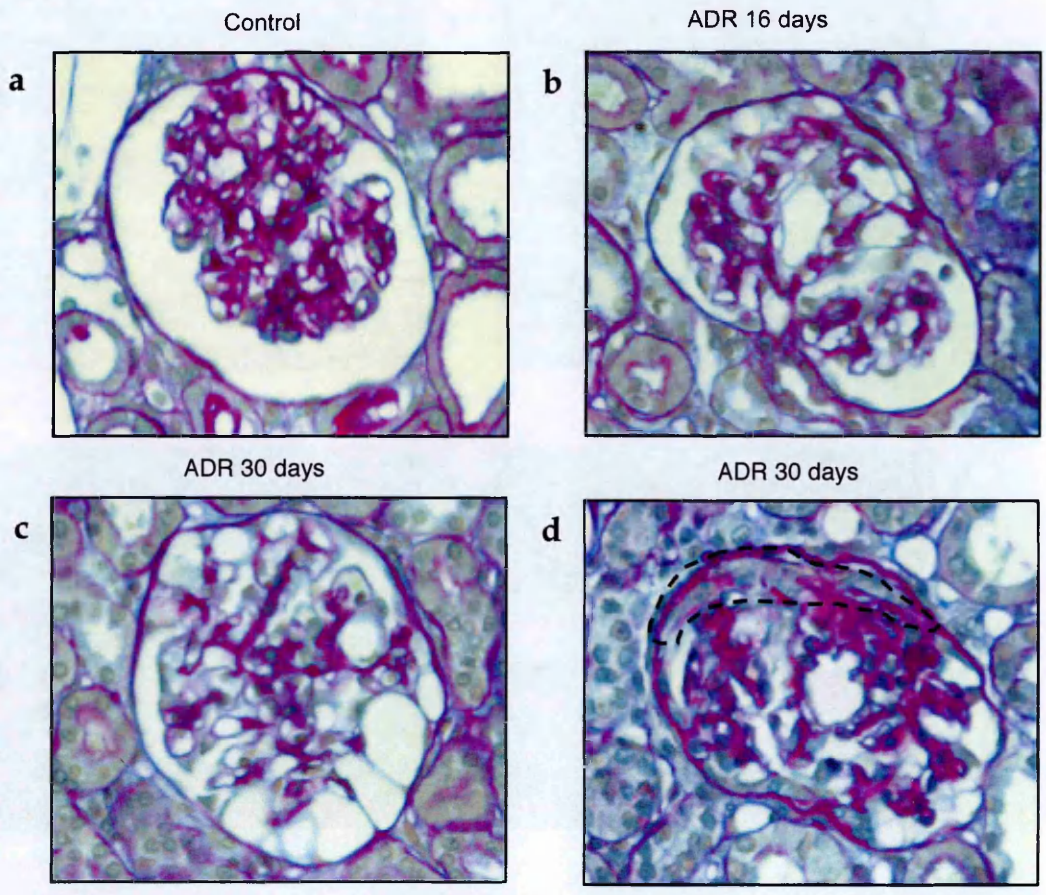

Figure 10.3: Glomerular lesions in rats with ADR nephropathy at 16 and 30 days.

Representative micrographs of kidney tissue from control (a) and ADR-rats (b-d). Synechiae (b) and more extensive adhesions or crescents-like lesions (c,d) were observed during time in ADR-treated rats. Original magnification, x400.

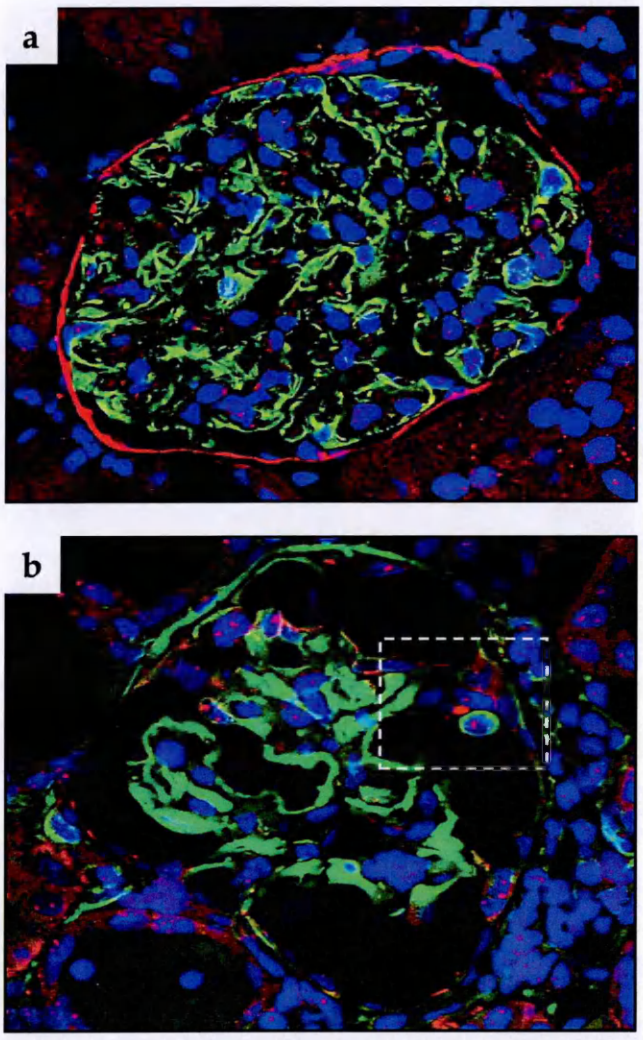

Figure 10.4: Formation of early synechiae in rats with ADR nephropathy at 16 days.

Representative images of claudin-1 (red) and nestin (green) in control (a) and ADR-rats (b). Inset shows claudin-1 and nestin positive cells that participated to the formation of early cellular bridge. Cells were co-stained with DAPI. Original magnification, x400.

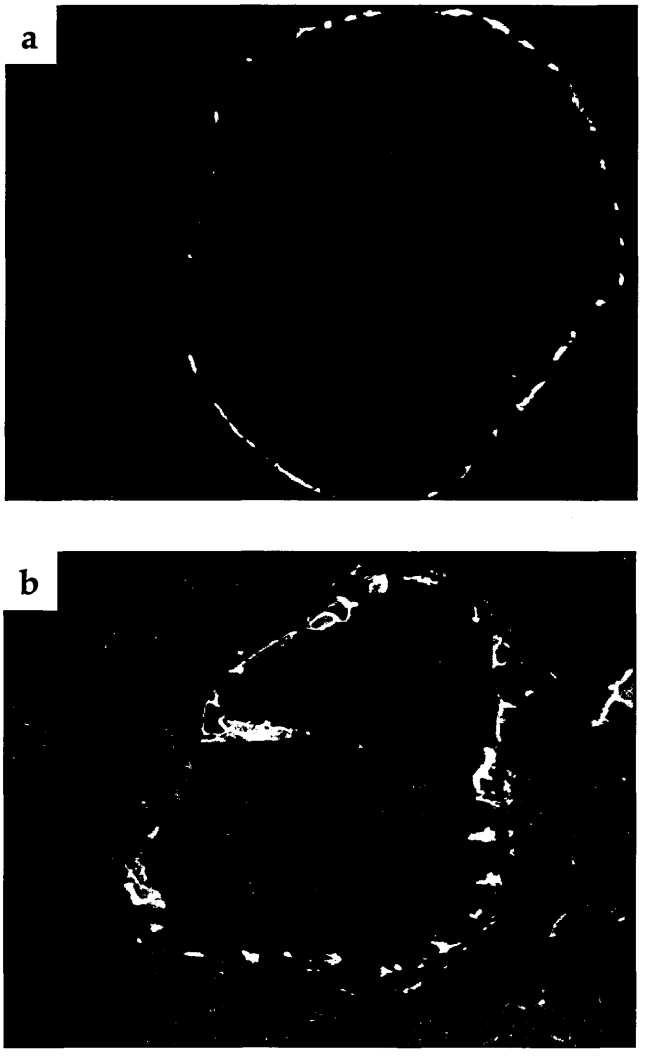

Figure 10.5: NCAM positive cells contributed to the formation of early lesions in ADR nephropathy at 16 days

Representative images of NCAM (red) in control (a) and ADR-rats (b). Cells were co-stained with DAPI. Original magnification, x400.

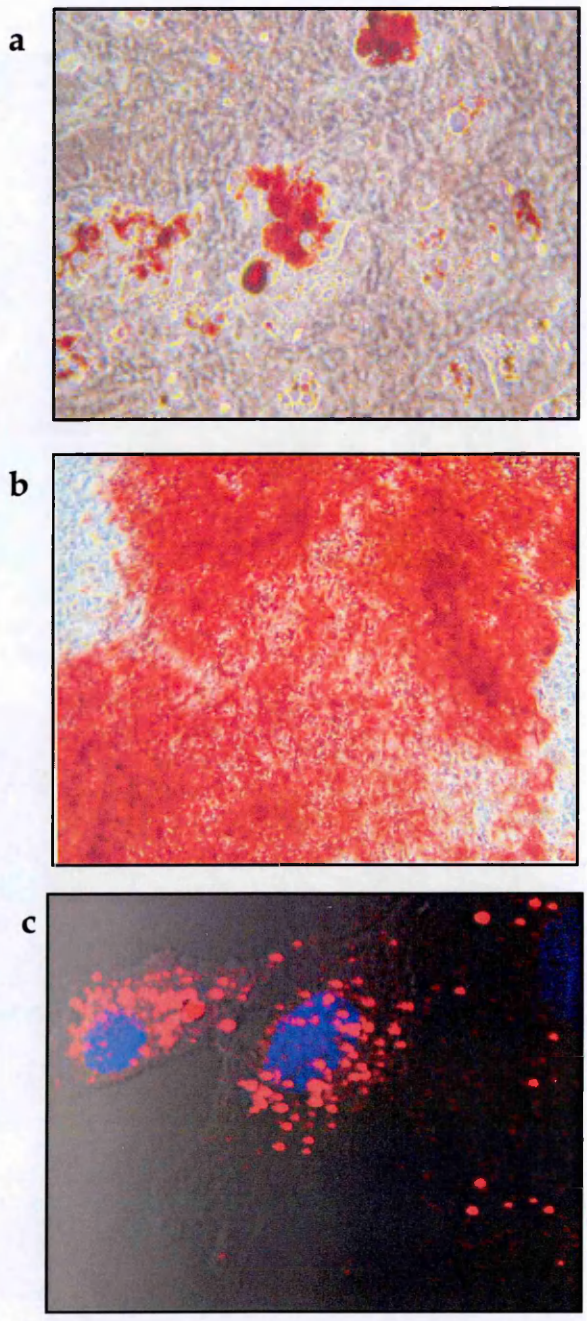

Figure 10.6: Differentiation potential and staining of MSCs

Representative micrographs of rat MSCs showing differentiation into adipocytes as visualized by intracellular lipid vacuoles detected with Oil Red O staining (a). The differentiation toward osteocytes is indicated by the formation of calcium-rich hydroxyapatite detected with Alizarin red (b). Representative image of fluo-NP labeled MSCs (red) co-stained with Hoechst 33258 for cell nuclei (blue) (c). Original magnification, x400.

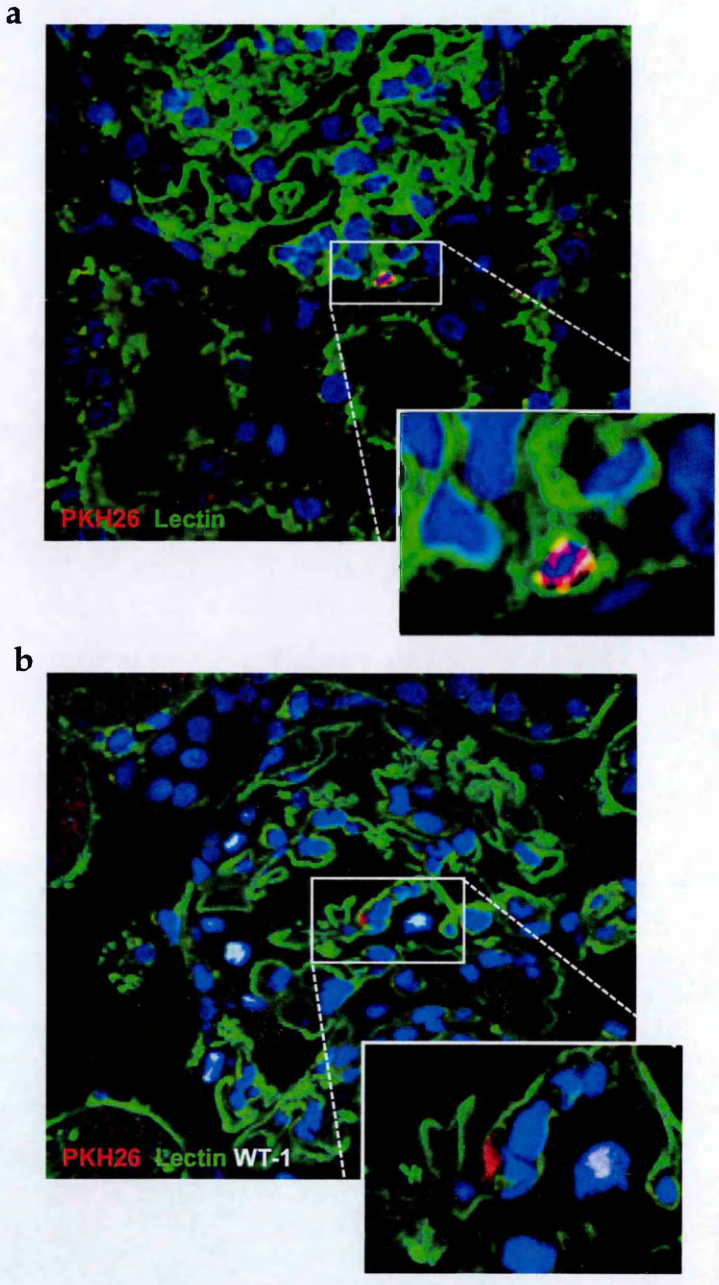

Figure 10.7: Localization of MSCs in renal tissue

Representative micrographs of kidney tissue from ADR-treated rats injected with PKH26-labeled MSCs (red) at 3 days (a). Representative micrograph of kidney section of ADR-treated rats injected with PKH-26-labeled MSCs (red) stained with the podocyte marker WT1 (white) at 16 days (b). Section were co-stained with lectin WGA and DAPI. Original magnification, x400.

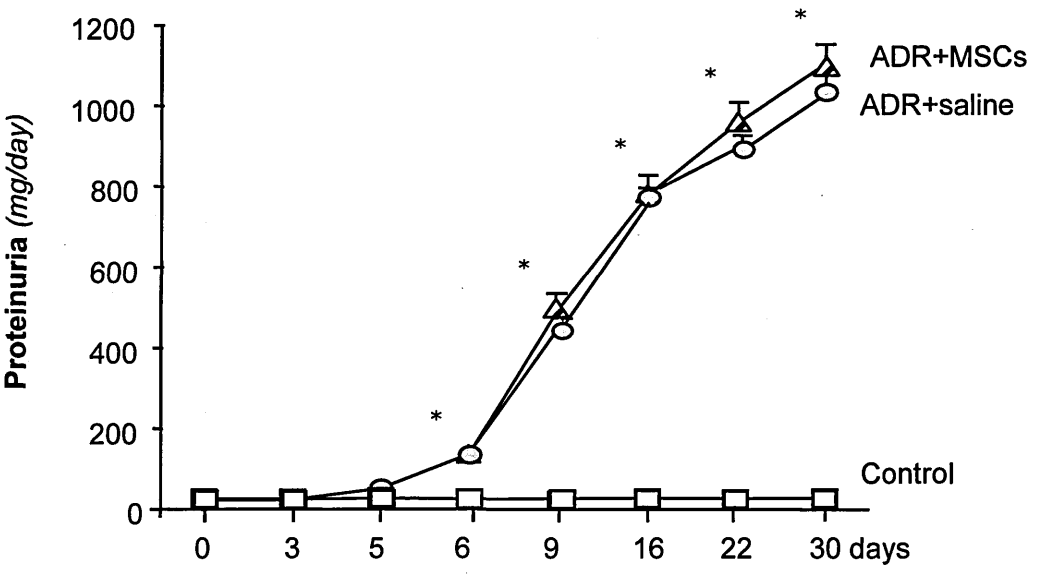

Figure 10.8: Effect of MSCs on proteinuria

Time course of urinary protein excretion in control (n=6) and ADR-rats treated with saline (n=16) or MSCs (n=16) . Data are mean ± SE. *P<0.01 vs control rats at corresponding time (Mann- Whitney test).

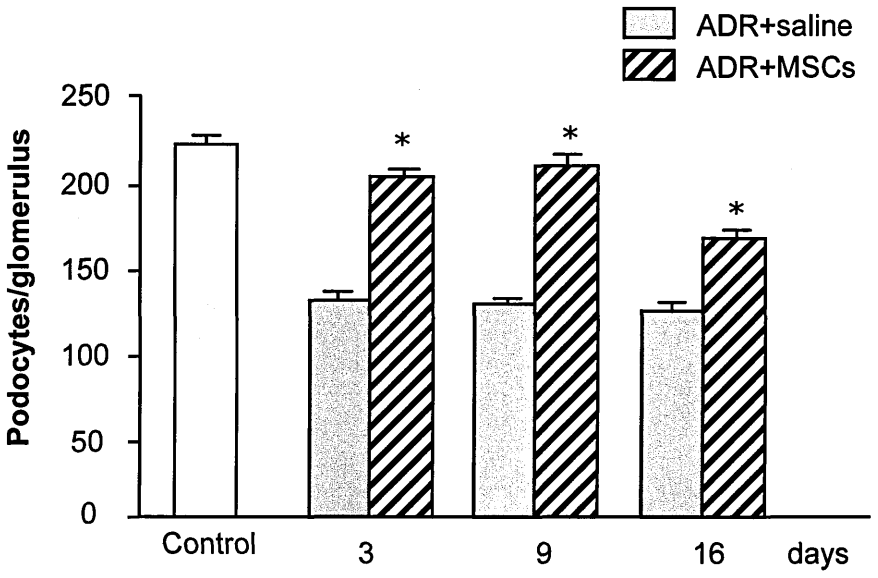

Figure 10.9: MSC treatment reduces podocyte loss in ADR-rats

Morphometrical estimation of average number of podocytes per glomerulus from 3 to 16 days in ADR-rats treated with saline (n=4 at each time point) or MSCs (n=4 at each time point), and in control rats (n=6). Values are expressed as mean±SE. *P<0.01 vs ADR+saline at corresponding time (ANOVA corrected with Bonferroni coefficient).

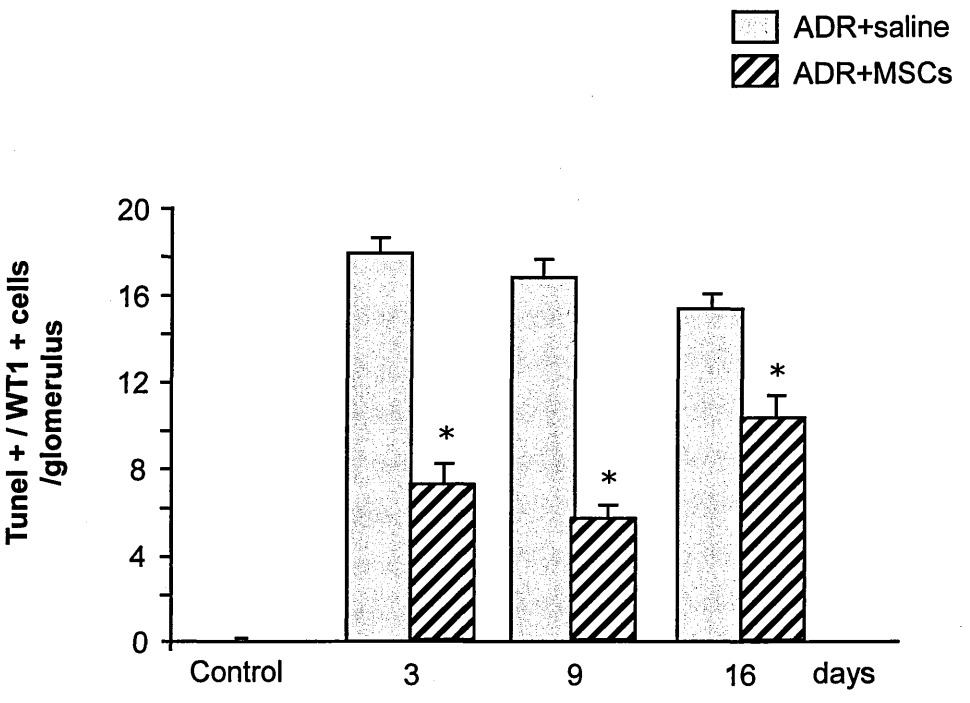

Figure 10.10: Effect of MSC injection on apoptotic podocytes in ADR-rats.

Quantification of apoptotic podocytes, double positive for TUNEL and WT-1 in glomeruli of ADR-rats given saline (n=4 at each time point) or MSCs (n=4 at each time point) at day 3, 9 and 16 and in control rats (n=6). Values are expressed as mean±SE. *P<0.01 vs ADR+saline at corresponding time (ANOVA corrected with Bonferroni coefficient).

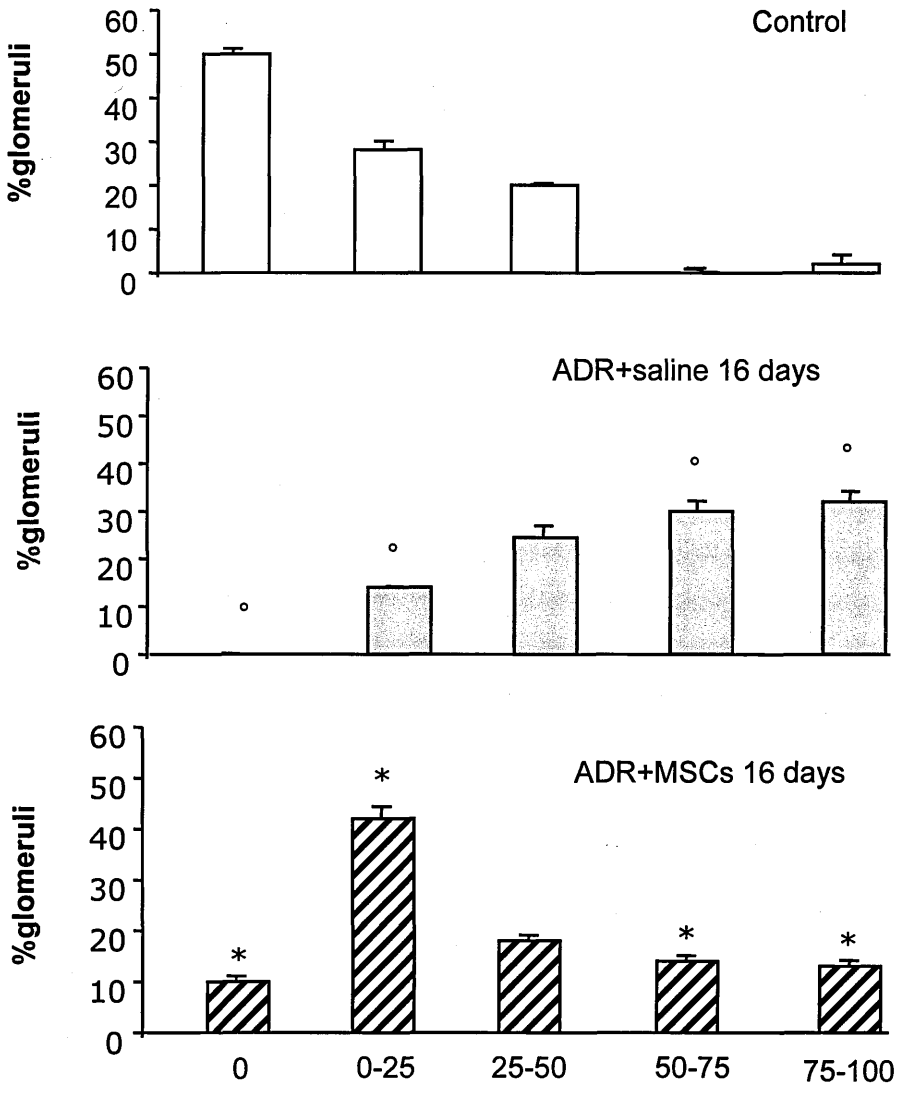

Figure 10.11: MSCs reduce formation of glomerular podocyte-PEC bridges in ADR-rats.

Percentage of glomeruli (mean±SE) affected by different degree of synechiae at 16 days in control (n=4) and ADR-rats receiving saline (n=4) or MSCs (n=4). °p<0.01 vs CTR.*P<0.01 vs ADR+saline (ANOVA corrected with Bonferroni coefficient).

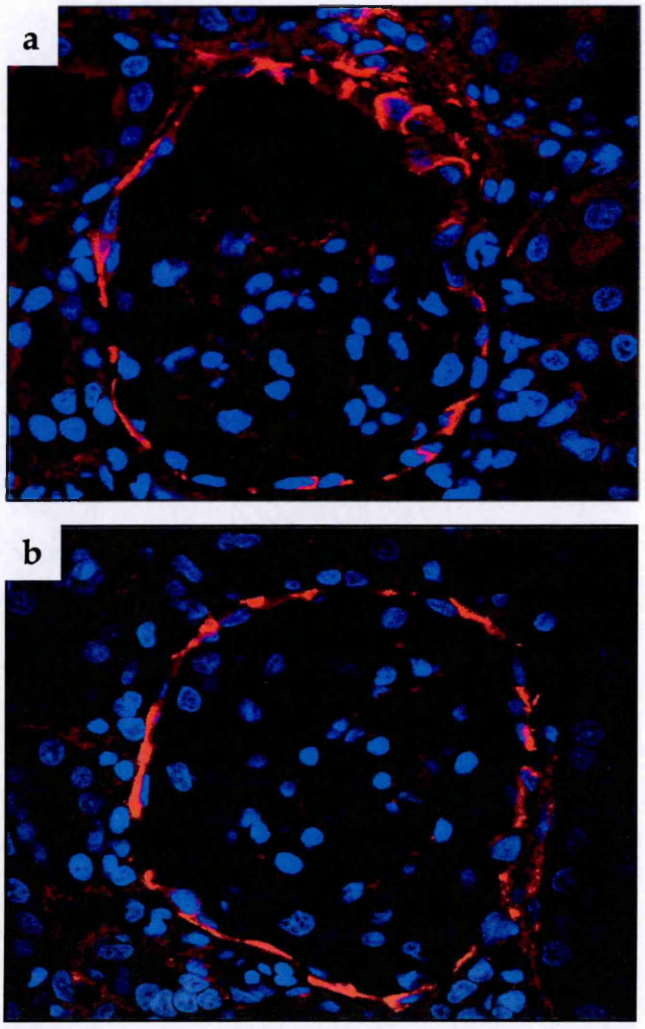

Figure 10.12: MSC treatment restores along the Bowman's capsule, the distribution of NCAM positive cells

Representative images of NCAM+ cells (red) in ADR-rats receiving saline (a) or MSCs (b) at 16 days. Cells were co-stained with DAPI. Original magnification, x400.

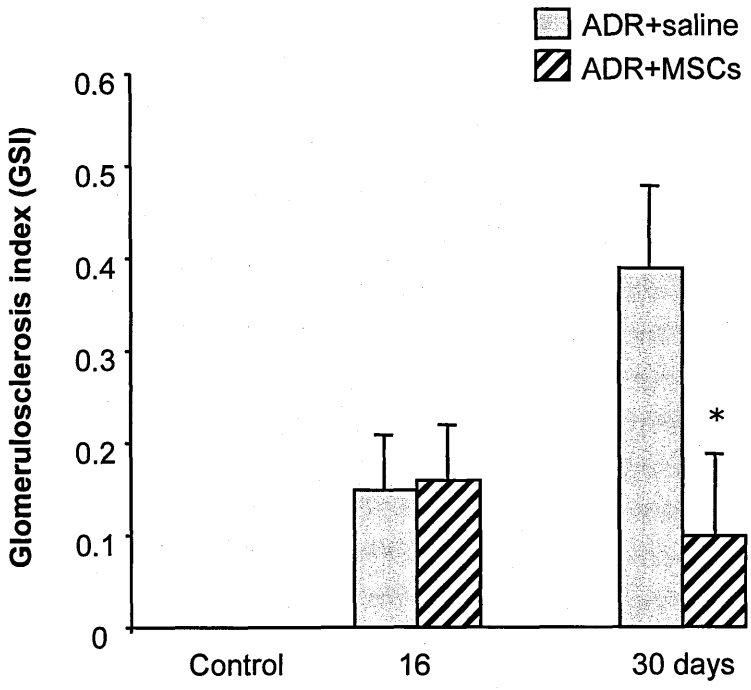

Figure 10.13: MSC treatment reduces glomerulosclerosis in ADR-rats at 30 days

Glomerulosclerosis index evaluated at 16 and 30 days in ADR-rats, receiving saline (n=4), MSCs (n=4) and in control rats (n=4). Original magnification, x400. Score values are mean±SE. *P<0.01 vs ADR+saline at corresponding time (Mann-Whitney).

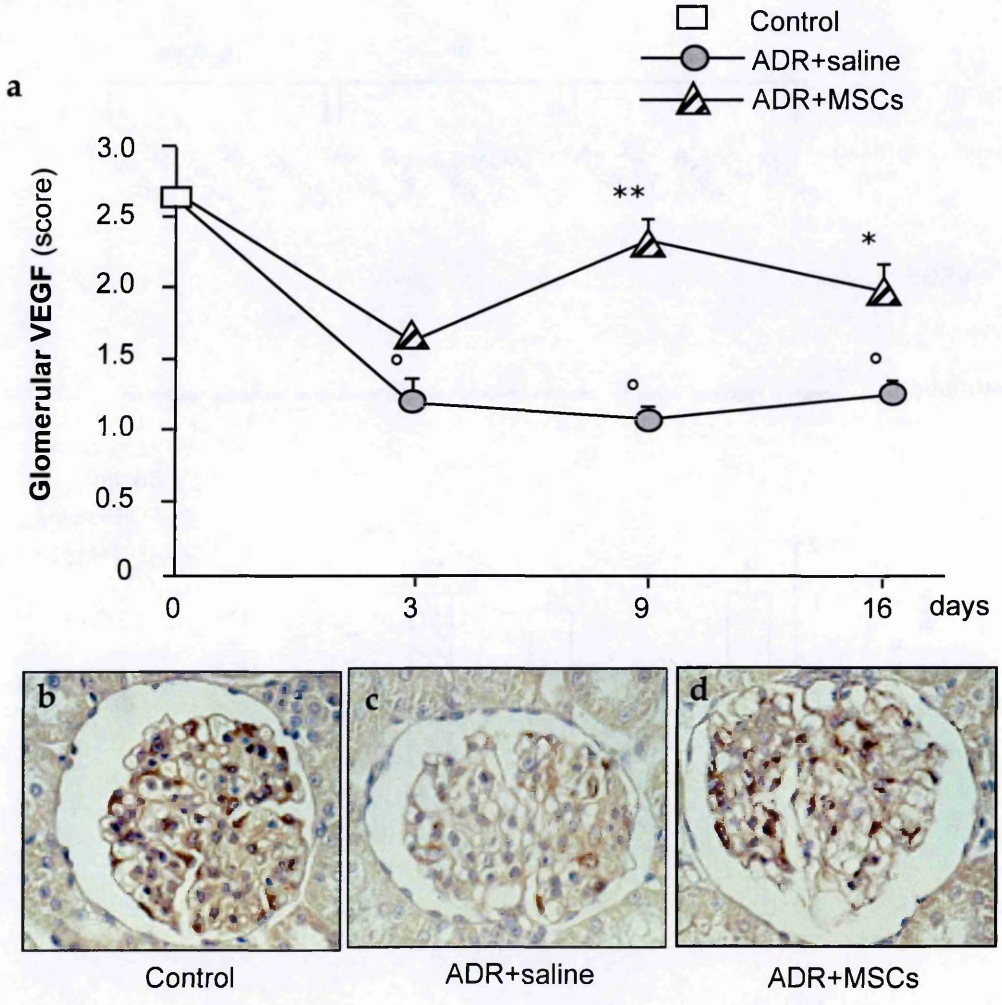

Figure 10.14: Effect of MSC treatment on glomerular VEGF expression

(a) Scores of glomerular VEGF expression evaluated at 3, 9 and 16 days after ADR in rats receiving saline (n=4), MSCs (n=4) or in control rats (n=4). Score values are mean±SE. *P<0.05 vs ADR+MSCs at corresponding time (t test). (b-d) Representative micrographs of VEGF expression at day 9 in control, ADR- rats receiving saline or MSCs. Original magnification, x400.

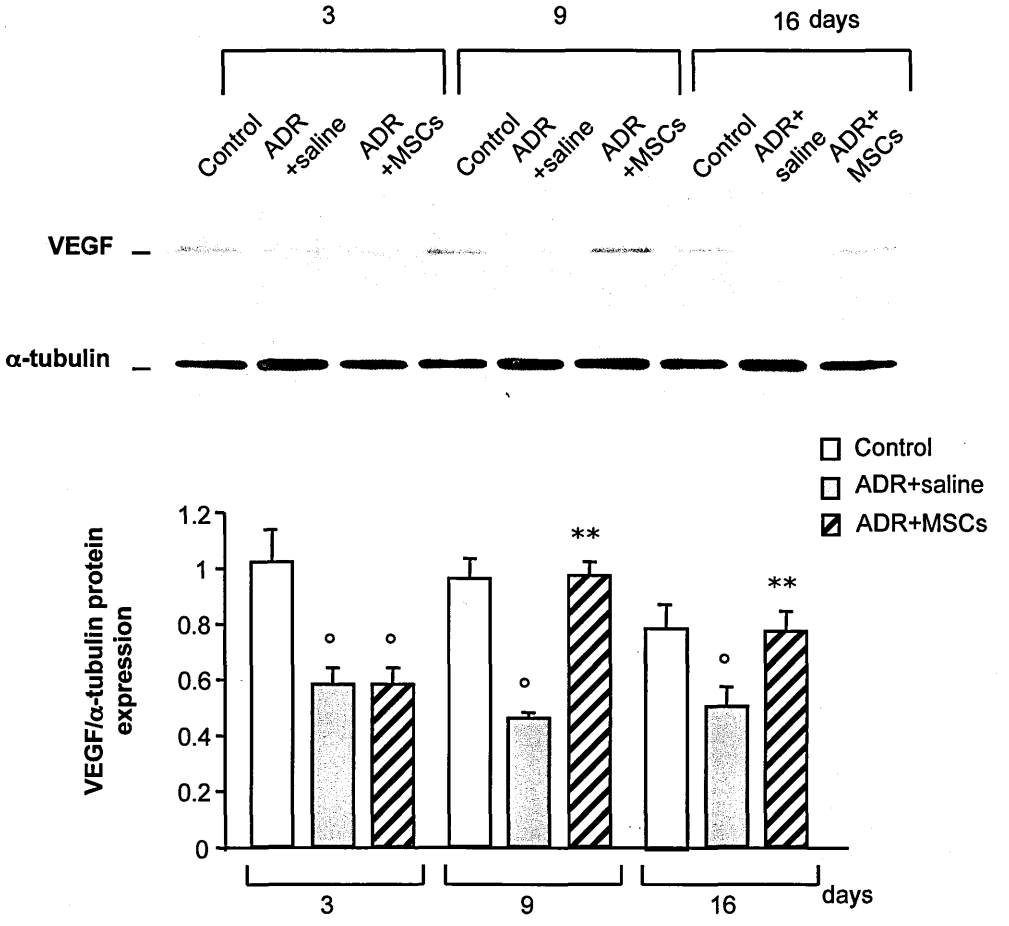

Figure 10.15:Effect of MSC treatment on glomerular VEGF expression

Western blot analysis of VEGF in kidney tissue of ADR-rats receiving saline (n=4) or MSCs (n=4), and control rats (n=4) at 3, 9, 16 days (top). The expression levels of VEGF are quantified relative to levels of α-tubulin (bottom). Data are means±SE. °P<0.01 vs. control; **P<0.01 vs. ADR+saline at corresponding time (ANOVA corrected with Bonferroni coefficient).

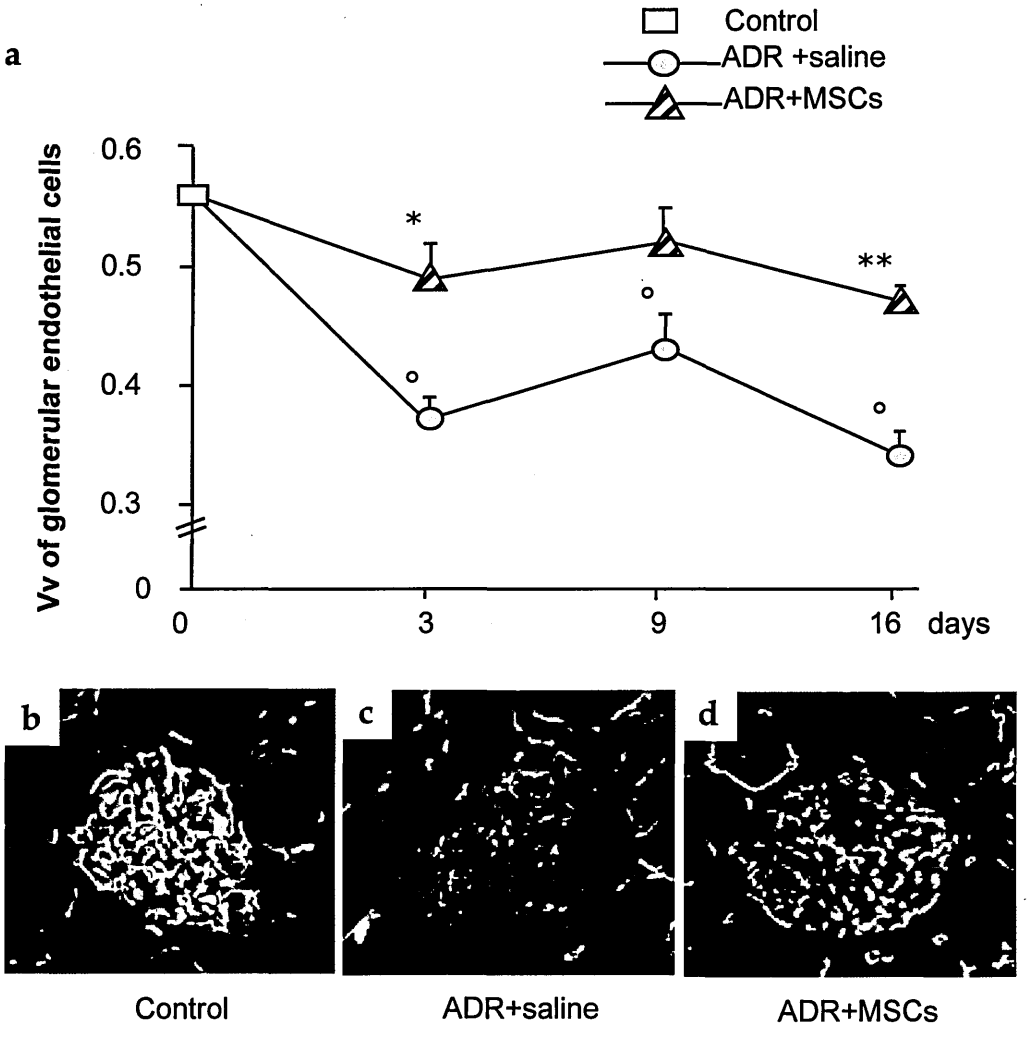

Figure 10.16: Effect of MSC treatment on volume density of endothelial cells.

Estimation of volume density (Vv) of glomerular endothelial cells stained for RECA during time (a). Score values are mean±SE. *P<0.01 vs ADR+saline at corresponding time (ANOVA followed Tuckey-Cicchetti). Representative micrographs at 9 days of glomerular RECA staining in control (n=4), ADR-rats receiving saline (n=4) or MSCs (n=4) (b-d). Original magnification, x400.

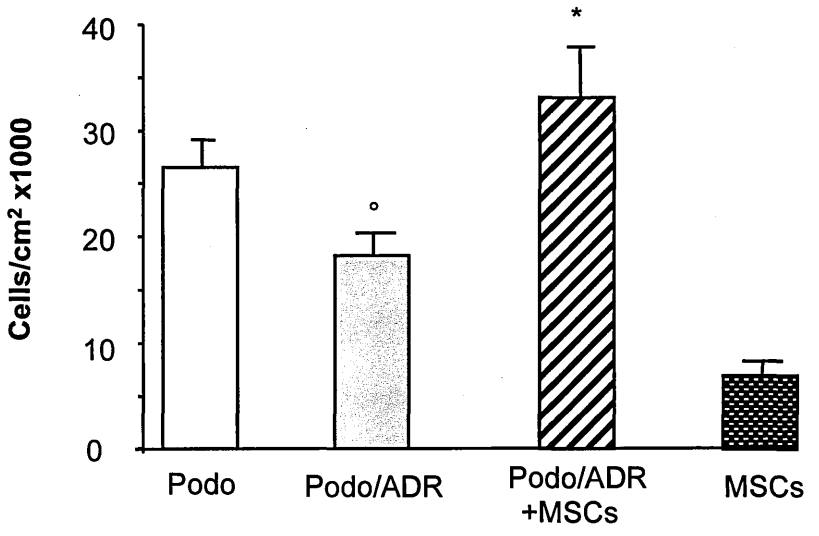

Figure 10.17: Effect of MSCs on ADR-treated podocytes : *in vitro* studies.

MSCs protected podocytes from ADR-induced damage after 72 hours of co-culture. Podocytes were incubated with 1.5 μM ADR for 6 hours, and after drug withdrawal, were co-cultured with murine MSCs. After 72 hours viable cells were counted. Data are expressed as mean±SE. °P<0.01 versus Podo, *P<0.01 versus Podo/ADR (ANOVA corrected with Bonferroni coefficient). The experiments were performed in triplicate and repeated 3 times.

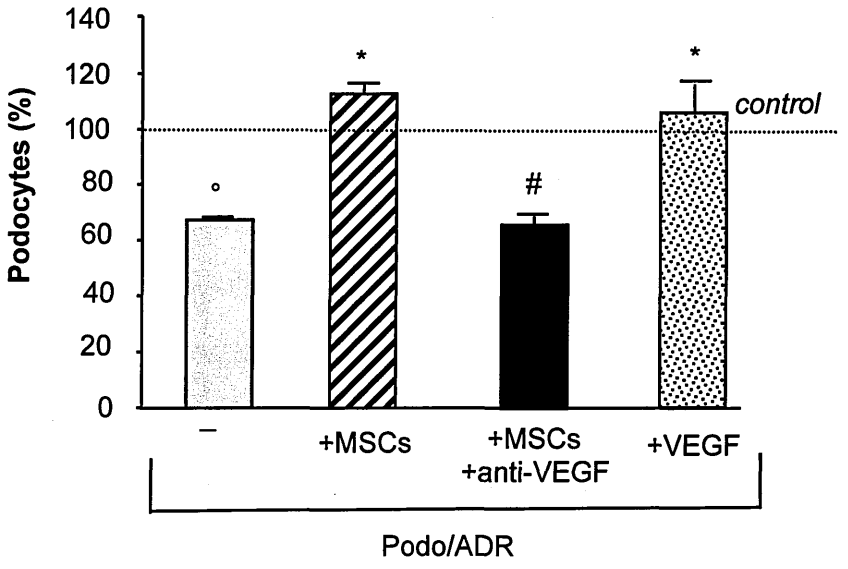

Figure 10.18: MSCs exert protective effect on ADR-damaged podocytes via VEGF

Percentage of viable ADR-treated podocytes alone or co-cultured with murine MSCs in the presence or absence of anti-VEGF antibody (10 mg/ml) for 72 hours. In additional samples, ADR-treated podocytes were incubated with exogenous VEGF (40 ng /ml) for 72 hours. Data (mean ± SE) are expressed as percentage of viable podocytes in each sample versus control podocytes imposed as 100%. °P<0.01 versus control, *P<0.01 versus Podo/ADR, #P<0.01 versus Podo/ADR+MSCs (ANOVA corrected with Bonferroni coefficient).
The experiments were performed in triplicate and repeated 3 times.

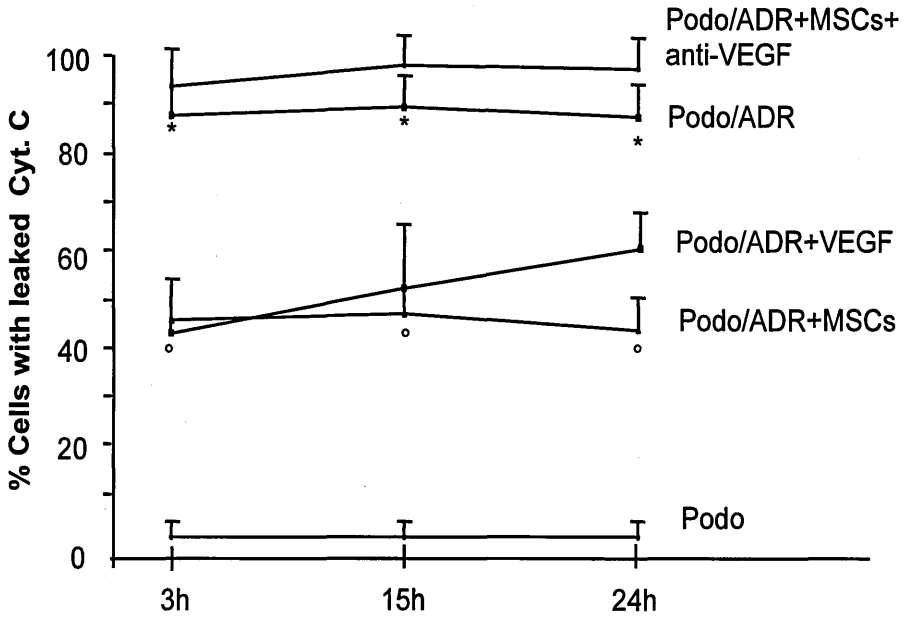

Figure 10.19: Effect of MSCs on podocyte apoptosis at different time intervals.

ADR-treated podocytes alone or co-cultured with MSCs in the presence or absence of functional blocking anti-VEGF antibody. In additional samples, ADR-treated podocytes were incubated with exogenous VEGF. Apoptosis was expressed as the percentage of podocytes with cytocrome (Cyt C) released into cell cytosol. *P<0.01 versus Podo, °P<0.01 versus Podo/ADR (ANOVA corrected with Bonferroni coefficient).

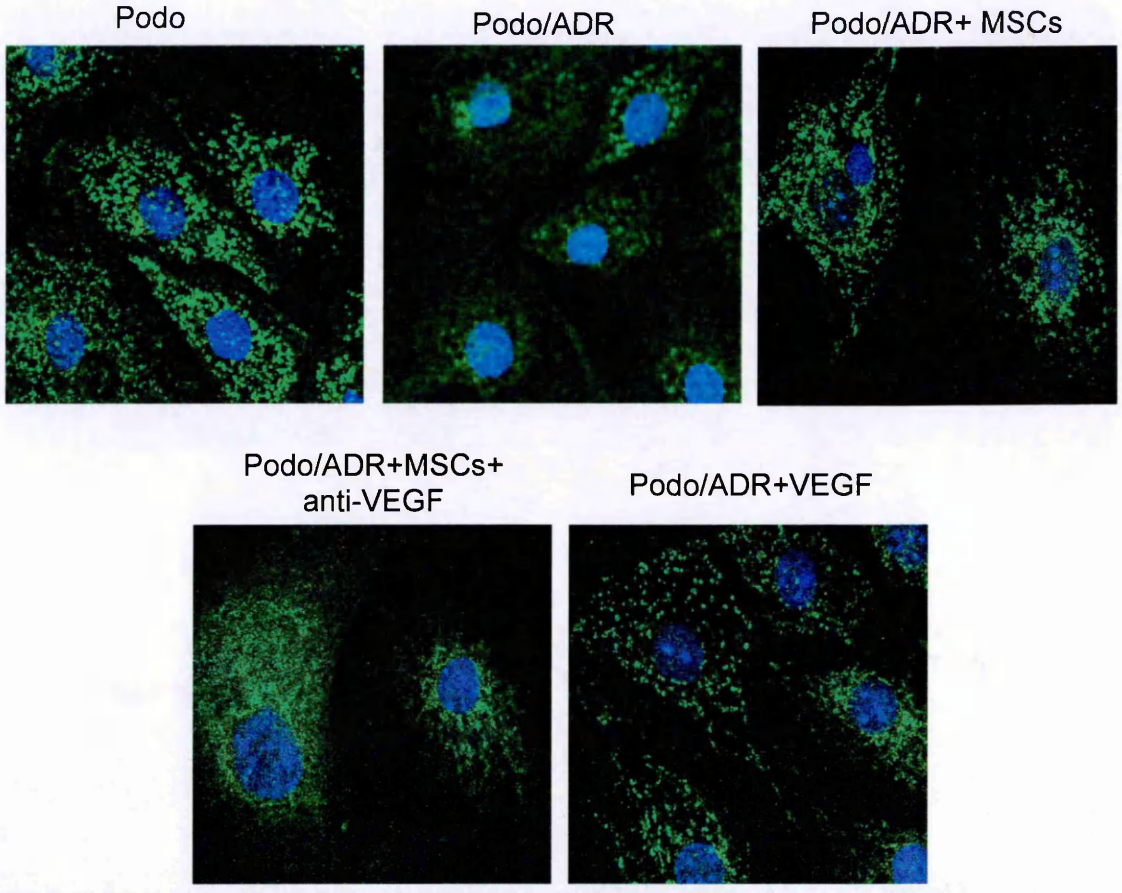

Figure 10.20: Effect of MSCs on Cyt C released on cytosol

Representative images of Cyt C expression in podocytes 3 hours after ADR incubation. Cyt C expression was also shown in ADR-treated podocytes co-cultured with MSCs with or without anti-VEGF antibody and in ADR-treated podocytes incubated with exogenous VEGF. Cells were co-stained with DAPI. Original magnification, x630.

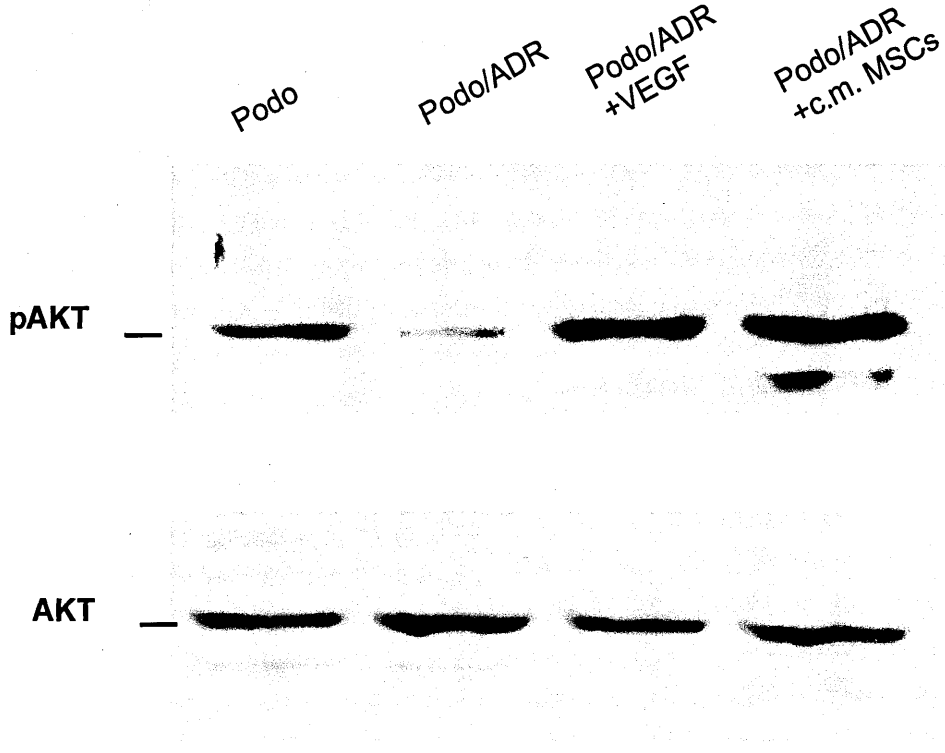

Figure 10.21: Effect of MSCs on Akt activation in ADR-damaged podocytes

Western blot analysis of Akt at 3 days. Expression level of phosphorylated (p)-Akt Ser437 and total Akt in control podocytes, ADR-treated podocytes, ADR-treated podocytes incubated with VEGF or with MSC conditioned medium (c.m. MSCs)

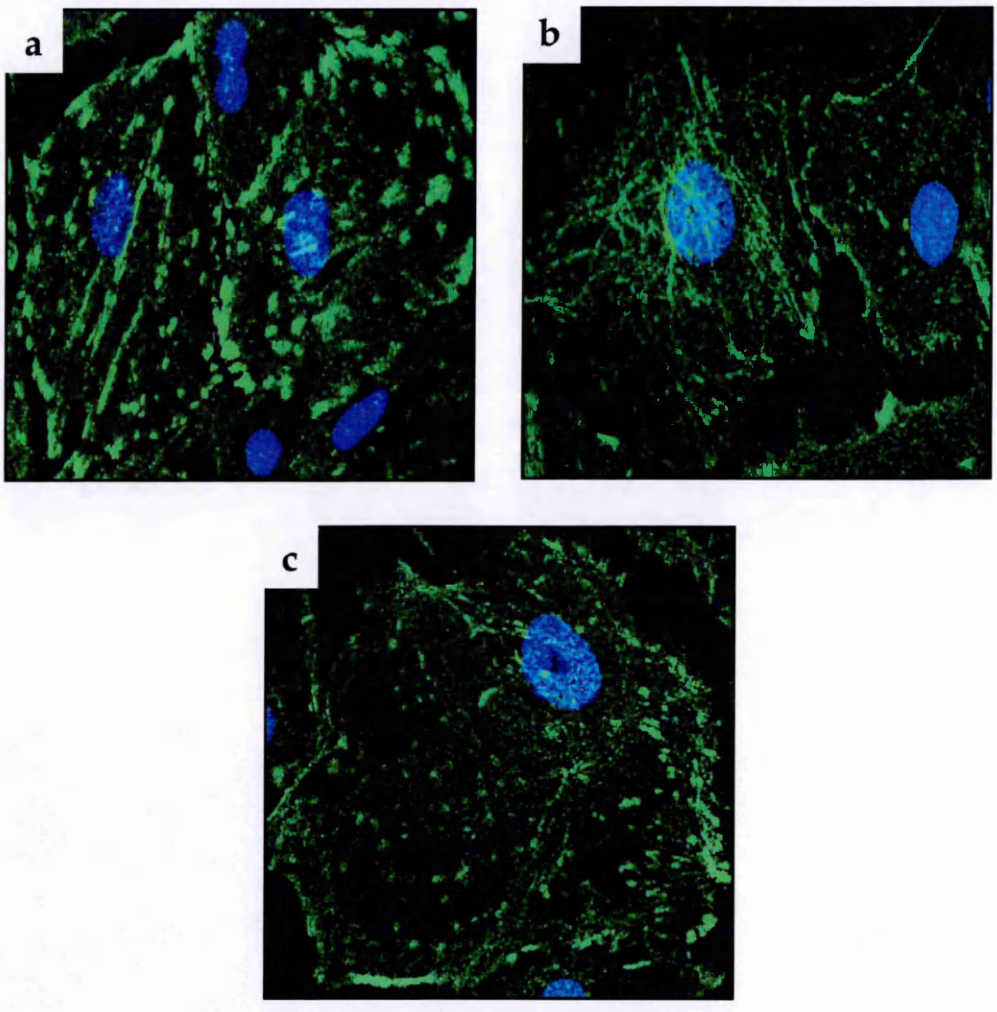

Figure 10.22: MSC treatment restores ILK staining in ADR-damaged podocytes

Representative images of ILK staining in untreated podocytes (a) or in cells exposed to ADR alone (b) or in co-culture with MSCs (c) for 24 hours. Cells were co-stained with DAPI. Original magnification, x630.

CHAPTER 11

GENERAL DISCUSSION

The kidney has been regarded as an organ with minimal cell turnover and limited capacity for repair. However, after acute damage, the kidney maintains a significant ability to undergo repair, and this is best illustrated by the power of tubular cells to replace damaged ones. The same, though, does not occur with glomeruli, their capacity for repair is rather limited, and once the damage has reached a certain point, the ability to recover from the injury may primarily depend on extrarenal stem cell sources. In experimental model of AKI, the renoprotective effect of BM-MSCs is well established, unfortunately, the therapeutic potential in CKD has not been completely demonstrated so far. This is probably due to the complexity of the chronic kidney damage, which involves different populations of renal cells.

In order to establish a therapeutic effect of BM-MSCs, we set up a model of nephropathy induced by adriamycin (ADR), an anthracycline antibiotic, used for the treatment of solid tumors. ADR-induced nephropathy is considered an accurate experimental model that mimics the primary focal segmental glomerulosclerosis (FSGS). To study the renoprotective effect of BM-MSCs, repeated intravenous injections of stem cells were performed, in order to maintain a constant number of MSCs into the damaged kidney.

The first important evidence of this study is that BM-MSCs are able to create a glomerular pro-regenerative environment in the glomerulus possibly by producing large amount of growth factors including VEGF. It is well established that VEGF regulates and

maintains podocyte and glomerular endothelial cell integrity and function (Sugimoto *et al.*, 2003; Eremina *et al.*, 2003). Moreover, VEGF is able to activate Akt, a kinase upstream target of anti-apoptotic and pro-survival pathways in podocytes.

It is plausible to hypothesize that BM-MSCs homing the glomeruli locally release VEGF that activates pro-survival pathways, thus rendering podocytes again metabolically active. Podocytes, in response to these pro-survival signals, start to synthesize again great amount of the pro-regenerative growth factor itself, through a self-repair process.

The second important finding is the preservation of the Bowman's capsule architecture with consequent reduction of formation of PEC-podocyte bridges and crescents. PECs response to injury by de/transdifferentiated into a mesenchymal/embryonic phenotype. This change leads to lose their polarity, microvilli and tight junctions (Le Hir *et al.*, 2001). As result of damage, podocytes undergo foot process effacement and prominent microvillus transformation that represents extensive membrane dynamics (Le Hir *et al.*, 2001). It is tempting to speculate that these changes enable podocytes to disjoin junction between PECs. This junctional instability could be provoked also by inflammatory environment present during the progression of CKD (Le Hir *et al.*, 2001). The rupture of junctions in the parietal epithelium at the site of intrusion by podocytes might play a central role in the proliferation of PECs and the organization of crescents. The restoration of podocyte number and function mediated by BM-MSC treatment,

limit migration and proliferation of parietal progenitor epithelial cells of the Bowman's capsule thereby reducing the early formation of PEC-podocyte bridges. In the future, it will be necessary to understand how podocytes and PECs communicate, and how PECs are activated by the damage in order to better understand the formation of cellular bridges.

The fact that BM-MSC treatment failed to reduce proteinuria could be ascribed to the limited recovery of the slit diaphragm proteins in the preserved podocytes. Future studies must investigate the reasons for this failure. Moreover, based on data described in literature, it becomes evident that potentiating renal migration, engraftment, survival and paracrine effects of administered stem cells through preconditioning or genetic modifications, may be possible to contribute to enhance the MSC local effect in the damaged kidneys thus improving also proteinuria and renal functional parameters. In particular, gene-modified and pre-conditioned BM-MSCs have shown enhanced therapeutic effects in preclinical model of AKI. BM-MSCs genetically modified with the serine protease kallikrein by adenovirus transduction were more resistant to oxidative stress-induced apoptosis and secreted high levels of VEGF in culture medium (Hagiwara *et al.*, 2008). Injection of kallikrein-modified BM-MSCs in rat with ischaemia/reperfusion injury enhanced renal function inhibiting apoptosis and inflammation (Hagiwara *et al.*, 2008). Other strategies to improve the ability of stem cells to survive and produce paracrine factors can be achieved by *in vitro* pretreatment with melatonin. Mias and coworkers have observed

that melatonin was able to increase the resistance of BM-MSCs to hydrogen peroxide-induced apoptosis by promoting overexpression of the antioxidant enzyme catalase and superoxidase dismutase (Mias *et al.,* 2008). Moreover, in a rat model of AKI, melatonin preconditioning allowed the long-term survival of BM-MSCs within the damaged kidney improving angiogenesis, proliferation and recovery of renal function (Mias *et al.,* 2008). Of note, the glial cell line-derived neurotrophic growth factor (GDNF), increased motility and survival of cultured MSCs and ameliorated acute renal damage (Shi *et al.,* 2008).

Another important finding of this study is the anti-inflammatory effect of BM-MSC therapy that markedly reduced glomerular macrophage infiltration and local release of chemo-attractants, possibly involved in PEC-podocyte activation. The role of inflammation in the progression of chronic kidney disease is well known and there is broad agreement that fibrosis often follows inflammation and that both associate with a decline of renal function in CKD. The relationship between inflammation and fibrosis remains under debate. However, it is now becoming clear the impact of distinct macrophage phenotypes on "inflammation", "epithelial healing", "mesenchymal healing" and the "resolution of fibrosis" (Anders *et al.,* 2011). At least four different types of macrophages should exist: proinflammatory macrophages, anti-inflammatory macrophages, profibrotic macrophages and fibrolytic macrophages (Anders *et al.,* 2011). However, as the histomorphological abnormalities in CKD are complex, it remains difficult to dissect their

presence in renal biopsies or their functional contribution to single disease. Much more work remains to be done to more clearly define functionally important macrophage phenotypes in the different stages of CKD. Equally, much work needs to be done to understand the effect of MSCs on macrophage-mediated inflammation.

In spite the BM-MSCs failed to improve renal function, our results demonstrated that BM-MSCs are able to create a pro-regenerative environment that restored glomerular architecture, limiting podocyte loss, endothelial dysfunction and moderating progenitor cell activation. Therefore, this study contributes to the advancement of knowledge in stem cell biology and provides a basis for a new therapeutic concept for the treatment of chronic kidney disease. Moreover, given the role of progenitor cells in the progression of the disease in chronic kidney injury future studies should investigate which mechanisms are induced by BM-MSCs to modulate renal progenitor cell activation.

CHAPTER 12

BIBLIOGRAPHY

Abbate M, Brown D, Bonventre JV. 1999. Expression of NCAM recapitulates tubulogenic development in kidneys recovering from acute ischemia. Am J Physiol. 277:F454-63.

Aejaz HM, Aleem AK, Parveen N, Khaja MN, Narusu ML, Habibullah CM. 2007. Stem cell therapy-present status. Transplant Proc. 39:694-9.

Anders HJ, Ryu M. 2011. Renal microenvironments and macrophage phenotypes determine progression or resolution of renal inflammation and fibrosis. Kidney Int. 80:915-25.

Appel D, Kershaw DB, Smeets B, Yuan G, Fuss A, Frye B, Elger M, Kriz W, Floege J, Moeller MJ. 2009. Recruitment of podocytes from glomerular parietal epithelial cells. J Am Soc Nephrol 20:333-43.

Arany I, Safirstein RL. 2003. Cisplatin nephrotoxicity. Semin Nephrol. 23: 460-4.

Bard JB, Gordon A, Sharp L, Sellers WI. 2001. Early nephron formation in the developing mouse kidney. J Anat. 199:385-92.

Baliga R, Ueda N, Walker PD, Shah SV. 1999. Oxidant mechanisms in toxic acute renal failure. Drug Metab Rev.31:971-97.

Benigni A, Morigi M, Remuzzi G. 2010. Kidney regeneration. Lancet. 375:1310-7.

Benigni A, Morigi M, Rizzo P, Gagliardini E, Rota C, Abbate M, Ghezzi S, Remuzzi A, Remuzzi G. 2011. Inhibiting angiotensin-converting enzyme promotes renal repair by limiting progenitor cell proliferation and restoring the glomerular architecture. Am J Pathol. 179:628-38.

Bertani T, Poggi A, Pozzoni R, Delaini F, Sacchi G, Thoua Y, Mecca G, Remuzzi G, Donati MB. 1982. Adriamycin-induced nephrotic syndrome in rats: sequence of pathologic events. Lab Invest. 46:16-23.

Berthiaume JM, Wallace KB. 2007. Adriamycin-induced oxidative mitochondrial cardiotoxicity. Cell Biol Toxicol. 23:15-25.

Betz AG. 2010. Immunology. Have you seen your mother, baby... Science. 330:1635-6.

Bi B, Schmitt R, Israilova M, Nishio H, Cantley LG. 2007. Stromal cells protect against acute tubular injury via an endocrine effect. J Am Soc Nephrol. 18:2486-96.

Bianco, P., M. Riminucci, S. Gronthos, and P.G. Robey. 2001. Bone marrow stromal stem cells: nature, biology, and potential applications. Stem Cells. 19: 180-92.

Bianco P, Robey PG, Simmons PJ. 2008. Mesenchymal stem cells: revisiting history, concepts, and assays. Cell Stem Cell. 2:313-9.

Blau, H.M., T.R. Brazelton, and J.M. Weimann. 2001. The evolving concept of a stem cell: entity or function? Cell. 105: 829-41.

Bodley A, Liu LF, Israel M, Seshadri R, Koseki Y, Giuliani FC, Kirschenbaum S, Silber R, Potmesil M. 1989. DNA topoisomerase II-mediated interaction of doxorubicin and daunorubicin congeners with DNA. Cancer Res. 49: 5969-78.

Bollini S, Pozzobon M, Nobles M, Riegler J, Dong X, Piccoli M, Chiavegato A, Price AN, Ghionzoli M, Cheung KK, Cabrelle A, O'Mahoney PR, Cozzi E, Sartore S, Tinker A, Lythgoe MF, De Coppi P. 2011. In vitro and in vivo cardiomyogenic differentiation of amniotic fluid stem cells. Stem Cell Rev. 7: 364-80.

Bonegio R, Lieberthal W. 2002. Role of apoptosis in the pathogenesis of acute renal failure. Curr Opin Nephrol Hypertens. 11: 301-8.

Bonventre, J.V. 2003. Dedifferentiation and proliferation of surviving epithelial cells in acute renal failure. J Am Soc Nephrol. 14 Suppl 1:S55-61.

Bossolasco P, Montemurro T, Cova L, Zangrossi S, Calzarossa C, Buiatiotis S, Soligo D, Bosari S, Silani V, Deliliers GL, Rebulla P, Lazzari L. 2006. Molecular and phenotypic characterization of human amniotic fluid cells and their differentiation potential. Cell Res. 16: 329-36.

Brady, H.R., B.C. Kone, M.E. Stromski, M.L. Zeidel, G. Giebisch, and S.R. Gullans. 1990. Mitochondrial injury: an early event in cisplatin toxicity to renal proximal tubules. Am J Physiol. 258:F1181-7.

Brooks C, Wei Q, Cho SG, Dong Z. 2009. Regulation of mitochondrial dynamics in acute kidney injury in cell culture and rodent models. J Clin Invest. May;119: 1275-85.

Bruno S, Grange C, Deregibus MC, Calogero RA, Saviozzi S, Collino F, Morando L, Busca A, Falda M, Bussolati B, Tetta C, Camussi G. 2009. Mesenchymal stem cell-derived microvesicles protect against acute tubular injury. J Am Soc Nephrol. 20:1053-67.

Bullock, A.N., and A.R. Fersht. 2001. Rescuing the function of mutant p53. Nat Rev Cancer. 1:68-76.

Bussolati B, Bruno S, Grange C, Buttiglieri S, Deregibus MC, Cantino D, Camussi G. 2005. Isolation of renal progenitor cells from adult human kidney. Am J Pathol. Feb;166:545-55.

Cai J, Ahmad S, Jiang WG, Huang J, Kontos CD, Boulton M, Ahmed A. 2003. Activation of vascular endothelial growth factor receptor-1 sustains angiogenesis and Bcl-2 expression via the phosphatidylinositol 3-kinase pathway in endothelial cells. Diabetes. 52: 2959-68.

Caldas HC, Hayashi AP, Abbud-Filho M. 2011. Repairing the chronic damaged kidney: the role of regenerative medicine. Transplant Proc. 43:3573-6.

Cananzi M, Atala A, De Coppi P. 2009. Stem cells derived from amniotic fluid: new potentials in regenerative medicine. Reprod Biomed Online. Suppl 1:17-27.

Cantley LG. 2005. Adult stem cells in the repair of the injured renal tubule. Nat Clin Pract Nephrol.1:22-32.

Capelli C, Domenghini M, Borleri G, Bellavita P, Poma R, Carobbio A, Micò C, Rambaldi A, Golay J, Introna M. 2007. Human platelet lysate allows expansion and clinical grade production of mesenchymal stromal cells from small samples of bone marrow aspirates or marrow filter washouts. Bone Marrow Transplant. 40:785-91.

Carraro G, Perin L, Sedrakyan S, Giuliani S, Tiozzo C, Lee J, Turcatel G, De Langhe SP, Driscoll B, Bellusci S, Minoo P, Atala A, De Filippo RE, Warburton D. 2008. Human amniotic fluid stem cells can integrate and differentiate into epithelial lung lineages. Stem Cells. 26:2902-11.

Cavaglieri RC, Martini D, Sogayar MC, Noronha IL. 2009. Mesenchymal stem cells delivered at the subcapsule of the kidney ameliorate renal disease in the rat remnant kidney model. Transplant Proc. Apr. 41: 947-51.

Chang F, Lee JT, Navolanic PM, Steelman LS, Shelton JG, Blalock WL, Franklin RA, McCubrey JA. 2003. Involvement of PI3K/Akt pathway in cell cycle progression, apoptosis, and neoplastic transformation: a target for cancer chemotherapy. Leukemia. 17: 590-603.

Challen GA, Martinez G, Davis MJ, Taylor DF, Crowe M, Teasdale RD, Grimmond SM, Little MH. 2004. Identifying the molecular phenotype of renal progenitor cells. J Am Soc Nephrol. 15:2344-57.

Challen GA, Bertoncello I, Deane JA, Ricardo SD, Little MH. 2006. Kidney side population reveals multilineage potential and renal functional capacity but also cellular heterogeneity. J Am Soc Nephrol. 17:1896-912.

Choi S, Park M, Kim J, Hwang S, Park S, Lee Y. 2009. The role of mesenchymal stem cells in the functional improvement of chronic renal failure. Stem Cells Dev. 18: 521-9.

Choi YH, Saric T, Nasseri B, Hühn S, Van Linthout S, Hetzer R, Tschöpe C, Stamm C. 2011. Cardiac cell therapies: the next generation. Cardiovasc Ther. 29:2-16.

Ciarimboli G, Ludwig T, Lang D, Pavenstädt H, Koepsell H, Piechota HJ, Haier J, Jaehde U, Zisowsky J, Schlatter E. 2005. Cisplatin nephrotoxicity is critically mediated via the human organic cation transporter 2. Am J Pathol. 167:1477-84.

Coca SG, Yusuf B, Shlipak MG, Garg AX, Parikh CR. 2009. Long-term risk of mortality and other adverse outcomes after acute kidney injury: a systematic review and meta-analysis. Am J Kidney Dis. 2009. 53:961-73.

Codreanu I, Perico N, Sharma SK, Schieppati A, Remuzzi G. 2006. Prevention programmes of progressive renal disease in developing nations. Nephrology.11:321-8.

Coimbra TM, Cieslinski DA, Humes HD. 1990 Epidermal growth factor accelerates renal repair in mercuric chloride nephrotoxicity. Am J Physiol. 259:F438-43.

Collins AJ, Foley RN, Herzog C, Chavers B, Gilbertson D, Ishani A, Kasiske B, Liu J, Mau LW, McBean M, Murray A, St Peter W, Guo H, Li Q, Li S, Li S, Peng Y, Qiu Y, Roberts T, Skeans M, Snyder J, Solid C, Wang C, Weinhandl E, Zaun D, Arko C, Chen SC, Dalleska F, Daniels F, Dunning S, Ebben J, Frazier E, Hanzlik C, Johnson R, Sheets D, Wang X, Forrest B, Constantini E, Everson S, Eggers P, Agodoa L. 2008. United States Renal Data System Annual Data Report. Am J Kidney Dis. 53:S1-374.

Costantini F, Shakya R. 2006. GDNF/Ret signaling and the development of the kidney. Bioessays. 28:117-27.

Couser WG, Remuzzi G, Mendis S, Tonelli M. 2011. The contribution of chronic kidney disease to the global burden of major noncommunicable diseases. Kidney Int. 80:1258-70.

Crisan M, Yap S, Casteilla L, Chen CW, Corselli M, Park TS, Andriolo G, Sun B, Zheng B, Zhang L, Norotte C, Teng PN, Traas J, Schugar R, Deasy BM, Badylak S, Buhring HJ, Giacobino JP, Lazzari L, Huard J, Péault B. 2008. A perivascular origin for mesenchymal stem cells in multiple human organs. Cell Stem Cell. 3:301-13.

Daley GQ, Scadden DT. 2008. Prospects for stem cell-based therapy. Cell. 132:544-8.

Dai C, Stolz DB, Bastacky SI, St-Arnaud R, Wu C, Dedhar S, Liu Y. 2006. Essential role of integrin-linked kinase in podocyte biology: Bridging the integrin and slit diaphragm signaling. J Am Soc Nephrol. 17:2164-75.

Datta SR, Brunet A, Greenberg ME. 1999. Cellular survival: a play in three Akts. Genes Dev. 13: 2905-27.

Davis BJ, Forbes JM, Thomas MC, Jerums G, Burns WC, Kawachi H, Allen TJ, Cooper ME. 2004. Superior renoprotective effects of combination therapy with ACE and AGE inhibition in the diabetic spontaneously hypertensive rat. Diabetologia. 47:89-97.

Davis, C.A., H.S. Nick, and A. Agarwal. 2001. Manganese superoxide dismutase attenuates Cisplatin-induced renal injury: importance of superoxide. J Am Soc Nephrol. 12:2683-90.

De Broe ME. 2005. Tubular regeneration and the role of bone marrow cells: 'stem cell therapy'--a panacea? Nephrol Dial Transplant. 11:2318-20.

De Coppi P, Bartsch G Jr, Siddiqui MM, Xu T, Santos CC, Perin L, Mostoslavsky G, Serre AC, Snyder EY, Yoo JJ, Furth ME, Soker S, Atala A. 2007. Isolation of amniotic stem cell lines with potential for therapy. Nat Biotechnol. 25:100-6.

Delmastro, D.A., J. Li, A. Vaisman, M. Solle, and S.G. Chaney. 1997. DNA damage inducible-gene expression following platinum treatment in human ovarian carcinoma cell lines. Cancer Chemother Pharmacol. 39:245-53.

Devarajan P. 2006. Update on mechanisms of ischemic acute kidney injury. J Am Soc Nephrol. 17:1503-20.

Dickey DT, Wu YJ, Muldoon LL, Neuwelt EA. 2005. Protection against cisplatin-induced toxicities by N-acetylcysteine and sodium thiosulfate as assessed at the molecular, cellular, and in vivo levels. J Pharmacol Exp Ther. 314:1052-8.

Ding, H., J.D. Kopple, A. Cohen, and R. Hirschberg. 1993. Recombinant human insulin-like growth factor-I accelerates recovery and reduces catabolism in rats with ischemic acute renal failure. J Clin Invest. 91:2281-7.

D'Ippolito G, Schiller PC, Ricordi C, Roos BA, Howard GA. 1999. Age-related osteogenic potential of mesenchymal stromal stem cells from human vertebral bone marrow. J Bone Miner Res. 14: 1115-22.

Ditadi A, de Coppi P, Picone O, Gautreau L, Smati R, Six E, Bonhomme D, Ezine S, Frydman R, Cavazzana-Calvo M, André-Schmutz I. 2009. Human and murine amniotic fluid c-Kit+Lin- cells display hematopoietic activity. Blood. 113:3953-60.

Dressler GR. 1996. Pax-2, kidney development, and oncogenesis. Med Pediatr Oncol. 27:440-4

Duffield, J.S., K.M. Park, L.L. Hsiao, V.R. Kelley, D.T. Scadden, T. Ichimura, and J.V. Bonventre. 2005. Restoration of tubular epithelial cells during repair of the postischemic kidney occurs independently of bone marrow-derived stem cells. J Clin Invest. 115:1743-55.

Edwards RG, Hollands P. 2007. Will stem cells in cord blood, amniotic fluid, bone marrow and peripheral blood soon be unnecessary in transplantation? Reprod Biomed Online. 14:396-401.

Eggers PW. 2011. Has the incidence of end-stage renal disease in the USA and other countries stabilized? Curr Opin Nephrol Hypertens. 20:241-5.

Eliopoulos N, Zhao J, Bouchentouf M, Forner K, Birman E, Yuan S, Boivin MN, Martineau D. 2010. Human marrow-derived mesenchymal stromal cells decrease cisplatin renotoxicity in vitro and in vivo and enhance survival of mice post-intraperitoneal injection. Am J Physiol Renal Physiol. 299:F1288-98.

Eliot H, Gianni L, Myers C. 1984. Oxidative destruction of DNA by the adriamycin-iron complex. Biochemistry. 23: 928-36.

Eremina V, Sood M, Haigh J, Nagy A, Lajoie G, Ferrara N, Gerber HP, Kikkawa Y, Miner JH, Quaggin SE. 2003. Glomerular-specific alterations of VEGF-A expression lead to distinct congenital and acquired renal diseases. J Clin Invest. Mar;111(5):707-16.

Eremina V, Cui S, Gerber H, Ferrara N, Haigh J, Nagy A, Ema M, Rossant J, Jothy S, Miner JH, Quaggin SE. 2006. Vascular endothelial growth factor a signaling in the podocyte-endothelial compartment is required for mesangial cell migration and survival. J Am Soc Nephrol. 17:724-35.

Erices A, Conget P, Minguell JJ. 2000. Mesenchymal progenitor cells in human umbilical cord blood. Br J Haematol. 109:235-42.

Escolar ML, Poe MD, Provenzale JM, Richards KC, Allison J, Wood S, Wenger DA, Pietryga D, Wall D, Champagne M, Morse R, Krivit W, Kurtzberg J. 2005. Transplantation of umbilical-cord blood in babies with infantile Krabbe's disease. N Engl J Med. 352: 2069-81.

Fang TC, Alison MR, Cook HT, Jeffery R, Wright NA, Poulsom R. 2005. Proliferation of bone marrow-derived cells contributes to regeneration after folic acid-induced acute tubular injury. J Am Soc Nephrol. 16:1723-32.

Figliuzzi M, Cornolti R, Perico N, Rota C, Morigi M, Remuzzi G, Remuzzi A, Benigni A. 2009. Bone marrow-derived mesenchymal stem cells improve islet graft function in diabetic rats. Transplant Proc. 41:1797-800.

Floege J, Jonson R and Feehally J. 2010. Comprehensive Clinical Nephrology, Fourth Edition.

Flynn A, Barry F, O'Brien T. 2007. UC blood-derived mesenchymal stromal cells: an overview. Cytotherapy.9:717-26.

Fogo AB. 2003. Animal models of FSGS: lessons for pathogenesis and treatment. Semin Nephrol. 23:161-71.

Foster RR, Saleem MA, Mathieson PW, Bates DO, Harper SJ. 2005. Vascular endothelial growth factor and nephrin interact and reduce apoptosis in human podocytes. Am J Physiol Renal Physiol. 288:F48-57.

Franklin, S.C., M. Moulton, G.A. Sicard, M.R. Hammerman, and S.B. Miller. 1997. Insulin-like growth factor I preserves renal function postoperatively. Am J Physiol. 272:F257-9.

García-Fernández M, Delgado G, Puche JE, González-Barón S, Castilla Cortázar I. 2008. Low doses of insulin-like growth factor I improve insulin resistance, lipid metabolism, and oxidative damage in aging rats. Endocrinology. 149:2433-42.

Gerber HP, McMurtrey A, Kowalski J, Yan M, Keyt BA, Dixit V, Ferrara N. 1998. Vascular endothelial growth factor regulates endothelial cell survival through the phosphatidylinositol 3'-kinase/Akt signal transduction pathway. Requirement for Flk-1/KDR activation. J Biol Chem. 273: 30336-43.

Gewirtz DA. 1999. A critical evaluation of the mechanisms of action proposed for the antitumor effects of the anthracycline antibiotics adriamycin and daunorubicin. Biochem Pharmacol. 57: 727-41.

Gianni L, Zweier JL, Levy A, Myers CE. 1985. Characterization of the cycle of iron-mediated electron transfer from Adriamycin to molecular oxygen. J Biol Chem.260: 6820-6.

Gluckman E, Broxmeyer HA, Auerbach AD, Friedman HS, Douglas GW, Devergie A, Esperou H, Thierry D, Socie G, Lehn P, et al. 1989. Hematopoietic reconstitution in a patient with Fanconi's anemia by means of umbilical-cord blood from an HLA-identical sibling. N Engl J Med. 321:1174

Gobe GC, Johnson DW. 2007. Distal tubular epithelial cells of the kidney: Potential support for proximal tubular cell survival after renal injury. Int J Biochem Cell Biol. 39:1551-61.

Goodell MA, Brose K, Paradis G, Conner AS, Mulligan RC. 1996. Isolation and functional properties of murine hematopoietic stem cells that are replicating in vivo. J Exp Med.183:1797-806.

Gordon, J.A., and V.H. Gattone, 2nd. 1986. Mitochondrial alterations in cisplatin-induced acute renal failure. Am J Physiol. 250:F991-8.

Green DR, Reed JC. 1998. Mitochondria and apoptosis. Science. 281:1309-12.

Grino JM. 1994. BN 52021: a platelet activating factor antagonist for preventing post-transplant renal failure. A double-blind, randomized study. The BN 52021 Study Group in Renal Transplantation. Ann Intern Med. Sep. 121:345-7.

Guan F, Villegas G, Teichman J, Mundel P, Tufro A. 2006. Autocrine VEGF-A system in podocytes regulates podocin and its interaction with CD2AP. Am J Physiol Renal Physiol. 291:F422-8.

Gupta, S., C. Verfaillie, D. Chmielewski, Y. Kim, and M.E. Rosenberg. 2002. A role for extrarenal cells in the regeneration following acute renal failure. Kidney Int. 62:1285-90.

Hagiwara M, Shen B, Chao L, Chao J. 2008. Kallikrein-modified mesenchymal stem cell implantation provides enhanced protection against acute ischemic kidney injury by inhibiting apoptosis and inflammation. Hum Gene Ther. 19: 807-19.

Hallan SI, Coresh J, Astor BC, Asberg A, Powe NR, Romundstad S, Hallan HA, Lydersen S, Holmen J. 2006. International comparison of the relationship of chronic kidney disease prevalence and ESRD risk. J Am Soc Nephrol. 17:2275-84.

Haynesworth SE, Baber MA, Caplan AI. 1996. Cytokine expression by human marrow-derived mesenchymal progenitor cells in vitro: effects of dexamethasone and IL-1 alpha. J Cell Physiol. 166:585-92.

Hartmann, J.T., and H.P. Lipp. 2003. Toxicity of platinum compounds. Expert Opin Pharmacother. 4:889-901.

Haug CE, Colvin RB, Delmonico FL, Auchincloss H Jr, Tolkoff-Rubin N, Preffer FI, Rothlein R, Norris S, Scharschmidt L, Cosimi AB. 1993. A phase I trial of immunosuppression with anti-ICAM-1 (CD54) mAb in renal allograft recipients. Transplantation. 55:766-72.

Hauser PV, De Fazio R, Bruno S, Sdei S, Grange C, Bussolati B, Benedetto C, Camussi G. 2010. Stem cells derived from human amniotic fluid contribute to acute kidney injury recovery. Am J Pathol. 177:2011-21.

Heiger-Bernays WJ, Essigmann JM, Lippard SJ. 1990. Effect of the antitumor drug cis-diamminedichloroplatinum(II) and related platinum complexes on eukaryotic DNA replication. Biochemistry. Sep 29:8461-6.

Herrera, M.B., B. Bussolati, S. Bruno, V. Fonsato, G.M. Romanazzi, and G. Camussi. 2004. Mesenchymal stem cells contribute to the renal repair of acute tubular epithelial injury. Int J Mol Med. 14:1035-41.

Herrera MB, Bussolati B, Bruno S, Morando L, Mauriello-Romanazzi G, Sanavio F, Stamenkovic I, Biancone L, Camussi G. 2007. Exogenous mesenchymal stem cells localize to the kidney by means of CD44 following acute tubular injury. Kidney Int. 72:430-41.

Hershberger, P.A., T.F. McGuire, W.D. Yu, E.G. Zuhowski, J.H. Schellens, M.J. Egorin, D.L. Trump, and C.S. Johnson. 2002. Cisplatin potentiates 1,25-dihydroxyvitamin D3-induced apoptosis in association with increased mitogen-activated protein kinase kinase kinase 1 (MEKK-1) expression. Mol Cancer Ther. 1:821-9.

Hirschberg, R., J. Kopple, P. Lipsett, E. Benjamin, J. Minei, T. Albertson, M. Munger, M. Metzler, G. Zaloga, M. Murray, S. Lowry, J. Conger, W. McKeown, M. O'Shea, R. Baughman, K. Wood, M. Haupt, R. Kaiser, H. Simms, D. Warnock, W. Summer, R. Hintz, B. Myers, K. Haenftling, W. Capra, and et al. 1999. Multicenter clinical trial of recombinant human insulin-like growth factor I in patients with acute renal failure. Kidney Int. 55:2423-32.

Hishikawa K, Marumo T, Miura S, Nakanishi A, Matsuzaki Y, Shibata K, Ichiyanagi T, Kohike H, Komori T, Takahashi I, Takase O, Imai N, Yoshikawa M, Inowa T, Hayashi M, Nakaki T, Nakauchi H, Okano H, Fujita T. 2005. Musculin/MyoR is expressed in kidney side population cells and can regulate their function. J Cell Biol. 169:921-8.

Hsu CY, Chertow GM, McCulloch CE, Fan D, Ordoñez JD, Go AS. 2009. Nonrecovery of kidney function and death after acute on chronic renal failure. Clin J Am Soc Nephrol. 4:891-8.

Humes, H.D., D.A. Cieslinski, T.M. Coimbra, J.M. Messana, and C. Galvao. 1989. Epidermal growth factor enhances renal tubule cell regeneration and repair and accelerates the recovery of renal function in postischemic acute renal failure. J Clin Invest. 84:1757-61.

Humes HD, Liu S. 1994. Cellular and molecular basis of renal repair in acute renal failure. J Lab Clin Med. 124:749-54.

Humphreys BD, Bonventre JV. 2008. Mesenchymal stem cells in acute kidney injury. Annu Rev Med. 59:311-25.

Hung SC, Pochampally RR, Hsu SC, Sanchez C, Chen SC, Spees J, Prockop DJ. 2007. Short-term exposure of multipotent stromal cells to low oxygen increases their expression of CX3CR1 and CXCR4 and their engraftment in vivo. PLoS One. 2:e416.

Hyun I. 2010. The bioethics of stem cell research and therapy. J Clin Invest. 120:71-5.

Imai N, Hishikawa K, Marumo T, Hirahashi J, Inowa T, Matsuzaki Y, Okano H, Kitamura T, Salant D, Fujita T. 2007. Inhibition of histone deacetylase activates side population cells in kidney and partially reverses chronic renal injury. Stem Cells.25:2469-75.

Imasawa T, Nagasawa R, Utsunomiya Y, Kawamura T, Zhong Y, Makita N, Muso E, Miyawaki S, Maruyama N, Hosoya T, Sakai O, Ohno T. 1999. Bone marrow transplantation attenuates murine IgA nephropathy: role of a stem cell disorder. Kidney Int. 56:1809-17.

Imberti B, Morigi M, Tomasoni S, Rota C, Corna D, Longaretti L, Rottoli D, Valsecchi F, Benigni A, Wang J, Abbate M, Zoja C, Remuzzi G. 2007. Insulin-like growth factor-1 sustains stem cell mediated renal repair. J Am Soc Nephrol. 18:2921-8.

Imgrund M, Gröne E, Gröne HJ, Kretzler M, Holzman L, Schlöndorff D, Rothenpieler UW. 1999. Re-expression of the developmental gene Pax-2 during experimental acute tubular necrosis in mice 1. Kidney Int. 56:1423-31.

In 't Anker PS, Scherjon SA, Kleijburg-van der Keur C, Noort WA, Claas FH, Willemze R, Fibbe WE, Kanhai HH. 2003. Amniotic fluid as a novel source of mesenchymal stem cells for therapeutic transplantation. Blood. 102: 1548-9.

Ip JE, Wu Y, Huang J, Zhang L, Pratt RE, Dzau VJ. 2007. Mesenchymal stem cells use integrin beta1 not CXC chemokine receptor 4 for myocardial migration and engraftment. Mol Biol Cell. 18:2873-82.

Iwatani, H., T. Ito, E. Imai, Y. Matsuzaki, A. Suzuki, M. Yamato, M. Okabe, and M. Hori. 2004. Hematopoietic and nonhematopoietic potentials of Hoechst (low)/side population cells isolated from adult rat kidney. Kidney Int. 65:1604-14.

Iwatani H, Imai E. 2010. Kidney repair using stem cells: myth or reality as a therapeutic option? J Nephrol. 23:143-6.

James MT, Tonelli M; Alberta Kidney Disease Network. 2011. Financial aspects of renal replacement therapy in acute kidney injury. Semin Dial. 24:215-9.

Jamieson ER, Lippard SJ. 1999. Structure, Recognition, and Processing of Cisplatin-DNA Adducts. Chem Rev.99:2467-98.

Ji JF, He BP, Dheen ST, Tay SS. 2004. Interactions of chemokines and chemokine receptors mediate the migration of mesenchymal stem cells to the impaired site in the brain after hypoglossal nerve injury. Stem Cells.22: 415-27.

Jiang M, Wei Q, Wang J, Du Q, Yu J, Zhang L, Dong Z. 2006. Regulation of PUMA-alpha by p53 in cisplatin-induced renal cell apoptosis. Oncogene. 25:4056-66.

Jiang M, Wei Q, Pabla N, Dong G, Wang CY, Yang T, Smith SB, Dong Z. 2007. Effects of hydroxyl radical scavenging on cisplatin-induced p53 activation, tubular cell apoptosis and nephrotoxicity. Biochem Pharmacol. 73:1499-510.

Jiang, Y., B.N. Jahagirdar, R.L. Reinhardt, R.E. Schwartz, C.D. Keene, X.R. Ortiz-Gonzalez, M. Reyes, T. Lenvik, T. Lund, M. Blackstad, J. Du, S. Aldrich, A. Lisberg, W.C. Low, D.A. Largaespada, and C.M. Verfaillie. 2002. Pluripotency of mesenchymal stem cells derived from adult marrow. Nature. 418:41-9.

Just PM, Riella MC, Tschosik EA, Noe LL, Bhattacharyya SK, de Charro F. 2008. Economic evaluations of dialysis treatment modalities. Health Policy. 86:163-80.

Kale, S., A. Karihaloo, P.R. Clark, M. Kashgarian, D.S. Krause, and L.G. Cantley. 2003. Bone marrow stem cells contribute to repair of the ischemically injured renal tubule. J Clin Invest. 112:42-9.

Kawaida, K., K. Matsumoto, H. Shimazu, and T. Nakamura. 1994. Hepatocyte growth factor prevents acute renal failure and accelerates renal regeneration in mice. Proc Natl Acad Sci USA. 91:4357-61.

Kelly, K.J., S.M. Meehan, R.B. Colvin, W.W. Williams, and J.V. Bonventre. 1999. Protection from toxicant-mediated renal injury in the rat with anti-CD54 antibody. Kidney Int. 56:922-31.

Kelly KJ, Molitoris BA. 2000. Acute renal failure in the new millennium: time to consider combination therapy. Semin Nephrol. 20:4-19.

Kern S, Eichler H, Stoeve J, Klüter H, Bieback K. 2006. Comparative analysis of mesenchymal stem cells from bone marrow, umbilical cord blood, or adipose tissue. Stem Cells. 24:1294-301.

Kim J, Lee Y, Kim H, Hwang KJ, Kwon HC, Kim SK, Cho DJ, Kang SG, You J. 2007. Human amniotic fluid-derived stem cells have characteristics of multipotent stem cells. Cell Prolif. 40: 75-90.

Kim SW, Han H, Chae GT, Lee SH, Bo S, Yoon JH, Lee YS, Lee KS, Park HK, Kang KS. 2006. Successful stem cell therapy using umbilical cord blood-derived multipotent stem cells for Buerger's disease and ischemic limb disease animal model. Stem Cells. 24: 1620-6.

Kim YG, Suga SI, Kang DH, Jefferson JA, Mazzali M, Gordon KL, Matsui K, Breiteneder-Geleff S, Shankland SJ, Hughes J, Kerjaschki D, Schreiner GF, Johnson RJ. 2000. Vascular endothelial growth factor accelerates renal recovery in experimental thrombotic microangiopathy. Kidney Int. 58: 2390-9.

Kögler G, Radke TF, Lefort A, Sensken S, Fischer J, Sorg RV, Wernet P. 2005. Cytokine production and hematopoiesis supporting activity of cord blood-derived unrestricted somatic stem cells. Exp Hematol. 33: 573-83.

Kolambkar YM, Peister A, Soker S, Atala A, Guldberg RE. 2007. Chondrogenic differentiation of amniotic fluid-derived stem cells. J Mol Histol. 38: 405-13.

Kopen, G.C., D.J. Prockop, and D.G. Phinney. 1999. Marrow stromal cells migrate throughout forebrain and cerebellum, and they differentiate into astrocytes after injection into neonatal mouse brains. Proc Natl Acad Sci USA. 96:10711-6.

Krause D, Cantley LG. 2005. Bone marrow plasticity revisited: protection or differentiation in the kidney tubule? J Clin Invest. 115:1705-8.

Kunter U, Rong S, Djuric Z, Boor P, Müller-Newen G, Yu D, Floege J. 2006. Transplanted mesenchymal stem cells accelerate glomerular healing in experimental glomerulonephritis. J Am Soc Nephrol. 17:2202-12.

Kunter U, Rong S, Boor P, Eitner F, Müller-Newen G, Djuric Z, van Roeyen CR, Konieczny A, Ostendorf T, Villa L, Milovanceva-Popovska M, Kerjaschki D, Floege J. 2007. Mesenchymal stem cells prevent progressive experimental renal failure but maldifferentiate into glomerular adipocytes. J Am Soc Nephrol. 18:1754-64.

Kuwana H, Terada Y, Kobayashi T, Okado T, Penninger JM, Irie-Sasaki J, Sasaki T, Sasaki S. 2008. The phosphoinositide-3 kinase gamma-Akt pathway mediates renal tubular injury in cisplatin nephrotoxicity. Kidney Int. 73:430-45.

Laflamme MA, Murry CE. 2005. Regenerating the heart. Nat Biotechnol. 23:845-56.

Lameire N, Van Biesen W, Vanholder R. 2008. Acute kidney injury. Lancet. 372: 1863-5.

Lange C, Tögel F, Ittrich H, Clayton F, Nolte-Ernsting C, Zander AR, Westenfelder C. 2005. Administered mesenchymal stem cells enhance recovery from ischemia/reperfusion-induced acute renal failure in rats. Kidney Int. 68:1613-7.

Lasagni L, Romagnani P. 2010. Glomerular epithelial stem cells: the good, the bad, and the ugly. J Am Soc Nephrol. Oct;21(10):1612-9.

Lattanzio MR, Kopyt NP. 2009. Acute kidney injury: new concepts in definition, diagnosis, pathophysiology, and treatment. J Am Osteopath Assoc. 109:13-9.

Laughlin MJ, Eapen M, Rubinstein P, Wagner JE, Zhang MJ, Champlin RE, Stevens C, Barker JN, Gale RP, Lazarus HM, Marks DI, van Rood JJ, Scaradavou A, Horowitz MM. 2004. Outcomes after transplantation of cord blood or bone marrow from unrelated donors in adults with leukemia. N Engl J Med. 351:2265-75.

Lazzari S, Moscatelli D, Codari F, Salmona M, Morbidelli M, Diomede L. 2012. Colloidal stability of polymeric nanoparticles in biological fluids. J Nanopart Res. 14: 920.

Lebrecht D, Setzer B, Rohrbach R, Walker UA. 2004. Mitochondrial DNA and its respiratory chain products are defective in doxorubicin nephrosis. Nephrol Dial Transplant. 19:329-36.

Lee OK, Kuo TK, Chen WM, Lee KD, Hsieh SL, Chen TH. 2004. Isolation of multipotent mesenchymal stem cells from umbilical cord blood. Blood. 103:1669-75.

Lee VW, Harris DC. 2011. Adriamycin nephropathy: a model of focal segmental glomerulosclerosis. Nephrology (Carlton). 16: 30-8.

Le Hir M, Keller C, Eschmann V, Hähnel B, Hosser H, Kriz W. 2001. Podocyte bridges between the tuft and Bowman's capsule: an early event in experimental crescentic glomerulonephritis. J Am Soc Nephrol.12:2060-71.

Levey AS, Stevens LA, Coresh J. 2009. Conceptual model of CKD: applications and implications. Am J Kidney Dis. 53:S4-16.

Li H, Jiang T, Lin Y, Zhao Z, Zhang N. 2006. HGF protects rat mesangial cells from high-glucose-mediated oxidative stress. Am J Nephrol.;26: 519-30.

Li J, Deane JA, Campanale NV, Bertram JF, Ricardo SD. 2007. The contribution of bone marrow-derived cells to the development of renal interstitial fibrosis. Stem Cells. 25:697-706.

Lieberthal, W., V. Triaca, and J. Levine. 1996. Mechanisms of death induced by cisplatin in proximal tubular epithelial cells: apoptosis vs. necrosis. Am J Physiol. 270:F700-8.

Lin, F., A. Moran, and P. Igarashi. 2005. Intrarenal cells, not bone marrow-derived cells, are the major source for regeneration in postischemic kidney. J Clin Invest. 115:1756-64.

Lindgren D, Boström AK, Nilsson K, Hansson J, Sjölund J, Möller C, Jirström K, Nilsson E, Landberg G, Axelson H, Johansson ME. 2011. Isolation and characterization of progenitor-like cells from human renal proximal tubules. Am J Pathol. 178:828-37.

Lindvall O, Kokaia Z. 2006. Stem cells for the treatment of neurological disorders. Nature. 441:1094-6.

Ling YH, Priebe W, Perez-Soler R. 1993. Apoptosis induced by anthracycline antibiotics in P388 parent and multidrug-resistant cells. Cancer Res. 53: 1845-52.

Little MH. 2006. Regrow or repair: potential regenerative therapies for the kidney. J Am Soc Nephrol. 17:2390-401

Liu CH, Hwang SM. 2005. Cytokine interactions in mesenchymal stem cells from cord blood. Cytokine. 32:270-9.

Liu ZJ, Zhuge Y, Velazquez OC. 2009. Trafficking and differentiation of mesenchymal stem cells. J Cell Biochem.106: 984-91.

Locatelli F, Giorgiani G, Di-Cesare-Merlone A, Merli P, Sparta V, Moretta F. 2008. The changing role of stem cell transplantation in childhood. Bone Marrow Transplant. 41:S3-7.

Ludwig T, Riethmüller C, Gekle M, Schwerdt G, Oberleithner H. 2004. Nephrotoxicity of platinum complexes is related to basolateral organic cation transport. Kidney Int. 66:196-202.

Madias, N.E., and J.T. Harrington. 1978. Platinum nephrotoxicity. Am J Med. 65:307-14.

Maeshima, A., S. Yamashita, and Y. Nojima. 2003. Identification of renal progenitor-like tubular cells that participate in the regeneration processes of the kidney. J Am Soc Nephrol. 14:3138-46.

Magnasco A, Corselli M, Bertelli R, Ibatici A, Peresi M, Gaggero G, Cappiello V, Chiavarina B, Mattioli G, Gusmano R, Ravetti JL, Frassoni F, Ghiggeri GM. 2008. Mesenchymal stem cells protective effect in adriamycin model of nephropathy. Cell Transplant. 17: 1157-67.

Manca MF, Zwart I, Beo J, Palasingham R, Jen LS, Navarrete R, Girdlestone J, Navarrete CV. 2008. Characterization of mesenchymal stromal cells derived from full-term umbilical cord blood. Cytotherapy.10: 54-68.

Mangi AA, Noiseux N, Kong D, He H, Rezvani M, Ingwall JS, Dzau VJ. 2003. Mesenchymal stem cells modified with Akt prevent remodeling and restore performance of infarcted hearts. Nat Med. 9:1195-201.

Metsuyanim S, Harari-Steinberg O, Buzhor E, Omer D, Pode-Shakked N, Ben-Hur H, Halperin R, Schneider D, Dekel B. 2009. Expression of stem cell markers in the human fetal kidney. PLoS One. 4:e6709.

Matsushima H, Yonemura K, Ohishi K, Hishida A. 1998. The role of oxygen free radicals in cisplatin-induced acute renal failure in rats. J Lab Clin Med. 131:518-26.

McCampbell KK, Wingert RA. 2012. Renal stem cells: fact or science fiction? Biochem J. 444:153-68.

McTaggart SJ, Atkinson K. 2007. Mesenchymal stem cells: immunobiology and therapeutic potential in kidney disease. Nephrology. 12:44-52.

Mias C, Trouche E, Seguelas MH, Calcagno F, Dignat-George F, Sabatier F, Piercecchi-Marti MD, Daniel L, Bianchi P, Calise D, Bourin P, Parini A, Cussac D. 2008. Ex vivo pretreatment with melatonin improves survival, proangiogenic/mitogenic activity, and efficiency of mesenchymal stem cells injected into ischemic kidney. Stem Cells. 26:1749-57.

Miller, S.B., D.R. Martin, J. Kissane, and M.R. Hammerman. 1992. Insulin-like growth factor I accelerates recovery from ischemic acute tubular necrosis in the rat. Proc Natl Acad Sci U S A. 89:11876-80.

Miller, S.B., D.R. Martin, J. Kissane, and M.R. Hammerman. 1994. Hepatocyte growth factor accelerates recovery from acute ischemic renal injury in rats. Am J Physiol. 266:F129-34.

Momparler RL, Karon M, Siegel SE, Avila F. 1976. Effect of adriamycin on DNA, RNA, and protein synthesis in cell-free systems and intact cells. Cancer Res. 36: 2891-5.

Moorefield EC, McKee EE, Solchaga L, Orlando G, Yoo JJ, Walker S, Furth ME, Bishop CE. 2011. Cloned, CD117 selected human amniotic fluid stem cells are capable of modulating the immune response. PLoS One. 6: e26535.

Morgan, S.E., and M.B. Kastan. 1997. p53 and ATM: cell cycle, cell death, and cancer. Adv Cancer Res. 71:1-25.

Morigi M, Imberti B, Zoja C, Corna D, Tomasoni S, Abbate M, Rottoli D, Angioletti S, Benigni A, Perico N, Alison M, Remuzzi G. 2004. Mesenchymal stem cells are renotropic, helping to repair the kidney and improve function in acute renal failure. J Am Soc Nephrol. 15:1794-804.

Morigi M, Benigni A, Remuzzi G, Imberti B. 2006. The regenerative potential of stem cells in acute renal failure. Cell Transplant. Suppl 1:S111-7.

Morigi M, Introna M, Imberti B, Corna D, Abbate M, Rota C, Rottoli D, Benigni A, Perico N, Zoja C, Rambaldi A, Remuzzi A, Remuzzi G. 2008. Human bone marrow mesenchymal stem cells accelerate recovery of acute renal injury and prolong survival in mice. Stem Cells. 26:2075-82.

Morigi M, Rota C, Montemurro T, Montelatici E, Lo Cicero V, Imberti B, Abbate M, Zoja C, Cassis P, Longaretti L, Rebulla P, Introna M, Capelli C, Benigni A, Remuzzi G, Lazzari L. 2010. Life-sparing effect of human cord blood-mesenchymal stem cells in experimental acute kidney injury. Stem Cells. 28:513-22.

Mundel P, Reiser J, Zúñiga Mejía Borja A, Pavenstädt H, Davidson GR, Kriz W, Zeller R. 1997. Rearrangements of the cytoskeleton and cell contacts induce process formation during differentiation of conditionally immortalized mouse podocyte cell lines. Exp Cell Res.236:248-58.

Mundel P, Reiser J, Kriz W. May 1997. Induction of differentiation in cultured rat and human podocytes. J Am Soc Nephrol.8:697-705.

Nagaya N, Fujii T, Iwase T, Ohgushi H, Itoh T, Uematsu M, Yamagishi M, Mori H, Kangawa K, Kitamura S. 2004. Intravenous administration of mesenchymal stem cells improves cardiac function in rats with acute myocardial infarction through angiogenesis and myogenesis. Am J Physiol Heart Circ Physiol. 287:H2670-6.

Nakamura, T., and K. Sakamoto. 2001. Reactive oxygen species up-regulates cyclooxygenase-2, p53, and Bax mRNA expression in bovine luteal cells. Biochem Biophys Res Commun. 284:203-10.

Narayan KM, Ali MK, Koplan JP. 2010. Global noncommunicable diseases--where worlds meet. N Engl J Med. 363:1196-8.

National Kidney Foundation. 2002. K/DOQI clinical practice guidelines for chronic kidney disease: evaluation, classification, and stratification. Am J Kidney Dis. 39:S1-266.

Naziroglu M, Karaoğlu A, Aksoy AO. 2004. Selenium and high dose vitamin E administration protects cisplatin-induced oxidative damage to renal, liver and lens tissues in rats. Toxicology. 195: 221-30.

Nigam S, Lieberthal W. 2000. Acute renal failure. III. The role of growth factors in the process of renal regeneration and repair. Am J Physiol Renal Physiol. 279:F3-F11.

Ninichuk V, Gross O, Segerer S, Hoffmann R, Radomska E, Buchstaller A, Huss R, Akis N, Schlöndorff D, Anders HJ. 2006. Multipotent mesenchymal stem cells reduce interstitial fibrosis but do not delay progression of chronic kidney disease in collagen4A3-deficient mice. Kidney Int. 70:121-9.

Norman, J., Y.K. Tsau, A. Bacay, and L.G. Fine. 1990. Epidermal growth factor accelerates functional recovery from ischaemic acute tubular necrosis in the rat: role of the epidermal growth factor receptor. Clin Sci (Lond). 78:445-50.

Odorico JS, Kaufman DS, Thomson JA. 2001. Multilineage differentiation from human embryonic stem cell lines. Stem Cells.19:193-204.

Ohse T, Pippin JW, Vaughan MR, Brinkkoetter PT, Krofft RD, Shankland SJ. 2008. Establishment of conditionally immortalized mouse glomerular parietal epithelial cells in culture. J Am Soc Nephrol. 19:1879-90.

Okada M, Sugita K, Inukai T, Goi K, Kagami K, Kawasaki K, Nakazawa S. 2004. Hepatocyte growth factor protects small airway epithelial cells from apoptosis induced by tumor necrosis factor-alpha or oxidative stress. Pediatr Res. 56:336-44.

Oliver, J.A., O. Maarouf, F.H. Cheema, T.P. Martens, and Q. Al-Awqati. 2004. The renal papilla is a niche for adult kidney stem cells. J Clin Invest. 114:795-804.

Orciani M, Emanuelli M, Martino C, Pugnaloni A, Tranquilli AL, Di Primio R. 2008. Potential role of culture mediums for successful isolation and neuronal differentiation of amniotic fluid stem cells. Int J Immunopathol Pharmacol. 21: 595-602.

Ostendorf T, Kunter U, Eitner F, Loos A, Regele H, Kerjaschki D, Henninger DD, Janjic N, Floege J. 1999. VEGF(165) mediates glomerular endothelial repair. J Clin Invest. 104: 913-23.

Ouellette AJ, Malt RA, Sukhatme VP, Bonventre JV. 1990. Expression of two "immediate early" genes, Egr-1 and c-fos, in response to renal ischemia and during compensatory renal hypertrophy in mice. J Clin Invest. 85:766-71.

Pabla N, Dong Z. 2008. Cisplatin nephrotoxicity: mechanisms and renoprotective strategies. Kidney Int. 73:994-1007.

Panepucci RA, Siufi JL, Silva WA Jr, Proto-Siquiera R, Neder L, Orellana M, Rocha V, Covas DT, Zago MA. 2004. Comparison of gene expression of umbilical cord vein and bone marrow-derived mesenchymal stem cells. Stem Cells.22: 1263-78.

Park MS, De Leon M, Devarajan P. 2002. Cisplatin induces apoptosis in LLC-PK1 cells via activation of mitochondrial pathways. J Am Soc Nephrol. Apr;13(4):858-65.

Pereira, R.F., K.W. Halford, M.D. O'Hara, D.B. Leeper, B.P. Sokolov, M.D. Pollard, O. Bagasra, and D.J. Prockop. 1995. Cultured adherent cells from marrow can serve as long-lasting precursor cells for bone, cartilage, and lung in irradiated mice. Proc Natl Acad Sci USA. 92:4857-61.

Perico N, Remuzzi G. 2012. Chronic kidney disease: a research and public health priority. Nephrol Dial Transplant. Oct;27 Suppl 3:iii19-26.

Perin L, Giuliani S, Jin D, Sedrakyan S, Carraro G, Habibian R, Warburton D, Atala A, De Filippo RE. 2007. Renal differentiation of amniotic fluid stem cells. Cell Prolif. 40: 936-48.

Perin L, Sedrakyan S, Giuliani S, Da Sacco S, Carraro G, Shiri L, Lemley KV, Rosol M, Wu S, Atala A, Warburton D, De Filippo RE. 2010. Protective effect of human amniotic fluid stem cells in an immunodeficient mouse model of acute tubular necrosis. PLoS One. 5: e9357.

Perry J, Ho M, Viero S, Zheng K, Jacobs R, Thorner PS. 2007. The intermediate filament nestin is highly expressed in normal human podocytes and podocytes in glomerular disease. Pediatr Dev Pathol. 10:369-82.

Perry S. 1969. Reduction of toxicity in cancer chemotherapy. Cancer Res. 29:2319-25.

Pinto FO, Roberts I. 2008. Cord blood stem cell transplantation for haemoglobinopathies. Br J Haematol. 141: 309-24.

Pippin JW, Brinkkoetter PT, Cormack-Aboud FC, Durvasula RV, Hauser PV, Kowalewska J, Krofft RD, Logar CM, Marshall CB, Ohse T, Shankland SJ. 2009. Inducible rodent models of acquired podocyte diseases. Am J Physiol Renal Physiol. 296:F213-29.

Pittenger, M.F., A.M. Mackay, S.C. Beck, R.K. Jaiswal, R. Douglas, J.D. Mosca, M.A. Moorman, D.W. Simonetti, S. Craig, and D.R. Marshak. 1999. Multilineage potential of adult human mesenchymal stem cells. Science. 284: 143-7.

Poulsom, R., S.J. Forbes, K. Hodivala-Dilke, E. Ryan, S. Wyles, S. Navaratnarasah, R. Jeffery, T. Hunt, M. Alison, T. Cook, C. Pusey, and N.A. Wright. 2001. Bone marrow contributes to renal parenchymal turnover and regeneration. J Pathol. 195:229-35.

Poulsom, R., M.R. Alison, S.J. Forbes, and N.A. Wright. 2002. Adult stem cell plasticity. J Pathol. 197:441-56.

Prockop, D.J. 1997. Marrow stromal cells as stem cells for nonhematopoietic tissues. Science. 276:71-4.

Prodromidi EI, Poulsom R, Jeffery R, Roufosse CA, Pollard PJ, Pusey CD, Cook HT. 2006. Bone marrow-derived cells contribute to podocyte regeneration and amelioration of renal disease in a mouse model of Alport syndrome. Stem Cells. 24:2448-55.

Prusa AR, Marton E, Rosner M, Bettelheim D, Lubec G, Pollack A, Bernaschek G, Hengstschläger M. 2004. Neurogenic cells in human amniotic fluid. Am J Obstet Gynecol. 191: 309-14.

Ramesh, G., and W.B. Reeves. 2002. TNF-alpha mediates chemokine and cytokine expression and renal injury in cisplatin nephrotoxicity. J Clin Invest. 110:835-42.

Ramesh G, Reeves WB. 2005. p38 MAP kinase inhibition ameliorates cisplatin nephrotoxicity in mice. Am J Physiol Renal Physiol. 289:F166-74.

Rebelatto CK, Aguiar AM, Moretão MP, Senegaglia AC, Hansen P, Barchiki F, Oliveira J, Martins J, Kuligovski C, Mansur F, Christofis A, Amaral VF, Brofman PS, Goldenberg S, Nakao LS, Correa A. 2008. Dissimilar differentiation of mesenchymal stem cells from bone marrow, umbilical cord blood, and adipose tissue. Exp Biol Med (Maywood). 233:901-13.

Rehni AK, Singh N, Jaggi AS, Singh M. 2007. Amniotic fluid derived stem cells ameliorate focal cerebral ischaemia-reperfusion injury induced behavioural deficits in mice. Behav Brain Res. 183: 95-100.

Remuzzi G, Ruggenenti P, Perico N. 2002. Chronic renal diseases: renoprotective benefits of renin-angiotensin system inhibition. Ann Intern Med. 136:604-15.

Remuzzi G, Benigni A, Remuzzi A. 2006. Mechanisms of progression and regression of renal lesions of chronic nephropathies and diabetes. J Clin Invest. 116:288-96.

Ronconi E, Sagrinati C, Angelotti ML, Lazzeri E, Mazzinghi B, Ballerini L, Parente E, Becherucci F, Gacci M, Carini M, Maggi E, Serio M, Vannelli GB, Lasagni L, Romagnani S, Romagnani P. 2009. Regeneration of glomerular podocytes by human renal progenitors. J Am Soc Nephrol. 20:322-32.

Rosenberg, B., L. Van Camp, E.B. Grimley, and A.J. Thomson. 1967. The inhibition of growth or cell division in Escherichia coli by different ionic species of platinum(IV) complexes. J Biol Chem. 242:1347-52.

Rosenberg, B., L. Vancamp, and T. Krigas. 1965. Inhibition of Cell Division in Escherichia Coli by Electrolysis Products from a Platinum Electrode. Nature. 205:698-9.

Rosner M, Mikula M, Preitschopf A, Feichtinger M, Schipany K, Hengstschläger M. 2012. Neurogenic differentiation of amniotic fluid stem cells. Amino Acids. 42: 1591-6.

Rüster B, Göttig S, Ludwig RJ, Bistrian R, Müller S, Seifried E, Gille J, Henschler R. 2006. Mesenchymal stem cells display coordinated rolling and adhesion behavior on endothelial cells. Blood. 108:3938-44.

Ryan MJ, Johnson G, Kirk J, Fuerstenberg SM, Zager RA, Torok-Storb B. 1994. HK-2: an immortalized proximal tubule epithelial cell line from normal adult human kidney. Kidney Int. 45:48-57.

Sagrinati C, Netti GS, Mazzinghi B, Lazzeri E, Liotta F, Frosali F, Ronconi E, Meini C, Gacci M, Squecco R, Carini M, Gesualdo L, Francini F, Maggi E, Annunziato F, Lasagni L, Serio M, Romagnani S, Romagnani P. 2006. Isolation and characterization of multipotent progenitor cells from the Bowman's capsule of adult human kidneys. J Am Soc Nephrol. 17:2443-56.

Sallustio F, De Benedictis L, Castellano G, Zaza G, Loverre A, Costantino V, Grandaliano G, Schena FP. 2010. TLR2 plays a role in the activation of human resident renal stem/progenitor cells. FASEB J. 24:514-25.

Sanchez-Ramos J. 2006. Stem cells from umbilical cord blood. Semin Reprod Med. 24:358-69.

Sariola H, Saarma M. 2003. Novel functions and signalling pathways for GDNF. J Cell Sci. 116: 3855-62.

Satoh, M., N. Kashihara, S. Fujimoto, H. Horike, T. Tokura, T. Namikoshi, T. Sasaki, and H. Makino. 2003. A novel free radical scavenger, edarabone, protects against cisplatin-induced acute renal damage in vitro and in vivo. J Pharmacol Exp Ther. 305:1183-90.

Schena FP. 1998. Role of growth factors in acute renal failure. Kidney Int Suppl. 66:S11-5.

Schmidt A, Ladage D, Schinköthe T, Klausmann U, Ulrichs C, Klinz FJ, Brixius K, Arnhold S, Desai B, Mehlhorn U, Schwinger RH, Staib P, Addicks K, Bloch W. 2006. Basic fibroblast growth factor controls migration in human mesenchymal stem cells. Stem Cells. 24:1750-8.

Scholzen T, Gerdes J. 2000. The Ki-67 protein: from the known and the unknown. J Cell Physiol. 182:311-22.

Schwartz, R.E., M. Reyes, L. Koodie, Y. Jiang, M. Blackstad, T. Lund, T. Lenvik, S. Johnson, W.S. Hu, and C.M. Verfaillie. 2002. Multipotent adult progenitor cells from bone marrow differentiate into functional hepatocyte-like cells. J Clin Invest. 109:1291-302.

Segers VF, Van Riet I, Andries LJ, Lemmens K, Demolder MJ, De Becker AJ, Kockx MM, De Keulenaer GW. 2006. Mesenchymal stem cell adhesion to cardiac microvascular endothelium: activators and mechanisms. Am J Physiol Heart Circ Physiol. 290:H1370-7.

Semedo P, Wang PM, Andreucci TH, Cenedeze MA, Teixeira VP, Reis MA, Pacheco-Silva A, Câmara NO. 2007. Mesenchymal stem cells ameliorate tissue damages triggered by renal ischemia and reperfusion injury. Transplant Proc.39:421-3.

Semedo P, Palasio CG, Oliveira CD, Feitoza CQ, Gonçalves GM, Cenedeze MA, Wang PM, Teixeira VP, Reis MA, Pacheco-Silva A, Câmara NO. 2009. Early modulation of inflammation by mesenchymal stem cell after acute kidney injury. Int Immunopharmacol. 9:677-82.

Semedo P, Correa-Costa M, Antonio Cenedeze M, Maria Avancini Costa Malheiros D, Antonia dos Reis M, Shimizu MH, Seguro AC, Pacheco-Silva A, Saraiva Camara NO. Dec 2009. Mesenchymal stem cells attenuate renal fibrosis through immune modulation and remodeling properties in a rat remnant kidney model. Stem Cells.27:3063-73.

Sener G, Satiroglu H, Kabasakal L, Arbak S, Oner S, Ercan F, Keyer-Uysa M. 2000. The protective effect of melatonin on cisplatin nephrotoxicity. Fundam Clin Pharmacol. 14:553-60.

Seres KB, Hollands P. 2010. Cord blood: the future of regenerative medicine? Reprod Biomed Online. 20:98-102.

Shah SH, Mehta RL. 2006. Acute kidney injury in critical care: time for a paradigm shift? Curr Opin Nephrol Hypertens. 15:561-5.

Shi H, Patschan D, Dietz GP, Bähr M, Plotkin M, Goligorsky MS. 2008. Glial cell line-derived neurotrophic growth factor increases motility and survival of cultured mesenchymal stem cells and ameliorates acute kidney injury. Am J Physiol Renal Physiol. 294: F229-35.

Shi M, Li J, Liao L, Chen B, Li B, Chen L, Jia H, Zhao RC. 2007. Regulation of CXCR4 expression in human mesenchymal stem cells by cytokine treatment: role in homing efficiency in NOD/SCID mice. Haematologica. 92: 897-904.

Shih NY, Li J, Cotran R, Mundel P, Miner JH, Shaw AS. 2001. CD2AP localizes to the slit diaphragm and binds to nephrin via a novel C-terminal domain. Am J Pathol. 159:2303-8.

Shimada IS, Spees JL. 2011. Stem and progenitor cells for neurological repair: minor issues, major hurdles, and exciting opportunities for paracrine-based therapeutics. J Cell Biochem. 112:374-80.

Smeets B, Angelotti ML, Rizzo P, Dijkman H, Lazzeri E, Mooren F, Ballerini L, Parente E, Sagrinati C, Mazzinghi B, Ronconi E, Becherucci F, Benigni A, Steenbergen E, Lasagni L, Remuzzi G, Wetzels J, Romagnani P. 2009. Renal progenitor cells contribute to

hyperplastic lesions of podocytopathies and crescentic glomerulonephritis. J Am Soc Nephrol. 20:2593-603.

Star RA. 1998. Treatment of acute renal failure. Kidney Int. 54:1817-31.

Stevens LA, Levey AS. 2009. Current status and future perspectives for CKD testing. Am J Kidney Dis. 53:S17-26.

Sugimoto H, Hamano Y, Charytan D, Cosgrove D, Kieran M, Sudhakar A, Kalluri R. 2003. Neutralization of circulating vascular endothelial growth factor (VEGF) by anti-VEGF antibodies and soluble VEGF receptor 1 (sFlt-1) induces proteinuria. J Biol Chem. 278:12605-8.

Sugimoto H, Mundel TM, Sund M, Xie L, Cosgrove D, Kalluri R. 2006. Bone-marrow-derived stem cells repair basement membrane collagen defects and reverse genetic kidney disease. Proc Natl Acad Sci U S A. 103:7321-6.

Strasser A, O'Connor L, Dixit VM. 2000. Apoptosis signaling. Annu Rev Biochem.;69:217-45.

Taal MW, Brenner BM. 2008. Renal risk scores: progress and prospects. Kidney Int. 73:1216-9.

Tang J, Xie Q, Pan G, Wang J, Wang M. 2006. Mesenchymal stem cells participate in angiogenesis and improve heart function in rat model of myocardial ischemia with reperfusion. Eur J Cardiothorac Surg. 30:353-61.

Thadhani R, Pascual M, Bonventre JV. 1996. Acute renal failure. N Engl J Med. 334:1448-60.

Takada M, Nadeau KC, Shaw GD, Marquette KA, Tilney NL. 1997. The cytokine-adhesion molecule cascade in ischemia/reperfusion injury of the rat kidney. Inhibition by a soluble P-selectin ligand. J Clin Invest. 99:2682-90.

Takahashi K, Yamanaka S. 2006. Induction of pluripotent stem cells from mouse embryonic and adult fibroblast cultures by defined factors. Cell. 126:663-76.

Tarver-Carr ME, Powe NR, Eberhardt MS, LaVeist TA, Kington RS, Coresh J, Brancati FL. 2002. Excess risk of chronic kidney disease among African-American versus white subjects in the United States: a population-based study of potential explanatory factors. J Am Soc Nephrol. Sep 13:2363-70.

Tetta C, Bruno S, Fonsato V, Deregibus MC, Camussi G. 2011. The role of microvesicles in tissue repair. Organogenesis. 7:105-15.

Togel, F., Z. Hu, K. Weiss, J. Isaac, C. Lange, and C. Westenfelder. 2005. Administered mesenchymal stem cells protect against ischemic acute renal failure through differentiation-independent mechanisms. Am J Physiol Renal Physiol. 289(1):F31-42.

Tögel F, Isaac J, Hu Z, Weiss K, Westenfelder C. May 2005. Renal SDF-1 signals mobilization and homing of CXCR4-positive cells to the kidney after ischemic injury. Kidney Int.67:1772-84.

Tögel F, Weiss K, Yang Y, Hu Z, Zhang P, Westenfelder C. 2007. Vasculotropic, paracrine actions of infused mesenchymal stem cells are important to the recovery from acute kidney injury. Am J Physiol Renal Physiol. 292:F1626-35.

Tögel F, Zhang P, Hu Z, Westenfelder C. 2009. VEGF is a mediator of the renoprotective effects of multipotent marrow stromal cells in acute kidney injury. J Cell Mol Med. 13:2109-14.

Toma, C., M.F. Pittenger, K.S. Cahill, B.J. Byrne, and P.D. Kessler. 2002. Human mesenchymal stem cells differentiate to a cardiomyocyte phenotype in the adult murine heart. Circulation. 105:93-8.

Torrente Y, Polli E. 2008. Mesenchymal stem cell transplantation for neurodegenerative diseases. Cell Transplant.17:1103-13.

Toubeau G, Nonclercq D, Zanen J, Laurent G, Schaudies PR, Heuson-Stiennon JA. 1994. Renal tissue expression of EGF and EGF receptor after ischaemic tubular injury: an immunohistochemical study. Exp Nephrol. 2:229-39.

Townsend, D.M., and M.H. Hanigan. 2002. Inhibition of gamma-glutamyl transpeptidase or cysteine S-conjugate beta-lyase activity blocks the nephrotoxicity of cisplatin in mice. J Pharmacol Exp Ther. 300:142-8.

Tryggvason K, Wartiovaara J. 2001. Molecular basis of glomerular permselectivity. Curr Opin Nephrol Hypertens. 10:543-9.

Tsai MS, Lee JL, Chang YJ, Hwang SM. 2004. Isolation of human multipotent mesenchymal stem cells from second-trimester amniotic fluid using a novel two-stage culture protocol. Hum Reprod. 19:1450-6.

Tsai MS, Hwang SM, Tsai YL, Cheng FC, Lee JL, Chang YJ. 2006. Clonal amniotic fluid-derived stem cells express characteristics of both mesenchymal and neural stem cells. Biol Reprod. 74: 545-51.

Tsuji H, Miyoshi S, Ikegami Y, Hida N, Asada H, Togashi I, Suzuki J, Satake M, Nakamizo H, Tanaka M, Mori T, Segawa K, Nishiyama N, Inoue J, Makino H, Miyado K, Ogawa S, Yoshimura Y, Umezawa A. 2010. Xenografted human amniotic membrane-derived mesenchymal stem cells are immunologically tolerated and transdifferentiated into cardiomyocytes. Circ Res. 106:1613-23.

Tsuruya K, Tokumoto M, Ninomiya T, Hirakawa M, Masutani K, Taniguchi M, Fukuda K, Kanai H, Hirakata H, Iida M. 2003. Antioxidant ameliorates cisplatin-induced renal tubular cell death through inhibition of death receptor-mediated pathways. Am J Physiol Renal Physiol. 285:F208-18.

Vassalotti JA, Stevens LA, Levey AS. 2007. Testing for chronic kidney disease: a position statement from the National Kidney Foundation. Am J Kidney Dis. 50:169-80.

Viappiani S, Schulz R. 2006. Detection of specific nitrotyrosine-modified proteins as a marker of oxidative stress in cardiovascular disease. Am J Physiol Heart Circ Physiol. 290:H2167-8.

Vogetseder A, Karadeniz A, Kaissling B, Le Hir M. 2005. Tubular cell proliferation in the healthy rat kidney. Histochem Cell Biol. 124:97-104.

Vogetseder A, Palan T, Bacic D, Kaissling B, Le Hir M. 2007. Proximal tubular epithelial cells are generated by division of differentiated cells in the healthy kidney. 292:C807-13.

Wagers AJ, Weissman IL. 2004. Plasticity of adult stem cells. Cell. 116:639-48.

Wagner W, Wein F, Seckinger A, Frankhauser M, Wirkner U, Krause U, Blake J, Schwager C, Eckstein V, Ansorge W, Ho AD. 2005. Comparative characteristics of mesenchymal stem cells from human bone marrow, adipose tissue, and umbilical cord blood. Exp Hematol. 33:1402-16.

Waikar SS, Liu KD, Chertow GM. 2008. Diagnosis, epidemiology and outcomes of acute kidney injury. Clin J Am Soc Nephrol. 3:844-61.

Wang D, Lippard SJ. 2005. Cellular processing of platinum anticancer drugs. Nat Rev Drug Discov. 2005. 4:307-20.

Wang M, Yang Y, Yang D, Luo F, Liang W, Guo S, Xu J. 2009. The immunomodulatory activity of human umbilical cord blood-derived mesenchymal stem cells in vitro. Immunology. 126: 220-32.

Weibel ER. Practical methods for biological morphometry. London: Academic Press,; Stereological Methods. 1979:pp 40-116.

Weimar IS, Miranda N, Muller EJ, Hekman A, Kerst JM, de Gast GC, Gerritsen WR. 1998. Hepatocyte growth factor/scatter factor (HGF/SF) is produced by human bone marrow stromal cells and promotes proliferation, adhesion and survival of human hematopoietic progenitor cells (CD34+). Exp Hematol. Aug. 26:885-94.

Wild S, Roglic G, Green A, Sicree R, King H. 2004. Global prevalence of diabetes: estimates for the year 2000 and projections for 2030. Diabetes Care. 27:1047-53.

Witzgall R, Brown D, Schwarz C, Bonventre JV. 1994. Localization of proliferating cell nuclear antigen, vimentin, c-Fos, and clusterin in the postischemic kidney. Evidence for a heterogenous genetic response among nephron segments, and a large pool of mitotically active and dedifferentiated cells. J Clin Invest. 93:2175-88.

Yamashita S, Maeshima A, Nojima Y. 2005. Involvement of renal progenitor tubular cells in epithelial-to-mesenchymal transition in fibrotic rat kidneys. J Am Soc Nephrol. 16:2044-51.

Yang CH, Murti A, Pfeffer SR, Kim JG, Donner DB, Pfeffer LM. 2001. Interferon alpha /beta promotes cell survival by activating nuclear factor kappa B through phosphatidylinositol 3-kinase and Akt. J Biol Chem. 276:13756-61.

Yang Y, Guo L, Blattner SM, Mundel P, Kretzler M, Wu C. 2005. Formation and phosphorylation of the PINCH-1-integrin linked kinase-alpha-parvin complex are important for regulation of renal glomerular podocyte adhesion, architecture, and survival. J Am Soc Nephrol. 16:1966-76.

Yokoo T, Ohashi T, Shen JS, Sakurai K, Miyazaki Y, Utsunomiya Y, Takahashi M, Terada Y, Eto Y, Kawamura T, Osumi N, Hosoya T. 2005. Human mesenchymal stem cells in rodent whole-embryo culture are reprogrammed to contribute to kidney tissues. Proc Natl Acad Sci U S A. 102: 3296-300.

Ysebaert DK, De Greef KE, Vercauteren SR, Ghielli M, Verpooten GA, Eyskens EJ, De Broe ME. 2000. Identification and kinetics of leukocytes after severe ischaemia/reperfusion renal injury. Nephrol Dial Transplant. 15:1562-74.

Ueda H, Nakamura T, Matsumoto K, Sawa Y, Matsuda H, Nakamura T. 2001. A potential cardioprotective role of hepatocyte growth factor in myocardial infarction in rats. Cardiovasc Res. 51:41-50.

Zha J, Harada H, Yang E, Jockel J, Korsmeyer SJ. 1996. Serine phosphorylation of death agonist BAD in response to survival factor results in binding to 14-3-3 not BCL-X(L). Cell. 87:619-28.

Zhou H, Li XM, Meinkoth J, Pittman RN. 2000. Akt regulates cell survival and apoptosis at a postmitochondrial level. J Cell Biol. 151:483-94.

Zhang B, Ramesh G, Norbury CC, Reeves WB. 2007. Cisplatin-induced nephrotoxicity is mediated by tumor necrosis factor-alpha produced by renal parenchymal cells. Kidney Int. 72:37-44.

Zuk, A., J.V. Bonventre, and K.S. Matlin. 2001. Expression of fibronectin splice variants in the postischemic rat kidney. Am J Physiol Renal Physiol. 280:F1037-53.

CHAPTER 13

APPENDICES

13.1 Contribution to the thesis by other researchers

Part of the thesis project was carried on with the collaboration of other researchers of the "Mario Negri" Institute in Bergamo that contributed to the research as follows:

- Real Time PCR experiments were performed together with Dr. Lorena Longaretti, Laboratory of Gene Therapy and Cellular Reprogramming, "Mario Negri" Institute.
- Animal care and treatments were conducted in collaboration with Daniela Corna, Unit of Experimental Models of Kidney Diseases, "Mario Negri" Institute.
- Technical assistance for electron microscopy was given by Daniela Rottoli, Unit of Pathologhy and Immunopathology, "Mario Negri" Institute.
- Western Blotting experiments were conducted in collaboration with Dr. Cristina Zanchi, Laboratory of Pathophysiology of Experimental Renal Disease and Interaction with other Organ systems, "Mario Negri" Institute.
- A great contribute to the project was given by Dr. Marina Morigi, head of the Laboratory of Cell Biology and Regenerative Medicine, the laboratory of Mario Negri Institute where the thesis was carried on. Dr. Morigi contributed to the work addressing research and supervising the progress of the study.

All the other techniques and experiments described in this thesis were performed by the PhD student, Cinzia Rota.

13.2 Publications emanating from the work described in this thesis

Morigi M, **Rota C**, Montemurro T, Montelatici E, Lo Cicero V, Imberti B, Abbate M, Zoja C, Cassis P, Longaretti L, Rebulla P, Introna M, Capelli C, Benigni A, Remuzzi G, Lazzari L. Life-sparing effect of human cord blood-mesenchymal stem cells in experimental acute kidney injury. Stem Cells, 28:513-22, 2010

Rota C, Imberti B, Pozzobon M, Piccoli M, De Coppi P, Atala A, Gagliardini E, Xinaris C, Benedetti V, Fabricio AS, Squarcina E, Abbate M, Benigni A, Remuzzi G, Morigi M. Human amniotic fluid stem cell preconditioning improves their regenerative potential. Stem Cells Dev, 21:1911-23, 2012

Zoja C., Garcia P., **Rota C.**, Conti S., Gagliardini E., Corna D., Zanchi C., Bigini P., Benigni A., Remuzzi G., Morigi M. Mesenchymal stem cell therapy promotes renal repair by limiting glomerular podocyte and progenitor cell dysfunction in adriamycin-induced nephropathy. Am J Physiol-Renal Physiol. 303:F1370-81, 2012.

13.3 Full list of publications by the candidate on topics not associated with the work described herein and/or previous to the commencement of the thesis project

Imberti B, Morigi M, Tomasoni S, **Rota C**, Corna D, Longaretti L, Rottoli D, Valsecchi F, Benigni A, Wang J, Abbate M, Zoja C, Remuzzi G. Insulin-like growth factor-1 sustains stem cell mediated renal repair. J Am Soc Nephrol, 18:2921-8, 2007

Morigi M, Introna M, Imberti B, Corna D, Abbate M, **Rota C**, Rottoli D, Benigni A, Perico N, Zoja C, Rambaldi A, Remuzzi A, Remuzzi G. Human bone marrow mesenchymal stem cells accelerate recovery of acute renal injury and prolong survival in mice. Stem Cells, 26: 2075-82, 2008

Figliuzzi M, Cornolti R, Perico N, **Rota C**, Morigi M, Remuzzi G, Remuzzi A, Benigni A. Bone marrow-derived mesenchymal stem cells improve islet graft function in diabetic rats. Transplant Proc, 41:1797-800, 2009

Benigni A, Morigi M, Rizzo P, Gagliardini E, **Rota C**, Abbate M, Ghezzi S, Remuzzi A, Remuzzi G. Inhibiting angiotensin-converting enzyme promotes renal repair by limiting progenitor cell proliferation and restoring the glomerular architecture. Am J Pathol, 179:628-38, 2011

Casiraghi F, Azzollini N, Todeschini M, Cavinato RA, Cassis P, Solini S, **Rota C**, Morigi M, Introna M, Maranta R, Perico N, Remuzzi G, Noris M. Localization of mesenchymal stromal cells dictates their immune or proinflammatory effects in kidney transplantation. Am J Transplant, 12:2373-83, 2012.

13.4 Congress presentations related to the work described in this thesis

Poster presentation

Prosurvival effect of mesenchymal stem cells on podocytes in rats with adriamycin-induced nephrosis. Zoja C, Bautista Garcia P, **Rota C**, Conti S, Gagliardini E, Corna D, Zanchi C, Bigini P, Benigni A, Remuzzi G, Morigi M. "World Congress of Nephrology" (WCN), Milan, Italy, 2009

Life-sparing effect of human cord blood-mesenchymal stem cells in experimental acute kidney injury. Morigi M, **Rota C**, Montemurro T, Montelatici E, Lo Cicero V, Imberti B, Abbate M, Zoja C, Cassis P, Longaretti L, Rebulla P, Introna M, Capelli C, Benigni A, Remuzzi G, Lazzari L. "International Society for Stem Cells Research (ISSCR)" Barcellona, Spain, 2009

Human amniotic fluid stem cell preconditioning improves their regenerative potential. **Rota C**, Imberti B, Pozzobon M, Piccoli M, De Coppi P, Atala A, Gagliardini E, Xinaris C, Benedetti V, Fabricio AS, Squarcina E, Abbate M, Benigni A, Remuzzi G, Morigi M. "3rd meeting FIRST: Forum of Italian researchers on mesenchymal and stromal stem cells" Milan, Italy, 2011.

Invited speaker

Life-sparing effect of human cord blood-mesenchymal stem cells in experimental acute kidney injury. "World Congress of Nephrology" (WCN), Milan, Italy, 2009

Life-sparing effect of human cord blood-mesenchymal stem cells in experimental acute kidney injury. "International Stem Cell Symphosium", Seoul, Korea, 2010

Human amniotic fluid stem cell preconditioning improves their regenerative potential. Meeting "Stem Cells and the Kidney" Genoa, Italy, 2010

ACKNOWLEDGMENTS

I would like to express my sincere appreciation and gratitude to Professor Silvio Garattini, Director of the "Mario Negri" Institute, and Professor Giuseppe Remuzzi, Researcher Coordinator of the "Mario Negri" Institute of Bergamo, for their steadfast devotion to promote scientific research and for their dedication in supporting the growth of young researchers. I would like to thank them for giving me the opportunity to attend PhD courses.

I am grateful to Dr. Ariela Benigni, Director of the Studies, for her help in supervising my work over these years and for her fundamental scientific support. This thesis' success couldn't have been possible without her kindness and support.

My sincerest gratitude goes to Dr. Patricia Murray. I have been honored to receive her tutoring and I have fully taken advantage from her expertise in the stem cell research field. I would like to acknowledge her for all the time she dedicated to supervise my research.

I am mainly indebted to Dr. Marina Morigi, head of the Cell Biology and Regenerative Medicine Laboratory, for her invaluable contributions to the success of this project, and moreover for generously guiding me in cultivating my scientific growth over these years.

Special thanks to all the people of the Department of Molecular Medicine who contributed to this study: Carla Zoja, Daniela Corna, Daniela Rottoli, Sara Conti and Lorena Longaretti. I would like to especially thank the colleagues and friends of my Laboratory that, with their support and cheerfulness, helped to relieve the fatigue of the hard work: Barbara, Valentina, Serena, Evangelia, Luca, Christos, Anna and Simona.

To my beloved Simone for his love and patience that he has shown throughout these years! To my loving family for their support and never ending encouragement.